SCUOLA DI DOTTORATO

UNIVERSITÀ DEGLI STUDI DI MILANO-BICOCCA

**School of Medicine and Surgery**

**PhD program in Translational and Molecular Medicine**

**Cycle XXXII**

Curriculum in Cellular and Molecular Mechanisms

# Relationship between repolarization and sarcoplasmic reticulum stability

Dr. Badone Beatrice

Registration number: 823332

Tutor: Prof. Zaza Antonio

Co-tutor: Prof. Volders Paul

Supervisor: Dr. Ronchi Carlotta

Coordinator: Prof. Biondi Andrea

**ACADEMIC YEAR 2018/2019**

# Table of content

*to my family and friends*

# Chapter 1

## *Introduction*

### *1.1 Acronyms*

| | |
|---|---|
| **ATII** | angiotensin II |
| **CaM** | calmodulin |
| **CICR** | $Ca^{2+}$-induced $Ca^{2+}$-release |
| **HF** | heart failure |
| **hiPSC-CMs** | human-induced pluripotent stem cell-derived cardiomyocytes |
| **LQTS** | Long-QT syndrome |
| **NO** | nitric oxide |
| **NOS1** | nitric oxide synthase 1 |
| **NOS1AP** | nitric oxide synthase 1 adaptor protein |
| **PLN** | phospholamban |
| **SERCA2a** | sarco/endoplasmic reticulum $Ca^{2+}$-ATPase type 2 |
| **SR** | sarcoplasmic reticulum |

In the cardiac muscle, the contraction is initiated by an electrical impulse that propagates through the sarcolemma, opening sarcolemmal voltage-activated $Ca^{2+}$ channels. $Ca^{2+}$ influx through these channels triggers $Ca^{2+}$ release from the sarcoplasmic reticulum (SR), the intracellular $Ca^{2+}$ store. This mechanism is called "$Ca^{2+}$-induced $Ca^{2+}$-release" (CICR). Subsequently, $Ca^{2+}$ binding to myofilaments initiates contraction [1].

This electro-mechanical coupling is in a dynamic equilibrium that strictly depends on the stability of the systems involved. In particular, SR function and stability are crucial in maintaining the efficiency of the CICR mechanism. This is because the SR has a pivotal role in maintaining the $Ca^{2+}$ influx/efflux balance. Indeed, after contraction, the reuptake of $Ca^{2+}$ by the $Ca^{2+}$-ATPase localized on the SR (SERCA2a), restores the diastolic levels of this ion in the cytosolic compartment, thus avoiding activation of stress signaling involved in  toxicity [2].

The presence of electrogenic channels and trasporters that are activated by cytosolic $Ca^{2+}$ changes, renders the sarcolemmal potential sensitive to $Ca^{2+}$ concentrations. This leads to electro-mechanical instability in pathological conditions, such as in heart failure (HF), where the SR function is compromised [3]. All of this could explain why the decline of mechanical function occurs along with an high incidence of arrhythmias, which are the main cause of death in HF.

The stability of the SR is preserved by several $Ca^{2+}$-binding proteins (i.e. CaM, calsequestrin), that cooperate in maintaining the homeostatic balance of intracellular $Ca^{2+}$. On the other hand, the cascade activated by $Ca^{2+}$ release from the SR, modulates these $Ca^{2+}$ sensitive elements, thus allowing a functional adaptation to demand [1, 2].

As mentioned before, the SR instability plays a central role in pathological conditions characterized by the concomitance of dysregulated $Ca^{2+}$ handling and arrhythmias.

The aim of this thesis was to study the mechanisms of cardiac functional impairment in three of such conditions:

1) the correlation between prolonged repolarization and the ATII signaling (**Chapter 2**);
2) the effect of NOS1AP polymorphisms which have been linked to arrhythmic risk in the context of Long-QT syndromes (LQTS) (**Chapter 3**);
3) the pathophysiological effect of a phospholamban (PLN) mutation (R14Del), a key protein in the SR stability and in $Ca^{2+}$ handling homeostasis (**Chapter 4**).

The outcome of these studies is summarized as follows:

1) ATII signaling is involved in cytosolic $Ca^{2+}$ handling and ROS production, both functions that are strictly correlated to SR stability. The results obtained from the first study (**Chapter 2**) confirm that prolonged repolarization and ATII signaling act as co-factors in inducing SR instability. This result has practical relevance because ATII receptor antagonists, commonly used in cardiovascular therapy with other indications, might be antiarrhythmic in patients affected by genetic or acquired conditions of prolonged repolarization. Moreover, the level of activation of ATII signaling, might be useful for arrhythmic risk stratification.
2) the work of the second study (**Chapter 3**) shows that the minor variant of NOS1AP gene affects the spatial localization of NOS1 and its activity. NOS1 inhibition caused upregulation of inward currents, further prolongation of repolarization, and, in the context of pre-existing prolonged repolarization (i.e. LQTS), it contributed to induce arrhythmogenic SR instability. This fits with the notion that NOS1 catalyzes the production of NO at sites relevant to intracellular $Ca^{2+}$ handling and SR stability. The final outcome of this work has a strong

translational value because it establishes a mechanistic link between NOS1AP polymorphisms and aggravation of the arrhythmia phenotype in prolonged repolarization syndromes. This allows the identification new therapeutic approaches;

3) in stem cell-derived cardiomyocytes (hiPSC-CMs) from carriers of the PLN-R14Del mutation, SERCA2a function is enhanced, thus suggesting a loss-of-function of PLN (**Chapter 4**). This novel result is partially unexpected, because previous findings from others have attributed the phenotype of the mutation (dilated and arrhytmogenic cardiomyopathy) to PLN gain-of-function, leading to SERCA2a insufficiency. The findings of our study suggest that an alternative mechanism must be considered to explain the disease phenotype. The work presented in this chapter has a powerful clinical potential, above all on the development of new therapeutic approaches.

### *1.2 References*


1. Bers, D.M., *Cardiac excitation–contraction coupling.* Nature, 2002. 415: p. 198-205.

2. Bers, D.M., *Calcium Cycling and Signaling in Cardiac Myocytes* Annu Rev Physiol, 2008 70: p. 23-49.

3. Santana, *How does the shape of the cardiac action potential control calcium signaling and contraction in the heart.* Journal of Molecular and Cellular Cardiology, 2010. 49(6): p. 901-903.

# Chapter 2

## *Action potential prolongation, β-adrenergic stimulation and angiotensin II as co-factors in sarcoplasmic reticulum instability*

Carlotta Ronchi[1], PhD, Beatrice Badone[1], MSc, Joyce Bernardi[1], PhD, and Antonio Zaza[1*], MD.

1. *Laboratory of Cardiac Cellular Physiology, Department of Biotechnology and Bioscience, University of Milano-Bicocca, Milan, Italy*

**Correspondence to:*

Antonio Zaza, MD, FESC
Dipartimento di Biotecnologie e Bioscienze
Università degli Studi Milano-Bicocca
P.za della Scienza 2, 20126 Milan (IT)
E-mail: antonio.zaza@unimib.it
Phone: +39 02 64483307

**[published; Front Physiol. 2018; 9: 1893. doi: 10.3389/fphys.2018.01893]**

### *2.1 Acronyms*

| | |
|---|---|
| **AP** | action potential |
| **APD** | action potential duration |
| **$APD_X$** | action potential duration at X% of repolarization |
| **AT1R** | angiotensin receptor type 1 |
| **ATII** | angiotensin II |
| **CL** | cycle length |
| **CICR** | $Ca^{2+}$-induced $Ca^{2+}$-released |
| **CM** | cardiomyocyte |
| **DADs** | delayed after depolarizations |
| **$I_m$** | total membrane current |
| **$I_{TI}$** | inward current transients |
| **$IP_3R$** | inositol 1,4,5-trisphospate-receptor |
| **ISO** | isoprotenerol |
| **ROS** | radical $O_2$ species |
| **RyR** | ryanodine receptor |
| **SCR** | spontaneous $Ca^{2+}$ release |
| **SR** | sarcoplasmic reticulum |

## *2.2 Abstract*

Increases in action potential duration (APD), genetic or acquired, and arrhythmias are often associated; nonetheless, the relationship between the two phenomena is inconstant, suggesting coexisting factors. β-adrenergic activation increases sarcoplasmic reticulum (SR) $Ca^{2+}$-content; angiotensin II (ATII) may increase cytosolic $Ca^{2+}$ and ROS production, all actions stimulating RyRs opening. Here we test how APD interacts with β-adrenergic and AT-receptor stimulation in facilitating spontaneous $Ca^{2+}$ release events (SCR)**. Methods**: under "action potential (AP) clamp", guinea-pig cardiomyocytes (CMs) were driven with long (200 ms), normal (150 ms), and short (100 ms) AP waveforms at a CL of 500 ms; in a subset of CMs, all the 3 waveforms could be tested within the same cell. SCR were detected as inward current transients ($I_{TI}$) following repolarization; $I_{TI}$ incidence and repetition within the same cycle were measured under increasing isoprenaline concentration ([ISO]) alone, or plus 100 nM ATII (30 min incubation+superfusion). **Results:** $I_{TI}$ incidence and repetition increased with [ISO]; at longer APs the [ISO]-response curve was shifted upward and $I_{TI}$ coupling interval was reduced. ATII increased $I_{TI}$ incidence more at low [ISO] and under normal (as compared to long) APs. Efficacy of AP shortening in suppressing $I_{TI}$ decreased in ATII-treated myocytes and at higher [ISO]. **Conclusions:** AP prolongation sensitized the SR to the destabilizing actions of ISO and ATII. Summation of ISO, ATII and AP duration effects had a "saturating" effect on SCR incidence, thus suggesting convergence on a common factor (RyRs stability) "reset" by the occurrence of spontaneous $Ca^{2+}$ release events.

**KEYWORDS:** Action Potential Duration, Angiotensin II, SR stability, Arrhythmias, Repolarization Reserve, β-adrenergic activation.

## *2.3 Introduction*

Prolonged ventricular repolarization, whether caused by myocardial remodeling [1], genetic defects [2] or drugs [3], may reduce myocardial electrical stability. Prolonged action potential duration (APD) may be a reporter of reduced "repolarization reserve", but it can also be causally linked to arrhythmogenesis through several mechanisms. Along with purely electrophysiological consequences (e.g increased repolarization heterogeneity) [4], APD prolongation affects the sarcolemmal $Ca^{2+}$ influx/efflux balance [5], thus it represents a stress-condition for intracellular $Ca^{2+}$ homeostasis requiring robust compensatory mechanisms. This might be critical under conditions, such as heart failure, in which intracellular $Ca^{2+}$ homeostasis is primarily impaired; indeed, "triggered activity" is common in the failing myocardium [6].

On the other hand, prolonged repolarization per se may be insufficient to induce arrhythmias, which might require the concomitance of multiple factors. This may be true also for primarily electrical disorders, such as genetic [7] and drug-induced [8] repolarization abnormalities. After the early identification of sympathetic activation as a powerful triggering mechanism [9], relatively little attention has been devoted to other biological variables that might theoretically converge with prolonged repolarization in reducing electrical stability. Their identification might pave the way to risk stratification and development of relatively simple preventive measures.

Myocardial and systemic production of angiotensin II (ATII) is increased in response to stress. Beside its well-known role in long-term structural remodeling of the failing heart, ATII has a couple of actions at the cellular level that might acutely compromise the compensations required to cope with prolonged repolarization.

AT-1 receptors (AT1R) stimulation by ATII induces $Ca^{2+}$ release from the sarcoplasmic reticulum (SR) through inositol 1,4,5-trisphospate-receptor channels (IP3R) and IP3R are functionally coupled to RYR2 in atrial myocytes [10, 11]. Although, in ventricular myocytes IP3R are less expressed [12], IP3R activation (by endothelin 1) has been reported to enhance CICR in rabbit ventricular myocytes [13]. Secondly, AT1R stimulation activates production of radical O2 species (ROS) by sarcolemmal NADPH-oxydases [14]; peroxydation destabilizes RyR2 closed state and is well known to facilitate spontaneous $Ca^{2+}$ release events (SCR) and related arrhythmias [15].

While an antiarrhythmic effect of ATII antagonism has been reported [16], acute proarrhythmia does not stand out as a direct consequence of increased ATII signaling, but what happens if the functional reserve provided by $Ca^{2+}$-homeostatic mechanisms is concomitantly decreased by prolonged repolarization?

Based on the above information, we hypothesize that stimulation of ATII receptors, may facilitate the occurrence of SCR events induced by APD prolongation and β-adrenergic stimulation. The aim of this study was to test such hypothesis.

The practical interest in this question also lies in the availability of widely used drugs limiting ATII cellular effects (AT1R antagonists), which might then be considered as complements in the prevention of ventricular arrhythmias under conditions of prolonged repolarization.

### *2.4 Materials and methods*

The investigation conforms to the Guide of the Care and Use of Laboratory Animals published by the US National Institute of Health (NIH publication No, 85-23). This study was reviewed and approved by the Animal Care Committee endorsed by University Milano -Bicocca.

#### *2.4.1 Cell isolation*

Dunkin-Hartley guinea pigs left ventricular cardiomyocytes were isolated by using a retrograde coronary perfusion method previously published [17], with minor modifications. Rod-shaped, $Ca^{2+}$-tolerant myocytes were used within 12 h from dissociation. No measure was taken to dissociate myocytes selectively from either the left or the right ventricle.

#### *2.4.2 Action potential clamp recordings*

Measurements were performed during superfusion with Tyrode's solution at 36.5 °C. Pre-recorded guinea-pig action potential (AP) waveforms were applied in V-clamp mode, as previously described [18], at a cycle length of 2 Hz. Three AP waveforms (obtained from previous I-clamp recordings under appropriate conditions) with different $APD_{90}$ (APD measured at 90% of repolarization) values were used: 200 ms (Long AP), 150 ms (Normal AP) and 100 ms (Short AP). $APD_{90}$ in the Long AP is 40% longer than in Normal AP, a change proportionally compatible with repolarization abnormalities seen in the clinical setting [19] (it would simulate a QTc change from e.g. 370 to 518 ms). According to the experimental protocol, the different AP waveforms were applied to different myocytes (group comparison) or within the same myocyte (internal control). Because of their design, internal control experiments involved application of both AP waveforms in a fixed sequence, thus requiring to exclude the dependence of $I_{TI}$ properties on the sequence itself. This was ruled out in preliminary experiments by applying Long-Short-Long AP sequences within the same

myocyte. Characteristics of AP waveforms are summarized in **Supplement Table S1**.

Total membrane current ($I_m$) during the AP-clamp cycle (**Figure 1A and Figure S1**) was recorded. Because the AP waveforms were not recorded within the same myocyte, $I_m$ during the AP was not null as expected under proper "self" AP-clamp conditions [20]; nonetheless, changes in the balance between $I_m$ inward and outward components could still be used as a gross estimate of interventions effect on systolic currents.

SCR events were detected as the occurrence of diastolic inward current transients ($I_{TI}$), known to result from activation of $Na^+/Ca^{2+}$ exchange by intracellular $Ca^{2+}$ transients. This method was preferred to direct recording of intracellular $Ca^{2+}$ because free from the contaminating effect of $Ca^{2+}$ buffering by fluorescent $Ca^{2+}$ probes; furthermore, $I_m$ is sensitive to sub-sarcolemmal $Ca^{2+}$ changes, which are relevant to membrane electrophysiology but poorly detected by epifluorescence measurements. Based on the baseline variance of diastolic current, $I_{TI}$ events were defined $I_{TI}$ exceeding a threshold of 15 pA; their incidence was defined as the percentage of myocytes in which at least 1 event was observed. Peak $I_{TI}$ amplitude (pA/pF) and $I_{TI}$ integral ($Q_{TI}$, in µC), which reports the charge moved by $Na^+/Ca^{2+}$ exchange, was used to quantify the magnitude of SCR events. Other parameters considered were $I_{TI}$ coupling interval after the preceding AP (CI in ms) and $I_{TI}$ latency (in sec) after the beginning of ISO infusion.

β-adrenergic stimulation was achieved by exposure to increasing isoprenaline concentrations ([ISO]); ATII-receptors were stimulated by 30 minutes preincubation in 100 nM ATII, which was also added to the superfusate.

Whether the effect of ATII was due to modulation of $IP_3R$ was tested by (5 min) exposure to 2 nM 2-aminoethyl diphenylborinate (2APB), an antagonist of $IP_3R$. Nifedipine 5 µM (NIFE) was used to compare 2APB effect on $I_m$ to that of L type $Ca^{2+}$ current ($I_{CaL}$) blockade.

### *2.4.3 Experimental solutions*

Tyrode's solution contained (in mM): 154 NaCl, 4 KCl, 2 $CaCl_2$, 1 $MgCl_2$, 5 HEPES-NaOH, 5.5 D-glucose, adjusted to pH 7.35 with NaOH. Myocytes were patch-clamped with borosilicate glass pipettes containing (mM): $K^+$-aspartate 110, KCl 23, $MgCl_2$ 3, HEPES KOH 5, EGTA KOH 1, GTP $Na^+$-salt 0.4, ATP $Na^+$-salt 5, creatine phosphate $Na^+$-salt 5, $CaCl_2$ 0.4 (calculated free-$Ca^{2+}$ = $10^{-7}$ M), adjusted to pH 7.3.

ISO and ATII were dissolved in water, NIFE in ethanol, and 2APB in DMSO. When used, compound solvents (ethanol or DMSO) were added to all solutions at the same final concentration, which never exceed 0.1%. All chemicals were purchased from Sigma.

### *2.4.4 Statistical analysis*

Student's paired or unpaired t-test was applied to compare means of continuous variables (latency, amplitudes etc). Difference between categorical variables (expressed as incidence %) was tested by chi-square (group comparison) or McNemar analysis (internal control) applied to absolute numbers; GLM regression for binomial data (R statistical package) was used to compare vectors of categorical variables (incidence in ISO dose-response curves). Statistical significance was defined as $P<0.05$. Sample size (n, number of cells) is specified for each experimental condition in the respective figure legend.

Categorical variables are expressed in percentages while the continuous variables are expressed as average ± standard error of the mean.

## *2.5 Results*

### *2.5.1 Effect of APD prolongation on ISO-induced $I_{TI}$ events*

The experimental protocol was optimized to test the effect of multiple [ISO] in each myocyte; because of limitations inherent to preparation stability, the effect of changing APD on the [ISO] vector had to be tested by comparing myocyte groups.

The incidence of $I_{TI}$ events was compared between myocytes clamped with either the Normal AP or the Long AP (group comparison) at baseline and during exposure to increasing ISO concentrations ([ISO]) (**Figure 1**). $I_{TI}$ incidence dose-dependently increased with [ISO] under both AP waveforms (**Figure 1B**); the Long APD moved the ISO concentration-response curve to significantly higher $I_{TI}$ incidences ($p<0.05$ at binomial GLM regression) and reduced the threshold concentration for ISO effect (lower vs upper panel in **Figure 1B**). As compared to Normal AP, Long AP shortened the time of $I_{TI}$ appearance after the beginning of ISO (or control) solution challenge; however, this effect became smaller as [ISO] was increased (**Figure 1C**).

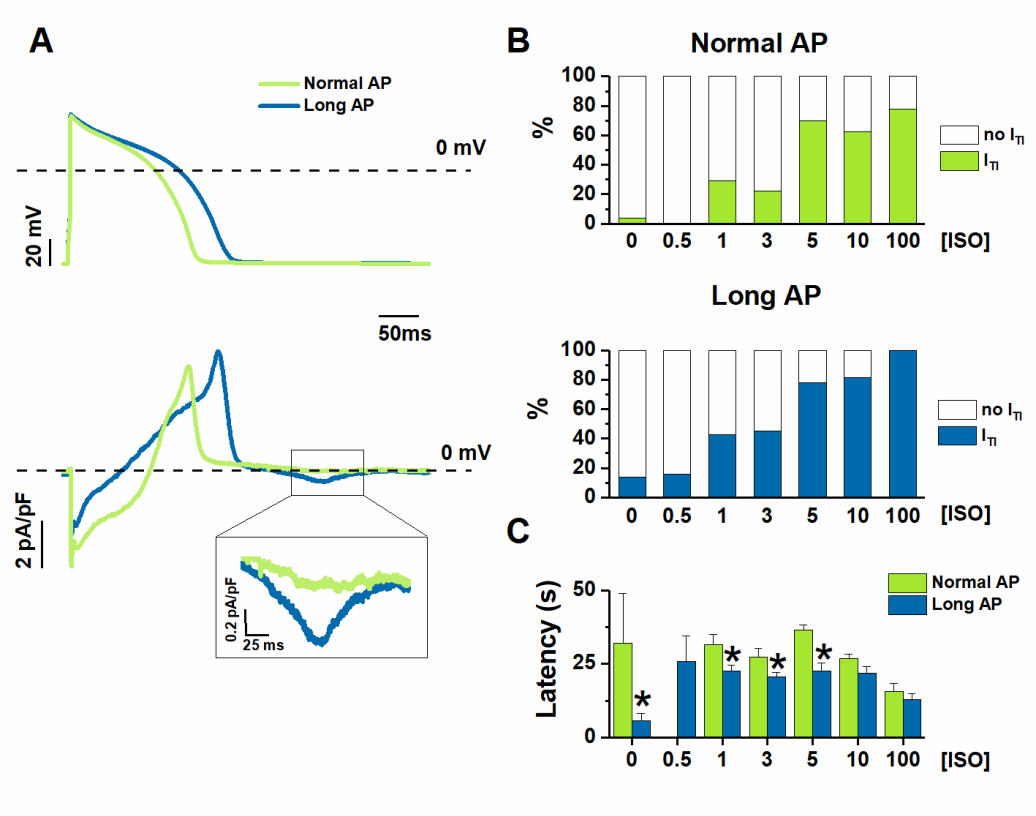


**Figure 1. [ISO]-dependency effect on $I_{TI}$ incidence under Normal AP and Long AP.** **(A)** Examples of Long AP and Normal AP waveforms used as a command in AP clamp (top) and the corresponding $I_m$ (bottom) during 1 nM ISO. **(B)** $I_{TI}$ incidence and **(C)** latency before $I_{TI}$ onset from starting ISO challenge at different ISO concentrations (nM). N> 10 for all data points. * P < 0.05 vs Normal AP.

*2.5.2 Effect of adding ATII*

The above experiments were repeated in cells treated with 100 nM ATII (ATII) and compared with untreated cells (no ATII) (**Figure 2**).

ATII alone ([ISO] = 0) had a very small effect on $I_{TI}$ incidence under Normal AP ($p<0.05$) and failed to change $I_{TI}$ significantly under Long AP (**Figure 2A**). Within each AP waveform, ATII moved the ISO concentration-response

curve to significantly higher $I_{TI}$ incidences. ATII effect was present with both AP waveforms, ($p<0.05$ at binomial GLM regression), but it was smaller and limited to low [ISO] during the Long AP (**Figure 2A**). ATII tended to shorten the time of $I_{TI}$ appearance after the beginning of ISO (or control) solution challenge but did so only under the Normal AP (**Figure 2B**).

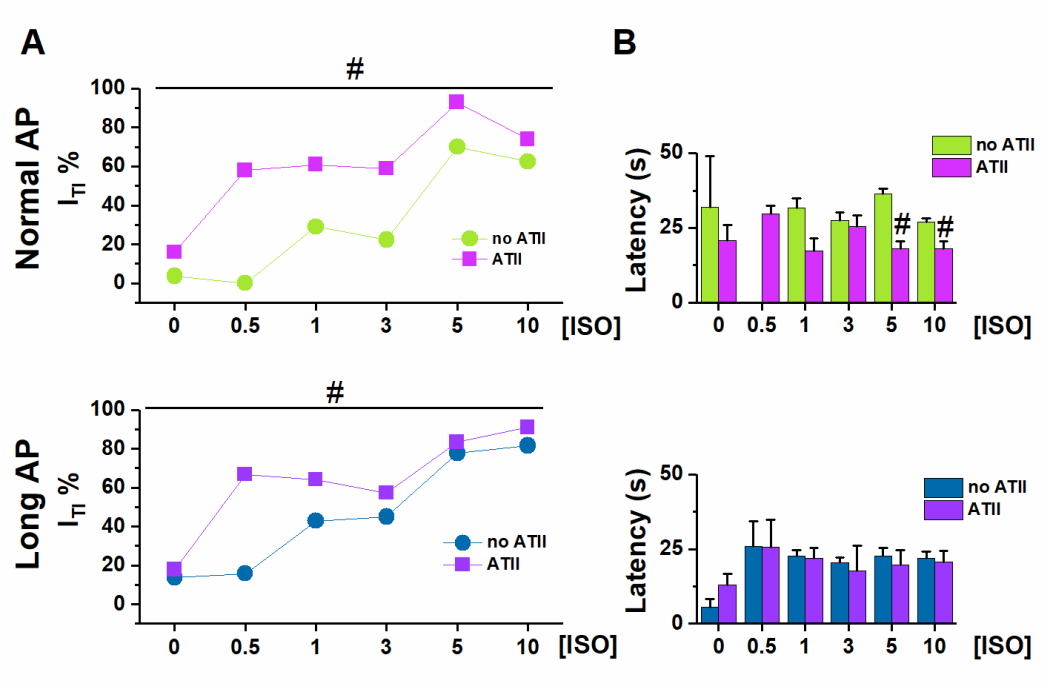


**Figure 2. Effect of adding ATII on $I_{TI}$ incidence under Normal AP and Long AP. (A)** $I_{TI}$ incidence observed and **(B)** latency before $I_{TI}$ onset from starting ISO challenge at different ISO concentrations (nM) in untreated (noATII) and ATII- treated (ATII) CMs. N> 20 for all groups. # $p<0.05$ vs ISO group.

*2.5.3 Effect of APD changes on $I_{TI}$ occurrence and properties*

This set of experiments was designed to test whether APD shortening would effectively modify $I_{TI}$ events induced by receptor stimulation. To this end, each myocyte in which $I_{TI}$ events occurred during the Long AP (incidence = 100% by default) was subsequently clamped with the Normal AP (internal control). This was repeated in myocyte groups, each exposed to a different [ISO] alone, or in the presence of ATII (**Figures 3-4**). $I_{TI}$ incidence and properties were measured.

Without ATII, (**Figure 3A**), switching from Long AP to Normal AP caused $I_{TI}$ to cease within several beats in 88% of the cells in basal conditions, in 46% under 1 nM ISO and in 33% under 10nM ISO ($p<0.05$ for $\Delta APD_{90}$ differences along the [ISO] vector). In ATII-treated myocytes, APD shortening terminated $I_{TI}$ in 55% of cells under basal conditions and termination rate decreased with increasing [ISO] (**Figure 3B**). The effect of APD shortening on $I_{TI}$ incidence was not significantly reduced by ATII.

In the absence of ATII, occurrence of two $I_{TI}$ events within the same cycle was not significantly affected by ISO. Surprisingly, ATII did not increase the occurrence of double $I_{TI}$ events and, if anything, tended to reduce it (**Figure 3C**).

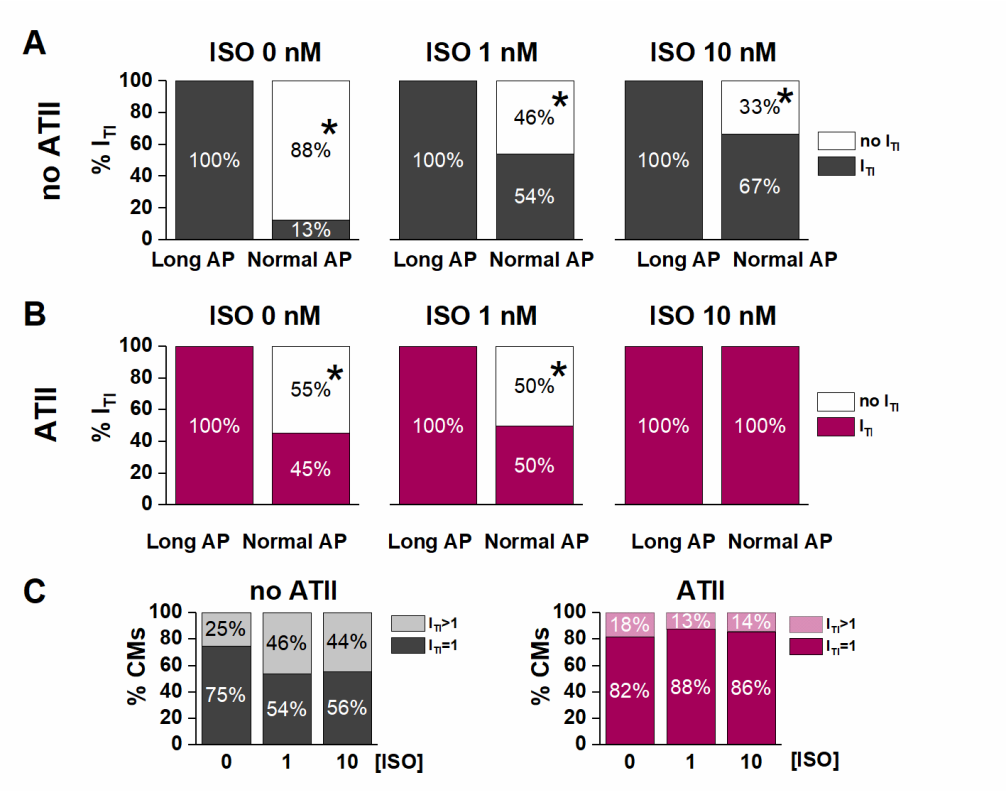


**Figure 3. Effect of APD shortening within the same cardiomyocytes in the absence (noATII) or presence of AT (ATII).** **(A-B)** $I_{TI}$ incidence and **(C)** number of cardiomyocytes with 1 $I_{TI}$ event or >1 $I_{TI}$ events under Long AP in basal condition (ISO 0) and during challenge with ISO 1 and 10 nM. CMs: cardiomyocytes. N > 8 for all groups. * $p < 0.05$ vs Long AP.

Similarly, $I_{TI}$ properties were affected by APD shortening (in the direction of smaller SCR with greater latency) only in the absence of β-adrenergic stimulation. ATII tended to increase $I_{TI}$ magnitude ($Q_{TI}$ and peak amplitude), but the effect of APD shortening was preserved (**Figure 4**).

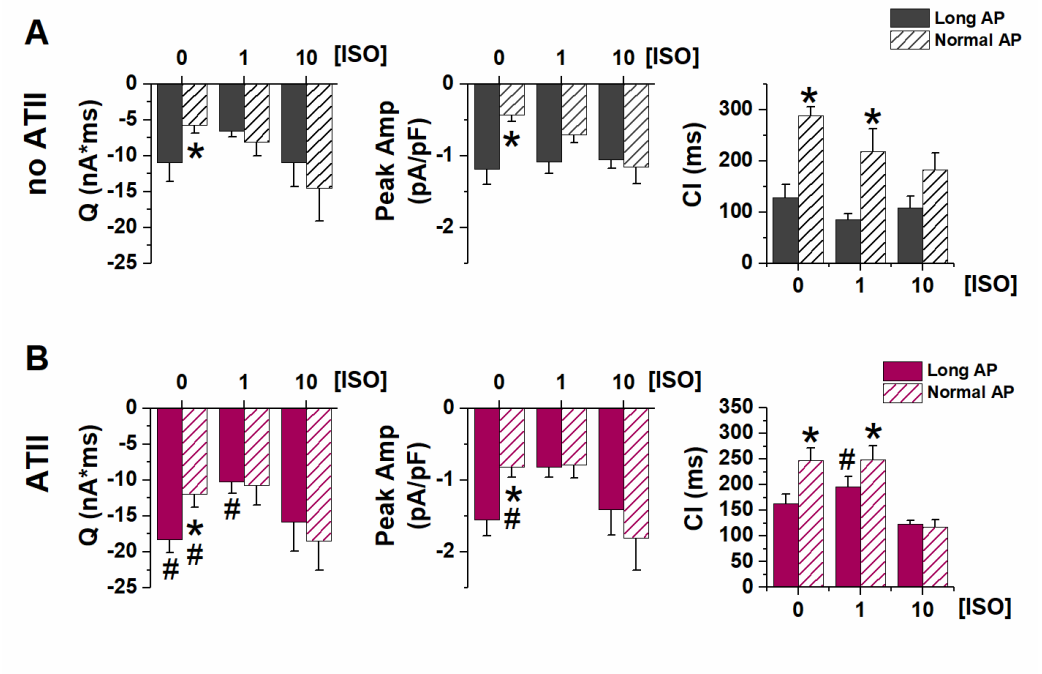


**Figure 4. Effect of APD shortening on $I_{TI}$ properties.** Statistic (mean ± S.E.) of $I_{TI}$ charge (Q), peak $I_{TI}$ amplitude (Peak Amp) and coupling interval (CI) in Untreated cardiomyocytes **(A)** and ATII-treated cardiomyocytes **(B).** N > 8 for all groups. * p < 0.05 vs Long AP; # p< 0.05 vs no ATII CMs.

To test whether APD affected $I_{TI}$ occurrence only if increased above its normal value, in a subset of myocytes the Short AP waveform was also tested (again by internal control) (**Figure 5**). $I_{TI}$ incidence and properties were incrementally modified by AP waveforms of shorter duration, suggesting that SR stability depends on APD in a continuous fashion. High [ISO] minimized the effect of APD shortening.

Overall, internal control experiments confirmed that APD shortening may counter the arrhythmogenic effect of receptor stimulation, but its impact was reduced at high levels of neurohumoral stimulation.

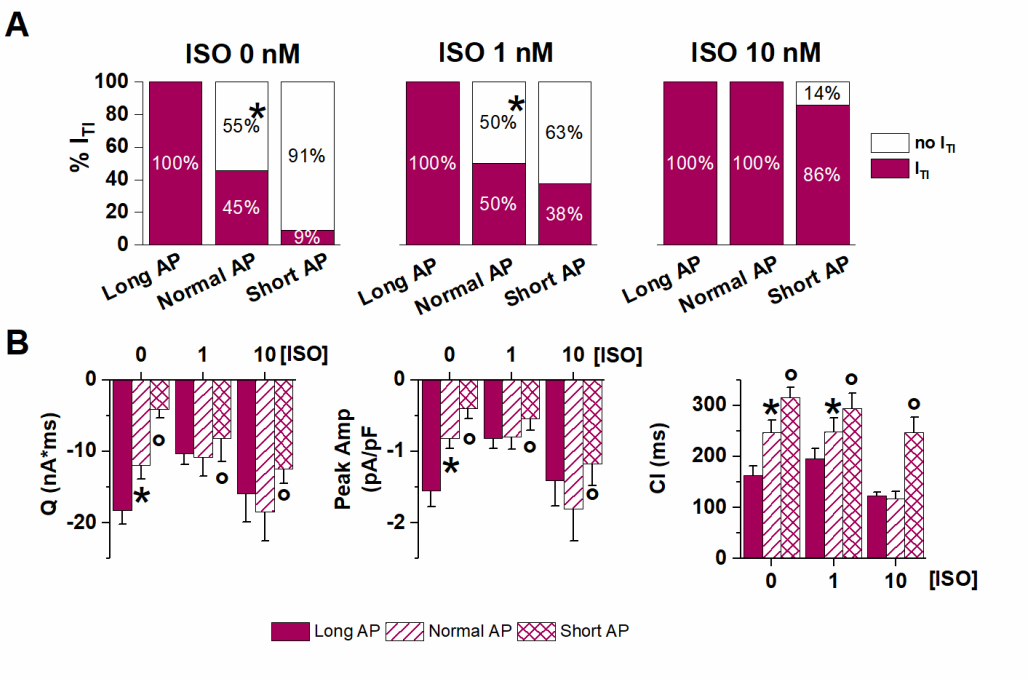


**Figure 5. Effect of APD shortening within the same ATII-treated cardiomyocytes (Long AP, Normal AP and Short AP waveforms). (A)** $I_{TI}$ incidence in basal condition (ISO 0) and in 1 nM and 10 nM ISO. **(B)** statistics (mean ± S.E.) of $I_{TI}$ charge (Q), peak $I_{TI}$ amplitude (Peak Amp) and coupling interval (CI). N >8 for all groups * $p<0.05$ vs Long AP; ° $p<0.05$ vs Normal AP.

### *2.5.4 $IP_3R$ contribution to ATII effect*

The contribution of $IP_3$ signaling to $I_{TI}$ facilitation by ATII was investigated by blocking $IP_3R$ (by 2APB) (**Figure 6**). To this end $I_{TI}$ incidence was measured, during Normal and Long APs, in the presence of 1 nM or 10 nM ISO + ATII only and after adding 2APB to the superfusate.

With 1 nM ISO, 2APB similarly reduced $I_{TI}$ incidence during Normal APD and Long APD (**Figure 6A**); the same was true for $I_{TI}$ charge (Q) (**Figure**

**6C**). When [ISO] was increased to 10 nM 2APB still reduced $I_{TI}$ incidence during Normal AP (by 60%) but had a much smaller effect during the Long AP (**Figure S2**).

This would suggest that $IP_3R$ stimulation significantly contributed to ATII-induced increment in SCR events; however, a substantial outward shift of $I_m$ during the AP (**Figure 6B**) opens the possibility of decreased $Ca^{2+}$ influx as the mechanism for $I_{TI}$ suppression. To test the hypothesis of direct $I_{CaL}$ blockade by 2APB, we compared the kinetics of its action on $I_m$ during the AP plateau to that of a saturating concentration of NIFE (**Figure S3**). The much slower kinetics of 2APB argues against direct $I_{CaL}$ blockade by 2APB.

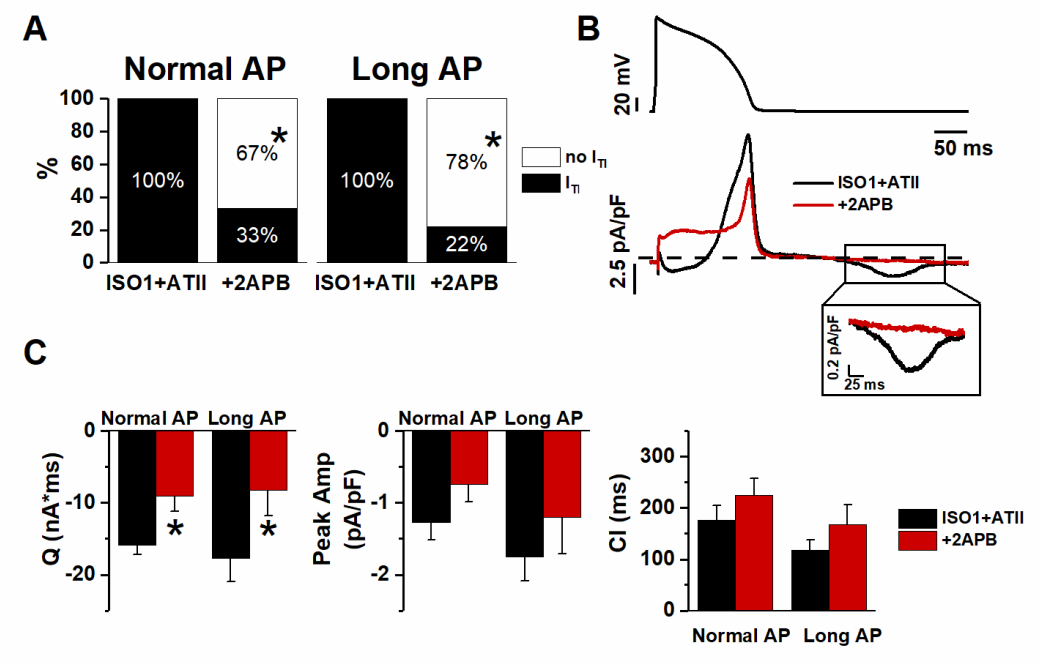


**Figure 6. Effect of 2APB on $I_{TI}$ evocated by ISO+ATII within same CMs. (A)** $I_{TI}$ incidence in ISO1+ATII alone and with 2APB. **(B)** Examples of Normal AP (top) and $I_m$ corresponding (bottom). **(C)** statistic (mean ± S.E.) of $I_{TI}$ charge (Q); peak $I_{TI}$ amplitude (Peak Amp) and coupling interval (CI). N=9 for both groups. * $p > 0.05$ vs ISO1+ATII.

### *2.6 Discussion*

The main findings of the present study were: ISO concentration-dependently induced SCR events and APD prolongation enhanced ISO effect; ATII increased SCR incidence preferentially when it was still far from 100%, i.e. with normal APD and in the lower range of [ISO].

While APD prolongation typically facilitates EADs through a mechanism at least partially independent of SCR [21, 22], its association with SCR is less straightforward. An increase in intracellular $Ca^{2+}$ content (both on the cytosolic and luminal sides of SR membrane) facilitates SCR [23, 24]. Because of net charge transport by the $Na^{+}/Ca^{2+}$ exchanger, $Ca^{2+}$ extrusion from the cell is favored at diastolic potentials; thus, assuming a constant cycle length (CL), APD prolongation can increase intracellular $Ca^{2+}$ content simply by decreasing the proportion of the cycle occupied by diastole [5]. Accordingly, modelling studies indicate that the amplitude and prematurity of DADs is expectedly related to APD because of APD-dependency of SR $Ca^{2+}$ load [22]. Nonetheless, blockade of a repolarizing current ($I_{Ks}$) in canine myocytes prolonged ventricular APD (by ~15%) but failed to induce DADs unless associated with β-adrenergic stimulation [25]. In the present study, APD prolongation (by 40%) alone tended to increase $I_{TI}$ incidence also in the absence of ISO; this effect was smaller than that previously reported in rabbit myocytes using more pronounced APD prolongation [26]. APD prolongation had a much larger effect in the presence of very low (nanomolar) ISO concentrations (**Figure 1**). This suggests that APD prolongation by amounts more relevant to the clinical setting may be relatively inconsequential on its own but becomes a powerful co-factor in the induction of SCR by adrenergic stimulation.

In the present experiments, APD was changed at a constant cycle length, thus reciprocally affecting diastolic interval. This implies that membrane "duty cycle" (the ratio between systolic and diastolic times), rather than APD itself, was considered. This approach was motivated by the consideration that repolarization

abnormalities are defined as changes of the rate-corrected QT interval, which implies that they are not accompanied by a commensurate change in cycle length. Furthermore, from a mechanistic standpoint, the sarcolemmal $Ca^{2+}$ flux balance depends on membrane duty cycle, rather than on APD alone [5]. Nonetheless, it is fair to stress that the present data may not describe the effect of changes in APD alone (i.e with constant diastolic interval).

In the presence of normal APD, ATII significantly facilitated $I_{TI}$ induction at all levels of β-adrenergic stimulation (**Figure 2**). ATII has been reported to exert "enhanced antagonism" of $I_{CaL}$ activation by β1-AR, reflecting inhibition of pre-activated adenylate cyclase [27]. Thus, $I_{TI}$ facilitation by ATII in the context of β1-AR activation may look contradictory. However, it should be noted that, in the present experiments, $I_{TI}$ facilitation by ATII prevailed at low ISO concentrations, which failed to induce $I_{TI}$ events on their own (**Figure 2**). Overall, this may suggest that ATII facilitated $I_{TI}$ events by mechanisms other than those triggered by β1-AR activation, but converging with them to impair SR stability.

ATII activates membrane phospholipase C (PLC) resulting in production of $IP_3$ and diacylglycerol. SR $Ca^{2+}$ release through $IP_3R$ channels is central in smooth muscle physiology and significantly contributes to intracellular $Ca^{2+}$ dynamics of atrial myocytes [11, 28]. Expression of $IP_3R$ in ventricular myocytes is lower, largely perinuclear and likely devoted to excitation-transcription coupling [13, 29, 30]; therefore, their role in intracellular $Ca^{2+}$ dynamics is debated. Nevertheless, $IP_3$-dependent enhancement of excitation-contraction coupling has been observed in rabbit ventricular myocytes [13]. Functional crosstalk between neighboring $IP_3R$ and RyR2 channels, caused by local $Ca^{2+}$ diffusion and amounting to direct activation of $Ca^{2+}$ release units, has been demonstrated in atrial myocytes [11]. In ventricular myocytes (including human ones), enhanced $IP_3R$-mediated SR $Ca^{2+}$ leak has been reported not to affect RyR2 function directly, but rather secondary to APD prolongation by the increment in $Na^+/Ca^{2+}$ exchanger current ($I_{NCX}$) [31]. Consistent with this interpretation, $IP_3R$ overexpression in a transgenic mouse model substantially enhanced SR $Ca^{2+}$ leak

without affecting the incidence of organized SCR events ($Ca^{2+}$ sparks or puffs) [32].

$IP_3R$ activation likely contributed to SCR facilitation by ATII in the present experiments, as suggested by the effect of 2APB (**Figure 6**). 2APB also shifted the current balance during the AP in the outward direction, a change compatible with an increased contribution of $I_{NCX}$ during $IP_3R$ activation [31]. Direct $I_{CaL}$ blockade by 2APB is unlikely because of the slow kinetics of 2APB effect (**Figure 6**) and of failure 2APB alone to affect $Ca^{2+}$ dynamics in ventricular myocytes [33]. The present results suggest that $IP_3R$ activation, possibly through an increment of cytosolic $Ca^{2+}$, may indeed facilitate $Ca^{2+}$ waves under the conditions generated by APD prolongation and β-adrenergic stimulation.

Albeit not investigated in the present work, activation of ROS production by ATII is a further mechanism potentially contributing to RyR2 destabilization [15]. Seen in the context of previous findings, the present results suggest that, albeit potentially inconsequential on its own, ATII may substantially facilitate SCR induction by β-adrenergic stimulation in ventricular myocytes.

Apparently in contrast with the hypothesis of a facilitatory role of APD prolongation, when APD was prolonged, ATII effect was smaller and limited to very low ISO concentrations (**Figure 2**). However, this can be viewed as "saturation" of the mechanisms responsible for SCR by APD prolongation (i.e. intracellular $Ca^{2+}$ load) and strong β-adrenergic stimulation. Notably, even at saturation, $I_{TI}$ incidence did not achieve 100% and events per cycle were limited to one or two. Such pattern is expected from convergence of the three co-factors (APD, ISO and ATII) on a common mechanism (RyR2 facilitation) with a "ceiling" effect. The ceiling can be conceivably caused by the SCR itself, which resets SR $Ca^{2+}$ content [23]. Considering that ATII facilitated SCR, we expected it to increase the occurrence of double $I_{TI}$ events within a cycle. The finding that the opposite was true can be tentatively interpreted by considering that ATII increased the magnitude of the first SCR event (**Q in Figure 4**); by causing larger SR $Ca^{2+}$ depletion, this might reduce the probability of a second SCR event.

The relevance of APD on $I_{TI}$ induction is highlighted by the ability of APD shortening to abrogate $I_{TI}$ once it was induced by either ISO alone or ISO plus ATII (**Figure 5**). Even when $I_{TI}$ persisted after AP normalization, its charge and amplitude were reduced, indicating that APD may affect the amount of $Ca^{2+}$ released by the SCR and, with it, the likelihood of triggering a propagated beat. In keeping with the convergence of factors, the ability of APD normalization to affect $I_{TI}$ occurrence and properties was reduced at high ISO concentrations and, further, in the presence of ATII.

### *2.7 Conclusion*

From the data obtained it is possible to conclude that ATII may act as a co-factor to facilitate the occurrence of SCR in the presence of AP prolongation and β-adrenergic stimulation.

### *2.8 Limitations*

Among small animals, guinea-pigs have an action potential contour which is closest to the human one; this justifies their adoption as experimental model. However, as compared to canine (and, possibly, human) myocytes, guinea-pig ones do not express $I_{TO}$ [34] and have a prominent sustained $I_{CaL}$, which likely supports a more positive action potential plateau [18]. This might exaggerate the impact of changes in APD in facilitating SCR events.

While $I_{TI}$ (measured under V-clamp) is a suitable reporter of SCR, the direct cause of arrhythmogenesis by SCR are DADs. Albeit $I_{TI}$ is the cause of DAD, their features do not necessarily coincide because V-clamp prevents the positive feed-back loop between depolarization and further current activation; moreover, the amplitude of DADs caused by a given $I_{TI}$ amplitude depends on membrane diastolic resistance and, thus, on the currents determining it (mostly $I_{K1}$). While absence of positive feed-back would lead to underestimate DADs

amplitude, the effect of the interventions tested on diastolic membrane resistance is unknown.

### *2.9 Practical implications*

ATII signaling is part of an homeostatic control system central to physiological adaptations; furthermore, ATII is also synthetized locally (cardiomyocytes, fibroblasts, vascular cells) in response to stress [35]; its production and its receptors (AT1R) are upregulated in cardiac disease [36]. Therefore, the extent of ATII signaling may well vary among subjects and, within a subject, in response to physiological and pathological states. The present results in cardiomyocytes suggest that ATII signaling might act as a variable co-factor in determining the impact of repolarization abnormalities on SR stability and the resulting arrhythmias. Thus, ATII antagonism might have an antiarrhythmic significance beyond prevention of myocardial remodeling, potentially extended to genetic and drug-induced conditions of prolonged repolarization. Considering that myocardial ATII production may be independent of the angiotensin converting enzyme (ACE) [35], direct antagonism of AT1 receptors should be considered as the logical intervention.

### *2.10 References*


1. Nattel, S., et al., Arrhythmogenic ion-channel remodeling in the heart: heart failure, myocardial infarction, and atrial fibrillation. Physiol Rev, 2007. 87(2): p. 425-456.

2. Schwartz, P.J., et al., Genotype-phenotype correlation in the long-QT syndrome: gene-specific triggers for life-threatening arrhythmias. Circulation, 2001. 103(1): p. 89-95.

3. Yang, T., D. Snyders, and D.M. Roden, Drug block of I(kr): model systems and relevance to human arrhythmias. Journal of Cardiovascular Pharmacology, 2001. 38(5): p. 737-744.

4. Winter, J. and M.J. Shattock, Geometrical considerations in cardiac electrophysiology and arrhythmogenesis. Europace, 2016. 18(3): p. 320-331.

5. Bers, D.M., Excitation-contraction coupling and cardiac contractile force. 2nd ed. 2001, Boston: Kluwer Academic Publishers.

6. Pogwizd, S.M., Nonreentrant mechanism underlying spontaneous ventricular arrhythmias in a model of nonischemic heart failure in rabbits. Circulation, 1995. 192: p. 1034-1048.

7. Napolitano, C., et al., Genetic modulators of the phenotype in the long QT syndrome: state of the art and clinical impact. Curr Opin Genet Dev, 2015. 33: p. 17-24.

8. Redfern, W.S., et al., Relationships between preclinical cardiac electrophysiology, clinical QT interval prolongation and torsade de pointes for a broad range of drugs: evidence for a provisional safety margin in drug development. Cardiovasc Res, 2003. 58(1): p. 32-45.

9. Malliani, A., P.J. Schwartz, and A. Zanchetti, Neural mechanisms in life-threatening arrhythmias. Am. Heart J, 1980. 100(5): p. 705-715.

10. Kockskamper, J., et al., Emerging roles of inositol 1,4,5-trisphosphate signaling in cardiac myocytes. J Mol Cell Cardiol, 2008. 45(2): p. 128-47.

11. Wullschleger, M., J. Blanch, and M. Egger, Functional local crosstalk of inositol 1,4,5-trisphosphate receptor- and ryanodine receptor-dependent Ca2+ release in atrial cardiomyocytes. Cardiovasc Res, 2017. 113(5): p. 542-552.

12. Garcia, M.I. and D. Boehning, Cardiac inositol 1, 4, 5-trisphosphate receptors. Biochimica et Biophysica Acta (BBA)-Molecular Cell Research, 2017. 1864(6): p. 907-914.

13. Domeier, T.L., et al., IP3 receptor-dependent Ca2+ release modulates excitation-contraction coupling in rabbit ventricular myocytes. Am J Physiol Heart Circ Physiol, 2008. 294(2): p. H596-604.

14. Kawai, T., et al., AT1 receptor signaling pathways in the cardiovascular system. Pharmacol Res, 2017. 125(Pt A): p. 4-13.

15. Prosser, B.L., et al., X-ROS signaling in the heart and skeletal muscle: stretch-dependent local ROS regulates [Ca(2)(+)]i. J Mol Cell Cardiol, 2013. 58: p. 172-81.

16. Garg, S., et al., Role of angiotensin receptor blockers in the prevention and treatment of arrhythmias. Am J Cardiol, 2006. 97(6): p. 921-5.

17. Zaza, A., et al., Dynamic Ca2+-induced inward rectification of K+ current during the ventricular action potential. Circulation Research, 1998. 82: p. 947-956.

18. Sala, L., et al., Action potential contour contributes to species differences in repolarization response to beta-adrenergic stimulation. Europace, 2018. 20(9): p. 1543-1552.

19. Schwartz, P.J., et al., Long QT Syndrome Patients With Mutations of the SCN5A and HERG Genes Have Differential Responses to Na+ Channel Blockade and to Increases in Heart Rate. Circulation, 1995. 92(12): p. 3381-3386.

20. Zaza, A., et al., Ionic currents during sustained pacemaker activity in rabbit sino-atrial myocytes. Journal of Physiology, 1997. 505(3): p. 677-688.

21. January, C.T. and J.M. Riddle, Early afterdepolarizations: Mechanism of induction and block. A role for L-type Ca2+ current. Circulation Research, 1989. 64: p. 977-990.

22. Song, Z., et al., Calcium-voltage coupling in the genesis of early and delayed afterdepolarizations in cardiac myocytes. Biophys J, 2015. 108(8): p. 1908-21.

23. Venetucci, L.A., et al., The sarcoplasmic reticulum and arrhythmogenic calcium release. Cardiovascular Research, 2008. 77(2): p. 285-292.

24. Egdell, R.M., A.I. De Souza, and K.T. MacLeod, Relative importance of SR load and cytoplasmic calcium concentration in the genesis of aftercontractions in cardiac myocytes. Cardiovascular Research, 2000. 47(4): p. 769-777.

25. Burashnikov, A. and C. Antzelevitch, Block of I(Ks) does not induce early afterdepolarization activity but promotes beta-adrenergic agonist-induced delayed afterdepolarization activity. J Cardiovasc Electrophysiol, 2000. 11(4): p. 458-65.

26. Wu, Y., D.M. Roden, and M.E. Anderson, Calmodulin kinase inhibition prevents development of the arrhythmogenic transient inward current. Circ Res, 1999. 84(8): p. 906-12.

27. Ai, T., et al., Accentuated antagonism by angiotensin II on guinea-pig cardiac L-type Ca-currents enhanced by β-adrenergic stimulation. Pflügers Archiv, 1998. 436(2): p. 168-174.

28. Li, X., et al., Endothelin-1-induced arrhythmogenic Ca2+ signaling is abolished in atrial myocytes of inositol-1,4,5-trisphosphate(IP3)-receptor type 2-deficient mice. Circ Res, 2005. 96(12): p. 1274-81.

29. Lipp, P., et al., Functional InsP3 receptors that may modulate excitation-contraction coupling in the heart. Curr Biol, 2000. 10(15): p. 939-42.

30. Wu, X., et al., Local InsP3-dependent perinuclear Ca2+ signaling in cardiac myocyte excitation-transcription coupling. J Clin Invest, 2006. 116(3): p. 675-82.

31. Signore, S., et al., Inositol 1, 4, 5-trisphosphate receptors and human left ventricular myocytes. Circulation, 2013. 128(12): p. 1286-97.

32. Blanch, I.S.J. and M. Egger, Obstruction of ventricular Ca(2+) -dependent arrhythmogenicity by inositol 1,4,5-trisphosphate-triggered sarcoplasmic reticulum Ca(2+) release. J Physiol, 2018.

33. Peppiatt, C.M., et al., 2-Aminoethoxydiphenyl borate (2-APB) antagonises inositol 1, 4, 5-trisphosphate-induced calcium release, inhibits calcium pumps and has a use-dependent and slowly reversible action on store-operated calcium entry channels. Cell calcium, 2003. 34(1): p. 97-108.

34. Nakajima, I., et al., Ca2+ overload evokes a transient outward current in guinea-pig ventricular myocytes. Circ J, 2002. 66(1): p. 87-92.

35. Varagic, J. and E.D. Frohlich, Local Cardiac Renin–Angiotensin System: Hypertension and Cardiac Failure. Journal of Molecular and Cellular Cardiology, 2002. 34(11): p. 1435-1442.

36. Szczepanska-Sadowska, E., K. Czarzasta, and A. Cudnoch-Jedrzejewska, Dysregulation of the Renin-Angiotensin System and the Vasopressinergic System Interactions in Cardiovascular Disorders. Curr Hypertens Rep, 2018. 20(3): p. 19.

### *2.11 Supplemental figures*

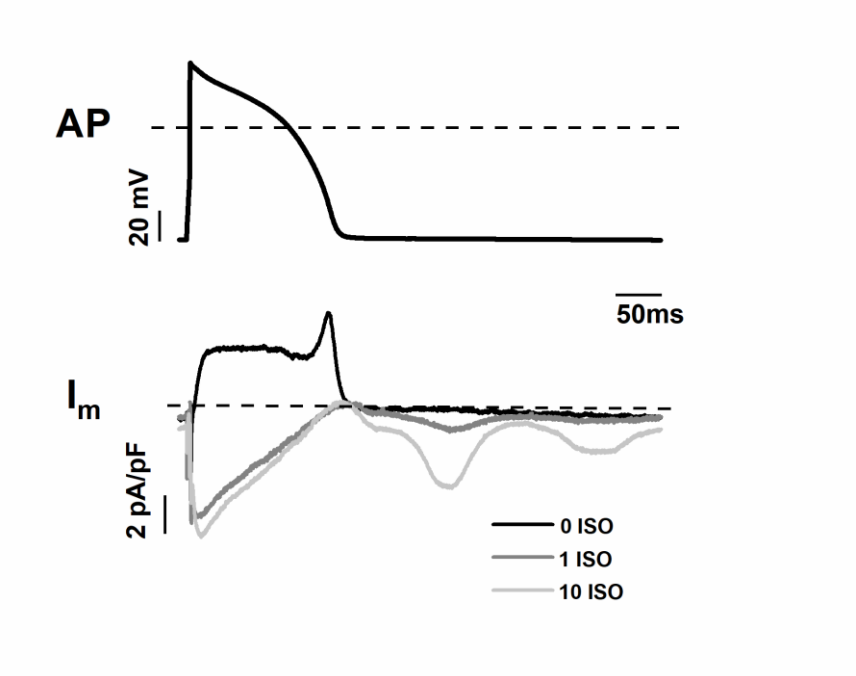


**Figure S1. [ISO]-dependency effect on $I_{TI}$ occurrence.** Examples of Normal AP waveform used as a command in AP clamp (top) and the corresponding $I_m$ (bottom) in basal condition and under ISO exposure.

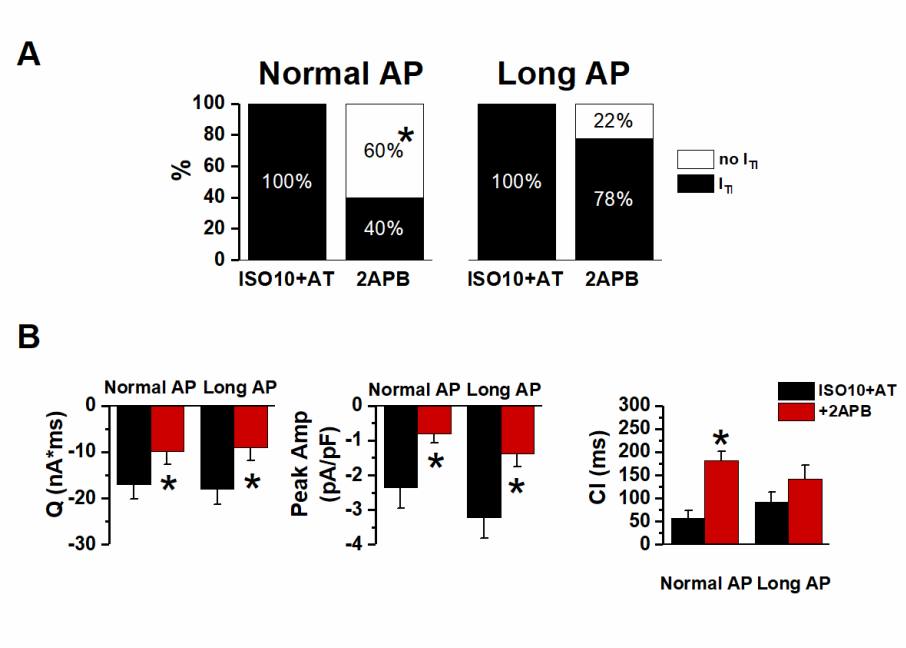


**Figure S2. 2APB effect on $I_{TI}$ evocated by ISO10+AT within same CMs. (A)** $I_{TI}$ incidence in ISO10+AT alone and with 2APB. **(B)** statistic (mean ± S.E.) of $I_{TI}$ charge (Q); peak ITI amplitude (Peak Amp) and coupling interval (CI). Normal AP N=10, Long AP N=9. * $p > 0.05$ vs ISO10+AT.

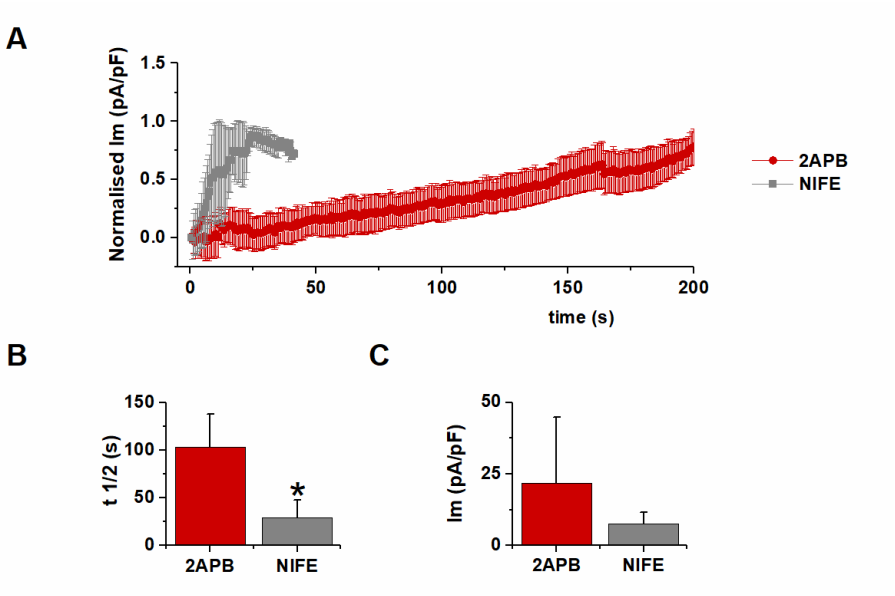


**Figure S3. 2APB and NIFE effect on $I_m$ during AP plateu phase under 10nM ISO exposure.** **(A)** Time course of means ± S.E. of normalized $I_m$ values during AP plateau phase in the presence of 2APB (red) or NIFE (grey). **(B)** Time for half-maximal effect of 2APB and NIFE. (C) Maximal effect of 2APB and NIFE on Im. 2APB N=6, NIFE N=5. * $p > 0.05$ vs 2APB.

| | Long AP | Normal AP | Short AP |
|---|---|---|---|
| $E_{diast}$ (mV) | -80.1103 | -80.354 | -80.5857 |
| PA (mV) | 47.8344 | 46.83809 | 53.33333 |
| $APD_{20}$ (ms) | 72.6823 | 61.297 | 37.41788 |
| $APD_{50}$ (ms) | 151.467 | 119.801 | 83.5066 |
| $APD_{90}$ (ms) | 185.34 | 148.88 | 97.8698 |
| $APD_{99}$ (ms) | 212.22 | 174.183 | 105.082 |

**Table S1.** Main parameters of AP waveforms. Diastolic potential ($E_{diast}$); peak amplitude of AP (PA) and action potential duration (APD) at different % of repolarization.

# Chapter 3

## *NOS1AP polymorphisms reduce NOS1 activity and interact with prolonged repolarization in arrhythmogenesis*

Carlotta Ronchi, PhD*[1]; Joyce Bernardi, PhD*[1]; Manuela Mura PhD*[2], Manuela Stefanello PhD[2], Beatrice Badone, MS[1]; Marcella Rocchetti PhD[1]; Lia Crotti, MD, PhD[3,4,5]; Paul Brink, MD[6], Peter J Schwartz, MD[3], Massimiliano Gnecchi[2,7,8#], MD, PhD, Antonio Zaza, MD[1,9#].

*These authors equally contributed to this work
[#] These senior authors equally contributed to this work

*Affiliations:*

1) *Department of Biotechnology and Bioscience, University of Milano-Bicocca, Milano (IT);*
2) *Coronary Care Unit and Laboratory of Experimental Cardiology for Cell and Molecular Therapy, Fondazione IRCCS Policlinico San Matteo, Pavia, (IT);*
3) Istituto Auxologico Italiano, IRCCS, Center for Cardiac Arrhythmias of Genetic Origin, Via Pier Lombardo 22, 20135, Milan, Italy;
4) *Department of Medicine and Surgery, University of Milano-Bicocca, Milano, (IT);*
5) *Department of Cardiovascular, Neural and Metabolic Sciences, San Luca Hospital, IRCCS Istituto Auxologico Italiano, Milan, (IT);*
6) *Department of Medicine, University of Stellenbosch, Tygerberg (SA);*
7) *Department of Molecular Medicine, Unit of Cardiology, University of Pavia, Pavia, (IT);*
8) *Department of Medicine, University of Cape Town, South Africa;*
9) *Cardiovascular Research Institute (CARIM), Maastricht University (NL).*

*Corresponding authors:*

Prof. Antonio Zaza, MD
Department of Biotechnologies and Biosciences, University Milano-Biococca
P.za della Scienza 2 20126, Milano Italy
E-mail. antonio.zaza@unimib.it
Phone: +39 02 64483307
Prof. Massimiliano Gnecchi, MD, PhD
University of Pavia and Fondazione IRCCS Policlinico San Matteo, Pavia, Italy
Viale Golgi 19, 27100, Pavia, Italy
Email: m.gnecchi@unipv.it
Phone: +39 0382-982107; Fax: +39 0382-502481

**[accepted]**

### *3.1 Acronyms*

| | |
|---|---|
| **4-AP** | 4-aminopyridine |
| **AP** | action potential |
| **APD** | action potential duration |
| **$APD_X$** | action potential duration at X% of repolarization |
| **AS** | asymptomatic |
| **$Ca_D$** | diastolic $Ca^{2+}$ |
| **$Ca_T$** | $Ca^{2+}$-transient amplitude |
| **$C_m$** | membrane capacitance |
| **cTT** | sarcomeric protein troponin T |
| **DADs** | delayed afterdepolarizations |
| **DC** | dynamic-clamp |
| **$E_{diast}$** | diastolic potential |
| **$g_{max}$** | maximal conductance of $I_{CaL}$ |
| **GP** | guinea-pig |
| **hiPSC** | human induced pluripotent stem cells |
| **hiPSC-CMs** | hiPSC derived cardiomyocytes |
| **$I_{CaL}$** | L-type $Ca^{2+}$ current |
| **$I_{NaL}$** | late $Na^+$ current |
| **$I_{Kr}$** | rapid delayed rectifier $K^+$ current |
| **$I_{Ks}$** | slow delayed rectifier $K^+$ current |
| **ISO** | isoprotenerol |

| | |
|---|---|
| **$I_{TI}$** | inward current transient |
| **Li-COR** | odyssey blocking buffer |
| **LQT1** | long-QT syndrome type 1 |
| **LQTS** | long-QT syndrome |
| **nNOS** | neuronal nitric oxide synthase |
| **NOS** | nitric oxide synthase |
| **PLA** | proximity ligation assay |
| **RyR2** | ryanodine receptor type 2 |
| **S** | symptomatic |
| **SA** | south africa |
| **SCR** | spontaneous $Ca^{2+}$ release events |
| **SDS-PAGE** | sodium dodecyl sulphate polyacrylamide gel electrophoresis |
| **SERCA** | sarco/endoplasmic reticulum $Ca^{2+}$ ATP-ase |
| **SR** | sarcoplasmic reticulum |
| **$t_{1/2}$** | time for half-maximal $I_{Ks}$ activation |
| **TEACl** | tetraethylammonium chloride |
| **TTX** | tetrodoxin |
| **T** | time constant of $I_{Ks}$ deactivation |

### *3.2 Abstract*

**Rationale:** NOS1AP SNPs correlate with QT prolongation and cardiac sudden death in patients affected by long QT syndrome type 1 (LQT1). NOS1AP targets NOS1 to intracellular effectors. We hypothesize that NOS1AP SNPs cause NOS1 dysfunction and this may converge with prolonged action potential duration (APD) to facilitate arrhythmias. **Objective:** To test 1) the effects of NOS1 inhibition and their interaction with prolonged APD in a guinea pig (GP) myocyte LQT1 model; 2) whether pluripotent stem cells-derived cardiomyocytes (hiPSC-CMs) from LQT1 patients differing for NOS1AP variants and mutation penetrance display a phenotype compatible with NOS1 deficiency. **Methods and Results:** In GP ventricular myocytes NOS1 was inhibited by SMTC (or L-VNIO); LQT1 was mimicked by $I_{Ks}$ blockade (JNJ203) and β-adrenergic stimulation (isoproterenol). HiPSC-CMs were obtained from symptomatic (S) and asymptomatic (AS) KCNQ1-A341V carriers, harboring the minor and major alleles of NOS1AP SNPs (rs16847548 and rs4657139) respectively. In GP cardiomyocytes: NOS1 inhibition prolonged APD, enhanced $I_{CaL}$ and $I_{NaL}$, slowed $Ca^{2+}$ decay and induced delayed afterdepolarizations. Under action-potential clamp, switching to shorter APD suppressed "transient inward current" events induced by NOS1 inhibition and reduced cytosolic $Ca^{2+}$. In S (vs AS) hiPSC-CMs: APD was longer and $I_{CaL}$ larger; NOS1AP and NOS1 expression and colocalization were decreased. **Conclusions:** the minor NOS1AP allele is associated with NOS1 loss of function. The latter may contribute to APD prolongation in LQT1, converge with it to perturb $Ca^{2+}$ handling and prevent catecholamine-induced APD shortening. This establishes a mechanistic link between NOS1AP SNPs and aggravation of the arrhythmia phenotype in prolonged repolarization syndromes.

**KEYWORDS**: LQT1, NOS1AP polymorphism, NOS1 deficiency, hiPSC-derived cardiomyocytes, arrhythmias.

### *3.3 Introduction*

The "neuronal" isoform of NO-synthase (NOS1 or nNOS) is abundantly expressed in cardiac myocytes and localized to a subcellular compartment highly relevant to $Ca^{2+}$ handling by an "anchoring protein" named NOS1AP (or CAPON) [1]. NOS1 activity is indeed crucial for modulation of L-type $Ca^{2+}$ current (ICaL) [2, 3], ryanodine receptor 2 (RyR2) [4] and SERCA2a [5, 6], thus contributing to sarcoplasmic reticulum (SR) stability.

Single nucleotide polymorphisms (SNPs) of the NOS1AP gene are associated with QT prolongation in the general population [7] and to increased incidence of sudden death in patients affected by type 1 long QT syndrome (LQT1) [8, 9]. Thus, even if the effect of NOS1AP SNPs on NOS1-mediated signaling still needs to be fully clarified, the existing evidence leads to hypothesize that a loss in NOS1 function/localization may act as a co-factor, facilitating the induction of arrhythmias in the setting of APD prolongation. If so, variability of NOS1 function might contribute to the markedly variable penetrance in genetic LQTS and of the inadequacy of QT interval in predicting arrhythmic events in acquired LQTS [10].

We tested this hypothesis using two different cell models: 1) mature guinea-pig (GP) cardiomyocytes and 2) human induced pluripotent stem cells (hiPSC)-derived cardiomyocytes (hiPSC-CMs) obtained from two carriers of the malignant KCNQ1-A341V LQT1 mutation [11, 12]. In the two carriers, respectively asymptomatic (AS) and symptomatic (S) for life-threatening arrhythmias, the LQT1 mutation was associated with either the major (in AS) or the minor (in S) NOS1AP variants.

The specific aims of the present study were: 1) to evaluate the effects of concomitant NOS1 inhibition and APD prolongation on membrane current and SR stability in mature GP cardiomyocytes; 2) to compare phenotypic differences between AS (major NOS1AP SNP) and S (minor NOS1AP SNP) hiPSC-CMs to the effects exerted by NOS1 inhibition in GP cardiomyocytes; 3) to test whether

in hiPSC-CMs the S status was associated with molecular changes compatible with reduced NOS1 function.

## *3.4 Materials and methods*

A detailed description of material and methods is provided in the Supplement.

### *3.4.1 Patients*

Two carriers of the KCNQ1-A341V mutation, belonging to a South African (SA) founder population thoroughly characterized by our group [8], were enrolled in the study. The two patients were selected as representative cases of asymptomatic (AS) and highly symptomatic (S) LQT1 phenotypes and because carriers of different NOS1AP SNPs. The study was approved by the the Health Research Ethics Committee of University of Stellenbosch (nr. N13/01/002) and Fondazione IRCCS Policlinico San Matteo, Pavia. Approved consent forms were provided in English or Afrikaans as appropriate. Clinical characteristics of S and AS carriers are summarized in the Supplement (Table S1).

### *3.4.2 Experimental models*

The experiments were carried out on isolated GP ventricular myocytes and hiPSC-CMs. All experiments involving animals (methods detailed in the Supplement) conformed to the guidelines for Animal Care endorsed by the University of Milano-Bicocca.

HiPSC-CMs were obtained from the S and the AS KCNQ1-A341V heterozygous mutation carriers (see “Patients”) and genotyped for the mutation and NOS1AP gene SNP variants:

- S hiPSC-CMs carried the minor variants rs16847548 and rs4657139 in homozygosis;
- AS hiPSC-CMs carried the major alleles of the respective positions.

HiPSC-CMs were also obtained from two healthy donors (i.e. wild-type for the KvLQT1 gene): one heterozygous for the minor NOS1AP rs16847548 SNP (patient belonging to the SA population; wt SA), the other carrying the major variants of all alleles (not belonging to the SA population; wt nonSA). Results concerning the healthy donors are presented in the Supplement only.

The generation and molecular characterization of hiPSC-CMs were carried out using a protocol previously published [13] and described in the Supplement.

### *3.4.3 Electrophysiology*

Electrophysiological measurements, performed GP and hiPSC-CMs, included I-clamp recordings, aimed at testing the phenotype and the effect of interventions on the electrical activity, and V-clamp recordings. Standard V-clamp protocols were used for evaluating ICaL, IKs and IKr; INaL was measured as the TTX-sensitive current during the AP plateau phase in action-potential clamp (AP-clamp) experiments. AP-clamp was also used to test the role of APD prolongation in facilitating “transient inward current” (ITI) events, reflective of SR instability.

All measurements were performed in the whole-cell configuration on freshly isolated GP ventricular myocytes at physiological temperature (36°C). Details on the recording solutions and signal acquisition for all protocols are provided in the Supplement.

### *3.4.4 Intracellular $Ca^{2+}$ recordings*

Cytosolic $Ca^{2+}$ was optically measured in cardiomyocytes loaded with 10 µM Fluo4-AM. $Ca^{2+}$ signals (expressed in normalized units F/F0) was evaluated as the amplitude of V-induced $Ca^{2+}$ transient (CaT), diastolic $Ca^{2+}$ (CaD), caffeine-induced $Ca^{2+}$ release (to measure SR $Ca^{2+}$ content, CaSR). The recordings were performed under control and NOS1 inhibition (by SMTC) in GP myocytes and AS hiPSC-CMs. Details on intracellular $Ca^{2+}$ measurements are provided in the Supplement.

### *3.4.5 Molecular studies*

Transcript and protein expression was measured by RT-PCR Western blot respectively. Protein expression and localization was detected by immunofluorescence; colocalization was assessed with the Duolink Proximity Ligation Assay (PLA).

### *3.4.6 Chemicals*

NOS1 was inhibited by SMTC (3µM, Caymal Chemical) [14] or by L-VNIO (Caymal Chemical, data in the Supplement) [5]. IKs, IKr and ICaL were blocked by JNJ303 (2 µM, Tocris Bioscience), E-4031 (5 µM, Alomone Labs) and nifedipine (5 µM, Sigma) respectively. INaL was blocked by TTX (1 µM, Tocris Bioscience). DMSO, ethanol, were used as solvents; their final concentration did not exceed 0.1%. All other chemicals were purchased from Sigma.

### *3.4.7 Statistical analysis*

Student's paired or unpaired t-test was applied as appropriate to test for significance between means. Difference between percentages was tested by chi-square analysis applied to raw numbers. Average data are expressed and plotted as mean ± standard error of the mean. Statistical significance was defined as $P<0.05$

(NS, not significant). Sample size (n/N, number of cells/ number of animals or differentiations) is specified for each experimental condition in the respective figure legend.

## *3.5 Results*

### *3.5.1 Studies in guinea pig cardiomyocytes*

#### *3.5.1.1 Effect of NOS1 inhibition on repolarization and occurrence of arrhythmogenic events*

This set of experiments aimed at testing the effect of NOS1 inhibition on repolarization ($APD_{90}$) and afterdepolarizations in basal conditions and when simulating the arrhythmogenic setting of LQT1 (β-adrenergic stimulation by ISO plus $I_{Ks}$ blockade by JNJ) [15, 16]. To this end, the effect of SMTC was tested before (basal) and during ISO+JNJ (LQT1 setting).

Under basal conditions, NOS1 inhibition markedly prolonged $APD_{90}$ (**Figure 1A-B**). $I_{Ks}$ blockade (JNJ) prolonged $APD_{90}$ only slightly and by a similar percent in CTRL and when NOS1 was inhibited (**Figure 1C**), thus suggesting that NOS1 inhibition did not interfere with $I_{Ks}$ channel activity. β-adrenergic stimulation was then superimposed on $I_{Ks}$ blockade: ISO further prolonged $APD_{90}$ and this prolongation was significantly larger when NOS1 was inhibited (39.7 ± 5.1 % vs 24.2 ± 4.0 %, $P<0.05$. **Figure 1D**).

Under basal conditions, delayed afterdepolarizations (DADs) occurred neither in CTRL, nor during NOS1 inhibition. In the presence of $I_{Ks}$ blockade, ISO 1 nM induced DADs, in 22% of cardiomyocytes; ISO effect was enhanced by NOS1 inhibition (DADs in 93% vs 22%; $P<0.01$) (**Figure 1E**). Moreover, the time at which DADs arose after the beginning of ISO perfusion was significantly shortened by NOS1 inhibition (**Figure 1F**). Triggered activity could be induced

during NOS1 inhibition by 10 nM ISO (**Figure 1G**). Possibly due to the relatively high pacing rate, EADs were never observed in GP myocytes.

To rule out that these observations resulted from SMTC effect other than NOS1 inhibition (ancillary effects), experiments were repeated using a different NOS1 inhibitor, L-VNIO. The results obtained with L-VNIO, detailed in the Supplement (**Figure S1**), were comparable to those described here for SMTC, thus indicating that the effect of these agents truly reflects NOS1 inhibition.

To summarize, NOS1 inhibition significantly prolonged $APD_{90}$ under basal condition, it did not change the effect of $I_{Ks}$ blockade, but it almost doubled the prolonging effect of superimposed ISO. NOS1 inhibition also facilitated induction of afterdepolarizations by ISO.

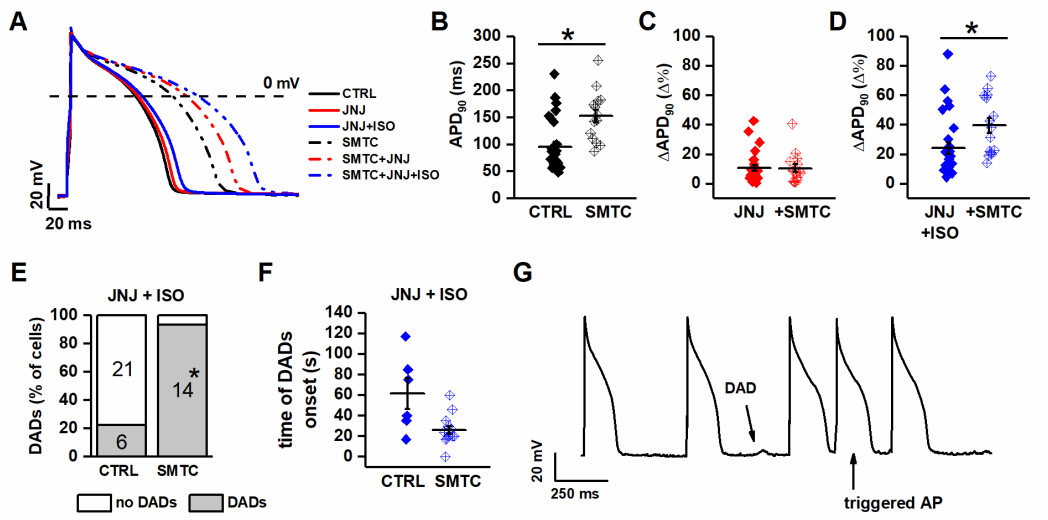


**Figure 1. Effect of NOS1 inhibition on APD and DADs in GP cardiomyocytes.** A) representative APs from control (CTRL, solid lines) and NOS1 inhibition (SMTC; dotted lines); color code: black = basal, red = $I_{Ks}$ blockade alone, blue = plus 1 nM ISO. B) Effect of NOS1 inhibition on $APD_{90}$ in basal condition. C) % change (Δ%) in $APD_{90}$ resulting from $I_{Ks}$ blockade in CTRL and during NOS1 inhibition; D) same as in C after

adding ISO. E) effect of NOS1 inhibition on DADs incidence (at 1 nM ISO); F) effect of NOS1 inhibition on the time of DADs onset after the beginning of ISO challenge; G) example of triggered activity observed during strong β-adrenergic stimulation in the presence of NOS1 inhibition (LVNIO+10 nM ISO). Sample sizes: CTRL n=27/12, SMTC n=15/4 for B, C, D and E; CTRL n=6/5, SMTC n=14/4 for F. *=*P*<0.05 vs control. Unpaired Student's and chi-squared tests.

#### *3.5.1.2 Effect of NOS1 inhibition on currents contributing to repolarization*

The aim of these experiments was to test the effect of NOS1 inhibition on the membrane currents more likely to account for its effect on repolarization (above). These include the inward components $I_{CaL}$ and $I_{NaL}$ and the outward ones $I_{Kr}$ and $I_{Ks}$.

Peak $I_{CaL}$ density was enhanced by NOS1 inhibition (**Figure 2A-B**) due to a 20.7 ± 0.4% increase in maximal conductance ($g_{max}$) (**Table S2**). $I_{CaL}$ steady-state activation and inactivation parameters, "window" current amplitude and inactivation rate were unaffected (**Figure 2C and Table S2**). SMTC markedly enhanced TTX-sensitive current during the AP plateau phase (**Figure 2D-F**); $I_{TTX}$ increment was maximal around +20 mV (**Figure 2E**), a potential compatible with an increment of $I_{NaL}$ as opposed to "window $I_{Na}$".

The outward components of repolarizing current ($I_{Kr}$ and $I_{Ks}$) were marginally affected by NOS1 inhibition, a slight slowing of $I_{Ks}$ activation being the only significant effect. Detail on $I_{Kr}$ and $I_{Ks}$ modulation are provided in the Supplement (**Figure S2 and S3**).

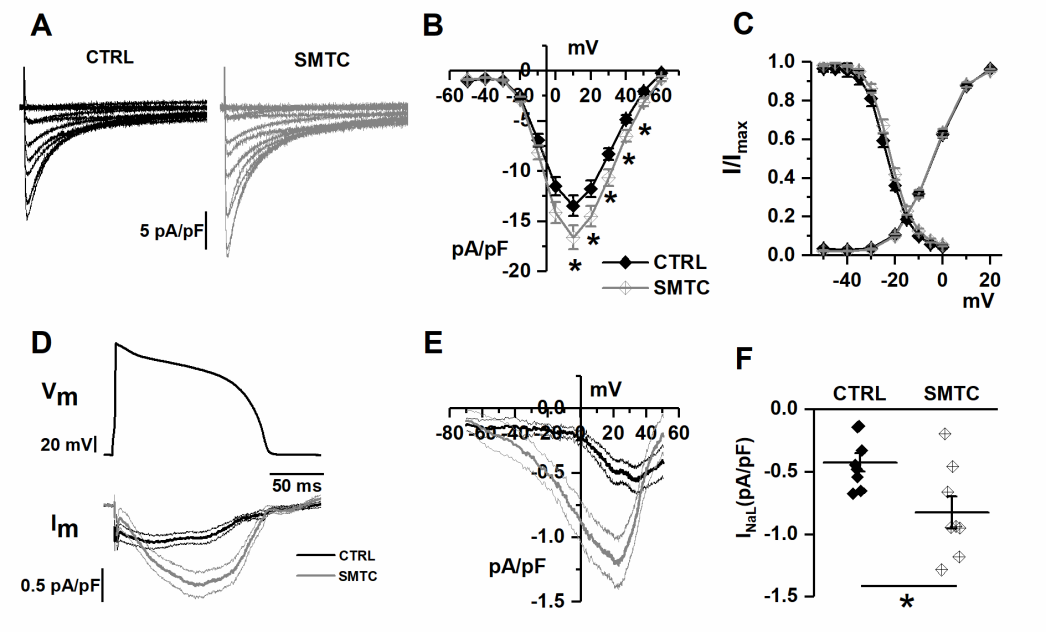


**Figure 2. Effect of NOS1 inhibition on $I_{CaL}$ and $I_{NaL}$ in GP cardiomyocytes.** A) representative $I_{CaL}$ recordings at different voltages in control (CTRL) and during NOS1 inhibition (SMTC); B) average (±SE) I/V relationships of peak $I_{CaL}$ density in CTRL and during NOS1 inhibition; C) average steady-state activation and inactivation curves in CTRL and NOS1 inhibition. D) Long AP waveform (top) and average traces of $I_{NaL}$ (bottom). E) Dynamic IV relationship of traces figured in D. F) TTX-sensitive current ($I_{NaL}$) in control and under NOS1 inhibition. Sample size CTRL n=25/4, SMTC n=20/3 for A-C panels. CTRL n=8/2 and SMTC n=8/2 for D-F panels. *=$P$<0.05 vs CTRL from two-way ANOVA for repeated measurements.

### *3.5.1.3 Effect of NOS1 inhibition on in intracellular $Ca^{2+}$ dynamics*

The above observations indicate that NOS1 inhibition *per se* results in SR instability (increased DADs incidence), likely contributed by intracellular $Ca^{2+}$ overload. We then investigated the effect of NOS1 inhibition (by SMTC) in the presence of ISO (1 nM) on intracellular $Ca^{2+}$ dynamics. Altogether, the results obtained are consistent with $I_{CaL}$ enhancement, increase $Ca^{2+}$ leak from the SR and

facilitation of spontaneous $Ca^{2+}$ release (SCR) (see Supplement, **Figure S4**). However, the magnitude of SMTC-induced changes, albeit statistically significant for some of the parameters, was smaller than expected. Moreover, in contrast to their electrical counterpart (DADs or $I_{TI}$), SCR events were observed with a surprisingly low frequency and in un-patched cells only (**Figure S4G**). This is likely to represent an artifact, originated from the experimental conditions required for $Ca^{2+}$ recordings (see Discussion). Accordingly, the results concerning the effect of NOS1 inhibition on intracellular $Ca^{2+}$ should be regarded as "quantitatively inaccurate" (underestimation) and are reported in detail in the Supplement only.

#### *3.5.1.4 Convergence of reduced NOS1 activity and slow repolarization in affecting ITI occurrence and $Ca^{2+}$ loading*

According to the working hypothesis, APD prolongation may amplify the effect of NOS1 inhibition on SR instability from an asymptomatic condition into an arrhythmogenic one. We tested this hypothesis evaluating the effect of changing APD (under AP-clamp conditions with 1 nM ISO) on membrane current events indicative of SR instability (**Figure 3A**).

In CTRL, $I_{TI}$ occurred in 68.7% of cardiomyocytes during the long AP; this incidence was not significantly affected by NOS1 inhibition (**Figure 3B**). The charge flowing during individual $I_{TI}$ events, reflecting the magnitude of spontaneous $Ca^{2+}$ release, was also not affected by NOS1 inhibition (31.4 ± 4.9 vs 37.91 ± 10.6 nC/pF, NS); nevertheless, whereas all CTRL cardiomyocytes displayed only single $I_{TI}$ events, up to 2 sequential $I_{TI}$ events were detected in 30% of cardiomyocytes during NOS1 inhibition ($P<0.05$ vs CTRL; **Figure 3C**). Switching to the shorter APD suppressed $I_{TI}$ in 81.8% and 100% of cardiomyocytes in CTRL and NOS1 inhibition respectively (**Figure 3D**); likely because the suppression rate observed in control conditions was already close to 100%, the effect of NOS1 inhibition only approached significance (P=0.06).

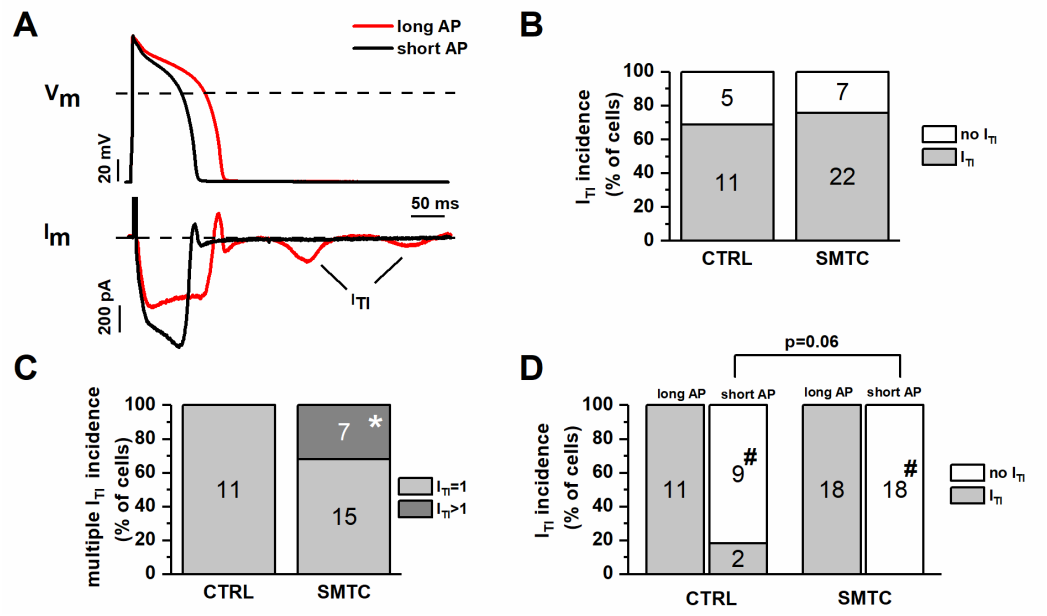


**Figure 3. Interaction between NOS1 inhibition and APD in inducing $I_{TI}$ events.** $I_{TI}$ events were induced by ISO 1 nM under AP-clamp. A) representative membrane current recordings during long ($APD_{90}$ = 140 ms, red) and short ($APD_{90}$=100 ms, black) AP waveforms in the same myocyte; $I_{TI}$ events are shown (arrows). B) percent of cells with no $I_{TI}$ (white) or at least 1 $I_{TI}$ (grey) event in CTRL and NOS1 inhibition; C) percent of cells with 1 $I_{TI}$ event (light grey) or >1 $I_{TI}$ events (dark grey) in CTRL and NOS1 inhibition; D) effect of APD shortening on $I_{TI}$ incidence in CTRL and NOS1 inhibition. (CTRL n=11/3, SMTC n=18/6) *=*P*<0.05 vs long AP. Chi squared test.

These results confirm that APD prolongation is a factor in the genesis of spontaneous $Ca^{2+}$ release events; we hypothesized that this is the consequence of changes in intracellular $Ca^{2+}$ loading. To test this hypothesis, we performed the same AP-clamp experiments described above (long to short AP in the presence of ISO 1 nM) while measuring diastolic $Ca^{2+}$ ($Ca_D$) and $Ca^{2+}$ transient amplitude ($Ca_T$) (**Figure 4A**). APD shortening reduced both $Ca_D$ and $Ca_T$; while the effect on $Ca_D$ was reversible, the one on $Ca_T$ was not (**Figure 4B**), possibly due to $I_{CaL}$ run-down during the long recording period.

NOS1 inhibition significantly prolonged the $t_{1/2}$ of $Ca^{2+}$ decay during the transient (**Figure 4C**), but affected neither $Ca_D$ nor $Ca_T$, nor their changes upon APD shortening (**Figure 4D**).

To rule out dependency of intracellular $Ca^{2+}$ parameters on the waveforms sequence, the latter was inverted in a subset of experiments. Irrespective of the waveform sequence, $Ca_D$ was consistently higher under the longer AP; as above, the response of $Ca_T$ was less consistent, in a way again compatible with $I_{CaL}$ run-down (**Figure S5**). In contrast to the high incidence of DADs and $I_{TI}$ events (in I-clamp and AP-clamp experiments respectively), diastolic $Ca^{2+}$ oscillations were never observed in Fluo4-AM loaded cardiomyocytes, possibly because of the buffering power of the dye.

Thus, facilitation of $I_{TI}$ occurrence by AP prolongation was associated with changes in $Ca^{2+}$ dynamics compatible with an increased intracellular $Ca^{2+}$ load. NOS1 inhibition increased the occurrence of multiple $I_{TI}$ events and slowed SR $Ca^{2+}$ reuptake. During NOS1 inhibition AP shortening suppressed $I_{TI}$ in all cardiomyocytes; under control conditions $I_{TI}$ suppression by AP shortening was less consistent but still frequent.

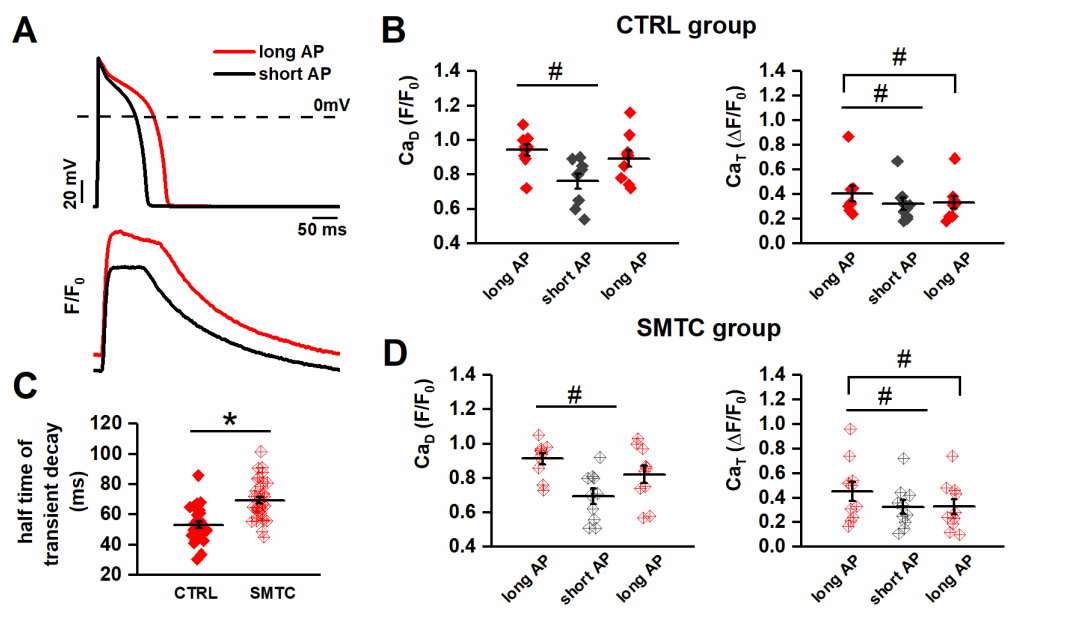


**Figure 4. Interaction between NOS1 inhibition and APD in affecting intracellular $Ca^{2+}$.** Cytosolic $Ca^{2+}$ was measured during ISO 1 nM under AP-clamp. A) AP waveforms (top) and the corresponding $Ca^{2+}$ transients (bottom) recorded in CTRL; B) effect of APD (long-short-long sequence within each myocyte) on diastolic $Ca^{2+}$ ($Ca_D$, left) and $Ca^{2+}$ transient amplitude ($Ca_T$, right) in CTRL; C) half-time of exponential $Ca^{2+}$ decay in CTRL and NOS1 inhibition; D) effect of APD (long-short-long sequence within each myocyte) on diastolic $Ca^{2+}$ ($Ca_D$) and $Ca^{2+}$ transient amplitude ($Ca_T$) under NOS1 inhibition (CTRL n=10/4, SMCT n=9/3; *=*P*<0.05 vs long AP, °=P<0.05 vs long AP). Paired Student's t-test and Two-way repeated measures ANOVA.

### *3.5.2 Studies in LQT1 hiPSC-CMs*

The aims of these experiments were: 1) to compare the functional phenotype of hiPSC-CMs derived from S and AS LQT1 patients and check, whether differences compatible with the effects of NOS1 inhibition in GP cardiomyocytes were detectable; 2) to test whether in hiPSC-CMs the S status (minor NOS1AP allele) was associated with molecular changes compatible with reduced NOS1 function. To assess the functional differences between S and AS hiPSC-CMs, we used the AP duration and $I_{CaL}$ density since these were the two parameters mostly affected by NOS1 inhibition in GP cardiomyocytes.

#### *3.5.2.1 S vs AS differences in electrical activity*

Membrane potential of hiPSC-CMs was recorded during pacing at 1 Hz in native and DC conditions (**Figure 5A**); AP parameters in the two conditions are summarized in **Table S3**. Membrane capacitance ($C_m$) was larger in S than in AS hiPSC-CMs (50.9 ± 4.8 pF vs 37.2 ± 4.2 pF, $P<0.05$). Diastolic membrane potential ($E_{diast}$) was around -40 mV in native conditions and approached -75 mV under DC; in both conditions, $E_{diast}$ was similar between S and AS hiPSC-CMs (**Table S3**). In both native and DC conditions, $APD_{90}$ was significantly longer (by 20.1% under DC) in S than in AS hiPSC-CMs (**Figure 5B**). Notably, albeit shortest in WT (with minor NOS1AP SNP) $APD_{90}$ was not significantly prolonged in AS (major NOS1AP SNP, KvLQT1 mutant) hiPS-CMs (Supplement and **Figure S6);** i.e. expression of the major NOS1AP allele partially countered the effect of KvLQT1 mutation on $APD_{90}$.

To verify whether such $APD_{90}$ differences could be ascribed to abnormality of NOS1AP-dependent signalling, we tested the effect of NOS1AP siRNA and NOS1 inhibition (by SMTC) in WT hiPS-CMs carrying the major NOS1AP SNP. Both the interventions prolonged $APD_{90}$ (**Figure S7**).

ISO effect was tested by internal comparison in a subset of KvLQT1-mutant hiPSC-CMs under DC. ISO 1nM failed to affect mean $APD_{90}$ significantly

in both S (ΔAPD: -2.7 ± 13.8 %, NS) and AS (ΔAPD: -4.2 ± 15 %, NS) hiPSC-CMs (**Figure 5C**), because of a high variability in the response. ISO 10 nM did not further modify $APD_{90}$ in either group (data not shown)**.**

EADs, DADs and triggered activity (**Figure 5D)** occurred (under DC conditions) in 46.15% (12/26) of S and in 18.2% (4/22) of AS hiPSC-CMs ($p<0.05$; **Figure 5E)**. Notably, both afterdepolarization types were often present within the same cell (e.g. rightmost panel in **Figure 5D).** APs containing EADs were not used for $APD_{90}$ measurement.

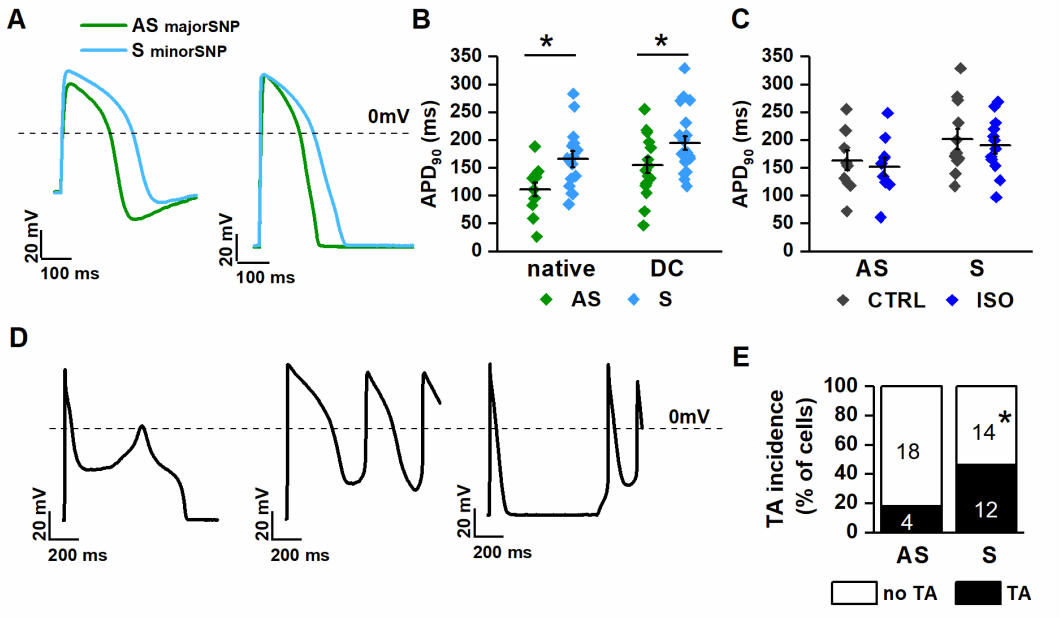


**Figure 5. Comparison of electrical activity between AS and S hiPSC-CMs.** A) representative AP tracings in native (left) and DC (right conditions); B) comparison of $APD_{90}$ between AS (green) and S (blue) hiPSC-CMs in native (left) and DC (right) conditions (AS nat n=12/6 S nat n=15/7, AS DC n=16/6, S DC n=21/7). C) ISO (1nM) effect on $APD_{90}$ in AS and S hiPSC-CMs in DC condition (AS n=12/6, S n=16/7). D) representative examples of afterpotentials and trigger activity (TA); E) incidence of TA in

AS and S hiPSC-CMs in DC condition (AS n=22/6; S n=26/7; *=*P*<0.05 vs AS). Unpaired Student's t-test and Chi squared test.

### *3.5.2.2 S vs AS differences in $I_{CaL}$*

Considering that the major effect of NOS1 inhibition in GP cardiomyocytes was $I_{CaL}$ enhancement, a comparison of this current between S and AS hiPSC-CMs was particularly interesting for the purpose of this study; $I_{CaL}$ parameters for the two experimental groups are reported in **Table S4**. Peak $I_{CaL}$ density was significantly larger in S than in AS hiPSC-CMs at all potentials (**Figure 6A-B**), reflecting an increase in maximal normalized conductance **Figure 6C**. Accordingly, no differences were observed in $I_{CaL}$ steady-state activation and inactivation curves (**Figure 6D and Table S4**).

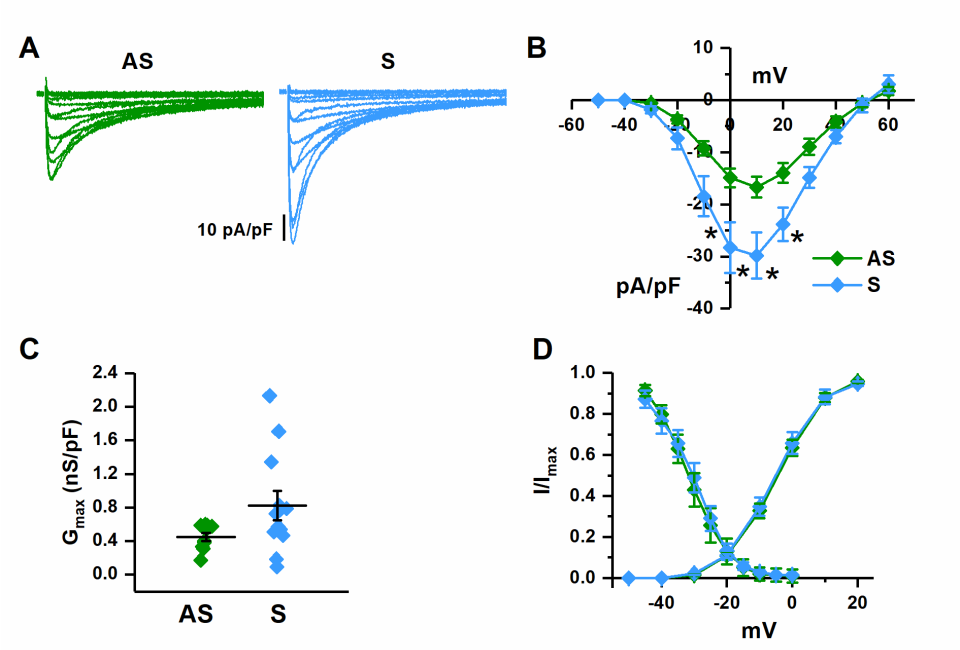


**Figure 6. $I_{CaL}$ properties in S vs AS hiPSC-CMs.** A) representative recordings of $I_{CaL}$ at different voltages in AS (green) and S (blue) hiPSC-CMs; B) comparison of I/V relationships of peak $I_{CaL}$ density; C) comparison of maximal $I_{CaL}$ conductance (normalized for membrane capacity); D) comparison of steady-state activation and

inactivation curves (AS n=10/3, S n=12/4 for all panels). *=$P<0.05$ vs AS from two-way ANOVA for repeated measurements.

### *3.5.2.3 Effect of NOS1 inhibition on in intracellular $Ca^{2+}$ dynamics in AS hiPSC-CMs*

To test whether modulation of intracellular $Ca^{2+}$ dynamics by endogenous NOS1 could be also observed in hiPSC-CMs, we applied SMTC to AS ones, i.e. those in which NOS1 signaling is expectedly intact (**Figure S8**). These experiments were performed under field-stimulation (un-patched cells) to avoid cytosol dialysis by the pipette solution. As for GP myocytes, SMTC effect on $Ca^{2+}$ parameters was unexpectedly small and dispersed, achieving statistical significance only for slowing of $Ca_T$ decay and increase in SR fractional $Ca^{2+}$ release, suggestive of RyRs facilitation. As mentioned in paragraph 3.1.3, the small magnitude of the changes is likely the consequence of a measurement artifact. The results are detailed in the Supplement.

### *3.5.2.4 Molecular characterization of hiPSC-CMs*

The presence of the KCNQ1-A341V heterozygous mutation was confirmed in S and AS hiPSC-CMs.

A first set of experiments aimed to test whether changes in NOS1AP and NOS1 expression and localization, compatible with loss of NOS1 function, could be detected in S hiPSC-CMs and, thus, ascribed to the minor variants of the NOS1AP SNPs.

NOS1AP signal was clearly detectable in hiPSC-CMs, in terms of transcript, protein levels (**Figure 7A**), and immunolocalization **(Figure 7B).** In AS hiPSC-CMs NOS1AP localization was cytosolic and roughly matched that of the sarcomeric protein cTnT **(Figure 7B)**; though, it should be noticed that variable orientation of myofibrils and lack of T-tubules periodicity make protein

colocalization with intracellular structures difficult in hiPSC-CMs. In S hiPSC-CMs NOS1AP transcript and protein levels were sharply reduced (**Figure 7A**); lower NOS1AP expression in S than in AS hiPSC-CMs was also visible at immunostaining as a weaker cytosolic signal (**Figure 7B**).

NOS1 signal was strong in the nucleus and diffuse in the cytosol, where it roughly overlapped with that of cTnT and RyR2 (**Figures 7C and S9).** NOS1 signal was lower, and its overlap with RyR2 weaker, in S than in AS hiPSC-CMs (**Figure S9**) Interaction between NOS1 and NOS1AP was investigated by the proximity ligation assay (PLA), in which interacting proteins appear as intracellular bright dots. The intensity and number of interaction dots were decreased in S hiPSC-CMs as compared to AS ones (**Figure 7D**). In the bottom panels of the figure, the interaction signal is overlapped with cTnT to show its relationship with cell structures.

A second set of experiments (reported in the Supplement) aimed to test whether the influence of NOS1AP SNP could be generalized to WT hiPSC-CMs. To this end, we compared two WT hiPSC-CMs samples (one from the SA population and the other from a different one), which differed for the NOS1AP SNP variant (only r16, in this case). The results of NOS1AP and NOS1 immunolabeling (**Figure S10 and S11**) match those obtained in LQT1 mutant cells, thus indicating that the effect of the r16 SNP variant on the expression and distribution of the two proteins is independent of the KvLQT1 genotype.

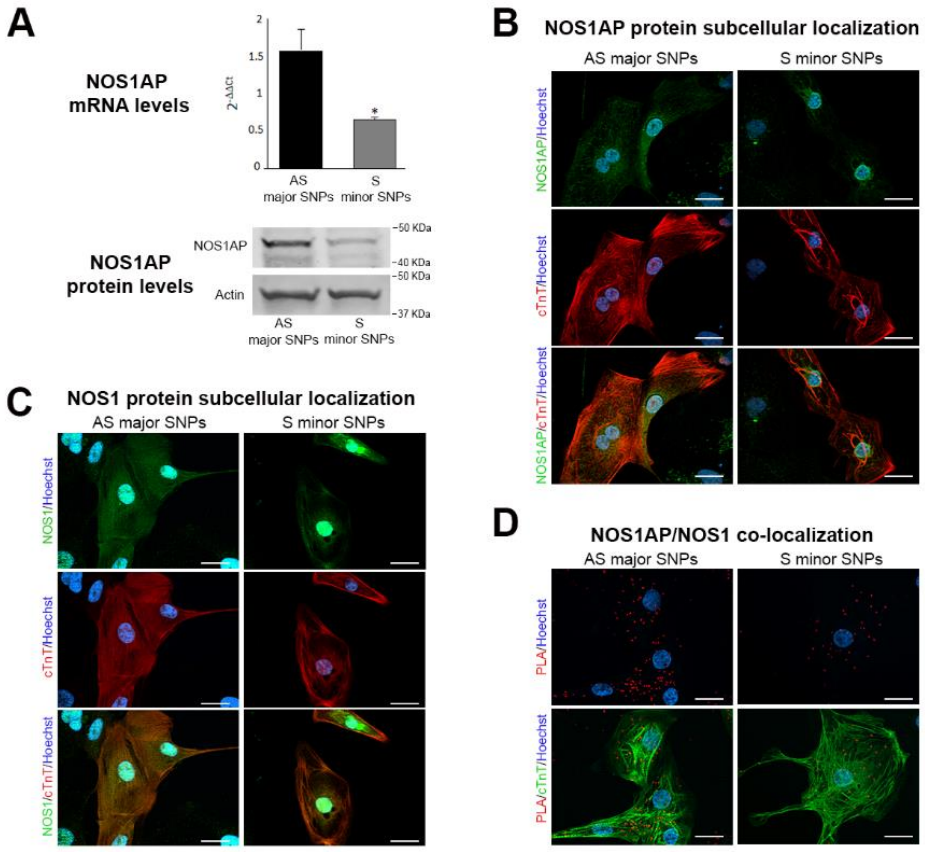


**Figure 7. NOS1AP and NOS1 expression and localization in S vs AS hiPSC-CMs**. A) comparison of NOS1AP transcript (top) and protein levels (bottom) between AS and S hiPSC-CMs (actin as loading control); B) immunostaining for NOS1AP protein (green) in AS and S hiPSC-CMs; C) immunostaining for NOS1 protein (green) in AS and S hiPSC-CMs. D) NOS1AP/NOS interaction evaluated by the proximity ligation assay (PLA), in AS and S hiPSC-CMs; interaction is revealed by bright red cytosolic dots. In B and C the lower panels show the same field stained for the cardiac sarcomeric protein troponin T (cTnT, red) alone (middle) and in overlap (bottom); in D PLA signals are overlapped with cTnT (bottom panel); nuclei in blue (Hoechst 33258). Scale bars = 20 µm. Sample size: AS n=6/3, S n=6/3 for A, *=$P$<0.01 vs AS from unpaired Student's t-test.

### *3.6 Discussion*

The main findings of this work can be summarized as follows. In a GP model of LQT1: 1) induction of marked SR instability by NOS1 inhibition induced enhancement of $I_{CaL}$ and $I_{NaL}$ and further prolonged APD; 2) SR instability induced by NOS1 inhibition did not ensue if APD was kept constant and, once present, was suppressed by shortening the APD (by AP-clamp). In hiPSC-CMs, larger $I_{CaL}$ ($I_{NaL}$ not tested), longer APD and more afterdepolarizations differentiated S cells (minor NOS1AP allele) from AS ones (major NOS1AP allele); furthermore, the expression and colocalization of NOS1AP and NOS1 proteins, were lower in S than in AS cells. The effects of NOS1 inhibition on intracellular $Ca^{2+}$ dynamics were consistent with those on electrophysiology, but of small magnitude; this was likely the consequence of $Ca^{2+}$ buffering by the $Ca^{2+}$-sensitive dye.

#### *3.6.1 Effect of NOS1 inhibition on APD and currents contributing to repolarization reserve*

In GP cardiomyocytes, NOS1 inhibition markedly increased APD; this effect was at least similar to that of $I_{Ks}$ blockade plus β-adrenergic stimulation and persisted when these factors were superimposed (**Figure 1**). Thus, defective NOS1 function may, by itself, delay repolarization, an effect adding to that of $I_{Ks}$ deficiency and β-adrenergic stimulation. Consistent with previous observations in $NOS1^{-/-}$ mice [2, 17], NOS1 inhibition increased $I_{CaL}$ density (**Figure 2**) an effect attributed to tonic, cGMP-mediated, $I_{CaL}$ inhibition by NO [18]. NOS1 inhibition also robustly enhanced $I_{NaL}$, an effect conceivably contributing to both APD prolongation and SR instability [19]. Previous work on $Na^+$ channel modulation by NO is controversial: both stimulation and inhibition are reported [20]. Notably the present findings are the only concerning NOS1 activity specifically and the "late" $I_{Na}$ component. The outward components of repolarization current ($I_{Kr}$ and $I_{Ks}$) were not affected by NOS1 inhibition in a functionally significant way (**Figures**

**S2 and S3**). In previous work, NOS1AP overexpression, leading to increased NOS1 activity, slightly increased $I_{Kr}$ [21]. Absence of $I_{Kr}$ modulation by NOS1 inhibition (present study) suggests that the results of overexpression studies may not mirror those of inhibition of endogenous activity. Lack of NOS1 effect on $I_{Ks}$ is consistent with the observation that $I_{Ks}$ upregulation is supported by NOS3 instead [22]; $I_{CaL}$ enhancement and APD prolongation would be expected to converge in causing EADs [23]; however, in GP myocytes, only DADs (also facilitated by $I_{NaL}$ enhancement) were observed. Although EADs have been previously reported in this species, they usually occur at very low pacing rates; faster rates (as the 2 Hz used here) are known to favor DADs instead. Both EADs and DADs occurred in hiPSC-CMs, often within the same cell; since spontaneous $Ca^{2+}$ release events can also underlie EADs [24], we speculate that, in the present setting, both types of afterpotentials may reflect SR instability.

### *3.6.2 Effect of NOS1 inhibition on SR stability*

Under conditions relevant to arrhythmogenesis in LQT1 ($I_{Ks}$ blockade and β-adrenergic stimulation), NOS1 inhibition (by two different agents) facilitated the occurrence of DADs, the arrhythmogenic epiphenomenon of spontaneous $Ca^{2+}$ release events (SCR). At least two mechanisms may contribute to SCR facilitation by NOS1 inhibition in the present setting: 1) NOS1 activity may be required to support RyR2 nitrosylation [4, 14], a redox modification contributing to stabilize the channel in its closed state [25]. Lack of this action in the presence of adrenergic modulation of other membrane effectors ($I_{CaL}$, SERCA2a etc.) may promote SCR during sympathetic activation; 2) NOS1 inhibition directly enhanced $I_{CaL}$ (**Figure 2**) and prolonged APD (**Figure 1**), thus conceivably changing the $Ca^{2+}$ influx/efflux balance [26]. The increment in intracellular $Ca^{2+}$, potentially resulting from such a change, is a well-known factor in facilitation of SCR [27]. Operation of this mechanism is also suggested by shortening of the coupling between DADs and the preceding V-induced $Ca^{2+}$ release (**Figure 1G**).

Intracellular $Ca^{2+}$ measurements were carried out to directly evaluate the effect of NOS1 inhibition on intracellular $Ca^{2+}$ handling. The low incidence of SCR events sharply contrasts with the high incidence of their electrical counterpart (DADs or $I_{TI}$), observed in experiments not requiring incubation with Fluo-4 AM. Partial $Ca^{2+}$ buffering by the dye may account for the above discrepancy, as well as for the smaller than expected SMTC effect on $Ca^{2+}$ handling (also NOS1 activation depends on cytosolic $Ca^{2+}$ levels [28]). Fluo-4 impact on $I_{TI}$ events, tested in preliminary experiments, support this view and suggests that $Ca^{2+}$ recordings may underestimate SMTC effects; nonetheless, they were assessed anyway, to pursue at least a qualitative match with the electrophysiological effects. Because SCR may deplete the SR, SMTC "primary" effects on $Ca^{2+}$ dynamics were assessed in their absence (GP experiments, **Figure S4B-C**). These effects, albeit small, are compatible with $I_{CaL}$ enhancement (increased release trigger and $Ca^{2+}$ influx) associated with a leakier SR. SMTC-induced increase in tetracaine-sensitive $Ca^{2+}$ leak (**Fig S4E**) and larger SR depletion caused by the leak period (**Fig S4F**) indeed suggest RyRs facilitation.

SMTC effect was even more elusive in AS hiPSC-CMs (**Figure S8**), but still compatible with RyRs facilitation (**Figure S8C and E**).

### *3.6.3 Interaction between NOS1 deficiency and APD prolongation in arrhythmogenesis and $Ca^{2+}$ dynamics*

The arrhythmogenic role acquired in LQT1 by otherwise inconsequential NOS1AP SNPs suggests that NOS1 deficiency and APD prolongation may converge to facilitate arrhythmogenic SCR. This hypothesis was addressed by imposing AP waveforms of different duration (AP-clamp), i.e. in the absence of potentially contaminating pharmacological interventions. This involved clamping membrane potential; therefore, $I_{TI}$ events were recorded, in lieu of DADs, to detect SCR. AP waveforms were selected to represent a 40% increase in APD starting from values normal for GP cardiomyocytes at 2 Hz; this change roughly

matches that induced by NOS1 inhibition (**Figure 1**). Consistent and reversible abrogation of $I_{TI}$ events by APD normalization (**Figure 3**) indicates that repolarization delay, such as that caused by KCNQ1 mutations, can indeed lead to SCR in the context of NOS1 deficiency. A plausible mechanism for such an effect is change in the balance between $Ca^{2+}$ influx (through $I_{CaL}$) and extrusion (by NCX) in each cyle, which may result in increased cell $Ca^{2+}$ content [26]. In support of this interpretation, diastolic $Ca^{2+}$ and $Ca^{2+}$ transient amplitude decreased upon APD shortening (**Figure 4**). Even if SR $Ca^{2+}$ accumulation may be limited by SCR events [29], the larger $Ca^{2+}$ transients amplitude suggests that APD changes did affect SR $Ca^{2+}$ content. Unfortunately, the latter could not be estimated, because incomplete reversal of caffeine effect makes measurements before and after APD change unreliable.

In murine cardiomyocytes under field stimulation, NOS1AP silencing [30] or NOS1 knockout [4] reduced $Ca^{2+}$ transient amplitude and increased SR $Ca^{2+}$ leak, an effect accounted for by reduced RyRs nitrosylation. In the present study, albeit increasing $I_{CaL}$, NOS1 inhibition failed to affect diastolic $Ca^{2+}$ or $Ca^{2+}$ transient amplitude appreciably when APD was kept constant (AP-clamp, **Figure 4B and D**) but increased them when APD was allowed to prolong (I-clamp, **Figure S4**). On the other hand, as previously described, SMTC facilitated RyRs opening (**Figures S4E-F**) and SCR induction (**Figures S4G**). Thus, in determining the overall effect of NOS1 deficit, increased $Ca^{2+}$ and $Na^{+}$ influx may be offset by destabilization of the $Ca^{2+}$ store. The findings also indicate that APD prolongation, also directly contributed by NOS1 dysfunction ($I_{NaL}$ and $I_{CaL}$ upregulation), may be crucial in unveiling $Ca^{2+}$ handling abnormality.

In conclusion, NOS1 deficiency may exaggerate APD prolongation caused by different mechanisms and act in concert with it to disrupt $Ca^{2+}$ handling and facilitate arrhythmogenic SCR events.

### *3.6.4 Differences between S and AS hiPSC-CMs obtained from KvLQT1 mutation carriers*

Others and we have shown that hiPSC-CMs recapitulate the typical features of LQTS associated with mutations of different proteins [31, 32]. HiPSC-CMs were obtained from a large and well characterized founder population; this provides a unique opportunity to study the effect of modifiers with the lowest possible degree of confounding factors [11]. Guided by the results obtained with NOS1 inhibition in GP cardiomyocytes, we chose to compare S and AS hiPSC-CMs for APD and $I_{CaL}$ properties. Both cell types carried the same mutation on KVLQT1 gene but differed for the expression of NOS1AP variants (minor allele in S and major in AS); therefore, the observed differences are likely to reflect changes in NOS1AP expression/function.

APD was longer and $I_{CaL}$ density was larger in S than in AS hiPSC-CMs (**Figures 5-6**), thus matching the effects of NOS1 inhibition in GP cardiomyocytes (**Figures 1-2**). The observation that NOS1AP SNPs may increase mortality even in users of dihydropyridine calcium channel blockers [33] might argue against a pathogenetic role of $I_{CaL}$ enhancement. However, it should be considered that, at therapeutic concentrations, dihydropyrydines mainly block vascular $I_{CaL}$, with the resulting vasodilation reflexly triggering sympathetic activation.

β-adrenergic stimulation failed to shorten APD in both S and AS hiPSC-CMs, (**Figure 6C**). Although $I_{Ks}$ was deficient (KvLQT1 mutation) in both groups, we still expected S hiPSC-CMs to respond differently because their $I_{CaL}$ was larger. To this concern, it should be stressed that ISO effect was quite heterogeneous among hiPSC-CMs, which might have obscured differences between samples of necessarily small size.

NOS1 function on specific targets may be reduced by changes in protein expression or subcellular localization. In agreement with functional experiments, NOS1AP and NOS1 expression and colocalization with sarcomeric and SR proteins was reduced in S hiPSC-CMs (**Figure 7**) Furthermore, the proximity

ligation assay (PLA) revealed reduced NOS1AP-NOS1 interaction in these cells (**Figure 7D**). This leads to the conclusion that the minor variant of NOS1AP gene may decrease NOS1AP expression, thus delocalizing NOS1 and reducing modulation of its compartment-specific targets.

The effect of NOS1AP variants associated with QT prolongation on NOS1AP expression is controversial. Our findings are consistent with the functional effect of NOS1AP or NOS1 overexpression in mammalian myocytes, the conditions mirroring what we observed in S hiPSC-CMs; indeed, in GP cardiomyocytes, these interventions decreased $I_{CaL}$ density and/or APD [3, 21, 34]. Nonetheless, an opposite relationship between QT prolonging NOS1AP SNPs and gene transcript (mRNA) was found by two studies in human myocardial samples [34, 35]. In these studies the association between the SNPs and QT prolongation was merely statistical and rather weak [34]; furthermore, one of them [34] reported that, in contrast to what expected from the findings in human samples, NOS1AP overexpression in mammalian myocytes shortened APD. Also, at variance with results in mammalian myocytes, NOS1AP knock-down caused APD shortening in zebra-fish [36], but this may simply reflect the large species difference.

Our observation that the effect of NOS1AP r16 SNP on proteins localization was also clearly detectable in WT hiPSC-CMs is consistent with the epidemiological notion that this gene variant is associated with longer repolarization and increased arrhythmia risk also in condtions other than LQT1 [7, 33].

### *3.7 Limitations*

A causative role of NOS1 dysfunction in $I_{CaL}$ enhancement, APD prolongation and SR instability of S hiPSC-CMs was inferred from the observation that the same effects were induced by NOS1 inhibition in GP myocytes. Correction of the NOS1AP gene variant, which would have lent further support to the conclusions, was not attempted because of limited availability of

patient-derived hiPSC-CMs with the desired features. Nonetheless, full reproducibility in S hiPSC-CMs of the rather complex pattern of changes resulting from NOS1 inhibition in GP myocytes is unlikely a matter of chance.

The interaction between NOS1 deficiency and APD has been evaluated in "acute" experiments. When repolarization is persistently prolonged, as in congenital LQTS, adaptive changes in the regulation of SR function may take place, thus potentially changing the relationship between the electrical cycle and intracellular $Ca^{2+}$ loading and/or the role of NOS1 signaling in SR stability.

Although NOS1 deficiency is more often reported to increase $I_{CaL}$ (and, therefore, APD) in isolated cardiomyocytes, the direction of NOS1 modulation of $I_{CaL}$ (and APD) might depend on the cell redox state, because of a change in the balance between channel S-nitrosylation and cGMP-regulated phosphorylation [17]. This suggests that redox state may be a further factor in the relationship between NOS1 function, prolonged repolarization and arrhythmias. The effect of NOS1 inhibition on intracellular $Ca^{2+}$ are likely underestimated because of $Ca^{2+}$ buffering by the dye; indeed, this may limit SCR occurrence and reduce the extent of NOS1 activity at baseline.

### *3.8 Conclusion and relevance*

The present findings in GP cardiomyocytes suggest that loss of NOS1 function and APD prolongation converge to generate conditions of SR instability; this is likely to contribute to arrhythmogenesis in both genetic and acquired LQTS. They also indicate that NOS1 deficiency can, on its own, be a cause of prolonged repolarization, or contribute to the imbalance between inward and outward currents when primary ion channel abnormalities coexist. The results obtained in hiPSC-CMs are compatible with loss of NOS1 localization and function in cells from the symptomatic patient, carrying the minor NOS1AP variant. With this, they support a cause-effect relationship between NOS1AP genotype, NOS1 function and proarrhythmia; this is of course a step beyond the

(merely correlative) demonstration of segregation of a genotype variant within a phenotype. The present results suggest that conditions leading to loss of NOS1 function (including, but not limited to NOS1AP SNPs) should be considered in the evaluation of the arrhythmogenic risk of prolonged repolarization syndromes in general. The results also point to $I_{CaL}$ and $I_{NaL}$ as potential therapeutic targets to minimize the aggravating role of the minor NOS1AP SNP under conditions of prolonged repolarization.

### *3.9 Sources of funding*

This work was funded by: Fondo Ricerca di Ateneo (FAR 2017 to A. Zaza) of Università Milano-Bicocca and Ricerca Corrente (RC to M. Gnecchi) of Fondazione IRCCS Policlinico San Matteo di Pavia.

J. Bernardi and B. Badone were supported by fellowships of the "DIMET" PhD program of Università Milano-Bicocca. C. Ronchi was supported by a Research Contract by the Department of Biotechnology and Bioscience of Università Milano-Bicocca.

### *3.10 Disclosures*

The Authors have no conflict of interest to disclose.

### *3.11 References*


1. Beigi, F., et al., Cardiac nitric oxide synthase-1 localization within the cardiomyocyte is accompanied by the adaptor protein, CAPON. Nitric Oxide, 2009. 21(3-4): p. 226-33.

2. Sears, C.E., et al., Cardiac neuronal nitric oxide synthase isoform regulates myocardial contraction and calcium handling. Circ Res, 2003. 92(5): p. e52-9.

3. Burkard, N., et al., Conditional neuronal nitric oxide synthase overexpression impairs myocardial contractility. Circ Res, 2007. 100(3): p. e32-44.

4. Gonzalez, D.R., et al., Deficient ryanodine receptor S-nitrosylation increases sarcoplasmic reticulum calcium leak and arrhythmogenesis in cardiomyocytes. Proc Natl Acad Sci U S A, 2007. 104(51): p. 20612-7.

5. Zhang, Y.H., et al., Reduced phospholamban phosphorylation is associated with impaired relaxation in left ventricular myocytes from neuronal NO synthase-deficient mice. Circ Res, 2008. 102(2): p. 242-9.

6. Bencsik, P., et al., Cardiac capsaicin-sensitive sensory nerves regulate myocardial relaxation via S-nitrosylation of SERCA: role of peroxynitrite. Br J Pharmacol, 2008. 153(3): p. 488-96.

7. Kao, W.H., et al., Genetic variations in nitric oxide synthase 1 adaptor protein are associated with sudden cardiac death in US white community-based populations. Circulation, 2009. 119(7): p. 940-51.

8. Crotti, L., et al., NOS1AP is a genetic modifier of the long-QT syndrome. Circulation, 2009. 120(17): p. 1657-63.

9. Tomas, M., et al., Polymorphisms in the NOS1AP gene modulate QT interval duration and risk of arrhythmias in the long QT syndrome. J Am Coll Cardiol, 2010. 55(24): p. 2745-52.

10. Schwartz, P.J. and R.L. Woosley, Predicting the Unpredictable: Drug-Induced QT Prolongation and Torsades de Pointes. J Am Coll Cardiol, 2016. 67(13): p. 1639-1650.

11. Brink, P.A., et al., Phenotypic variability and unusual clinical severity of congenital long-QT syndrome in a founder population. Circulation, 2005. 112(17): p. 2602-10.

12. Crotti, L., et al., The common long-QT syndrome mutation KCNQ1/A341V causes unusually severe clinical manifestations in patients with different ethnic backgrounds: toward a mutation-specific risk stratification. Circulation, 2007. 116(21): p. 2366-75.

13. Mura, M., et al., The KCNH2-IVS9-28A/G mutation causes aberrant isoform expression and hERG trafficking defect in cardiomyocytes derived from patients affected by Long QT Syndrome type 2. Int J Cardiol, 2017. 240: p. 367-371.

14. Cutler, M.J., et al., Aberrant S-nitrosylation mediates calcium-triggered ventricular arrhythmia in the intact heart. Proc Natl Acad Sci U S A, 2012. 109(44): p. 18186-91.

15. Wang, Q., et al., Positional cloning of a novel potassium channel gene: KVLQT1 mutations cause cardiac arrhythmias. Nat Genet, 1996. 12(1): p. 17-23.

16. Schwartz, P.J., et al., Genotype-phenotype correlation in the long-QT syndrome - Gene-specific triggers for life-threatening arrhythmias. Circulation, 2001. 103(1): p. 89-95.

17. Campbell, D.L., J.S. Stamler, and H.C. Strauss, Redox modulation of L-type calcium channels in ferret ventricular myocytes. Dual mechanism regulation by nitric oxide and S-nitrosothiols. J Gen Physiol, 1996. 108(4): p. 277-93.

18. Sumii, K. and N. Sperelakis, cGMP-dependent protein kinase regulation of the L-type Ca2+ current in rat ventricular myocytes. Circ Res, 1995. 77(4): p. 803-12.

19. Zaza, A. and M. Rocchetti, The late Na+ current--origin and pathophysiological relevance. Cardiovasc Drugs Ther, 2013. 27(1): p. 61-8.

20. Marionneau, C. and H. Abriel, Regulation of the cardiac Na+ channel NaV1.5 by post-translational modifications. J Mol Cell Cardiol, 2015. 82: p. 36-47.

21. Chang, K.C., et al., CAPON modulates cardiac repolarization via neuronal nitric oxide synthase signaling in the heart. Proc Natl Acad Sci U S A, 2008. 105(11): p. 4477-82.

22. Bai, C.X., et al., Role of nitric oxide in Ca2+ sensitivity of the slowly activating delayed rectifier K+ current in cardiac myocytes. Circ Res, 2005. 96(1): p. 64-72.

23. January, C.T. and J.M. Riddle, Early afterdepolarizations: mechanism of induction and block. A role for L-type Ca2+ current. Circ Res, 1989. 64(5): p. 977-90.

24. Zhao, Z., et al., Revisiting the ionic mechanisms of early afterdepolarizations in cardiomyocytes: predominant by Ca waves or Ca currents? Am. J. Physiol Heart Circ. Physiol, 2012. 302(8): p. H1636-H1644.

25. Vielma, A.Z., et al., Nitric Oxide Synthase 1 Modulates Basal and beta-Adrenergic-Stimulated Contractility by Rapid and Reversible Redox-Dependent S-Nitrosylation of the Heart. PLoS One, 2016. 11(8): p. e0160813.

26. Bers, D.M., Cardiac excitation-contraction coupling. Nature, 2002. 415(6868): p. 198-205.

27. Stevens, S.C., et al., Intra-sarcoplasmic reticulum Ca2+ oscillations are driven by dynamic regulation of ryanodine receptor function by luminal Ca2+ in cardiomyocytes. J Physiol, 2009. 587(Pt 20): p. 4863-72.

28. Weissman, B.A., et al., Activation and inactivation of neuronal nitric oxide synthase: characterization of Ca(2+)-dependent [125I]Calmodulin binding. Eur J Pharmacol, 2002. 435(1): p. 9-18.

29. Venetucci, L.A., A.W. Trafford, and D.A. Eisner, Increasing ryanodine receptor open probability alone does not produce arrhythmogenic calcium waves: threshold sarcoplasmic reticulum calcium content is required. Circ Res, 2007. 100(1): p. 105-11.

30. Treuer, A.V. and D.R. Gonzalez, NOS1AP modulates intracellular Ca(2+) in cardiac myocytes and is up-regulated in dystrophic cardiomyopathy. Int J Physiol Pathophysiol Pharmacol, 2014. 6(1): p. 37-46.

31. Kiviaho, A.L., et al., Distinct electrophysiological and mechanical beating phenotypes of long QT syndrome type 1-specific cardiomyocytes carrying different mutations. Int J Cardiol Heart Vasc, 2015. 8: p. 19-31.

32. Rocchetti, M., et al., Elucidating arrhythmogenic mechanisms of long-QT syndrome CALM1-F142L mutation in patient-specific induced pluripotent stem cell-derived cardiomyocytes. Cardiovasc Res, 2017. 113(5): p. 531-541.

33. Becker, M.L., et al., A common NOS1AP genetic polymorphism is associated with increased cardiovascular mortality in users of dihydropyridine calcium channel blockers. Br J Clin Pharmacol, 2009. 67(1): p. 61-7.

34. Kapoor, A., et al., An enhancer polymorphism at the cardiomyocyte intercalated disc protein NOS1AP locus is a major regulator of the QT interval. Am J Hum Genet, 2014. 94(6): p. 854-69.

35. Saba, S., et al., Cardiac levels of NOS1AP RNA from right ventricular tissue recovered during lead extraction. Heart Rhythm, 2012. 9(3): p. 399-404.

36. Milan, D.J., et al., Drug-sensitized zebrafish screen identifies multiple genes, including GINS3, as regulators of myocardial repolarization. Circulation, 2009. 120(7): p. 553-9.

### *3.12 Supplemental methods*

## Experimental Models

### *Guinea pig (GP) ventricular myocytes*

Dunkin-Hartley GP were euthanized by cervical dislocation under anesthesia with zolazepam + tiletamine (Telazol 100 mg/Kg i.p.). Ventricular cardiomyocytes were enzymatically dissociated by using a retrograde coronary perfusion method previously published 21, with minor modifications. Rod-shaped, $Ca^{2+}$ -tolerant cardiomyocytes were used within 12 hours from dissociation. All experiments conformed to the guidelines for Animal Care endorsed by the University of Milano-Bicocca. A total of 15 animals were used.
To reproduce the LQT1 phenotype we subjected GP ventricular cardiomyocytes to $I_{Ks}$ blockade (2µM JNJ303) and adrenergic stimulation (Isoproterenol, ISO 1 nM). In these cells we measured electrical activity, membrane currents and intracellular $Ca^{2+}$ dynamics, in basal condition (CTRL group) and under selective inhibition of NOS1 activity by incubation with 3µM S-methyl-L-thiocitrulline (SMTC) [1] for at least 30 minutes (SMTC group). As a confirmation, for some experiments we also used another NOS1 inhibitor, Vynil-L-NIO (L-VNIO) [2]. NOS1 inhibitors were added both in the perfusion solution and dialyzed into the cell through the patch pipette.

### *HiPSC-CMs preparation*

#### *Features of S and AS hiPSC-CMs donors*
The clinical features of the KCNQ1 mutation carriers from which hiPSC-CMs were obtained are reported in **Table S1**.

#### *Cell culture*
Human dermal fibroblasts (HDFs), mouse embryonic fibroblasts (MEFs), and 293T were cultured in HDF medium composed of Dulbecco Modified Eagle Medium (DMEM), 10% Fetal Bovine Serum (FBS), 2mM L-glutamine, 50 U/ml penicillin, 50 U/ml streptomycin, 1% Non Essential Amminoacid (NEAA). Human induced pluripotent stem cells (hiPSCs) were maintained on irradiated MEF in human embryonic stem cell (hESC) medium composed of DMEM-F12, 20% KnockOut serum replacement (KO-SR), 10 ng/ml basic fibroblast growth factor (bFGF), 1 mM-glutamine, 1% NEAA, 50 U/ml penicillin, 50 U/ml streptomycin, and 0.1 mM 2-mercaptoethanol.

#### *Retrovirus preparation*
293T packaging cells were co-transfected with each of the 4 retroviral vectors encoding for human OCT4, SOX2, KLF4 and cMYC (Addgene), and with the packaging vector pCL-Eco (Addgene), using the calcium/phosphate method. The

viral particles released in the medium were collected, filtered with 0.45 µm PVDF filters and immediately used to infect HDFs.

***Generation of hiPSCs***
HDFs were transduced with a mix of the 4 retroviruses in two consecutive rounds of infection, in the presence of 4 µg/ml polybrene (Sigma Aldrich). 6 days after transduction, HDFs were harvested and re-plated onto MEF feeders in hESC medium. 24 days after infection, the emerging hiPSC clones were mechanically isolated.

***Embryoid body formation and three germ layer differentiation in vitro***
HiPSCs were grown for 7 days in non-adherent conditions in a modified hESC medium deprived of bFGF, and containing 20% FBS in place of KO-SR. Forming embryoid bodies (EBs) were then transferred to gelatin-coated dishes to allow differentiation for other 7 days in adhesion. Three germ layer formation was assessed by immunocytochemistry.

***Genotyping***
Genomic DNA was extracted from hiPSCs using the QIAmp DNA Blood Mini kit (Qiagen) according to the manufacturer's instructions. The regions of interest on KCNQ1 and NOS1AP genes were amplified by PCR using specific primers, and then sequenced (Lightrun service - GATC Biotech AG-Germany; www.gatc-biotech.com/lightrun).

***Karyotyping***
HiPSCs were blocked at metaphase by exposure for 3 hours to 10 µg/ml demecolcine solution. Karyotype analysis was performed using G-banding chromosome analysis, according to standard procedures (International System for Human Cytogenetic Nomenclature 2013).

***Alkaline phosphatase colorimetric assay***
Alkaline phosphatase (AP) colorimetric assay was performed on hiPSCs seeded on feeders in 24-multiwells using the Alkaline Phosphatase Staining kit (Stemgent) and following manufacturer's instructions.

***Differentiation into cardiomyocytes (CMs)***
HiPSCs were differentiated into CMs with the PSC Cardiomyocyte Differentiation Kit (ThermoFisher). Contracting hiPSC-CMs appeared as early as 11 days after the initiation of the differentiation protocol. HiPSC-CMs were characterized by RT-PCR and immunofluorescence for cardiac-specific proteins at different time points.

***Dissociation of contracting EBs***
Spontaneously contracting EBs were micro-sectioned, dissociated with 1 mg/ml collagenase B at 37°C for 40 minutes, and adhered onto gelatin-coated dishes or glass slides.

**Electrophysiology**

The baseline solution for all patch-clamp recordings was standard Tyrode's solution containing (mM): 154 NaCl, 4 KCl, 2 $CaCl_2$, 1 $MgCl_2$, 5 HEPES-NaOH, 5.5 D-glucose, adjusted to pH 7.35 with NaOH. Membrane capacitance and series resistance were measured and automatically compensated in every cell. Signals were acquired with a MultiClamp 700B amplifier (Axon Instrument), connected to a Digidata 1440A (Molecular Devices) and filtered with an appropriate Bessel filter via pClamp 10 (Molecular Devices). All measurements were performed at 36.5°C.

***I-clamp and Dynamic Clamp recordings***
Membrane potential was recorded during steady-state pacing at a cycle length of 2 Hz for GP cardiomyocytes and 1 Hz for hiPSC-CMs.
Cells were patch-clamped with borosilicate glass pipettes containing (mM): $K^+$-aspartate 110, KCl 23, $MgCl_2$ 3, HEPES KOH 5, EGTA KOH 0.1, GTP $Na^+$-salt 0.4, ATP $Na^+$-salt 5, creatine phosphate $Na^+$-salt 5, $CaCl_2$ 0.04 (calculated free-$Ca^{2+}$ = $10^{-7}$ M), adjusted to pH 7.3. Series resistance was <5 MΩ and was compensated to 80% of its value.

In hiPSC-CMs, "synthetic" $I_{K1}$ was injected by the dynamic-clamp (DC) technique to correct for low endogenous $I_{K1}$ expression. $I_{K1}$ conductance required to achieve a diastolic potential (Ediast) around -80 mV was 1.9 nS/µF (kept constant in all cells); this abolished automatic activity and resulted in physiological AP contours (examples in manuscript **Figure 5**). HiPSC-CMs with ventricular-like APs were selected based on an APD90/APD50 ratio lower than 2 (under DC conditions), as previously reported [3, 4]. The following parameters were considered: AP duration at 90% repolarization (APD90, measured beat by beat by an automated routine); incidence and time of occurrence of afterdepolarizations (EADs and DADs), defined as transient membrane depolarizations > 0.5 mV occurring before and after AP repolarization respectively [5]. "Triggered activity", observed in hiPSC-CMs only, was defined as APs arising from afterdepolarizations; it was distinguished from "automaticity" because of the absence of a proper diastolic depolarization phase (**Figure S1**).

Only cells in which DC successfully polarized diastolic potential were used. Synthetic $I_{K1}$ was generated by a human numerical current model derived from Rudy-O'Hara one [6] and injected in the cell using the Real-Time eXperiment Interface (RTXI) as previously described [7]. $I_{K1}$ conductance was set to achieve a diastolic potential ($E_{diast}$) around -80 mV; the value of $I_{K1}$ conductance was the same in all cells.

***Standard V-clamp experiments***

$I_{CaL}$ was isolated by using a $Na^+$- and $K^+$-free extracellular solution, in which the two ions were replaced, containing (mM): 154 tetraethylammonium chloride (TEACl), 1 $MgCl_2$, 2 $CaCl_2$, 5 HEPES, 5.5 D-glucose, with pH adjusted to 7.4 with TEAOH. Intracellular solution contained (mM): 115 CsCl, 20 TEACl, 0.5 $MgCl_2$, 10 EGTA CsOH, 5 HEPES CsOH, 5 ATP $Mg^{2+}$-salt, 5 creatine phosphate Tris-salt, 0.4 GTP Tris-salt; at pH 7.2 with CsOH. For $I_{CaL}$ recordings in hiPSC-CMs, extracellular $CaCl_2$ and D-glucose were elevated to 5 mM and 10 mM respectively; 2 mM 4-aminopyridine (4-AP) and 10 μM tetrodotoxin (TTX) were added. To construct peak I/V relationships, $I_{CaL}$ was elicited by 300 ms steps (range -50 to +60 mV) from a holding potential of -40 mV. Activation and inactivation curves were obtained from peak current I/V relationship and fitted with Boltzmann functions to extract gating parameters. The latter included voltage of half-maximal activation/inactivation ($V_{0.5}$, mV), slope factor (k, mV), maximal conductance ($g_{max}$, nS). Series resistance was compensated up to 80% to minimize voltage error.

$I_{NaL}$ was measured under AP-clamp (see below) and dissected as the current sensitive to 1μM TTX. A representative AP, recorded under NOS1 inhibition (by SMTC), was used as the command signal. The measurement was performed during Tyrode's superfusion (see above), with pipette solution containing 0.1mM EGTA.

$I_{Ks}$ and $I_{Kr}$ were isolated by subtraction, as currents sensitive to their specific blockers JNJ303 (2 μM) and E-4031 (5 μM) respectively. Pipette solution contained (mM): 110 $K^+$-aspartate, 23 KCl, 3 $MgCl_2$, 2 $CaCl_2$, 5 HEPES-KOH, 5 EGTA-KOH, 5 ATP $Na^+$-salt, 5 creatine phosphate $Na^+$-salt, 0.4 GTP $Na^+$-salt, pH adjusted to 7.3 with KOH. 5 μM nifedipine was added to rule out interference by $I_{CaL}$. From a holding potential of -40 mV, depolarizing steps (range -50 to +50 mV) of 5s for $I_{Ks}$ and of 1 s for $I_{Kr}$ were applied (interpulse interval was 11 s for $I_{Ks}$ and 3 s for $I_{Kr}$). $I_{Ks}$ amplitude was measured as peak current occurring upon returning to holding potential ("tail current" amplitude). $I_{Kr}$ was measured at the end of the activating step and as tail current; the "rectification ratio", which reflects channel inactivation, was estimated from the ratio between the step and tail current amplitudes. The time-course of changes was described by the time constant (τ) of monoexponential fitting, or by the time to half-maximal transition ($t_{1/2}$) when monoexponential fitting was inadequate.

***Action-potential clamp (AP-Clamp) experiments***

Short ($APD_{90}$ = 100 ms) and long ($APD_{90}$ = 140 ms) AP waveforms were selected from previous I-clamp recordings in control and during NOS1 inhibition respectively. Their $APD_{90}$ differed by a proportion (40%) roughly representative of clinically observable QT prolongation. The AP waveforms were applied as "command potential" in V-clamp mode at the same rate at which they were recorded (2 Hz for both AP waveforms); thus, the longer AP was associated with a shorter diastolic interval. Because the AP waveforms were not obtained from the

same myocyte in which they were applied, membrane current was not null during the AP and was disregarded. The relevant parameter in these experiments was the occurrence of inward current transients ($I_{TI}$) during diastole, assumed to reflect the occurrence of intracellular $Ca^{2+}$ waves, a sign of SR instability. The proportion of cells in which at least 1 $I_{TI}$ event occurred was measured to obtain $I_{TI}$ incidence. Furthermore, the number of $I_{TI}$ events within each cycle, the time of onset of the earliest event and the $I_{TI}$ integral (representative of charge flowing in each event) were considered. Measurements were carried out under superfusion with 1 nM isoproterenol (ISO) to simulate conditions of arrhythmia occurrence in LQTS. In general, the long AP was applied first and, when $I_{TI}$ events were stably detected, V-clamp was continued, within the same myocyte, with short AP. Nevertheless, to rule out time as a cause of changes in $I_{TI}$ occurrence, in preliminary experiments a long-long sequence of APs, with each phase lasting > 15 seconds, was applied. This did not result in changes of $I_{TI}$ occurrence (n= 7). Furthermore, in myocytes in which long-short-long sequences could be applied, $I_{TI}$ suppression by short AP was reversed by switching back to long AP in 7/8 cells (**Figure S5**).

**Intracellular $Ca^{2+}$ recordings**

Guinea pig ventricular myocytes were incubated for 30 minutes in 10 µM Fluo4-AM and washed. The dye was excited at a wavelength of 494 nm and emission was collected through a 535 nm band pass filter. Light emission was amplified, converted to voltage, low-pass filtered (200 Hz) and digitized at 2 kHz. Background luminescence was recorded from a cell free field and subtracted; the fluorescence signal recorded from the cell in the quiescent state (before any intervention) was used as reference fluorescence ($F_0$) for signal normalization ($F/F_0$). Intracellular $Ca^{2+}$ was expressed in $F/F_0$ units.

The amplitude of V-triggered $Ca^{2+}$ transients ($Ca_T$) was measured as the difference between diastolic $Ca^{2+}$ ($Ca_D$) and $Ca_T$ peak; the half time of $Ca_T$ decay ($t_{1/2}$) was measured after estimating the decay asymptote by mono-exponential fitting; SR $Ca^{2+}$ content ($Ca_{SR}$) was measured as the amplitude of the caffeine-induced (10 mM, 5 s) $Ca^{2+}$ transient; fractional release (FR) was calculated as the $Ca_T/Ca_{SR}$ ratio. To evaluate $Ca^{2+}$ leak through RyR2 channels, cells were field-stimulated (2Hz) to steady-state $Ca_T$; stimulation was then discontinued and $Ca^{2+}$ bild-up was measured in the presence of $Na^+/Ca^{2+}$ exchanger inhibition ($Na^+$- and $Ca^{2+}$-free superfusion). The protocol was then repeated in the same cell after exposure to tetracaine (0.1 mM) and tetracaine-sensitive $Ca^{2+}$-leak was estimated by subtraction (the control-tetracaine sequence was swapped in alternate cells to avoid systematic time-dependent artefact). Spontaneous $Ca^{2+}$ release events (SCR) were defined as clearly identifiable diastolic oscillations of the $Ca^{2+}$ signal and their incidence expressed as % of cells in which they occurred.

To test the effect of changes in AP duration under control and NOS1 inhibition $Ca^{2+}$ recordings were performed under AP-clamp (see above). In other experiments (as detailed in the results) intracellular $Ca^{2+}$ was measured under I-clamp. Whenever measurements were likely affected by pipette dialysis (in hiPS-

CMs, or when SR $Ca^{2+}$ leak was measured), intracellular $Ca^{2+}$ recordings were obtained during field-stimulation of un-patched cells.

**Molecular studies**

***Reverse transcription, PCR and real Time qPCR***

Total RNA was extracted from hiPSCs and from CMs using Trizol® Reagent (Invitrogen) according to the manufacturer's instructions, and used for cDNA synthesis with SuperScript IV Reverse Transcriptase (ThermoFisher). cDNA were amplified by PCR with Phire Green Hot Start II PCR Master Mix (ThermoFisher), or by Real Time PCR with Power SYBR Green PCR Master Mix (Applied Biosystems, Carlsbad, California, USA) and the ABI Prism 7900HT Fast Real Time PCR System (Applied Biosystems). Primers for PCR were designed by using the 'Primer3 input' software and the specificity of each primer was confirmed using the BLAST software (NCBI).

***Western blot***

Cells were lysed in ice-cold RIPA buffer supplemented with protease inhibitors. The extracted proteins were separated by sodium dodecyl sulphate polyacrylamide gel electrophoresis (SDS-PAGE), and then transferred onto nitrocellulose membrane by a Transblot Turbo (BioRad Laboratories, Hercules, CA, USA). For immunoblotting, membranes were blocked in Odyssey Blocking Buffer (Li-COR), and then incubated overnight at 4ºC with anti-CAPON (R-300) antibody (sc-9138, Santa Cruz Biotechnology) or anti-actin antibody (ab3280, Abcam) diluted in Odyssey Blocking Buffer. At the end of the incubation, membranes were washed in PBS 0.1% tween 20 and subsequently incubated for 1 hour with IRDYE 800-conjugated secondary antibody at room temperature. After further washes, bands were visualized with the Odyssey Infrared Imaging System (Li-COR).

***Immunofluorescence***

Cells were fixed in 4% paraformaldehyde for 15 minutes, rinsed 3 times in PBS, and permeabilized in 0.2% Triton X-100 for 5 minutes. Samples were blocked with 1% bovine serum albumin (BSA) for 1 hour. The cells were incubated for 1 hour at room temperature or overnight at 4°C with antibody diluted in 1% BSA, and then rinsed 3 times for 5 minutes with PBS. Further incubation was performed with the appropriate secondary antibody for 60 minutes at room temperature. The cells were rinsed once more, counterstained with Hoechst 33258, and analyzed with the AxioObserver.Z1 (Zeiss, Oberkochen, Germany).

***Duolink Proximity Ligation Assay (PLA)***

The interaction between NOS1AP and NOS1 in hiPSC-CMs was detected using the Duolink In situ Orange Starter Kit Mouse/Rabbit (DUO92102, Sigma Aldrich) according to manufacturer’s instructions. Primary antibody incubation against NOS1AP (sc-9138 rabbit antibody, Santa Cruz Biotechnology) and NOS1

(610309 mouse antibody, BD Transduction Laboratories) was performed using the same conditions as immunostaining. The cells were visualized using the AxioObserver Z1 (Zeiss, Oberkochen, Germany).

### *3.13 Supplemental results*

**Guinea-pig experiments:**

***Effect of NOS1 inhibition by L-VNIO on repolarization and DADs occurrence***

To rule out that the observations resulted from SMTC effect other than NOS1 inhibition (ancillary effects), experiments were repeated using a different NOS1 inhibitor, L-VNIO (100 μM). This concentration was selected because previously shown to mimic the effect of NOS1 gene knock-out in murine ventricular myocytes [8]. The experiments were performed on a background of $I_{Ks}$ blockade plus 1 or 10 nM ISO.

L-VNIO significantly prolonged APD (73.3 ± 2.9 vs 94.3 ± 10.1 ms; $P<0.05$). The lower ISO concentration induced DADs in none of 11 CTRL myocytes and in 6 of 9 L-VNIO treated myocytes (0% vs 66.7%; $P<0.01$. **Figure S1A**). At the higher ISO concentration DADs occurred in 100% of both CTRL and L-VNIO treated myocytes (**Figure S1B**); however, the time of DADs occurrence was significantly shorter in L-VNIO than in CTRL (**Figure S1C**). Furthermore, at the higher ISO concentration, DADs occasionally (4 of 9 cells) resulted in triggered activity in L-VNIO but never in CTRL ($P<0.01$ vs CTRL. **Figure S1D**). L-VNIO effect was fully consistent with that of SMTC (reported in the manuscript).

***Effect of NOS1 inhibition by SMTC on membrane currents $I_{Kr}$ and $I_{Ks}$***

While $I_{CaL}$ modulation by SMTC is illustrated in a manuscript figure (**Figure 3**), $I_{Kr}$ and $I_{Ks}$ modulation was minor and probably irrelevant to the effect of NOS1 inhibition on repolarization; therefore, the respective figures are shown here only.

$I_{Kr}$ maximal conductance, steady-state activation parameters and rectification ratio (reflecting channel inactivation) were not affected by NOS1 inhibition (**Figure S2 and Table S2**).

$I_{Ks}$ density, maximal conductance and steady-state activation parameters were similarly unaffected by NOS1 inhibition (**Figure S3A-B**, **Table S2**). The $t_{1/2}$ for $I_{Ks}$ activation was slightly but significantly prolonged by NOS1 inhibition (**Figure S3C**). Deactivation kinetics was well fitted by a single exponential, whose time constant ($\tau$) was not affected by NOS1 inhibition (**Figure S3D and Table S2**).

Overall, NOS1 inhibition did not affect $I_{Kr}$ and moderately slowed $I_{Ks}$ activation. The observation that the effect of $I_{Ks}$ blockade on APD was similar in SMTC-treated and CTRL cardiomyocytes (**Figure 1C**) suggests that $I_{Ks}$ modulation was unlikely to account for APD prolongation induced by NOS1 inhibition.

***Effect of NOS1 inhibition by SMTC on intracellular $Ca^{2+}$ dynamics***

Intracellular $Ca^{2+}$ dynamics was measured in patched myocytes under I-clamp conditions (APD free to change). SMTC did not affect diastolic $Ca^{2+}$ (**Fig S4A**), increased $Ca_T$ amplitude (**Fig S4B),** slowed $Ca^{2+}$ decay (**Fig S4C**) and tended to increase SR $Ca^{2+}$ content (**Fig S4D).**

Tetracaine-sensitive SR $Ca^{2+}$ leak, SR $Ca^{2+}$ content after the leak period and the incidence of spontaneous $Ca^{2+}$ release events (SCR) were measured under field-stimulation (no dialysis, APD free to change). SMTC increased $Ca^{2+}$ leak (**Fig S4E),** as also indicated by the reduced SR $Ca^{2+}$ content at the end of the leak period (**Fig S4F**). Under field stimulation, SMTC increased the incidence of SCR events (**Fig S4G**).

***Effect of APD on intracellular $Ca^{2+}$ and $I_{TI}$ occurrence: reproducibility with different waveform sequences***

To rule out dependency of intracellular $Ca^{2+}$ parameters on the order of waveforms sequence, the latter was inverted in a subset of experiments. Irrespective of the waveform sequence, $Ca_D$ was consistently higher under the longer AP; as above, the response of $Ca_T$ was less consistent, in a way again compatible with $I_{CaL}$ run down (**Figure S5**).

**hiPSC-CMs experiments:**

***Comparison of AP parameters between native and DC conditions***

Action potential parameters of AS and S hiPSC-CMs are reported for native and DC conditions in **Table S3**.

Under native conditions hiPSC-CMs displayed a depolarized and unstable diastolic potential, which often resulted in automatic activity (see manuscript **Figure 5**). The majority of cells had a ventricular-like AP contour (see criteria in Methods) for both S and AS groups; cells with other contours were discarded. Whereas diastolic potential was similar between S and AS hiPSC-CMs, APD was significantly longer in S than in AS hiPSC-CMs, also under native conditions (**Figure 5**).

$I_{K1}$ injection by DC hyperpolarized diastolic potential to -80 mV (the target potential in setting $I_{K1}$ conductance value), abolished automatic activity and prolonged APD. Since $I_{K1}$ is an outward current, APD prolongation must be the consequence of dependency of currents other than $I_{K1}$ on diastolic potential. The difference in APD between S and AS hiPSC-CMs was preserved under DC conditions.

***Interaction between KvLQT1 mutation and NOS1AP SNPs in affecting APD***

To assess the interaction between the KvLQT1 mutation and NOS1AP minor allele in prolonging repolarization, APD was compared between KvLQT1 mutant hiPSC-CMs (AS and S) and WT hiPSC-CMs (from the same population)

harboring the minor NOS1AP allele (**Figure S6**). Among hiPS-CMs carrying the minor NOS1AP allele, the KvLQT1 mutation was associated with longer APD; however, APD was similar between KvLQT1-mutant hiPS-CMs carrying the major NOS1AP allele and WT ones carrying the minor NOS1AP allele. Thus, the APD difference caused by the KvLQT1mutation was "compensated" by expression of the major NOS1AP allele. However, because of the small size of the WT sample, this result has to be interpreted with caution.

***Comparison of $I_{CaL}$ parameters between S and AS cells*** $I_{CaL}$ in S and AS hiPSC-CMs is compared in manuscript **Figure 6**. $I_{CaL}$ parameters measured in those experiments are summarized in **Table S4**.

***Effect of NOS1 inhibition by SMTC on intracellular $Ca^{2+}$ dynamics***
Intracellular $Ca^{2+}$ dynamics and SCR incidence were measured in unpatched hiPS-CMs under field stimulation (no dialysis, APD free to change). SMTC slowed $Ca^{2+}$ decay ($t_{1/2}$, **Figure S8C**) and increased fractional $Ca^{2+}$ release (FR, **Figure S8E**), but failed to affect the remaining parameters.

***Molecular characterization***
To test the effect of NOS1AP variants independently of KvLQT1 mutation, NOS1 expression and its colocalization with RyRs and cTNT was compared between different NOS1AP alleles in WT hiPSC-CMs from two unrelated populations (**Figure S10**). Also in WT hiPSC-CMs the minor NOS1AP allele was associated to reduced NOS1 expression and with its reduced colocalization with RyRs and cTnT (**Figure S11**).

### *3.14 Supplemental figures*

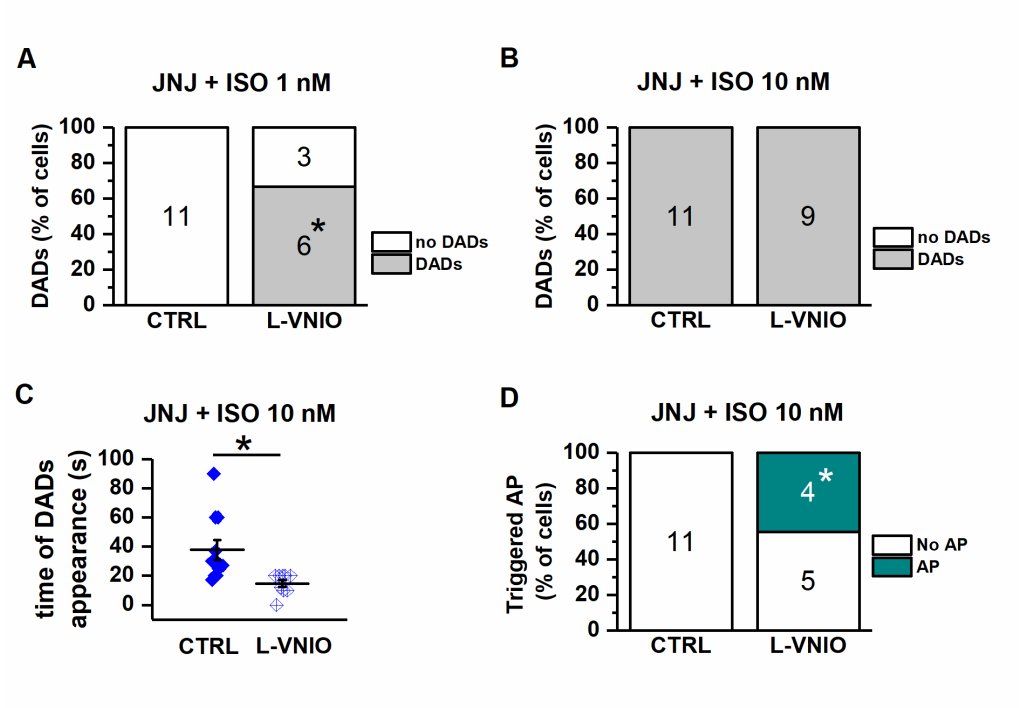


**Figure S1. Effect of NOS1 inhibition by L-VNIO on DADs incidence and properties in GP myocytes with a LQT1 background**. L-VNIO was tested in the presence of $I_{Ks}$ blockade and β-adrenergic stimulation (by 1 and 10 nM ISO); A) DADs incidence at 1 nM ISO in CTRL and L-VNIO; B) DADs incidence at 10 nM ISO in CTRL and L-VNIO; C) Time of DADs onset after repolarization at 10 nM ISO in CTRL and L-VNIO; D) Incidence of triggered APs at 10 nM ISO in CTRL and L-VNIO. Sample sizes: CTRL n=11/4, L-VNIO n=9/3 for all panels. *=$P$<0.05 vs CTRL from unpaired Student's test and chi squared test.

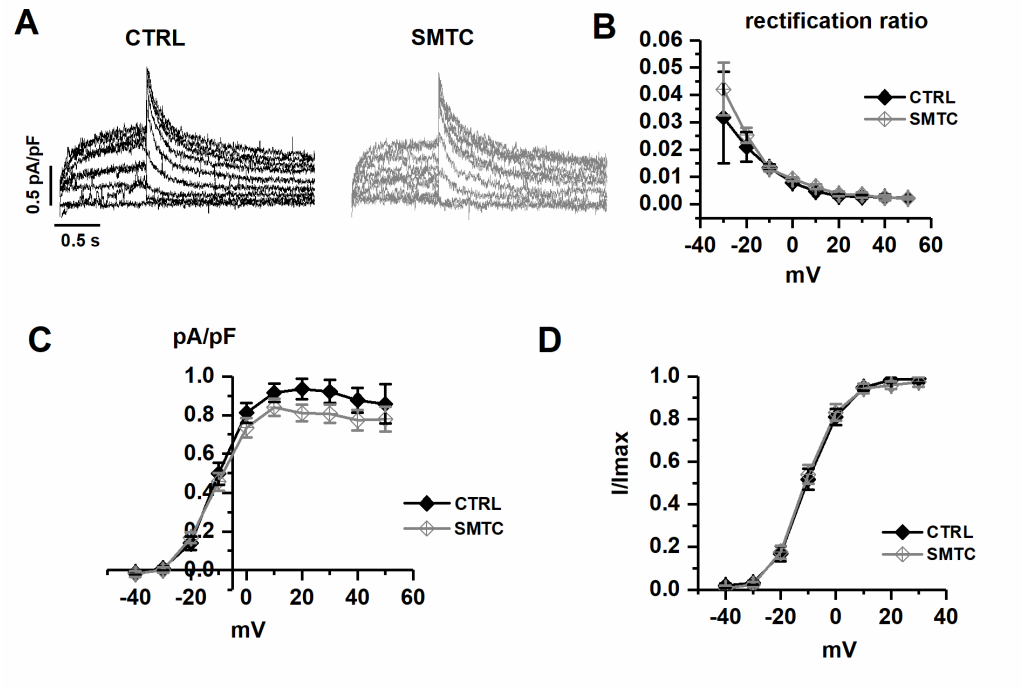


**Figure S2. Effect of NOS1 inhibition on $I_{Kr}$.** Data for CTRL and SMTC are presented in each panel. A) Records of $I_{Kr}$ during step and tail at different step voltages; B) V-dependency of $I_{Kr}$ rectification ratio (inactivation). C) I/V relationships of $I_{Kr}$ tail current density; D) $I_{Kr}$ activation curve. Sample sizes: CTRL n=14/5, SMTC n=23/5 for all panels.

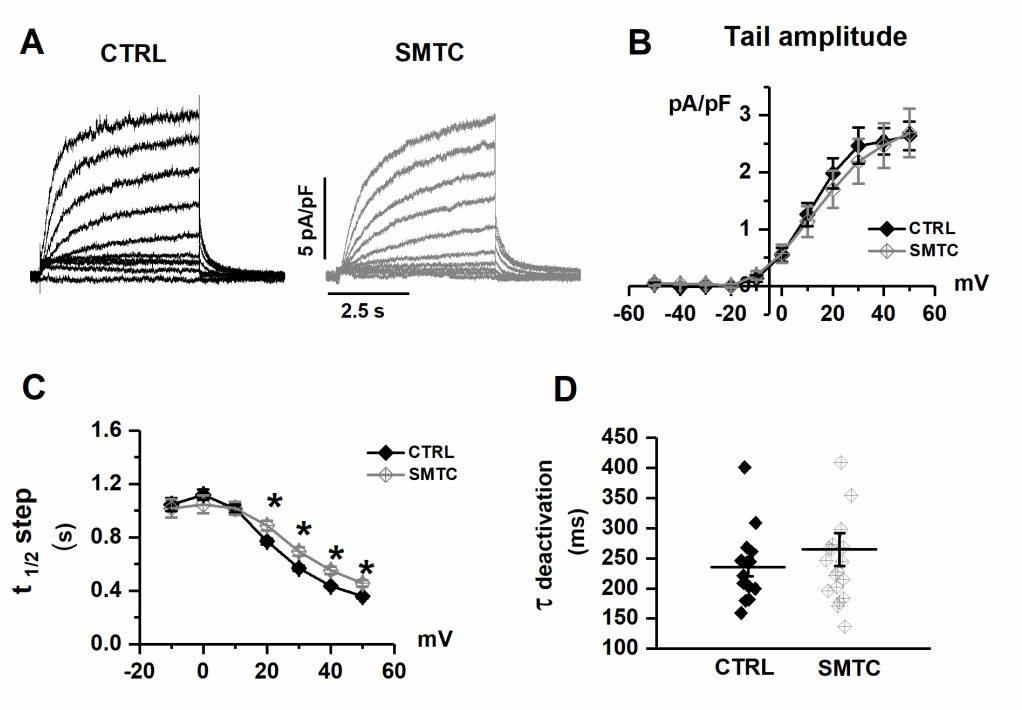


**Figure S3. Effect of NOS1 inhibition on $I_{Ks}$.** Data for CTRL and SMTC are presented in each panel. A) Records of $I_{Ks}$ during step and tail at different step voltages; B) I/V relationship of $I_{Ks}$ tail current; C) V-dependency of the time for half $I_{Ks}$ activation ($t_{1/2}$) during the step; D) V-dependency (+40mV) of the time constant of $I_{Ks}$ deactivation ($\tau$) during the tail current. Sample sizes: CTRL n=16/7, SMTC n=19/6 for all panels. *=$P$<0.05 vs CTRL. From two-way ANOVA for repeated measurements.

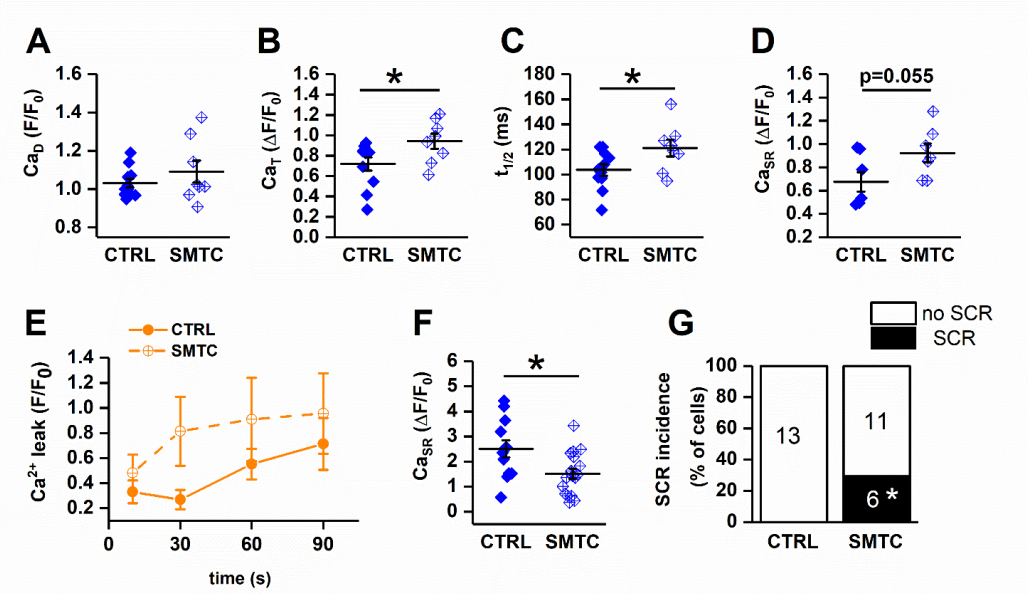


**Figure S4. Effect of NOS1 inhibition on $Ca^{2+}$ dynamics in GP myocytes.** *Upper panels:* I-clamp recordings. SMTC-induced changes in diastolic $Ca^{2+}$ ($Ca_D$, A), $Ca^{2+}$ transient amplitude ($Ca_T$, B), half-time of $Ca^{2+}$ decay ($t_{1/2}$, C) and SR $Ca^{2+}$ content ($Ca_{SR}$ D). These results refer to myocytes in which SCR did not occur. *Lower panels:* field stimulation recordings. SMTC-induced changes in tetracaine-sensitive $Ca^{2+}$ leak (E), $Ca_{SR}$ (F), and SCR incidence (G). Sample sizes: CTRL n=7/2, SMTC n=7/2 for panels A-D; CTRL n=13/4, SMTC n=17/3for panels E-G. *=$P$<0.05 vs CTRL from unpaired Student's test and chi squared test.

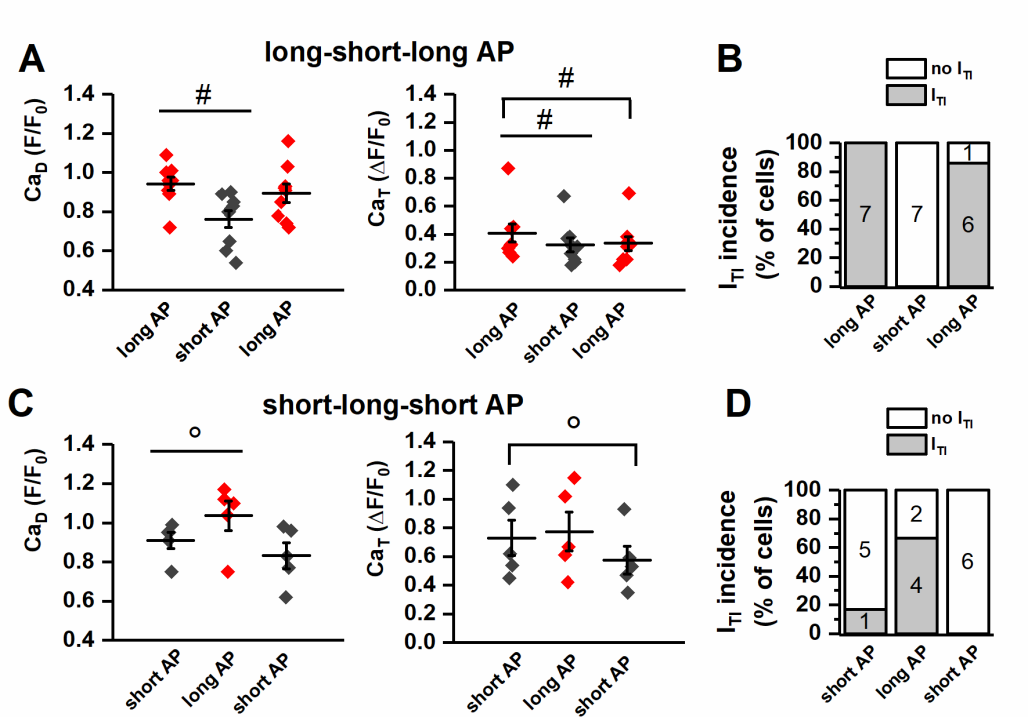


**Figure S5. Reproducibility of APD effect on $Ca^{2+}$ transient parameters.** Changes in diastolic $Ca^{2+}$ ($Ca_D$), $Ca^{2+}$ transient amplitude ($Ca_T$) and $I_{TI}$ incidence caused by change in AP waveform, in the long-short-long sequence or short-long-short one. Sample sizes: n=7/4 for A and B; n=6/2 for C and D. #=*P*<0.05 vs long AP; ° =*P*<0.05 vs short AP from two-way ANOVA for repeated measurements.

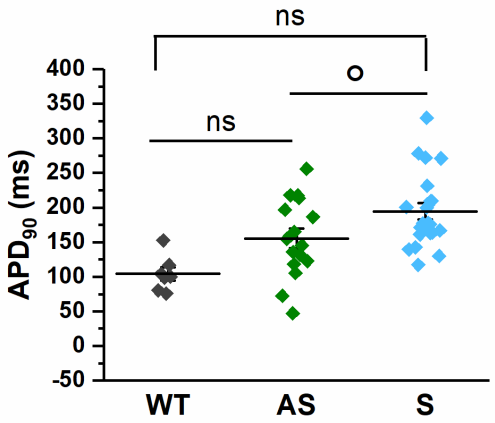


**Figure S6. Effect of KLVQT1 mutation and SNP variant on APD in hiPSC-CMs.** For clarity, only the data obtained under dynamic-clamp (DC) conditions are shown; similar results were obtained in the absence of DC. Comparison of $APD_{90}$ between S KVLQT1-mutant (minor NOS1AP SNP), WT (minor NOS1AP SNP) and AS KVLQT1-mutant (major NOS1AP SNP). Sample sizes: S n=21/7, WT n=7/3. AS n=16/6. °=$P$<0.05 vs S from unpaired Student's test.

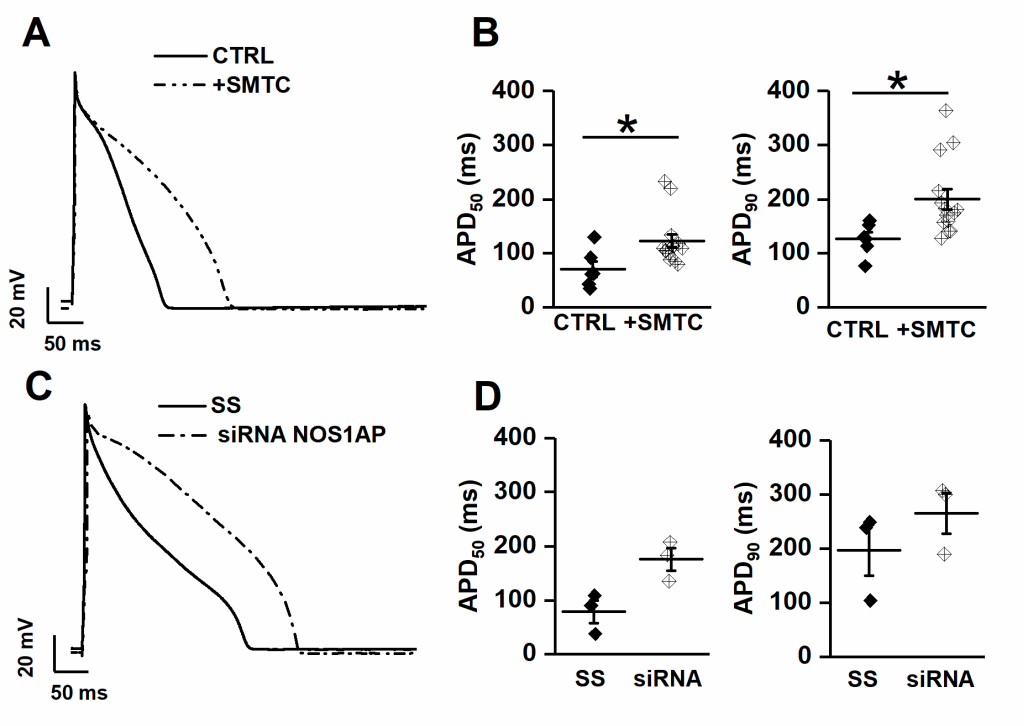


**Figure S7. Effect of NOS1AP-dependent signaling on APD in WT hiPS-CMs carrying the major NOS1AP SNP.** *Upper panels (A, B):* effect of NOS1AP knock-down (scramble sequence, SS solid line; siRNA, dotted line) on AP contour, $APD_{50}$ and $APD_{90}$; *lower panels (C, D)*: effect of NOS1 inhibition (control CTRL solid line, +SMTC, dotted line) on AP contour, $APD_{50}$ and $APD_{90}$. Sample sizes: upper panels SS n= 3/1; siRNA n=3/1; lower panels CTRL n= 15/4; +SMTC n=15/4; *= $P<0.05$ vs CTRL from unpaired Student's test (calculated only if n>5).

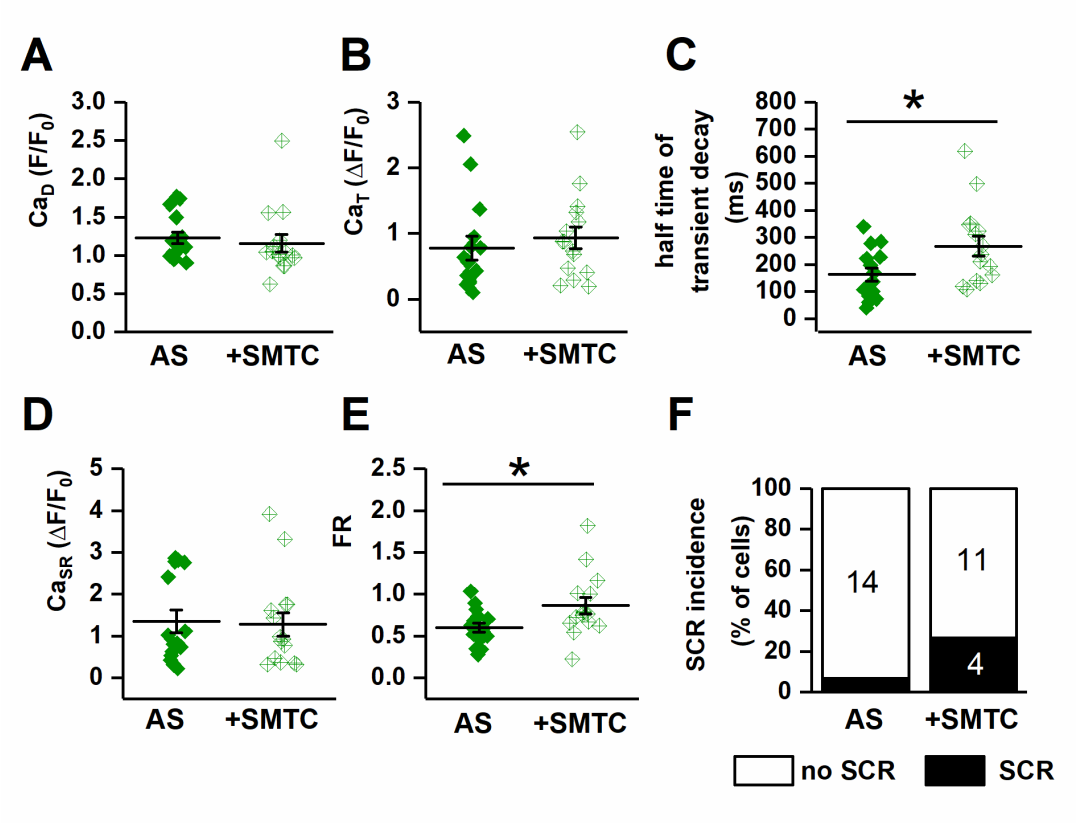


**Figure S8. Effect of NOS1 inhibition on $Ca^{2+}$ dynamics in KLVQT1-mutant AS hiPS-CMs (carrying the major SNP).** Field-stimulation recordings. SMTC-induced changes in diastolic $Ca^{2+}$ ($Ca_D$, A), $Ca^{2+}$ transient amplitude ($Ca_T$, B), half-time of $Ca^{2+}$ decay ($t_{1/2}$, C), SR $Ca^{2+}$ content ($Ca_{SR}$ D), fractional SR release (FR, E) and SCR incidence (F). Sample sizes: AS n= 14/4; +SMTC n=15/4. *= $P$<0.05 vs AS from unpaired Student's test.

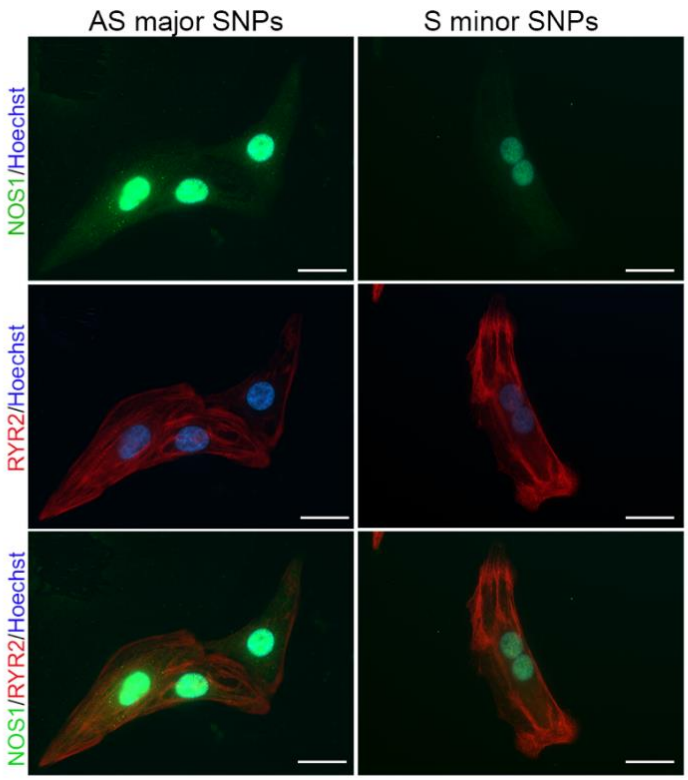


**Figure S9. NOS1 expression and localization in KvLQT1-mutant hiPSC-CMs carrying the major (left) or minor (right) NOS1AP SNPs respectively.** KvLQT1-mutant hiPSC-CMs carrying the major (left) and minor (right) NOS1AP alleles respectively were stained for NOS1 protein (green, upper panels), RyR2 protein (red, middle panel). NOS1-RyR2 overlap images (bottom panels). Nuclei in blue (Hoechst). Scale bars 20 μm.

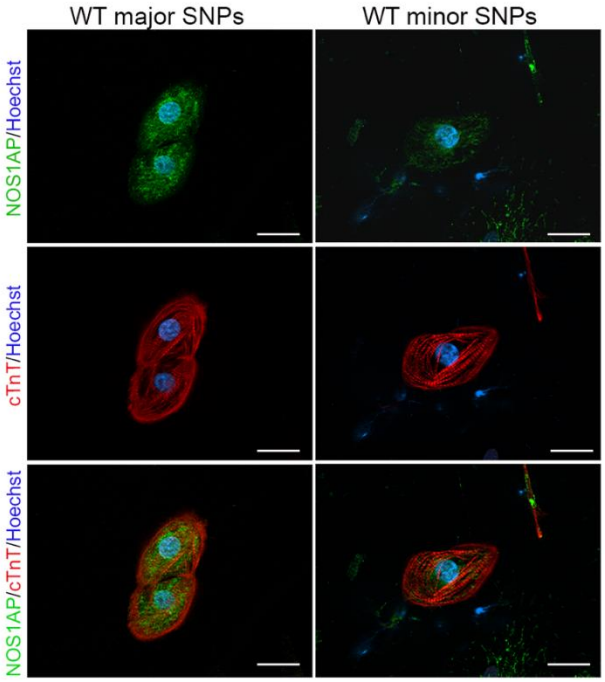


**Figure S10. NOS1AP expression and localization in WT hiPS-CMs carrying the major or minor (right) NOS1AP SNPs respectively**. WT hiPS-CMs carrying the major (left) and minor (right) NOS1AP alleles respectively were collected. Immunofluorescence staining of the same field for NOS1AP protein (green, upper panels, cardiac sarcomeric protein troponin T (red, middle panel). NOS1AP-CTnT overlap images (bottom panels). Nuclei in blue (Hoechst). Scale bars 20 µm.

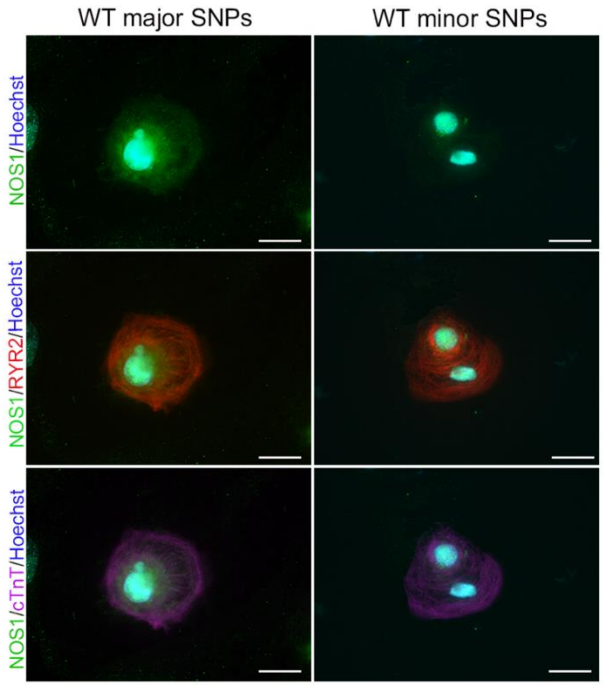


**Figure S11. NOS1 expression and localization in WT hiPS-CMs carrying the minor or major NOS1AP SNPs respectively**. WT hiPS-CMs carrying the major (left) and minor (right) NOS1AP alleles respectively were collected from different donor populations. Immunofluorescence staining of the same field for NOS1 protein (green, upper panels), NOS1-RyR2 overlap image (RyR2 red, middle panel). NOS1-cTnT overlap images (cTnT purple, bottom panels). Nuclei in blue (Hoechst). Scale bars 20 μm.

### *3.15 Supplemental tables*

| Patient | Gender | Age at enrollment | Clinical history |
|---|---|---|---|
| **S** | **Female** | **64** | **Negative family history for SCD. Symptomatic for syncope from the age of 16. Triggers for cardiac events: emotion and exercise. One cardiac arrest requiring DC shock at age of 35, β-blocker therapy (propranolol 40 mg x3) started; no more events since therapy initiation.**<br>**ECG at age of 52 (β-blocker wash out): QT 500 ms, RR 710 ms; QTc 593 ms, HR 84 bpm** |
| **AS** | **Female** | **53** | **Daughter died at age of 12 while ice-skating after many misdiagnosed syncopes. The patient never had symptoms and was never on therapy.**<br>**ECG at age 42: QT 452 ms, RR 860 ms; QTc 488, HR 69 bpm.** |

**Table S1. Clinical parameters of hiPSC-CMs donors.**

| $I_{CaL}$ parameters | CTRL | SMTC |
|---|---|---|
| peak current density (pA/pF) | -13.5 ± 1.0 | -16.6 ± 1.2* |
| $g_{max}$ (nS/pF) | 0.29 ± 0.02 | 0.35 ± 0.02* |
| $E_{rev}$ (mV) | 60.3 ± 0.9 | 62.2 ± 1.0 |
| $V_{0.5}$ A (mV) | -3.6 ± 0.7 | -3.9 ± 0.5 |
| A slope (mV) | 7.0 ± 0.1 | 6.9 ± 0.1 |
| $V_{0.5}$ I (mV) | -23.8 ± 1.0 | -22.1 ± 0.6 |
| I slope (mV) | 4.8 ± 0.5 | 4.4 ± 0.2 |
| $I_{Kr}$ parameters | CTRL | SMTC |
| $I_{max}$ (pA/pF) | 0.98 ± 0.05 | 0.89 ± 0.04 |
| $V_{0.5}$ A (mV) | -10.6 ± 1.3 | -10.9 ± 1.2 |
| A slope (mV) | 5.4 ± 0.3 | 5.3 ± 0.4 |
| $I_{Ks}$ parameters | CTRL | SMTC |
| $I_{max}$ (pA/pF) | 2.94 ± 0.3 | 2.78 ± 0.4 |
| $V_{0.5}$ A (mV) | 14.4 ± 1.1 | 16.9 ± 1.7 |
| A slope (mV) | 8.6 ± 0.5 | 9.4 ± 0.6 |
| τ deactivation (ms) | 235.6 ± 15.5 | 261.9 ± 25.8 |

**Table S2. Current ($I_{CaL}$, $I_{Kr}$ and $I_{Ks}$) parameters in CTRL and SMTC treated GP myocytes**. $g_{max}$= normalized maximal conductance; $E_{rev}$ = reversal potential; $V_{0.5}$ A = voltage of half-maximal activation; A slope = slope factor (mV) of activation $V_{0.5}$ I = voltage of half-maximal inactivation; I slope = slope factor (mV) of inactivation; τ deactivation = time constant of tail current deactivation. *$P$<0.05 vs CTRL.

| | Native | | Dynamic Clamp (DC) | |
|---|---|---|---|---|
| | **AS** | **S** | **AS** | **S** |
| **$E_{diast}$ (mV)** | -40.2 ± 11.5 | -38.7 ± 4.7 | -75.2 ± 3.4 | -76.3 ± 1.08 |
| **APA (mV)** | 40.9 ± 4.9 | 47.1 ± 5.2 | 39.8 ± 7.2 | 52.2 ± 3.1* |
| **$APD_{90}$ (ms)** | 109.5 ± 27.5 | 169.6 ± 34.8* | 135.5 ± 35.9 | 196.2 ± 33.03* |
| **$APD_{50}$ (ms)** | 79.6 ± 22.4 | 131.9 ± 39.3* | 92.1 ± 29.2 | 142.3 ± 30.7* |
| **$APD_{20}$ (ms)** | 45.6 ± 13.3 | 73.3 ± 18.6* | 46.7 ± 18.6 | 76.2 ± 28.9 |
| **$ADP_{90}/ADP_{50}$** | 1.4 ± 0.1 | 1.3 ± 0.07 | 1.5 ± 0.17 | 1.4 ± 0.13 |

**Table S3. AP parameters in S and AS hiPSC-CMs under native and Dynamic Clamp conditions.** $E_{diast}$ = diastolic potential; APA = action potential amplitude; $APD_x$= action potential duration at the indicated repolarization level (%). (S nat n=13 AS nat n=11, S DC n=16, AS DC n=13). *=*P*<0.05 vs AS.

| $I_{CaL}$ Parameters | S | AS |
|---|---|---|
| **Peak density (pA/pF)** | -29.8 ± 4.4 * | -16.7 ± 2.0 |
| **$g_{max}$ (nS/pF)** | 0.8 ± 0.1 | 0.45 ± 0.04 |
| **$E_{rev}$ (mV)** | 57.5 ± 3.8 | 52.5 ± 3.0 |
| **$V_{0.5}$ A(mV)** | -4.8 ± 1.6 | -4.4 ± 1.2 |
| **A slope (mV)** | 6.7 ± 0.3 | 7.1 ± 0.31 |
| **$V_{0.5}$ I (mV)** | -31.4 ± 1.9 | -31.3 ± 1.8 |
| **I slope (mV)** | 5.4 ± 0.5 | 5.0 ± 0.1 |

**Table S4. $I_{CaL}$ parameters in S vs AS hiPSC-CMs.** $g_{max}$ = normalized maximal conductance; $E_{rev}$ = reversal potential; Act $V_{0.5}$ A = voltage of half-maximal activation; A slope = slope factor (mV) of activation; $V_{0.5}$ I = voltage of half-maximal inactivation; I slope = slope factor (mV) of inactivation. (AS n=10, S n=12). *=$P$<0.05 vs AS.

### *3.16 Supplemental references*


1. Cutler MJ, Plummer BN, Wan X, Sun QA, Hess D, Liu H, Deschenes I, Rosenbaum DS, Stamler JS and Laurita KR. Aberrant S-nitrosylation mediates calcium-triggered ventricular arrhythmia in the intact heart. *Proc Natl Acad Sci U S A*. 2012;109:18186-91.

2. Babu BR and Griffith OW. N5-(1-Imino-3-butenyl)-L-ornithine. A neuronal isoform selective mechanism-based inactivator of nitric oxide synthase. *J Biol Chem*. 1998;273:8882-9.

3. Matsa E, Rajamohan D, Dick E, Young L, Mellor I, Staniforth A and Denning C. Drug evaluation in cardiomyocytes derived from human induced pluripotent stem cells carrying a long QT syndrome type 2 mutation. *Eur Heart J*. 2011;32:952-62.

4. Rajamohan D, Kalra S, Duc Hoang M, George V, Staniforth A, Russell H, Yang X and Denning C. Automated Electrophysiological and Pharmacological Evaluation of Human Pluripotent Stem Cell-Derived Cardiomyocytes. *Stem Cells Dev*. 2016;25:439-52.

5. Paavola J, Viitasalo M, Laitinen-Forsblom PJ, Pasternack M, Swan H, Tikkanen I, Toivonen L, Kontula K and Laine M. Mutant ryanodine receptors in catecholaminergic polymorphic ventricular tachycardia generate delayed afterdepolarizations due to increased propensity to Ca2+ waves. *Eur Heart J*. 2007;28:1135-42.

6. O'Hara T, Virag L, Varro A and Rudy Y. Simulation of the undiseased human cardiac ventricular action potential: model formulation and experimental validation. *PLoS Comput Biol*. 2011;7:e1002061.

7. Altomare C, Bartolucci C, Sala L, Bernardi J, Mostacciuolo G, Rocchetti M, Severi S and Zaza A. IKr Impact on Repolarization and Its Variability Assessed by Dynamic Clamp. *Circ Arrhythm Electrophysiol*. 2015;8:1265-75.

8. Zhang YH, Zhang MH, Sears CE, Emanuel K, Redwood C, El-Armouche A, Kranias EG and Casadei B. Reduced phospholamban phosphorylation is associated with impaired relaxation in left ventricular myocytes from neuronal NO synthase-deficient mice. *Circ Res*. 2008;102:242-9.

# Chapter 4

## *Characterization of PLN-R14Del mutation in human induced pluripotent stem cell-derived cardiomyocytes*

Beatrice Badone[1], MSc, Carlotta Ronchi[1], PhD, and Antonio Zaza[1], MD

1. *Laboratory of Cardiac Cellular Physiology, Department of Biotechnology and Bioscience, University of Milano-Bicocca, Milan, Italy*

**[in preparation]**

### *4.1 Acronyms*

| | |
|---|---|
| **ACM** | arrhythmogenic cardiomyopathy |
| **DCM** | dilated cardiomyopathy |
| **ECC** | excitation-contraction coupling |
| **HF** | heart failure |
| **hiPSC-CMs** | human-induced pluripotent stem cell-derived cardiomyocytes |
| **ML** | monolayer |
| **NKA** | $Na^+/K^+$-ATPase |
| **NMR** | nuclear magnetic resonance |
| **NT** | Normal Tyrode's |
| **PKA** | protein-kinase A |
| **PLN** | phospholamban |
| **ROI** | region of interest |
| **SERCA2a** | sarco/endoplasmic reticulum $Ca^{2+}$ ATP-ase type 2a |
| **SR** | sarcoplasmic reticulum |
| **$t_{1/2}$** | half time of $Ca^{2+}$-transient decay |
| **V-induced** | voltage-induced |

### *4.2 Abstract*

Phospholamban (PLN) is the natural inhibitor of the sarco/endoplasmic reticulum $Ca^{2+}$ ATP-ase (SERCA2a) in cardiac cells. Their interaction, and its regulation, is crucial for the excitation-contraction coupling (ECC) in cardiomyocytes. The R14Del mutation is characterized by a deletion of Arg-14 of PLN and it is associated with a severe phenotype of arrhythmogenic and dilated cardiomyopathy. The mutation has been already studied in several models, such as HEK293, mice, and human-induced pluripotent stem cell-derived cardiomyocytes (hiPSC-CMs). Here we wanted to: 1) test how PLN-R14Del (MUT) hiPSC-CMs and their isogenic controls (WT) cultured in a standard monolayer (ML) format differ in terms of $Ca^{2+}$ dynamics; 2) test in both groups the pure SERCA2a activator PST3093, which prevents the interaction PLN/SERCA2a. **Methods:** both WT and MUT hiPSC-CMs were thawed and plated in single glass petri dishes, to allow simultaneous electrophysiological recordings and $Ca^{2+}$ measurements. $Ca^{2+}$-transient recordings were performed in field stimulation at 1 Hz (or increasing frequencies). All experiments were performed under Tyrode's (TYR) superfusion. **Results:** V-induced $Ca^{2+}$-transients did not differ between WT and MUT MLs (1.99±0.17 $F/F_0$, n=37 WT vs 2.10±0.28 $F/F_0$, n=32 MUT); the sarcoplasmic reticulum (SR) $Ca^{2+}$-content, was not significantly different between groups (3.13±0.35 $F/F_0$, n=20 WT vs 3.88±0.44 $F/F_0$, n=27 MUT). Nevertheless, the SR $Ca^{2+}$-content tended to be higher in MUT MLs. The half time of $Ca^{2+}$-transient decay ($t_{1/2}$) was significantly faster (small $t_{1/2}$) in MUT MLs than the WT ones (241.86±9.61 ms, n=43 WT vs 203.54±14.08 ms, n=36 MUT, $P<0.05$). The pure SERCA2a stimulator PST3093 (1 μM) significantly accelerates the decay (small $t_{1/2}$) in both WT (241.86±9.58 ms, n=43 TYR vs 140.95±4.74 ms, n=34 PST3093 1 μM, $P<0.0001$) and MUT MLs (203.54±14.08 ms, n=36 TYR vs 143.04±9.62 ms, n=28 PST3093 1 μM, $P<0.01$). Data obtained from the staircase protocol (application of four increasing frequencies) for the diastolic $Ca^{2+}$, showed a flat staircase in MUT MLs and a

steeply positive one (implying accumulation of $Ca^{2+}$ in the cytosol) in WT MLs ($P<0.05$ vs MUT, two-way ANOVA). PST3093 1 μM significantly reduced the accumulation of diastolic $Ca^{2+}$ in WT ($P<0.01$), whereas it was similar to basal conditions in MUT MLs. **Conclusions:** these results suggest that the PLN-R14Del mutation lead to a PLN loss-of-function for the following reasons: 1) the faster decay (small $t_{1/2}$) in MUT compared to the WT; 2) the lack of effect of PST3093 during the staircase protocol in MUT MLs. In particular, the latter indicates that, in MUT MLs SERCA2a function is enhanced.

**KEYWORDS:** Phospholamban mutation, R14Del mutation, SERCA2a/PLN interaction, hiPSC-CMs, cardiac ECC.

### *4.3 Background*

Phospholamban (PLN) is a crucial regulator of $Ca^{2+}$ cycling in cardiomyocytes. In the non- phosphorylated state (monomeric PLN structure), it inhibits the sarco/endoplasmic reticulum $Ca^{2+}$-ATPase (SERCA2a), which controls $Ca^{2+}$ removal from cytosol and the degree of sarcoplasmic reticulum (SR) $Ca^{2+}$ load [1]. On the contrary, phosphorylation by protein-kinase A (PKA) on the Ser16 residue in the PLN cytosolic domain leads to the relief of the inhibition (pentameric PLN structure), increasing the velocity of $Ca^{2+}$ reuptake by SERCA2a.

In the last decade, several PLN mutations have been strictly associated with arrhythmogenic cardiomyopathy (ACM) and dilated cardiomyopathy (DCM). One of them is the PLN-R14Del, characterized by a loss of arginine at position 14. This mutation, first discovered in a Greek family affected by DCM, has been classified as the most prevalent cardiomyopathy-related mutation in the Netherlands [2]. More than a decade ago, Haghighi and co-workers have defined the R14Del as a "superinhibitory" [3] mutation. The underlying mechanisms have been related to an imbalance between the pentameric and monomeric structure of PLN, resulting in increased PLN monomers concentration, thus increased SERCA2a inhibition. Moreover, PLN monomers phosphorylation by PKA was hindered by the dominant effect of the mutation. Nevertheless, it remains unclear how the mutation leads to the severe phenotype (biventricular dysfunction, arrhythmias, fibrofatty replacement and interstitial fibrosis), observed in ACM and DCM patients. Therefore, other mechanisms need to be elucidated.

Recently, other hypothesis on the PLN-R14Del mutation have been considered. First, Vostrikov and co-workers [4] have demonstrated by nuclear magnetic resonance (NMR) in reconstituted lipid vesicles that the PLN-R14Del mutation presents a reduced inhibition of SERCA2a due to a conformational

change of mutant PLN into a membrane detached state, with increased flexibility of the cytosolic domain. In addition to this, Rijdt et al. [5] have proved that PLN-R14Del mutation lead to the formation of perinuclear aggregates, resulting in cellular toxicity. These additional findings open the possibility to consider different mechanisms involved in the pathophysiology of this PLN mutation.

The aim of the present work is to compare PLN-R14Del human-induced pluripotent stem cell-derived cardiomyocytes (hiPSC-CMs), plated in a monolayer (ML) format, with their CRISPR-Cas9 isogenic controls, to better understand the pathophysiology of the PLN-R14Del mutation. In addition, by the use of a pure SERCA2a stimulator developed in our lab, the PST3093, we specifically want to investigate on the PLN/SERCA2a binding, since the drug prevents their interaction. The latter pharmacological approach on PLN/SERCA2a interaction could be considered as a promising approach to improve life of heart failure (HF) patients [6], where $Ca^{2+}$ handling is compromised.

## *4.4 Methods*

### *4.4.1 HiPSC-CMs preparation*

HiPSC-CMs were kindly shared by Prof. Eschenhagen's lab (University Medical Center Hamburg-Eppendorf, Hamburg, Germany). PLN-R14Del (MUT group) hiPSC-CMs derived from a carrier harboring this mutation in the coding region of the PLN gene; the mutation has been reverted through the CRISPR-Cas9 genome editing system, obtaining their isogenic controls (WT group). Both WT and MUT hiPSC-CMs vials were kept in liquid nitrogen until the thawing procedure. After thawing, cells were plated in 24-multiwell coated dishes (200.000cells/$cm^2$ in a ML format) consisting of 1:100 Geltrex LDEV-Free matrix (Gibco by Life Technologies, A14133), DMEM low-glucose (Sigma Aldrich,

D5921), 1% Penicillin/streptomycin (Sigma Aldrich, P0781), 10% HI Horse Serum (Gibco by Life Technologies, 26050-088), 10µg/ml Human recombinant insulin (Sigma Aldrich, I9278), 33µg/ml Aprotinin from bovine lung (Sigma Aldrich, A1153), 10 µmol/l RHO protein kinase inhibitor GSK 269962A (Biaffin, 850664-21-0). The RHO protein kinase inhibitor was removed 24-h after thawing. The day of thawing, both groups of hiPSC-CMs were at day 17$^{th}$ post-differentiation; therefore, to reach a complete maturation, MLs were maintained for at least 2 weeks in the incubator. At days 28-30$^{th}$ post-differentiation, MLs were washed with room temperature PBS (Invitrogen, 14040) and then divided with a digestion mix (0.08 ml/cm$^2$) consisting of StemPro Accutase (Gibco by Life Technologies, A11105) and Trypsin 2.5% (Gibco by Life Technologies, 15090), at room temperature from 20 up to 40 min. After counting, cells were plated in single glass petri dishes in ML format (35.000cells/1.5cm$^2$) to allow simultaneous electrophysiological recordings and $Ca^{2+}$ measurements.

### *4.4.2 Intracellular $Ca^{2+}$ recordings*

Recordings were made between days 30-34$^{th}$ post differentiation. All experiments were performed under NT superfusion (adapted from [7]), constisting of (mM): 137 NaCl, 5.4 KCl, 2 $CaCl_2$, 1 $MgCl_2$, 10 Hepes, 10 Glucose, pH adjusted to 7.4 with NaOH. Intracellular $Ca^{2+}$-recordings were optically measured in hiPSC-CMs incubated with Fluo-4AM (5 µM) for 20 mins at 37°C, and then washed for 5 min with Tyrode's (TYR) solution. All fluorescence values were normalized to $F_0$, which was recorded at rest before V-stimulation. Group-compared recordings were performed in field stimulation (Multiplexing Pulse Booster, Ugo Basile) giving 60-100 mA per pulse, to allow $Ca^{2+}$-transients measurements; the recorded ML area enclosed not more than three/four cells to avoid propagation effect (region of interest, ROI). Four-five ROIs were analyzed for each plate. Bath and perfusate temperature was 35-37°C. MLs were always stimulated at 1 Hz of frequency. Nevertheless, in some experiments we applied

the “staircase” protocol [8, 9], which consist of giving a series of increasing frequencies (1 Hz, 1.3 Hz, 1.7 Hz and 2 Hz) within the same ROI, to look at MLs adaptation to frequency.

### *4.4.3 Chemicals*

After the achievement of the steady-state at 1 Hz of stimulation, MLs were superfused with: 1) caffeine (10 mM) for 5 sec, to look at the SR $Ca^{2+}$-content; 2) thapsigargin (10 µM) for 5 min, to test if SERCA2a function was preserved.

In our lab, are available some pure SERCA2a stimulators which are still under patent. In this work, we tested one of these compounds, the PST3093, which prevents the inhibitory interaction between PLN and SERCA2a (see next paragraph). We tested PST3093 at three increasing concentrations (100 nM, 500 nM and 1 µM) by incubation for 30 mins at 37°C. Therefore, its effect was analysed by comparing plates with and without drug (group comparison). Thapsigargin was dissolved in DMSO, whereas PST3093 in water. All chemicals (unless PST3093) were purchased from Sigma Aldrich.

### *4.4.4 SERCA2a stimulators*

Istaroxime [(*E,Z*)-3-((2-aminoethoxy)imino) androstane-6,17-dione hydrochloride)] or PST2744 is a new small-molecule drug under clinical development for the treatment of HF. Istaroxime is characterized by a double mechanism of action inhibiting $Na^+/K^+$- ATPase (NKA) [10, 11] while stimulating SERCA2a [11, 12] (**Figure 1A)**, thus improving both inotropy and lusitropy. Compared to Digoxin, which is a pure NKA inhibitor, SERCA2a stimulation by Istaroxime reduces the proarrhythmic effects at the same level of inotropy [12]. This has been confirmed also in clinical studies [13]. Despite its benefits, Istaroxime presents some negative features. The aminoethoxyimino moiety of the molecule undergoes to metabolic transformation which can leads to

possible genotoxicity. Moreover, Istaroxime is active only by intravenous administration and its administration to patients is not suitable for chronic therapy due to its short half-life in the blood. Finally, NKA inhibition could predispose to arrhythmias. For all this reasons, finding a compound possibly administrable by oral route, and able to stimulate SERCA2a without inhibiting NKA to avoid proarrhythmic effects, would considerably improve lusitropy and heart function.

PST3093 is the final long-lasting metabolite of Istaroxime. Compared to Istaroxime, PST3093 retains the oxime moiety at position 3 with the amino-chain substituted with a carboxyl group, while the 6-keto group of Istaroxime is reduced to a 6β-hydroxyl group **(Figure 1B)**. In particular, it is the PST3093 carboxyl group hydrolysis that produces an hydroxyamide that is the one with high genotoxicity. Unlike Istaroxime, PST3093 is active only as a SERCA2a activator, without affecting NKA. Moreover, it has now been found that certain PST3093 derivatives exhibit pure or predominantly pure SERCA2a activation, giving to those compounds a remarkable potential for clinical development.

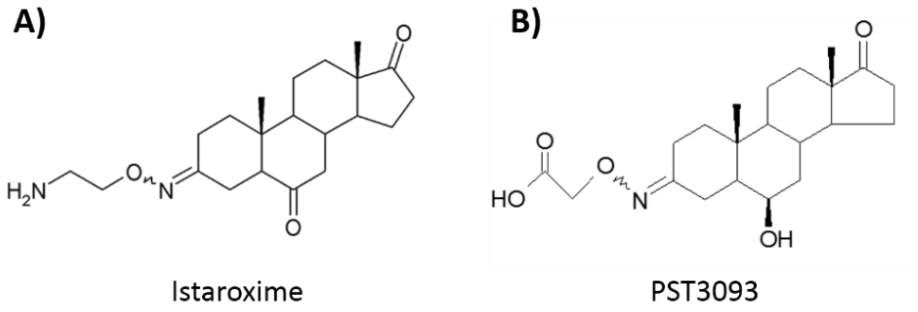


**Figure 1. Istaroxime (A) and PST3093 (B) chemical structures.**

### *4.4.5 Statistics*

OriginPro 2019 (OriginLab software, Northampton, Massachusetts, USA) and GraphPad Prism 8 (GraphPad software, San Diego, CA, USA) were used for statistical analysis. Student's unpaired t-test was used to test for significance between means of continuous variables (amplitudes, $t_{1/2}$). Two-way ANOVA was used to compare two groups at different time points (staircase analysis). Average data are expressed and plotted as mean ± standard error of the mean (SEM). Statistical significance was defined as $P<0.05$*, $P<0.01$**, $P<0.001$*** and $P<0.0001$****. Sample size (n, number of ROIs) is specified for each experimental condition in the respective figure legend.

## *4.5 Results*

### *4.5.1 Voltage- and caffeine-induced $Ca^{2+}$-transient amplitude*

These set of experiments were performed in field stimulation at 1 Hz after reaching the steady state, which usually appeared within 10 beats. V-induced $Ca^{2+}$-transient amplitude did not differ between groups (1.99±0.17 $F/F_0$, n=37 WT vs 2.10±0.28 $F/F_0$, n=32 MUT), as shown in **Figure 2A**. Nonetheless, as clearly visible in the figure, $Ca^{2+}$-transient profile diverged between the experimental groups (**Figure 2A, bottom**), suggesting different contributions from $Ca^{2+}$ handling mechanisms between WT and MUT MLs. This issue will be addressed in detail in the next paragraph (4.5.2).

After reaching the steady state at a stimulation rate of 1 Hz, a caffeine pulse (10 mM) was applied for 5 sec. The amplitude of caffeine-induced $Ca^{2+}$-transients, reflective of SR $Ca^{2+}$-content, tended to be higher in MUT (3.13±0.35 $F/F_0$, n=20 WT vs 3.88±0.44 $F/F_0$, n=27 MUT) (**Figure 2B**); however the difference was small and did not achieve statistical significance.

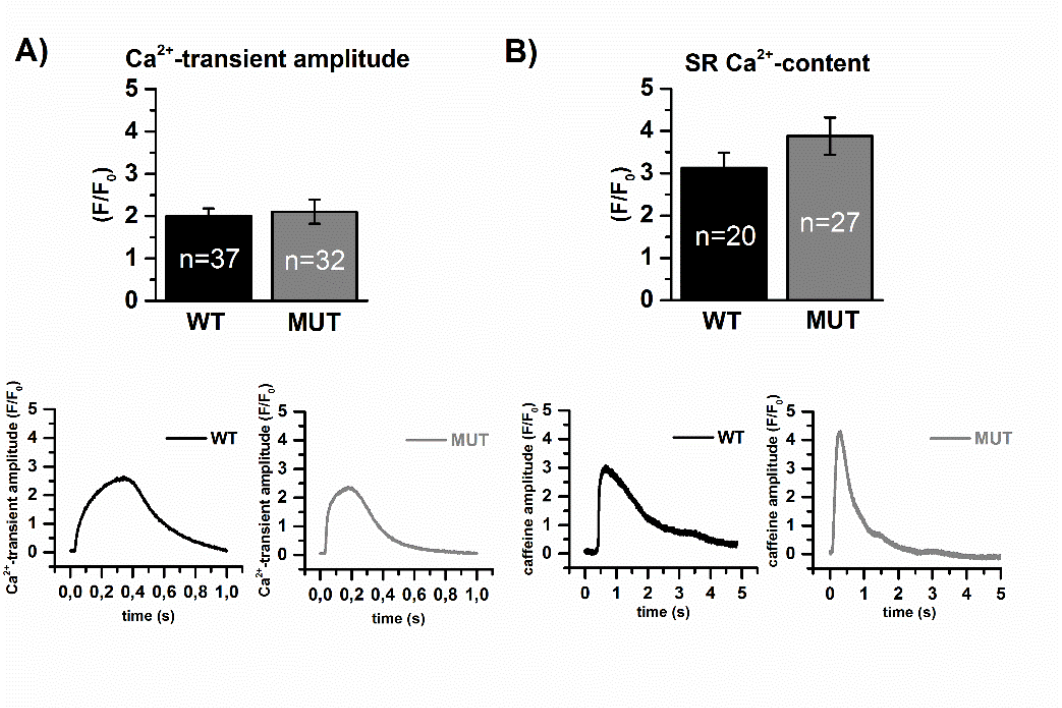


**Figure 2. V-induced $Ca^{2+}$-transient amplitude and SR $Ca^{2+}$-content in WT and MUT MLs**. The figure shows: **(A)** average values ± standard error (top) and representative traces (bottom) of V-induced $Ca^{2+}$-transient amplitude; **(B)** average values ± standard error (top) and representative traces (bottom) of caffeine-induced $Ca^{2+}$-transient, reflective of SR $Ca^{2+}$-content.

### *4.5.2 HiPSC-CMs $Ca^{2+}$-transient profiles*

During electrophysiological recordings, we noticed a variety of $Ca^{2+}$-transient profiles in both WT and MUT MLs. As shown in **figure 3**, five different $Ca^{2+}$ transient profiles (T1, T2, T3, T4, T5), each with different peculiarities on the rise and decay parts, could be identified. Among them, T1 was seldom observed (5,4% in WT, 8,6% in MUT), whereas T5 was observed only in WT (5,4%) (**Figure 3**). T2 was by far the most frequent in MUT MLs (77,2%) (**Figure 3B**), T3 prevailed in WT cells (43,2%) (**Figure 3A**), and T4 was present only in the WT (29,7%) (**Figure 3A**).

Thus, we classified MLs on the basis of their $Ca^{2+}$-transient profile, obtaining different rise time (ms) and half time of $Ca^{2+}$-transient decay ($t_{1/2}$, ms) values (**Figure 3C**). The T2 profile had very fast rise time and, in the majority of cases, a very fast decay (small $t_{1/2}$). The T4 profile instead, was characterized by a very slow rise time, associated to a relatively fast decay (small $t_{1/2}$). The T3 profile showed intermediate values between T2 and T4. Since T1 and T5 were too rare to allow a systematic analysis of their distribution, they were not considered in this type of analysis.

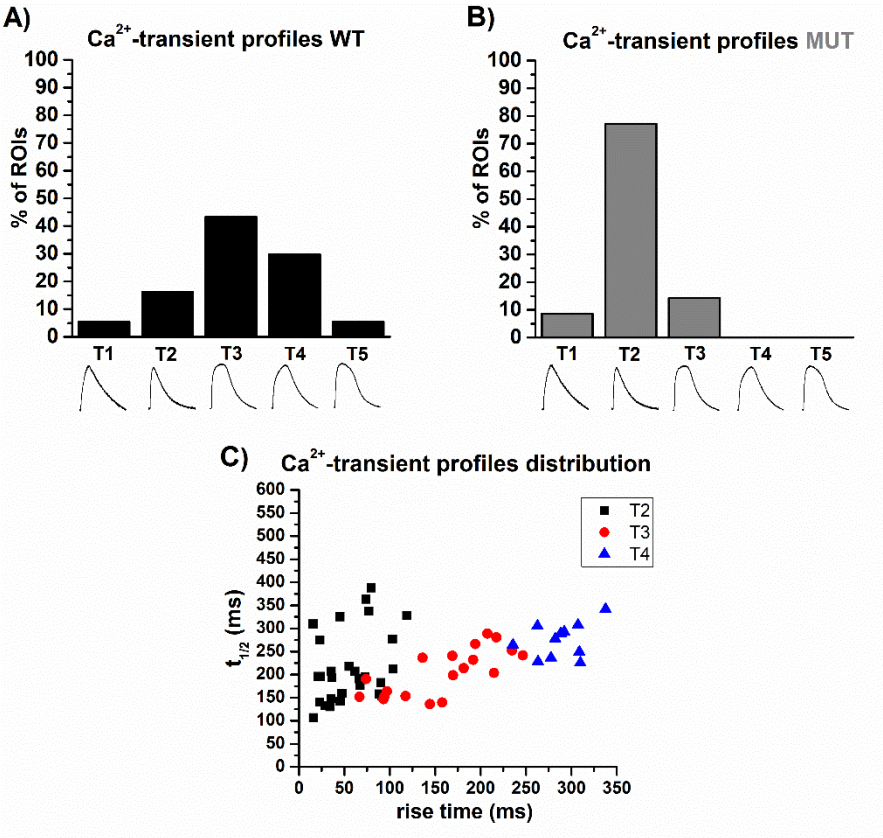


**Figure 3. $Ca^{2+}$-transient profiles distribution in WT and MUT MLs**. The figure shows $Ca^{2+}$-transient profiles distribution (in %) are shown in panel **(A)** for WT and **(B)** for MUT MLs. In panel **(C)** is shown the correlation between $t_{1/2}$ and rise time of only T2, T3 and T4. Since T1 and T5 were too rare to allow a systematic analysis of their distribution, they were not considered in this type of analysis.

We suggest that the profiles differences between WT and MUT MLs were caused by a different SERCA2a activity. To verify this hypothesis we tested thapsigargin (THAPSI, 10 µM), a potent inhibitor of SERCA2a on V-induced $Ca^{2+}$-transients. After the achievement of the steady state at 1 Hz in basal condition (TYR), THAPSI was superperfused for 5 minutes. As shown in the representative traces of both WT and MUT (**Figure 4A**), THAPSI superfusion visibly changed $Ca^{2+}$ transient profile. In MUT cells with a T2 profile (as shown above in **Figure 3B**), the application of THAPSI changed it to T3/T4 ones, which are the most prevalent in WT cells (see above **Figure 3A**). Notably the T2 profile is more similar than the T3/T4 ones to that of mature cardiomyocytes (see discussion). Furthermore, THAPSI lowered $Ca^{2+}$-transient amplitude, increased diastolic $Ca^{2+}$ and slowed the decay (long $t_{1/2}$), in both WT **(**n=5) and MUT (n=3) (**Figure 4B-D**), all changes compatible with decreased SERCA2a function.

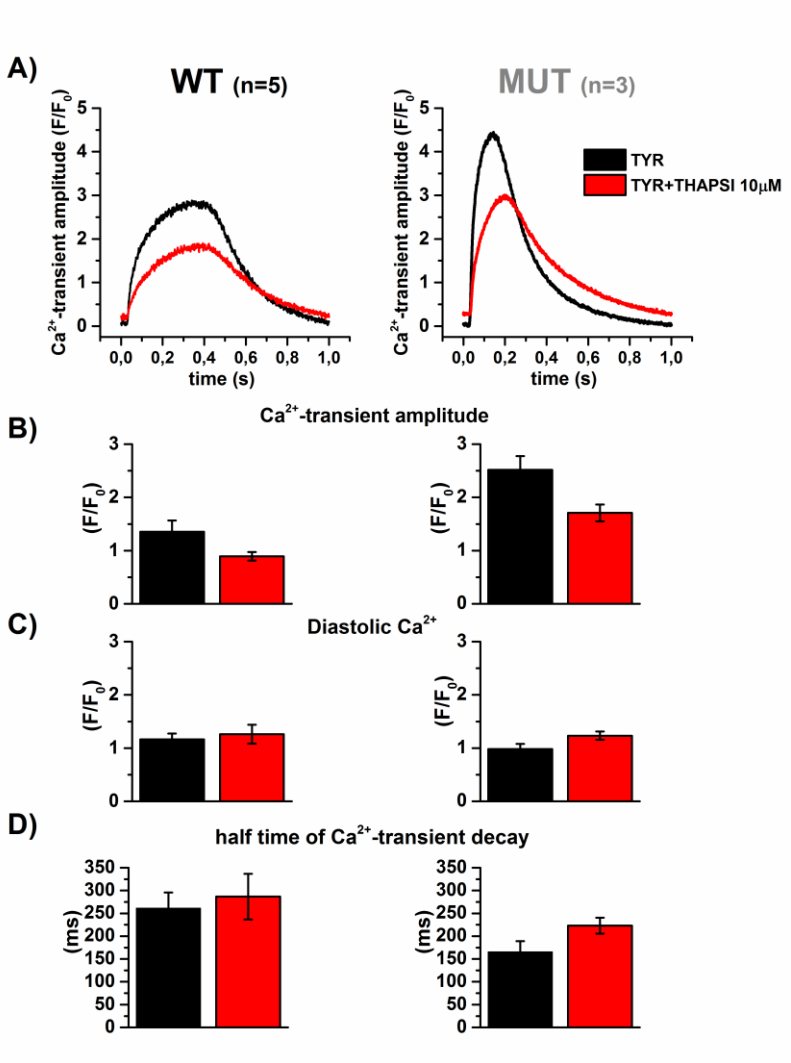


**Figure 4. Thapsigargin changes $Ca^{2+}$-transient profiles in WT and MUT MLs.** In panel **(A)** are represented example traces of both groups (WT n=5, left column and MUT n=3, right column), that show a clear difference in $Ca^{2+}$ transient profiles in basal condition (TYR, black) and after superfusion of thapsigargin (TYR+THAPSI, red), within the same ROI. THAPSI effect was confirmed by the analysis of $Ca^{2+}$-transient parameters **(B)** decreased $Ca^{2+}$ transient amplitude, **(C)** increased diastolic $Ca^{2+}$ **(D)** slower half time of $Ca^{2+}$-transient decay) in both WT (n=5, left column) and MUT (n=3, right column).

*4.5.3 Half time of $Ca^{2+}$-transient decay*

The half time of $Ca^{2+}$-transient decay ($t_{1/2}$), has been estimated as the time required for halving the $Ca^{2+}$-transient amplitude, calculated as the difference between signal peak and its asymptote during diastole. MUT MLs showed a significantly faster decay (small $t_{1/2}$) compared to the WT ones (241.86±9.61 ms, n=43 WT vs 203.54±14.08 ms, n=36 MUT, P<0.05) (**Figure 5**), suggesting enhanced SERCA2a function in MUT MLs.

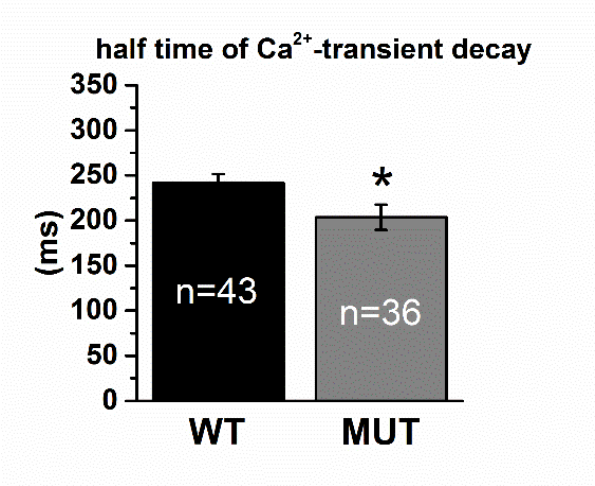


**Figure 5. Half time of $Ca^{2+}$-transient decay in WT and MUT MLs.** The figure shows the difference of the half time of $Ca^{2+}$-transient decay ($t_{1/2}$) between WT and MUT MLs. * $p < 0.05$ vs WT (Student's t test).

*4.5.4 Effect of PST3093 on V-induced $Ca^{2+}$-transient amplitude*

The effect of the SERCA2a stimulator PST3093 (see paragraph 4.4.3) was tested at different concentrations (100 nM, 500 nM, 1 µM), in the range of those previously found to be effective in guinea pig/rat ventricular cardiomyocytes (data not shown).

As shown in **figure 6**, there was not a clear dose-dependent response neither in WT nor in MUT MLs. Thus there was no reason to make statistics in this set of experiments.

At 100 nM, PST3093 tended to increase V-induced $Ca^{2+}$-transient amplitude in WT (1.99±0.17 $F/F_0$, n=37 TYR vs 2.44±0.18 F/F0, n=43 PST3093 100 nM) (**Figure 6A**) but not in MUT MLs (2.10±0.28 $F/F_0$, n=32 TYR vs 2.07±0.33 $F/F_0$, n=30 PST3093 100 nM) (**Figure 6B**). In WT MLs, PST3093 500 nM decreased $Ca^{2+}$-transient amplitude (1.99±0.17 $F/F_0$, n=37 TYR vs 1.32±0.16 $F/F_0$, n=24 PST3093 500 nM, $P<0.01$) (**Figure 6A**); the same result was obtained for MUT MLs (2.10±0.28 $F/F_0$, n=32 TYR vs 1.17±0.21 $F/F_0$, n=30 PST3093 500 nM) (**Figure 6B**). At 1 µM concentration instead, there were not significant differences neither in WT (1.99±0.17 $F/F_0$, n=37 TYR vs 2.40±0.26 $F/F_0$, n=13 PST3093 1 µM) (**Figure 6A**), nor in MUT MLs (2.10±0.28 $F/F_0$, n=32 TYR vs 1.98±0.23 $F/F_0$, n=28 PST3093 1 µM) (**Figure 6B**).

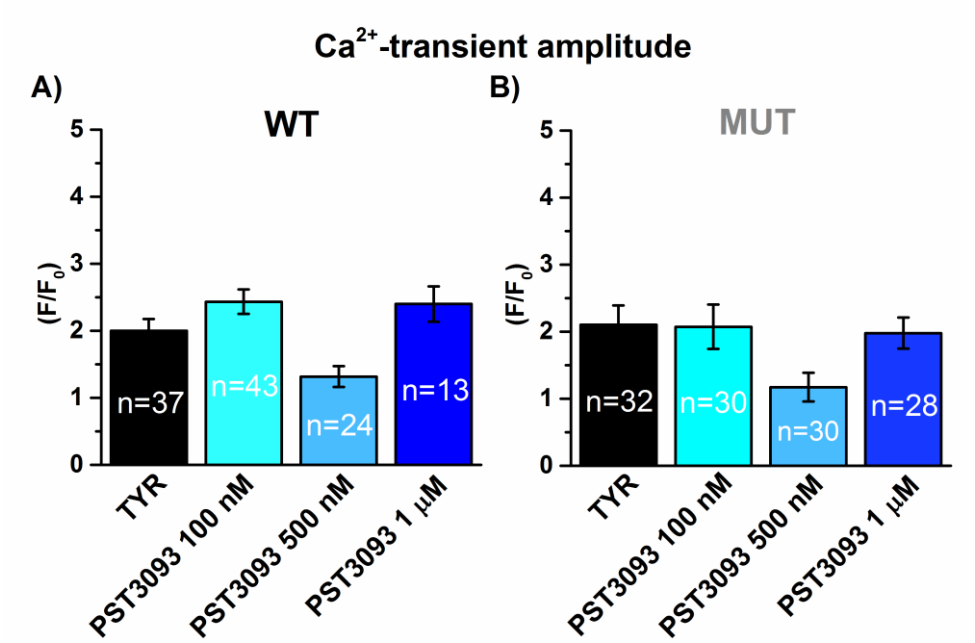


**Figure 6. PST3093 effect on V-induced $Ca^{2+}$-transient amplitude in WT and MUT MLs.** The figure shows the effects of PST3093 (SERCA2a stimulator) at different concentrations (100 nM, 500 nM, 1 µM) on V-induced $Ca^{2+}$-transient amplitude in WT **(A)** and MUT **(B)** MLs.

PST3093 effect was visible when it was compared between the variety of $Ca^{2+}$-transient profiles. In particular, PST3093 (mostly at 1 µM) reverted the $Ca^{2+}$-transient profile to the T2 one in a dose-dependent manner, partially in WT (**Figure 7A**) and completely in MUT MLs (**Figure 7B**). The T2 profile, which is representative of MUT MLs in basal conditions, seems to be the most physiological profile above all others (see discussion). PST3093, allowing PLN release from SERCA2a, would accelerate the decay (small $t_{1/2}$), as confirmed in **Figure 9**, thus improving $Ca^{2+}$-handling. This suggests that MLs with the T2 profile are the one with a most physiological ECC compared to the others (**Figure 7**).

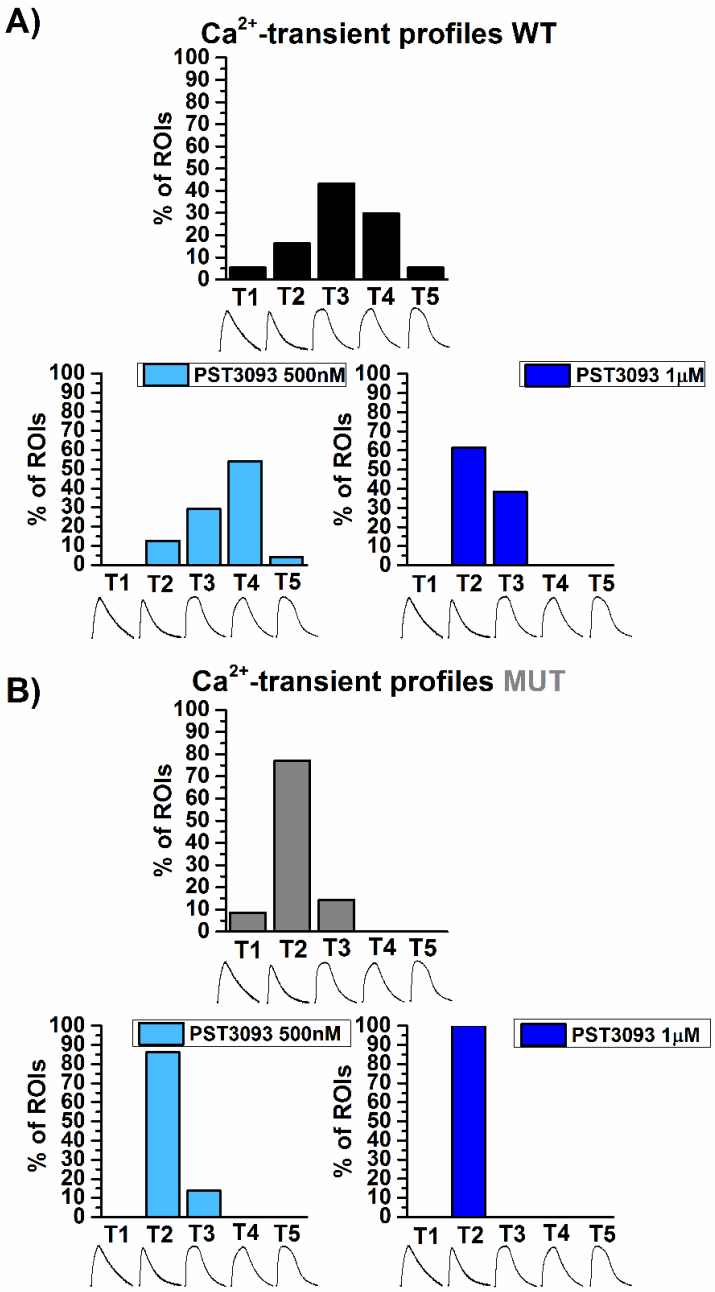


**Figure 7**. **Effect of PST3093 on $Ca^{2+}$-transient profiles.** The figure shows the % of ROIs that showed a certain $Ca^{2+}$-transient profile in WT **(A)** and in MUT **(B)** MLs.

*4.5.5 Effect of PST3093 on caffeine-induced $Ca^{2+}$-transient amplitude*

As shown during $Ca^{2+}$-transient recording (see above), also the SR $Ca^{2+}$-content did not shown a clear dose-dependent response (**Figure 8**).

PST3093 100 nM tended to increase the SR $Ca^{2+}$-content in WT (3.13±0.35 $F/F_0$, n=20 TYR vs 3.97±0.28 $F/F_0$, n=37 PST3093 100 nM) (**Figure 8A**), but not in MUT MLs (3.88±0.44 $F/F_0$, n=27 TYR vs 3.73±0.50 $F/F_0$, n=31 PST3093 100 nM) (**Figure 8B**). At 500 nM, PST3093 showed no effect in neither group (WT: 3.13±0.35 $F/F_0$, n=20 TYR vs 2.31±0.16 $F/F_0$, n=10 PST3093 500 nM; MUT: 3.88±0.44 $F/F_0$, n=27 TYR vs 2.54±0.29 $F/F_0$, n=20 PST3093 500 nM) (**Figure 8**). At 1 µM mean values were similar to controls in both WT and MUT MLs (WT: 3.13±0.35 $F/F_0$, n=20 TYR vs 3.34±0.28 $F/F_0$, n=12 PST3093 1 µM; MUT: 3.88±0.44 $F/F_0$, n=27 TYR vs 3.28±0.42 $F/F_0$, n=28 PST3093 1 µM) (**Figure 8**).

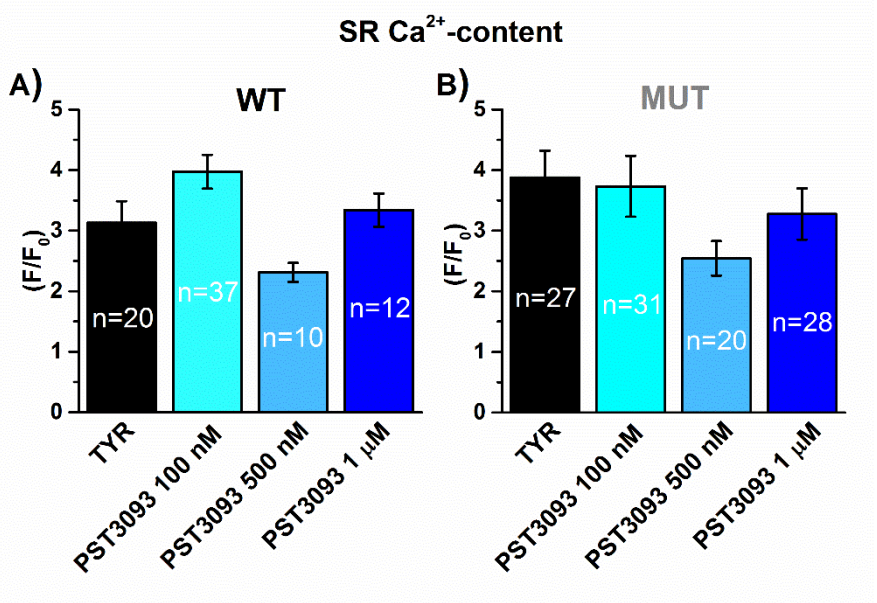


**Figure 8. PST3093 effect on caffeine-induced $Ca^{2+}$-transient amplitude in WT and MUT MLs.** The figure shows the effect of PST3093 at different concentrations on caffeine-induced $Ca^{2+}$-transients in WT **(A)** and MUT **(B)** MLs.

*4.5.6 Effect of PST3093 on the half time of $Ca^{2+}$-transient decay*

PST3093 effect on $t_{1/2}$ showed a clear dose-dependency in both groups. In WT MLs, the drug significantly accelerated the decay (small $t_{1/2}$) at 1 µM (241.86±9.58 ms, n=43 TYR vs 140.95±4.74 ms, n=34 PST3093 1 µM, P<0.0001) (**Figure 9A**), whereas there were not significant changes at the other concentrations (241.86±9.58 ms, n=43 TYR vs 262.18±12.78 ms, n=51 PST3093 100 nM; TYR vs 226.01±15.44 ms, n=26 PST3093 500 nM) (**Figure 9A**). The same results were obtained in MUT MLs, with a significant acceleration of decay (small $t_{1/2}$) at 1 µM (203.54±14.08 ms, n=36 TYR vs 143.04±9.62 ms, n=28 PST3093 1 µM, P<0.01) (**Figure 9B**); as in the WT MLs, there were no significant differences for the other tested concentrations (203.54±14.08 ms, n=36 TYR vs 208.92±12.69 ms, n=34 PST3093 100 nM; TYR vs 166.53±13.28 ms, n=13 PST3093 500 nM) (**Figure 9B**).

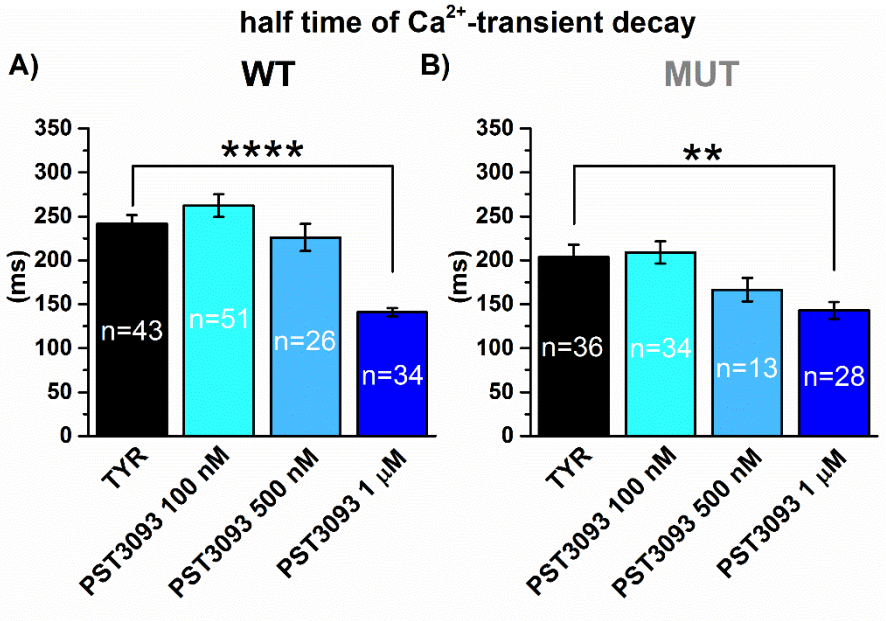


**Figure 9. PST3093 effect on the half time of $Ca^{2+}$-transient decay in WT and MUT MLs.** The figure shows the effect of PST3093 at different concentrations on $t_{1/2}$ in WT **(A)** and in MUT **(B)** MLs. ** p < 0.01 vs TYR; **** p < 0.0001 vs TYR (Student's t test).

*4.5.7 Staircase*

The staircase phenomenon was described for the first time in muscle cells by Bowditch [8, 9], in 1871. It has been attributed to changes in the distribution of intracellular $Ca^{2+}$ ions. The concept is that after succession of contractions at increasing frequencies, the force of contraction increases. At the single cell level, the basis of the phenomenon correlates with the acceleration of $Ca^{2+}$ reuptake into the SR (due to SERCA2a) and with the extrusion of $Ca^{2+}$ outside the cell (due to the $Na^{+}/Ca^{2+}$ exchanger, NCX). The increased heart rate shorten the diastolic interval, leading to the accumulation of cytosolic $Ca^{2+}$ at each beat. In this way, SERCA2a works at increased $Ca^{2+}$ concentration, pumping more $Ca^{2+}$ into the SR, thus leading to more $Ca^{2+}$ available for the next $Ca^{2+}$-transient. At increased frequencies, the movement of $Ca^{2+}$ ions is limited towards troponin C (allowing contraction) and to the SR, whereas $Ca^{2+}$ extrusion through NCX decrease. On the contrary when heart rate slows, intracellular $Na^{2+}$ levels decreases and $Ca^{2+}$ extrusion through the NCX is more evident.

In this work, we describe for the first time in literature the staircase phenomenon to investigate on frequency adaptation in our model of hiPSC-CMs. We applied four different increasing frequencies (1, 1.3, 1.7 and 2 Hz) within the same ROI, to investigate on $Ca^{2+}$-transient amplitude and levels of diastolic $Ca^{2+}$, in both WT and MUT MLs (**Figure 10**). For $Ca^{2+}$-transient amplitude, both groups showed a negative staircase, with no differences in its steepness between WT and MUT MLs (**Figure 10A**). Nevertheless, diastolic $Ca^{2+}$, which mostly depends on the speed of $Ca^{2+}$ reuptake into the SR, showed a flat staircase in MUT MLs (**Figure 10B**), and a steeply positive one (implying accumulation of $Ca^{2+}$ in the cytosol) in WT ones ($P<0.05$ vs MUT, two-way ANOVA) (**Figure 10B**). The latter result suggests that $Ca^{2+}$ reuptake during diastole is more complete in MUT than in WT, an observation consistent with a functional SERCA2a (i.e. PLN loss-of-function).

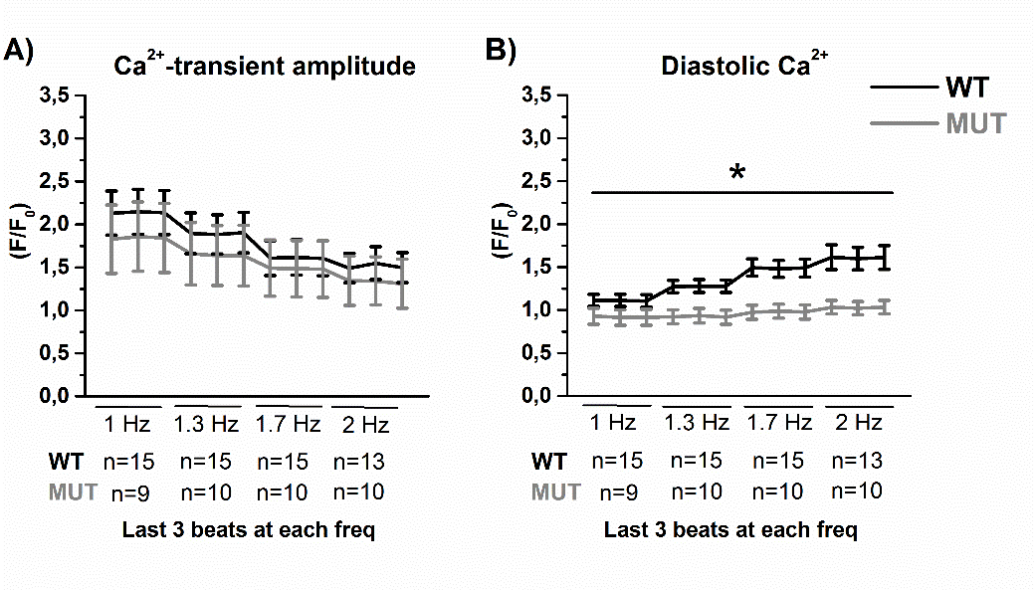


**Figure 10. Effect of the staircase protocol in WT and MUT MLs.** The figure shows results obtained from the staircase protocol (application of four increasing frequencies) in WT and MUT MLs. **(A)** $Ca^{2+}$-transients amplitude **(B)** diastolic $Ca^{2+}$. *p < 0.05 vs MUT (two way ANOVA test).

PST3093 1 µM (**Figure 11**), significantly reduced the accumulation of diastolic $Ca^{2+}$ in WT MLs (P<0.005, two-way ANOVA), implying SERCA2a function enhancement (**Figure 11B**); on the contrary, in MUT MLs the levels of diastolic $Ca^{2+}$ were similar to basal conditions (**Figure 11D**). This suggests that MUT MLs have a functional SERCA2a in basal conditions. During the application of the staircase protocol, there were no significant changes in $Ca^{2+}$-transient amplitude in neither group (**Figure 11A,C**).

The staircase protocol was tested also at the other drug concentrations (100 nM and 500 nM, data not shown); however, the results obtained were somehow confused although going in the same direction of the 1 µM concentration.

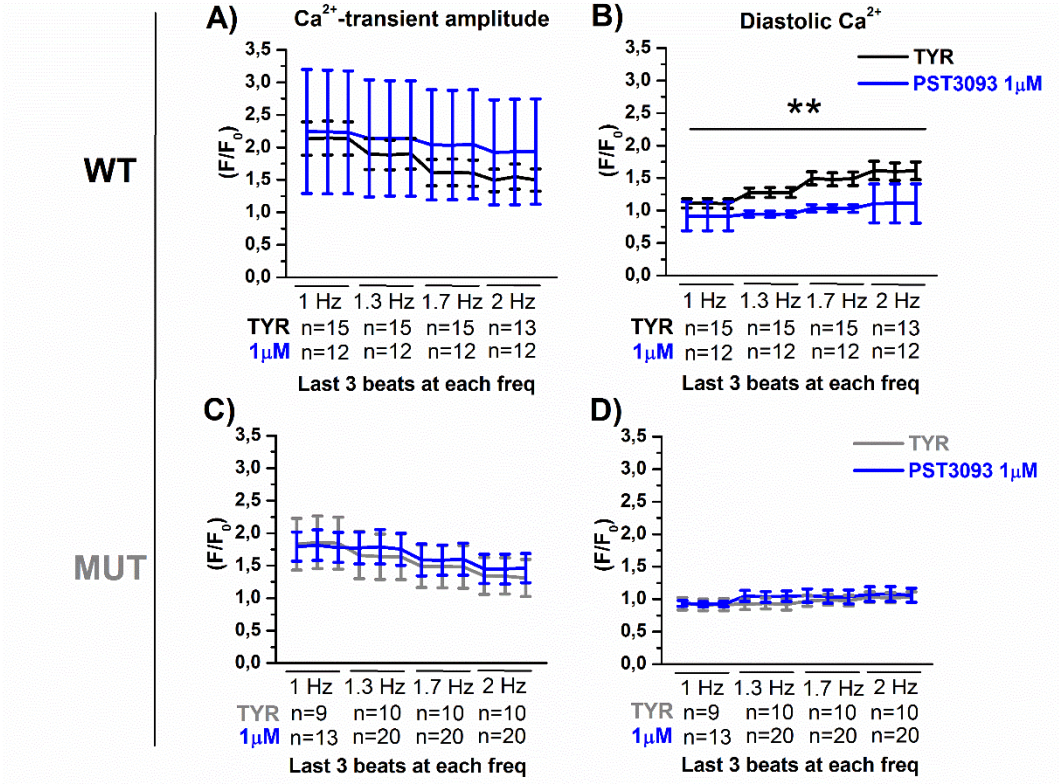


**Figure 11. PST3093 1 µM effect during the staircase protocol in WT and MUT MLs.** The figure shows the PST3093 effect on $Ca^{2+}$ dynamics during the application of the staircase protocol in WT **(A)** $Ca^{2+}$ transients, **(B)** diastolic $Ca^{2+}$ and MUT **(C)** $Ca^{2+}$ transients, **(D)** diastolic $Ca^{2+}$ MLs. ** $p<0.01$ vs WT, two-way ANOVA.

### *4.6 Discussion*

The main results of this study are: 1) $Ca^{2+}$-transient amplitude (V- or caffeine-induced) does not differ between WT and MUT MLs (if anything, with a trend to larger SR $Ca^{2+}$-content in MUT); 2) the prevalence of $Ca^{2+}$-transient profiles suggestive of a larger SERCA2a contribution; 3) a faster decay (smaller $t_{1/2}$) in MUT MLs compared to the WT ones; 4) the lack of rate-dependent diastolic accumulation in MUT MLs.

All of these findings do not support the concept of a superinhibitory action of the PLN-R14Del mutation that was described by Haghighi et al. in 2006 [4]; indeed our results point to a PLN loss-of-function in MUT MLs, leading to enhanced SERCA2a activity.

The lack of difference in the amplitude of V-induced $Ca^{2+}$ transients (**Figure 2**) should be interpreted considering the different profiles (**Figure 3**). Overall, the findings suggest that $Ca^{2+}$-transient amplitude may be under the control of homeostatic mechanisms [14] which reduce the impact of differences in SERCA2a function. The latter may instead be unveiled by the analysis of profiles and protocols as the rate-dependency of $Ca^{2+}$ accumulation (staircase protocol). We hypothesized that the T2 profile, reflecting that of mature cardiomyocytes (**Figure 7**), was representative of a larger SERCA2a activity and it was the most representative of MUT MLs. Thus MUT MLs are endowed with a greatest SERCA2a function than WT ones, thus suggesting a PLN loss-of-function in MUT MLs.

Our results obtained from the $t_{1/2}$ showed that in basal conditions MUT MLs have a faster decay (small $t_{1/2}$) compared to the WT ones (**Figure 5)**, strictly consistent with the PLN loss-of-function hypothesis (i.e. no superinhibitory effect). PST3093 1 μM showed a significant effect on $t_{1/2}$ values in both groups and the acceleration of decay (small $t_{1/2}$) induced by the drug was higher in WT than MUT MLs (Δ%: 42% WT vs 30% MUT) (**Figure 9A, B**), again suggesting low SERCA2a inhibition by PLN in the latter. PST3093 is the long-lasting

metabolite of Istaroxime [11], a well-known luso/inotropic drug which has been deeply studied in previous works from our lab [10, 15]. The activity of Istaroxime and its effect have been studied in microsomes [16], where it has been demonstrated that it stimulates SERCA2a by relieving PLN inhibition. This means that PLN presence on the SR is necessary for the action of the drug. Research on PST3093 is still ongoing, but we already known that it stimulates SERCA2a, without affecting NKA (data not shown), as instead, Istaroxime does.

The staircase protocol [8, 9], which consisted of giving four increasing frequencies within the same ROI, was tested with the purpose of looking at both WT and MUT MLs adaptation to frequency. In particular, we investigated on $Ca^{2+}$-transient amplitude and diastolic $Ca^{2+}$ parameters. In ventricular myocytes of most mammalian species (i.e. guinea pigs, humans), the staircase phenomenon for $Ca^{2+}$-transients has shown to be positive, due to the acceleration of $Ca^{2+}$ reuptake by the SR at increased frequencies, together with the allosteric modulation of SERCA2a by PLN [14, 17]. Both phenomena, lead to larger $Ca^{2+}$-transients at each beat, enhancing contractility [18]. Nevertheless, pathological conditions such as HF, where SERCA2a function is depressed (depressed ECC), $Ca^{2+}$-transient staircase from positive becomes negative [19, 20]. Also in rodents, the force–frequency response has been found to be flat or even negative [18, 19], due to their very short action potential (less $Ca^{2+}$ plateau at each beat), showing depressed contractility at higher frequencies, due to a decline in the amplitude of $Ca^{2+}$-transients [19, 21]. In any case, the balance of the contribution between SERCA2a and NCX has a fundamental value in the response to rate-dependent adaptation. In a functional heart, the response at higher frequencies leads to enhanced $Ca^{2+}$ reuptake by SERCA2a avoiding diastolic $Ca^{2+}$ accumulation in the cytosol.

In the present work, during the staircase protocol, V-induced $Ca^{2+}$-transient of both experimental groups showed a negative staircase (**Figure 10A-11A,C**), that was not expected, since this model derived from an human patient harboring the PLN-R14Del mutation (humans have a positive staircase [19]).

However, several differences of hiPSC-CMs features compared to adult cardiomyocytes could contribute to a negative staircase of $Ca^{2+}$-transient (i.e. immaturity, lack of t-tubules, slower $Ca^{2+}$ transport by SERCA2a) [22, 23].

Moreover, diastolic $Ca^{2+}$ in WT MLs was accumulated at each step of frequency (**Figure 10A**), whereas it was similar to basal conditions in MUT MLs (**Figure 10B**). This suggests that WT MLs have not an efficient ECC compared to the MUT ones, a difference compatible with the immaturity of the experimental model.

During the incubation with PST3093 1 μM, WT MLs showed a reduced accumulation of diastolic $Ca^{2+}$ during the staircase protocol, compatible with enhancement of SERCA2a activity (**Figure 11B**). In MUT MLs instead (**Figure 11D**), PST3093 1 μM effect was superimposed on the basal condition, suggesting that MUT MLs have a functional SERCA2a already in basal conditions. In both WT and MUT MLs, drug effect on $Ca^{2+}$-transient amplitude during the staircase protocol showed no differences in neither group (**Figure 11 A,C**).

Overall, SERCA2a activity is enhanced in MUT MLs, in a way not compatible to a PLN superinhibition. Nevertheless, the negative staircase observed in the $Ca^{2+}$-transient amplitude of both groups suggest that hiPSC-CMs in general, despite plated in the MLs format, which should prevent isolation-induced changes, have a weak ECC, compared to mature human myocytes.

### *4.7 Conclusions*

In summary, in this work, we failed to observe in MUT cells the signs of reduced SERCA2a activity expected from the superinhibition hypothesis (PLN gain-of-function) [4]. To the contrary, the results of protocols suitable to detect allosteric SERCA2a modulation by cytosolic $Ca^{2+}$, a process mediated by PLN, suggest loss-of-function in mutant PLN. Moreover, the response to drugs preventing PLN/SERCA2a interaction (PST3093) differed between MUT vs WT

MLs in a direction pointing to the same conclusion. Therefore, if the PLN loss-of-function hypothesis is correct, the PLN-R14Del mutation lead to less PLN protein on the SR and, accordingly to this, PST3093 would fail to stimulate SERCA2a due to the absence of PLN.

The study also discloses for the first time that $Ca^{2+}$-transient profiles and rate-responsiveness of ECC in hiPSC-CMs show aspects of immaturity, and that drug-induced SERCA2a stimulation may minimize them. This leads to conclude that response of SERCA2a to allosteric activation by $Ca^{2+}$ may be immature in hiPSC-CMs, also because the immature phenotype of this model [23].

Moreover, two recent works [4, 5] have demonstrated that other mechanisms that not directly involved the SR (i.e. cytosolic aggregates formation, detachment of PLN from the SR), would impact on the phenotype observed in ACM and DCM patients affected by this mutation. For these reasons, further hypothesis need to be investigated.

### *4.8 Acknowledgements*

We thank Prof. Eschenhagen to share with us the hiPSC-CMs.

### *4.9 References*


1. MacLennan, D.H. and E.G. Kranias, Phospholamban: a crucial regulator of cardiac contractility. Nat Rev Mol Cell Biol, 2003. 4(7): p. 566-77.

2. van der Zwaag, P.A., et al., Phospholamban R14del mutation in patients diagnosed with dilated cardiomyopathy or arrhythmogenic right ventricular cardiomyopathy: evidence supporting the concept of arrhythmogenic cardiomyopathy. Eur J Heart Fail, 2012. 14(11): p. 1199-207.

3. Haghighi, K., et al., A mutation in the human phospholamban gene, deleting arginine 14, results in lethal, hereditary cardiomyopathy. Proc Natl Acad Sci U S A, 2006. 103(5): p. 1388-93.

4. Vostrikov, V.V., et al., Effects of naturally occurring arginine 14 deletion on phospholamban conformational dynamics and membrane interactions. Biochim Biophys Acta, 2015. 1848(1 Pt B): p. 315-22.

5. Te Rijdt, W.P., et al., Phospholamban p.Arg14del cardiomyopathy is characterized by phospholamban aggregates, aggresomes, and autophagic degradation. Histopathology, 2016. 69(4): p. 542-50.

6. Bers, D.M., Cardiac excitation-contraction coupling. Nature, 2002. 415(6868): p. 198-205.

7. Zhang, X.H., et al., Ca2+ signaling in human induced pluripotent stem cell-derived cardiomyocytes (iPS-CM) from normal and catecholaminergic polymorphic ventricular tachycardia (CPVT)-afflicted subjects. Cell Calcium, 2013. 54(2): p. 57-70.

8. Niedergerke, R., The staircase phenomenon and the action of calcium on the heart. J Physiol, 1956. 134(3): p. 569-83.

9. Hajdu, S., Mechanism of the Woodworth staircase phenomenon in heart and skeletal muscle American Journal of Physiology, 1969. 216: p. 206-214.

10. Micheletti R, et al., Istaroxime, a Stimulator of Sarcoplasmic Reticulum Calcium Adenosine Triphosphatase Isoform 2a Activity, as a Novel Therapeutic Approach to Heart Failure. Am J Cardiol., 2007. 99(2A): p. 24A-32A.

11. Huang, C.L., SERCA2a stimulation by istaroxime: a novel mechanism of action with translational implications. Br J Pharmacol, 2013. 170(3): p. 486-8.

12. Rocchetti, Modulation of Sarcoplasmic Reticulum Function by Na /K Pump Inhibitors with Different Toxicity: Digoxin and PST2744 [(E,Z)-3-((2-Aminoethoxy)imino)androstane-6,17-dione Hydrochloride]. The Journal Of Pharmacology and Experimental Therapeutics, 2005. Vol. 313(No. 1 ): p. 207–215.

13. Gheorghiade, M., et al., Hemodynamic, echocardiographic, and neurohormonal effects of istaroxime, a novel intravenous inotropic and lusitropic agent: a randomized controlled trial in patients hospitalized with heart failure. J Am Coll Cardiol, 2008. 51(23): p. 2276-85.

14. Gustavsson, M., et al., Allosteric regulation of SERCA by phosphorylation-mediated conformational shift of phospholamban. Proc Natl Acad Sci U S A, 2013. 110(43): p. 17338-43.

15. Rocchetti, M., et al., Modulation of sarcoplasmic reticulum function by PST2744 [istaroxime; (E,Z)-3-((2-aminoethoxy)imino) androstane-6,17-dione hydrochloride)] in a pressure-overload heart failure model. J Pharmacol Exp Ther, 2008. 326(3): p. 957-65.

16. Ferrandi, M., et al., Istaroxime stimulates SERCA2a and accelerates calcium cycling in heart failure by relieving phospholamban inhibition. British Journal of Pharmacology, 2013. 169: p. 1849–1861.

17. Kranias, E.G., Regulation of Ca2+ transport by cyclic 3',5'-AMP-dependent and calcium-calmodulin-dependent phosphorylation of cardiac sarcoplasmic reticulum. Biochim Biophys Acta, 1985. 844(2): p. 193-9.

18. Hattori, Y., J. Toyama, and I. Kodama, Cytosolic calcium staircase in ventricular myocytes isolated from guinea pigs and rats Cardiovascular research, 1991. 25: p. 622-629.

19. Palomeque, J., M.G. Vila Petroff, and A. Mattiazzi, Pacing staircase phenomenon in the heart: from Bodwitch to the XXI century. Heart Lung Circ, 2004. 13(4): p. 410-20.

20. Palomeque, J., et al., Multiple alterations in Ca2+ handling determine the negative staircase in a cellular heart failure model. J Card Fail, 2007. 13(2): p. 143-54.

21. Henry, P.D., Positive staircase effect in the rat heart. Am J Physiol, 1975. 228(2): p. 360-4.

22. Hwang, H.S., et al., Comparable calcium handling of human iPSC-derived cardiomyocytes generated by multiple laboratories. J Mol Cell Cardiol, 2015. 85: p. 79-88.

23. Machiraju, P. and S.C. Greenway, Current methods for the maturation of induced pluripotent stem cellderived cardiomyocytes. World Journal of Stem Cells, 2019. 11(1): p. 33-43.

# Chapter 5

## *Summary and Conclusions*

The interplay between ventricular repolarization and intracellular $Ca^{2+}$ handling is crucial to maintain the physiological ECC in cardiomyocytes. Both intracellular $Ca^{2+}$ and SR $Ca^{2+}$ load play a crucial role in this mechanism and they are influenced, and controlled, by several factors. Among them, the non-physiological action potential duration (APD) prolongation affects the sarcolemmal $Ca^{2+}$ influx/efflux balance [1] thus it represents a stress-condition for intracellular $Ca^{2+}$ homeostasis, requiring robust compensatory mechanisms [2]. This may be critical in pathological conditions, such as HF, where intracellular $Ca^{2+}$ handling is impaired. Indeed, conditions in which the SR $Ca^{2+}$ handling is altered could represent a trigger to induce arrhythmogenic afterdepolarizations (DADs or EADs) [3]. On the other hand, prolonged repolarization and arrhythmias are often associated, albeit the concomitance of multiple factors, such as peptides or polymorphisms in proteins involved in the ECC, might be necessary to produce arrhythmogenesis.

This thesis has the purpose to demonstrate how APD prolongation per se could be insufficient to induce arrhythmias, thus the presence of concomitant factors such as ATII (**Chapter 2**) or NOS1AP polymorphisms (**Chapter 3**), are necessary to produce arrhytmogenesis.

Similarly, other mechanisms not strictly correlated to the SR, seem to be involved in the generation of the phenotype of HF patients affected by the PLN-R14Del mutation (**Chapter 4**).

In particular, in **Chapter 2** we wanted to demonstrate how ATII correlates with β-adrenergic stimulation (isoproterenol-induced) and APD prolongation to induce SR instability [4]. APD prolongation per se significantly increased $I_{TI}$ incidence and reduced the threshold for $I_{TI}$ induction by isoproterenol. In the presence of a normal APD, ATII significantly facilitated $I_{TI}$ induction at all concentrations of β-adrenergic stimulation. However, $I_{TI}$ facilitation by ATII prevailed at low isoproterenol concentrations, which failed to induce $I_{TI}$ events on

their own. Thus, in the presence of ATII, isoproterenol effect approached saturation. Overall, this may suggest that ATII facilitated $I_{TI}$ events by mechanisms other than those triggered by β-adrenergic activation, but converging with them to impair SR stability.

The arrhytmogenic effect of β-adrenergic stimulation occurring in APD prolongation conditions was abolished by APD shortening. However, ATII increased the incidence and magnitude of $I_{TI}$ and it reduced the efficacy of APD shortening in abolishing $I_{TI}$.

Considering that ATII activates membrane phospholipase C, resulting in production of $IP_3$ and diacylglycerol, in this work it has been assessed whether $IP_3R$ activation could contribute to spontaneous $Ca^{2+}$ release facilitation by ATII. Indeed IP3R blockade reduced incidence and magnitude of $I_{TI}$ events evoked by ATII and isoproterenol. The present results suggest that $IP_3R$ activation, possibly through an increment of cytosolic $Ca^{2+}$, may indeed facilitate $Ca^{2+}$ waves under the conditions generated by APD prolongation and β-adrenergic stimulation.

Overall, this work suggests that, in cardiomyocytes, ATII signaling might act as a variable co-factor in determining the impact of repolarization abnormalities on SR stability and the resulting arrhythmias.

Since ATII and its receptor AT1R are upregulated in cardiac diseases, drugs commonly used in cardiovascular therapy, such as ACE inhibitors or AT1R antagonists, would find a new indication in the prevention of arrhythmias in genetic and acquired conditions of prolonged repolarization.

In **Chapter 3**, we wanted to test the effects of NOS1 inhibition and their interaction with prolonged APD in a guinea pig myocyte LQT1 model. Moreover, we wanted to investigate whether hiPSC-CMs from LQT1 patients differing for NOS1AP variants and mutation penetrance display a phenotype compatible with NOS1 deficiency.

In the animal model of LQT1, induction of marked SR instability by NOS1 inhibition was associated with $I_{CaL}$ and $I_{NaL}$ enhancement and further APD

prolongation. SR instability induced by NOS1 inhibition did not ensue if APD was kept constant and, once present, was suppressed by shortening the APD.

In hiPSC-CMs from symptomatic (S) and asymptomatic (AS) LQT1 patients, larger $I_{CaL}$, longer APD and more afterdepolarizations differentiated S (carrying the minor NOS1AP allele) from AS (carrying the major NOS1AP allele) cells. Moreover, the expression and co-localization of NOS1AP and NOS1 proteins were lower in S than in AS cells. The effects of NOS1 inhibition on intracellular $Ca^{2+}$ dynamics were consistent with those on electrophysiology, but of small magnitude.

Overall, the findings of this chapter establish a mechanistic link between NOS1AP SNPs and aggravation of the arrhythmia phenotype in prolonged repolarization syndromes.

The work of **Chapter 4**, which is still in preparation, is focused on the characterization of a PLN mutation, the R14Del, which has been correlated with SR and $Ca^{2+}$ handling dysfunctions [5]. Patients carrying this mutation present severe symptoms of both dilated and arrhythmogenic cardiomyopathies, and in the long term, the development of fibrosis and cardiac remodeling. Nevertheless, the molecular mechanisms involved in the pathophysiology of the mutation are still not clear.

Among all PLN mutations [6], the PLN-R14Del has been considered the most superinhibitory mutation so far [5, 6]; nevertheless, recent findings have demonstrated other suitable mechanisms involved in the pathophysiology of this mutation [7, 8]. In a model of hiPSC-CMs carrying the PLN-R14Del mutation, plated in a monolayer format, our preliminary results suggest that the mutation leads to a PLN loss-of-function, which is in contrast with the superinhibitory phenotype observed previously by others. By the use of PST3093, the long-lasting metabolite of Istaroxime [9], which is a luso/inotropic drug that binds PLN and prevents PLN/SERCA2a interaction, we demonstrated that mutant hiPSC-CMs

have a functional SR, with enhanced SERCA2a activity, compared to their isogenic controls.

The results obtained from this study change the actual knowledge on the PLN-R14Del mutation. Our hypothesis is that the latter does not specifically correlate with PLN/SERCA2a interaction, but the severe phenotype of the patients is probably due to a displacement of PLN from the SR, which maybe accumulate in the cytosol leading to cellular toxicity. This last chance needs to be confirmed in the future.

## CONCLUSIONS

In conclusion, this thesis wants to focus on the mechanisms involved in SR-correlated genetic pathologies, which have both a fundamental and translational value. This could be useful to help patients affected by cardiac diseases, in the context of prolonged repolarization syndromes and $Ca^{2+}$ handling dysfunction.

## References


1. Bers, D.M., Cardiac excitation-contraction coupling. Nature, 2002. 415(6868): p. 198-205.

2. Nattel, S., et al., Arrhythmogenic ion-channel remodeling in the heart: heart failure, myocardial infarction, and atrial fibrillation. Physiol Rev, 2007. 87(2): p. 425-56.

3. Nattel, S. and D. Dobrev, The multidimensional role of calcium in atrial fibrillation pathophysiology: mechanistic insights and therapeutic opportunities. European Heart Journal, 2012. 33: p. 1870–1877.

4. Ronchi, C., et al., Action Potential Prolongation, beta-Adrenergic Stimulation, and Angiotensin II as Co-factors in Sarcoplasmic Reticulum Instability. Front Physiol, 2018. 9: p. 1893.

5. Haghighi, K., et al., A mutation in the human phospholamban gene, deleting arginine 14, results in lethal, hereditary cardiomyopathy. PNAS, 2006. 103: p. 1388–1393.

6. Hof, I.E., et al., Prevalence and cardiac phenotype of patients with a phospholamban mutation. Neth Heart J, 2019. 27(2): p. 64-69.

7. Rijdt, W.P.t., et al., Phospholamban p.Arg14del cardiomyopathy is characterized by phospholamban aggregates, aggresomes, and autophagic degradation. Histopathology, 2016. 69: p. 542–550.

8. Vostrikov, V.V., et al., Effects of naturally occurring arginine 14 deletion on phospholamban conformational dynamics and membrane interactions. Biochimica et Biophysica Acta, 2015. 1848: p. 315-322.

9. Ferrandi, M., et al., Istaroxime stimulates SERCA2a and accelerates calcium cycling in heart failure by relieving phospholamban inhibition. Br J Pharmacol, 2013. 169(8): p. 1849-61.

# Chapter 6

## *Published papers*

1. **Badone, B.**, Ronchi, C., Kotta, M. C., Sala, L., Ghidoni, A., Crotti, L., & Zaza, A. (2018). Calmodulinopathy: functional effects of CALM mutations and their relationship with clinical phenotypes. *Frontiers in cardiovascular medicine*, *5*.

2. Kotta, M. C., Sala, L., Ghidoni, A., **Badone, B.**, Ronchi, C., Parati, G., ... & Crotti, L. (2018). Calmodulinopathy: a novel, life-threatening clinical entity affecting the young. *Frontiers in cardiovascular medicine*, *5*, 175.

frontiers in Cardiovascular Medicine

REVIEW
published: 11 December 2018
doi: 10.3389/fcvm.2018.00176

# Calmodulinopathy: Functional Effects of CALM Mutations and Their Relationship With Clinical Phenotypes

*Beatrice Badone[1], Carlotta Ronchi[1], Maria-Christina Kotta[2], Luca Sala[2], Alice Ghidoni[2], Lia Crotti[2,3,4†] and Antonio Zaza[1*†]*

[1] Department of Biotechnology and Bioscience, University of Milano-Bicocca, Milan, Italy, [2] Center for Cardiac Arrhythmias of Genetic Origin and Laboratory of Cardiovascular Genetics, Istituto Auxologico Italiano, IRCCS, Milan, Italy, [3] Department of Medicine and Surgery, University of Milano-Bicocca, Milan, Italy, [4] Department of Cardiovascular, Neural and Metabolic Sciences, San Luca Hospital, Istituto Auxologico Italiano, IRCCS, Milan, Italy

In spite of the widespread role of calmodulin (CaM) in cellular signaling, CaM mutations lead specifically to cardiac manifestations, characterized by remarkable electrical instability and a high incidence of sudden death at young age. Penetrance of the mutations is surprisingly high, thus postulating a high degree of functional dominance. According to the clinical patterns, arrhythmogenesis in CaM mutations can be attributed, in the majority of cases, to either prolonged repolarization (as in long-QT syndrome, LQTS phenotype), or to instability of the intracellular $Ca^{2+}$ store (as in catecholamine-induced tachycardias, CPVT phenotype). This review discusses how mutations affect CaM signaling function and how this may relate to the distinct arrhythmia phenotypes/mechanisms observed in patients; this involves mechanistic interpretation of negative dominance and mutation-specific CaM-target interactions. Knowledge of the mechanisms involved may allow critical approach to clinical manifestations and aid in the development of therapeutic strategies for "calmodulinopathies," a recently identified nosological entity.

**Keywords: calmodulin mutations, ion channels, repolarization, $Ca^{2+}$ handling, arrhythmia mechanisms**

OPEN ACCESS

***Edited by:***
*Gaetano M. De Ferrari, University of Pavia, Italy*

***Reviewed by:***
*Osmar Antonio Centurion, Universidad Nacional De Asunción, Paraguay*
*Anna Pfenniger, Northwestern Medicine, United States*

***Correspondence:**
*Antonio Zaza*
*antonio.zaza@unimib.it*

*†These authors share senior authorship*

***Specialty section:***
*This article was submitted to Cardiac Rhythmology, a section of the journal Frontiers in Cardiovascular Medicine*

***Received:*** *05 September 2018*
***Accepted:*** *22 November 2018*
***Published:*** *11 December 2018*

***Citation:***
*Badone B, Ronchi C, Kotta M-C, Sala L, Ghidoni A, Crotti L and Zaza A (2018) Calmodulinopathy: Functional Effects of CALM Mutations and Their Relationship With Clinical Phenotypes. Front. Cardiovasc. Med. 5:176. doi: 10.3389/fcvm.2018.00176*

## INTRODUCTION

As other ions, $Ca^{2+}$ is used as a charge carrier to modulate membrane potential; however, $Ca^{2+}$ also has a central role as a diffusible signaling molecule and as a trigger of diverse cellular functions. While some of these are clearly complementary in achieving a functional goal (e.g., cAMP signaling in functional upregulation) and can coexist, others are devoted to apparently competing aims (e.g., apoptosis pathway) and need to be separated. This requires mechanisms allowing intracellular $Ca^{2+}$ to act on its targets with high specificity. Several strategies are employed by the cell to achieve this goal. $Ca^{2+}$ buffering by intracellular proteins and small molecules, leads to a strictly controlled mobility of the ion. Active $Ca^{2+}$ compartmentalization within organelles allows to keep "resting" $Ca^{2+}$ concentration in the general (or "bulk") cytosolic compartment at very low levels (around $10^{-7}$ M), i.e., below the threshold required to activate downstream effectors; at the same time, structural organization (e.g., T-tubules) allows very small $Ca^{2+}$ fluxes to achieve high $Ca^{2+}$ concentration in the specific subcellular compartment hosting the target effector (1).

The presence of molecules devoted to detect $Ca^{2+}$ and transduce its concentration changes into specific actions is a further strategy, pivotal to the integrated operation of $Ca^{2+}$-dependent processes. Perhaps the most diffuse of such "$Ca^{2+}$ sensor" molecules is calmodulin (CaM), a protein present in all cell types and highly conserved throughout evolution (1). Most $Ca^{2+}$-binding proteins are characterized by "EF hand" domains, which constitute the ion binding site. Whereas, in proteins involved in $Ca^{2+}$ buffering and controlled mobility the EF hand is simply a binding site, in $Ca^{2+}$ sensors the EF domain changes protein conformation in response to $Ca^{2+}$ binding, thus triggering a variety of downstream events (2).

Essential to CaM's targeting role, is its property to stably bind to many of its downstream effectors. This corresponds to the presence on the latter of specific CaM-binding sequences, which make CaM an integral component of the target protein. Thus, CaM can exist as a freely diffusible signal (cytosolic pool), or as a sensor intrinsic to a given effector (bound pool), thus affording either diffuse or highly confined signaling. Furthermore, in various cells types, the cytosolic CaM pool can be redistributed to the nuclear compartment upon a rise in $Ca^{2+}$ levels, thus broadening the targets range (3, 4). Also, except in selected cell types (e.g., mitotic cells), local CaM concentrations may follow $Ca^{2+}$ oscillations, thus generating spatial and temporal patterns which may play a crucial role in biological processes (5).

In keeping with its central and evolutionarily conserved function, CaM is generated in a highly redundant mode. Indeed, an identical amino acid sequence is encoded by 3 CaM genes (CALM 1, 2, and 3) (5). Such redundancy is in apparent contrast with the high penetrance of heterozygous CaM mutations. While the possible role of transcriptional regulation of these genes is discussed in the accompanying article (6), specific molecular mechanisms may contribute to negative dominance in a mutation's effect.

In cardiac muscle cells, $Ca^{2+}$ at the same time contributes as a charge carrier to electrical excitation (the "action potential," AP) and triggers the development of mechanical force; therefore, $Ca^{2+}$ is crucial to excitation-contraction coupling (ECC) (7). Several processes central to beat-to beat control of intracellular $Ca^{2+}$ dynamics are CaM-mediated; furthermore, CaM acts a $Ca^{2+}$ sensor in the control of gene expression, thus playing a role in long-term modulation of cell function and fate (8). This might lead to the expectation that a CaM loss of function should result in general myocyte dysfunction and death. However, this is contradicted by the observation that CaM mutations affect only the function of specific targets, leading to mutation-specific phenotypes with pronounced electrical instability as a common feature (9).

Our objective is to revise the information available on the various aspects of CaM structure/function that we see as potentially relevant to a mechanistic interpretation of CaM mutations phenotypes, with a focus on cardiac ones.

## CaM Structure, $Ca^{2+}$-Sensing and Target Recognition

CaM is composed of 149 amino acid residues to form a 17 kDa protein. The protein is ubiquitous and expressed in all eukaryotic cells, with 100% identity in its amino acid sequence among vertebrates. Three genes (CALM1, CALM2, and CALM3) encode CaM with an identical amino acid sequence, thus resulting in potential redundancy (10).

CaM is formed of two "lobes," named N and C, respectively, according to their position with respect to protein ends, connected by an α-helix "linker" containing a flexible region ("hinge") (**Figure 1**) (12); this allows each lobe to move relative to the other. Each lobe consists of two "EF hand" domains (EF) with one $Ca^{2+}$ binding site each (2 $Ca^{2+}$ binding sites per lobe). All EF hand domains can bind $Ca^{2+}$; however, while the N-lobe (EF I and EF II) has higher affinity for $Mg^{2+}$, the C-lobe (EF III and EF IV) binds $Ca^{2+}$ with ten times higher affinity (13). Another functional distinction between the two CaM lobes is the rate of $Ca^{2+}$ binding and unbinding, faster for the N-lobe than for the C-lobe (14).

Knowledge of CaM's 3D structure has evolved since its first description in 1985 (15), with a major contribution provided, 10 years later, by nuclear magnetic resonance (16). Whereas, this technology revealed detail of the linker helix accounting for its flexibility (17, 18), more recent studies added information about recognition of target proteins and how it can be affected by CaM complexing with $Ca^{2+}$ (12, 19).

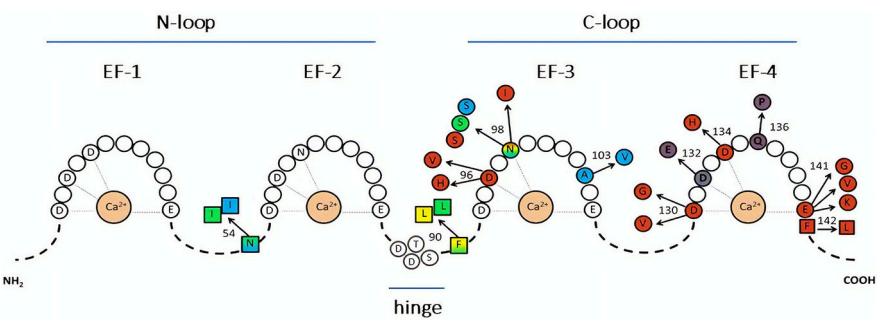


**FIGURE 1 |** Representation of CaM sequence and relative disease-associated mutations. The letters identify amino acids directly involved in $Ca^{2+}$ binding (within the EF-hands), or in the hinge region. Color-substituted amino acids represent mutations in the EF-hands (circles) or in the linkers (squares); colors correspond to the associated phenotype: catecholaminergic polymorphic ventricular tachycardia (CPVT, light blue), long QT syndrome (LQTS, red), idiopathic ventricular fibrillation (IVF, yellow), other unexplained sudden death (green). LQTS/CPVT overlap mutations are shown in shaded color. Modified from Crotti and Kotta, (11).

The interplay between structure and function is relevant to the three components of CaM signaling: $Ca^{2+}$ binding, target binding, and target modulation.

The first aspect of interest is CaM's interaction with $Ca^{2+}$. In apo-CaM (the $Ca^{2+}$ unloaded CaM), EF I and EF II (N-lobe) are in a packed conformation, thus with low affinity for $Ca^{2+}$; EF III and EF IV (C-lobe) are instead in a partially open conformation, more prone to $Ca^{2+}$ binding. At resting $Ca^{2+}$ levels (about $10^{-7}$ M), all CaM binding sites are typically unoccupied. When $Ca^{2+}$ rises, its binding to the C-lobe sites triggers a conformational change leading the N-lobe to increase its affinity for $Ca^{2+}$. In other words, $Ca^{2+}$ binding to CaM is "cooperative," i.e., the overall affinity increases when $Ca^{2+}$ concentration exceeds the threshold for C-lobe occupation. CaM can potentially bind 1–4 $Ca^{2+}$ ions; activation of downstream targets requires CaM being loaded with 3 $Ca^{2+}$ ions at least (12), a configuration referred to as "holo-CaM."

Also of interest are the structural aspects of CaM's interaction with target proteins, which are necessary for modulation of their activity. "Anchor" domains on target proteins are characterized by hydrophobic residue sequences flanked by negatively charged ones; the latter provide electrostatic interaction that may orient CaM binding (12). Many CaM targets (e.g., $Ca_v1.2$) are characterized by the presence of a typical basic amino acid sequence called the "IQ motif." The IQ motif is closely preceded by a "preIQ" region, which is a common site of permanent CaM binding (20). CaM interaction with the IQ motif itself is instead more likely responsible for downstream signaling (8, 14); indeed, specificity of the IQ sequence may dictate whether $Ca^{2+}$-CaM signaling leads to target activation or inhibition (20). A well-studied instance of preIQ-IQ binding is CaM interaction with the voltage-dependent L-type $Ca^{2+}$-channel ($Ca_v1.2$); the detailed mechanism and $Ca^{2+}$-dependency of this specific interaction will be described in paragraph Voltage-gated $Ca^{2+}$ channels (Cav1.2).

As for $Ca^{2+}$ sensing, CaM domains mainly involved in target binding are the lobes. Both CaM lobes contain nine methionine residues, playing a key role in target recognition, whose high flexibility provides plasticity crucial for this function (21).

The CaM binding interface is highly structured, but it may dynamically accommodate various binding modes in a metastable equilibrium. $Ca^{2+}$ may stabilize a given interface conformation (12). $Ca^{2+}$-dependency of CaM binding differs among target proteins. While holo-CaM is strictly required for strong target binding in some cases, in others target interaction occurs preferentially at lower levels of occupancy by $Ca^{2+}$. This accounts for the finding that CaM may be bound to many targets at resting $Ca^{2+}$ concentrations (8, 12, 22). At low $Ca^{2+}$ the N-lobe has higher stability than the C-lobe (23), which favors its binding in the apo form (pre-association) (8). On the other hand, due to its higher $Ca^{2+}$ affinity, the C-lobe is more often involved in $Ca^{2+}$-dependent target binding than the N-lobe (12, 24) and both the N- and C-lobes may participate to stabilize the protein-target complex (25).

$Ca^{2+}$ binding changes CaM conformation to expose hydrophobic (methionine-rich) sites, either at the N-lobe or at the C-lobe, suitable to interact with hydrophobic residues in the anchor (18). The large size and flexibility of CaM interaction landscape is essential to accommodate a variety of "anchor" side-chains, thus providing CaM with its extraordinary pleiotropicity. Nonetheless, the observation that single site mutations may selectively affect CaM binding to a specific target suggests high specificity of the binding interface. Less information exists about the target binding mode of apo-CaM. The main differences with holo-CaM binding may concern the N-lobe and a larger involvement of electrostatic interactions (12).

Consistent with the notion that CaM lobes change their conformation when interacting with the target, the relationship between target and $Ca^{2+}$ binding by CaM is mutual: binding to the target may increase CaM affinity for $Ca^{2+}$ (12); this generates cooperativity in $Ca^{2+}$-dependency of CaM-target interactions. According to modeling data (26), differences among targets in the extent of such cooperativity contribute to specificity of target recognition.

The third aspect of CaM signaling is modulation of target function which, depending on the target, can be either stimulatory or inhibitory. Target modulation can be either enacted by apo-CaM, or require $Ca^{2+}$ binding and its mechanism differs among targets (see below examples for RyR and $Ca_v1.2$ channels). As a general interpretational scheme, CaM binding may stabilize an otherwise short-lived configuration, spontaneously assumed by the target protein and associated with a specific functional state (12).

## "Free" and "Pre-Bound" CaM Pools

Many CaM targets have been described so far. These include proteins involved in cell cycle, cell proliferation and autophagy (in healthy cells), tumor progression proteins (in cancerous cells) (5), proteins essential to cell communication and metabolism (27), and a wide number of ion channels (28–30). Most of these targets strictly require CaM pre-association to allow their regulation (31).

To better understand the role of CaM in cells, we need to consider its distribution between the "free" (cytosolic) and "pre-bound" pools. As mentioned previously, such a distribution may vary according to CaM's occupancy by $Ca^{2+}$ (25).

Total CaM concentration is variable among tissues: it usually ranges between 5 and 40 $\mu$M (e.g. ,about 6 $\mu$M in intact myocytes) (32), but values up to 100 $\mu$M have been described in specific cell types (e.g., in the testis) (33). In cardiomyocytes, even at diastolic $Ca^{2+}$ concentration, 99% of total intracellular CaM is bound to cellular proteins, leaving about 50-100 nM of free CaM (1%) in the cell (32). Nonetheless, the proportion of CaM in the pre-bound pool is variable among tissue types (e.g., 11% in testis and 63% in spleen), and it may differ between normal and pathological cells and depend on environmental factors, such as cell density in culture (5). The pre-bound CaM pool includes mainly apo-CaM or CaM with incomplete occupancy, depending on the target (32); its functional relevance may be to increase speed of target response to local $Ca^{2+}$ elevation.

The pre-bound CaM pool localizes to structures in the plasma membrane as well as in intracellular organelles; under resting $Ca^{2+}$ concentrations (e.g., 100 nM), pre-bound CaM may largely exist as apo-CaM. Pre-bound apo-CaM may even be released to the free CaM pool in response to $Ca^{2+}$ elevation,

thus representing a local diffusible CaM store (22); this is true particularly in growing cells, where CaM is highly expressed.

As $Ca^{2+}$ occupancy increases, CaM becomes almost completely bound to targets, thus leaving a very small pool of freely diffusible holo-CaM. Competition among targets for this pool may be of significance for their reciprocal regulation (32). Even if the CaM-target interaction is generally facilitated by $Ca^{2+}$, the pattern is quite complex. Chin and Means (22) identified at least six CaM target groups, according to their CaM recognition sequences and $Ca^{2+}$-dependency of binding. Some of them are strongly pre-bound to apo-CaM, for others binding is stronger for holo-CaM, while, finally, apo-CaM binding to a class of targets can be released by $Ca^{2+}$, thus providing a local reservoir for free CaM.

# CAM MODULATION OF VOLTAGE-GATED CHANNELS

## Voltage-Gated $Ca^{2+}$ Channels ($Ca_v1.2$)

$Ca^{2+}$ current from $Ca_v1.2$ channels ($I_{CaL}$) is the most abundant type in cardiomyocytes (34). The symbol "L" recapitulates the main features of this channel (as compared to other $Ca^{2+}$ ones): large conductance, activation at larger depolarizations and long lasting openings. The activation of this channel is driven by the action potential upstroke, with $I_{CaL}$ reaching a peak in 2–7 ms. Thereafter, channels inactivate with time constants in the order of 50–100 ms at plateau potential, due to both $Ca^{2+}$ and voltage-dependent gating (35). $Ca^{2+}$ influx through $I_{CaL}$ leads to a rapid increase of cytosolic $Ca^{2+}$ concentration in the confined space between the sarcolemmal and sarcoplamic reticulum (SR) membranes (also called "dyadic cleft"). This is responsible for the opening of ryanodine receptors (RyRs), $Ca^{2+}$-activated $Ca^{2+}$channels clustered in the SR membrane facing $Ca_v1.2$ channels.

$I_{CaL}$ is modulated by two feedback signals that, albeit of opposite sign, are both dependent on the rise of $Ca^{2+}$ concentration close to cytosolic mouth of the channel and involve CaM. $Ca^{2+}$-dependent inactivation (CDI) is responsible for most of the rapid $I_{CaL}$ decay occurring during sustained depolarization (35). $Ca^{2+}$-dependent facilitation (CDF), a weaker phenomenon, reflects instead the increase in $I_{CaL}$ peak conductance that may be observed during repetitive activation at high rates (36). Both CDF and CDI depend on $Ca^{2+}$-CaM complexing (37). Earlier studies (37) reported that, whereas replacement of isoleucine or glutamine to alanine in the IQ motif of the C-terminal region of the $Ca_v1.2$ channel $\alpha_{1C}$ subunit abolished CDI but enhanced CDF, replacement of isoleucine to glutamate in the same region abolished both forms of auto-regulation. This led to the conclusion that CDI and CDF had different mechanisms, but that CaM binding to the IQ motif is involved in both cases.

$Ca_v1.2$ channels are constitutively associated with apo-CaM. Such pre-association is required since CaMs from the cytosolic bulk are unable to adequately access the binding site on $Ca_v1.2$ during $Ca^{2+}$ inflow (38); pre-association to the C-terminal region of $Ca_v1.2$ places CaM within a nanodomain at channel cytosolic mouth. This location confers to the C-lobe of pre-bound CaM the ability to sense $Ca^{2+}$ changes in temporal relation to channel gating (14).

### CDI Mechanism

According to a recent interaction model, apo-CaM is constitutively tethered (pre-bound pool) to a pre-IQ motif present on the C-terminus of the $\alpha_{1C}$ channel subunit. Such "pre-association" involves the N-lobe and occurs at resting $Ca^{2+}$ concentrations. Signaling activation by $Ca^{2+}$ elevation (i.e., CDI induction) requires $Ca^{2+}$ binding to the C-lobe, whose affinity for the target IQ motif is thus increased; C-lobe interaction with the IQ motif stabilizes the channel conformational state associated with CDI (8) (**Figure 2**). CDI has been further modeled as transitions between different states: apo-CaM release from the pre-association site, formation of the $Ca^{2+}$-CaM complex, its subsequent binding to the effector site (14). The novel and most relevant feature of this model is that, using the difference in the kinetics of $Ca^{2+}$ binding and unbinding between the C- and N-lobes (faster for the N-lobe), identifies their respective role in sensing $Ca^{2+}$ at the channel mouth (local sensing, largely insensitive to intracellular $Ca^{2+}$ buffering) vs. global cell $Ca^{2+}$ (sensitive to even weak $Ca^{2+}$ buffering). Unlike in neuronal channel isoforms, $Ca_v1.2$ channels retain robust CDI even in the presence of strong $Ca^{2+}$ buffering; such form of CDI is entirely triggered by $Ca^{2+}$ association with the C-lobe (39). Numerical modeling provides the (counterintuitive) conclusion that, if associated with slow CaM-channel interaction kinetics, fast $Ca^{2+}$ binding/unbinding (typical of the N-lobe) may best support selective sensing of a smaller but sustained $Ca^{2+}$ signal (14). The latter is typical of CDI in non-cardiac channel isoforms (39).

### CDF Mechanism

As discussed above, earlier studies indicated that CDF requires an intact anchoring region on the channel C-terminus, thus suggesting that pre-bound CaM is involved (37). Nonetheless, there is now general agreement that, unlike CDI, CDF is operated by $Ca^{2+}$-CaM dependent activation of calmodulin-kinase II (CaMKII), which then phosphorylates the $Ca_v1.2$ channel at two serine residues close to the EF-hand motif (40) (**Figure 2**); mutation of these two serine residues abolished CDF but did significantly affect CDI (40), hence confirming independent mechanisms for these processes. Notably, CaMKII phosphorylation of nearby serine residues also induces Mode2 gating of the channel (41). Thus, at variance with CDI, CDF is the consequence of protein phosphorylation, dependent on CaM, but not directly operated by it.

## Voltage-Gated $K^+$ Channels ($K_v7.1$)

$K_v7.1$ is a $K^+$-selective channel which, in association with KCNE subunits, carries the slow component of the delayed-rectifier current ($I_{Ks}$). $I_{Ks}$ gating is positively regulated by cytosolic $Ca^{2+}$ through a CaM-dependent process (42), with an effect similar to that of the membrane constituent phosphatidylinositol-4,5-bisphosphate (PIP2). Indeed, PIP2 and the N-lobe of CaM competitively interact at the same site on the $K_v7.1$ protein (the helix B on the proximal C terminus). Interpretation of the

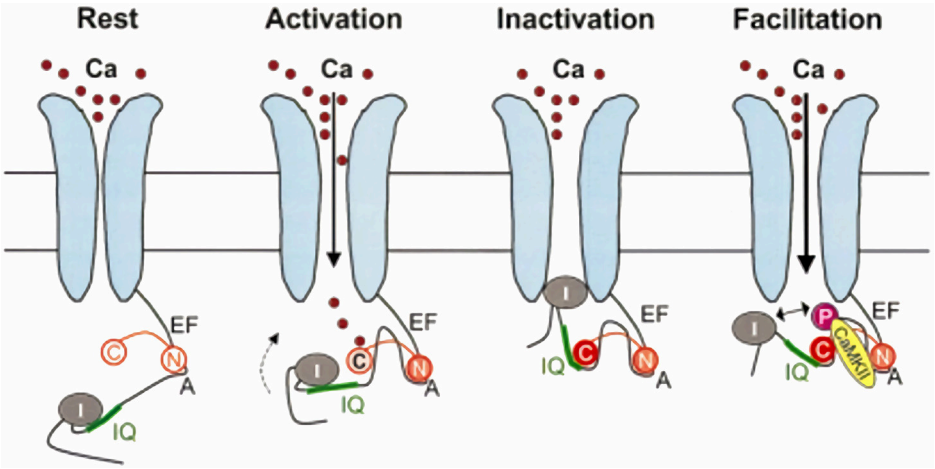


**FIGURE 2 |** Model for CaM-dependent modulation of $Ca_v1.2$ channels ($I_{CaL}$). *CDI mechanism*: in the channel closed state (Rest), the N-lobe of apo-CaM (N) is constitutively bound to a pre-IQ region (A) in the channel C-terminus. When the channel opens (Activation), the CaM C-lobe (C) binds to the entering $Ca^{2+}$, which increases its affinity for the channel IQ-domain; this moves the channel inactivation particle (I) in the permeation path (Inactivation). *CDF mechanism*: holo-CaM binding to CaMKII promotes channel phosphorylation, which results in repulsion of the inactivation particle from the permeation pore (Facilitation). Modified from Maier and Bers (8).

effect of a helix B $K_v7.1$ mutant (K526E) and of interference of $Ca^{2+}$-CaM with $K_v7.1$ pull-down by PIP2 has led to the following model: at diastolic $Ca^{2+}$ levels, CaM is bound to a non-activating $K_v7.1$ site (helix A) by its apo-C-lobe; the N-lobe is displaced from the helix B site. As cytosolic $Ca^{2+}$ increases, calcification of the C-lobe causes its dissociation from helix A and the N-lobe then interacts with its site on the helix B; this results in stabilization of the channel open state (43). According to an alternative model, at resting $Ca^{2+}$ levels the C- and N-lobes are permanently bound to the channel (at helices A and B, respectively) and limit its open probability; when $Ca^{2+}$ increases, N-lobe binding is reinforced and C-lobe is released thereby relieving the inhibitory effect on channel gating (44).

Both models imply that CaM binding to $K_v7.1$ and positive regulation of $I_{Ks}$ are separate processes. Binding occurs in the apo-CaM form (pre-bound pool), $I_{Ks}$ enhancement requires $Ca^{2+}$ elevation. Furthermore, both CaM lobes are involved and a preserved C-lobe $Ca^{2+}$ affinity is essential for the signaling function.

PIP2 is a membrane phospholipid degraded by phospholipase C (PLC) to produce inositol 3-phosphate (IP3) in response to activation of a number of membrane receptors associated with $G_q$ proteins. Receptor activation may result in PIP2 depletion, which would reduce $I_{Ks}$; however, IP3-induced $Ca^{2+}$ release from the sarcoplasmic reticulum may compensate PIP2 reduction by activating positive $I_{Ks}$ regulation by $Ca^{2+}$-CaM. This may represent the main physiological role of $I_{Ks}$ modulation by $Ca^{2+}$-CaM, which would therefore be of particular relevance during activation of the PLC-IP3 signaling pathway.

CaM integrity may also be necessary for $K_v7.1$ channel trafficking; indeed, mutations disrupting N- and C-lobe integrity reduce channel membrane expression (44).

It has been reported that holo-CaM complexing with KCNE4 (channel β-subunit) inhibits $I_{Ks}$ (45). While this would provide antagonism to direct holo-CaM modulation of the channel α-subunit, the physiological role of CaM-KCNE4 interaction remains unclear.

CaM-mediated $I_{Ks}$ regulation also occurs indirectly by CaMKII-mediated phosphorylation of the channel at serine 484; contrary to direct CaM modulation, phosphorylative modulation is inhibitory and may account for $I_{Ks}$ downregulation upon sustained β-adrenergic receptor activation (46).

## Voltage-Gated $Na^+$ Channels ($Na_v1.5$)

Among all voltage-gated channels involved in arrhythmogenesis, $Na_v1.5$ channels also interact with CaM. CaM binds to an IQ motif on the C-terminus of this channel in a $Ca^{2+}$-independent manner. Binding reduces CaM's affinity for $Ca^{2+}$ and does not induce the conformational changes that have been observed for $Ca_v1.2$ channels; therefore, similarities in the binding site may not necessarily translate into similarities of channel modulation. Nonetheless, disruption of the CaM binding site (by mutation of the $Na_v1.5$ IQ motif) leads to the enhancement of persistent $Na^+$ current, thus suggesting a role of CaM in stabilizing the inactivated state (47), possibly by fostering the interaction between the channel C-terminus and the II-IV linker. According to another model, CaM binding to $Na_v1.5$ channels would obstruct their direct modulation by $Ca^{2+}$; holo-CaM would lose its affinity for the channel, thus unveiling the direct modulatory site (48). In this case, failure of CaM interaction with the channel (as in the case of holo-CaM) causes a "leftward" (negative) shift of the steady-state inactivation curve (48); this would presumably reduce channel availability at diastolic potential as well as the "window" component of $I_{Na}$.

Overall, while CaM interaction with $Na_v$ and $Ca_v$ channels are somewhat similar, the consequences of CaM-dependent modulation on $Na_v$ function are less defined and, possibly, quantitatively less important.

## RYRS MODULATION BY $Ca^{2+}$ AND $Ca^{2+}$-CAM

RyRs are homotetramers of ∼2,200 kDa (each subunit is >550 kDa), containing ∼5,035 amino acid residues in total, sharing the general structure of the six-transmembrane ion channel superfamily (49). Since RyRs span the SR membrane, they have domains facing both the cytosol and the SR lumen. Of the three isoforms present in nature, RyR2 is the predominant one in cardiac myocytes, where it is organized in large clusters on the SR membrane (50). In T-tubules, RyR2 clusters are separated from sarcolemmal $Ca_v1.2$ channels by a 10–15 nm gap; thus, small $Ca^{2+}$ influx through $I_{CaL}$ exposes them to very high $Ca^{2+}$ concentrations (50, 51). This structural arrangement is generally referred to as "couplon" (52). The RyR/$Ca_v$ ratio in couplons is up to 15-fold higher in cardiac than in skeletal muscle and differs between species (53).

RyRs are strongly regulated by $Ca^{2+}$ in CaM-independent ways. At the same time, they are regulated by CaM in both $Ca^{2+}$-dependent and -independent ways. This makes investigation of CaM's role in RyRs' regulation very complex.

### CaM-Independent RyR Regulation by $Ca^{2+}$

RyR gating is highly sensitive to $Ca^{2+}$ on both sides of the SR membrane in a CaM-independent way. Although not the focus of the present review, a brief discussion of such "direct" regulation by $Ca^{2+}$ is required to understand the potential difficulty in isolating the CaM-dependent one.

Each of the N- and C-terminal domains of RyR2 contains two EF-hand $Ca^{2+}$ binding motifs (54), similar to those of CaM. These motifs are both on the cytosolic domain of RyR2; they show high (C-terminal) and low (N-terminal) affinity for $Ca^{2+}$ and induce channel opening and inactivation, respectively (55, 56). Since RyR2 inactivation occurs at $Ca^{2+}$ concentrations exceeding the physiological range, $Ca^{2+}$-dependent activation is the dominant phenomenon and the basis for the $Ca^{2+}$-induced-$Ca^{2+}$release (CICR) mechanism (7).

SR luminal $Ca^{2+}$ modulates RyR2 open probability by two CaM-independent mechanisms. The indirect one involves stabilization of the closed state by a macromolecular complex, involving calsequestrin (CASQ) and is disrupted by increases in luminal $Ca^{2+}$ (57). Sensitivity to luminal $Ca^{2+}$ is preserved after CASQ knock out. This stands for the presence of a $Ca^{2+}$-sensing mechanism on the RyR protein itself, located in a luminal domain also involved in control of $Ca^{2+}$ permeation (58). Direct lumenal $Ca^{2+}$ sensing may be important for channel activation under conditions of SR overload (59).

### CaM-Dependent RyR Regulation

CaM-dependent modulation of RyRs differs between channel isoforms, which have only ∼70% of gene homology and contain three divergent regions (60). In general, conductance of all the three RyR isoforms is reduced by CaM when cytosolic $Ca^{2+}$ is above 1 μM. At lower $Ca^{2+}$ concentrations, favoring apo-CaM and more relevant to diastole, CaM increases the open probability of RyR1 and RyR3 (61, 62), but it stabilizes the closed conformation of RyR2 (54).

RyR2 channels have high affinity (nanomolar $K_d$) for both apo-CaM and holo-CaM, thus resulting in a pre-bound CaM pool (54, 63). Apo-CaM may actually be a stronger inhibitor of RyR2 opening than holo-CaM, as indicated by relief of inhibition at $Ca^{2+}$ concentrations in the μM range (64). Therefore, CaM modulation of RyR2 gating may be largely $Ca^{2+}$-independent. Increasing $Ca^{2+}$ up to 100 μM has been reported to increase the number of CaM molecules bound to RyR2 (from 1 to 7.5 per RyR2 tetramer) (54); however, it is difficult to relate responses to such an abnormally high $Ca^{2+}$ concentration to physiological function.

Given that CaM binding domains are highly homologous between RyR1 and RyR2 (65), what may explain the $Ca^{2+}$-dependent discrepancy of CaM effects on RyR opening between RyR1 and RyR2 channels?

Mutations in both the N-terminal and central RyR2 regions similarly destabilize the channel closed state; this suggests that the latter may require interaction between these two regions ("zipping" model of RyR gating). This view is confirmed by the effect of peptides (e.g., DPc-10) interfering with such interaction (66). On the other hand, CaM binds to a domain other than those involved in zipping. According to the "inter-domain hypothesis," CaM binding to RyR2 may induce a protein conformation change that allosterically stabilizes the zipping interaction (and the closed state) (**Figure 3**). Vice versa, agents interfering with the zipping interaction may reduce CaM binding affinity (66).

A different gating model has been proposed for RyR1 channels, in which the channel CaM binding domain is followed, within about 450 residues, by a CaM-like sequence. FRET data indicate that, at high $Ca^{2+}$, the two channel domains interact with each other in the folded protein; such $Ca^{2+}$-dependent interaction is required for channel opening. Binding of holo-CaM to the channel may disrupt the activating interdomain interaction, thus explaining CaM-induced RyR1 inhibition at high $Ca^{2+}$ concentrations (68). However, this model does not explain why low $Ca^{2+}$ concentrations (favoring apo-CaM) may produce CaM-dependent RyR1 activation, which remains an open question.

Cryo-EM studies in RyR1 indicate that increasing $Ca^{2+}$ shifts CaM binding to the channel by about 3 nM, corresponding in the 3D structure to two different protein domains. In view of the fact that CaM activates RyR1 at low $Ca^{2+}$ and inhibits it at high $Ca^{2+}$, the two domains may be seen as activator and inhibitory sites, respectively. Importantly, these studies indicate that the $Ca^{2+}$-dependent shift in CaM binding site is a consequence of a rearrangement of the binding surface of CaM, rather than of RyR1 conformation (69) (which is also $Ca^{2+}$-dependent). The same technique shows that in RyR2 CaM binds to the "inhibitory site" (as identified in RyR1) already at low $Ca^{2+}$; this might explain why RyR2 is inhibited by CaM in a $Ca^{2+}$-independent way (69). Apparently at odd with these observations, FRET experiments (in the same study), measuring the position of CaM

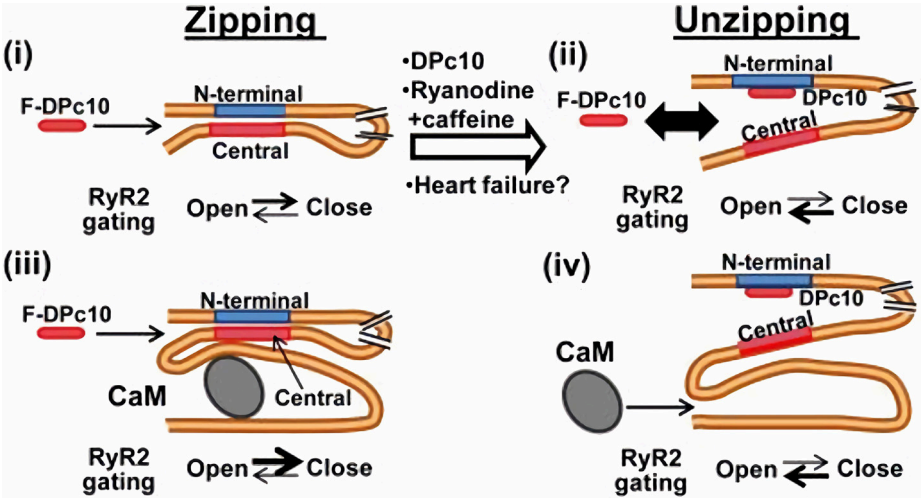


**FIGURE 3 |** CaM-dependent modulation of RyR2 channels. RyR2 closed state is stabilized by the interaction (zipping) between "terminal" and "central" regions of the N-terminal (cytosolic) tail of the protein. If such interaction is removed (unzipping), the channel closed state is destabilized. Apo-CaM binds to a domain distal to the "zipping" one, but the resulting conformation allosterically facilitates the zipping interaction, thus stabilizing RyR2 closed state. CaM and F-DPc10 (a peptide obstructing the zipping interaction) allosterically "compete" for binding to RyR2. Similarly, the unzipped state, promoted by drugs and reactive oxygen species which facilitate RyR2 opening, reduces RyR2 affinity for CaM (67). F-DPc10 is a peptide fragment designed to prevent the interaction between the central and N-terminal protein domains (a tool in testing the unzipping model). From Oda et al. (66).

relative to that of FKBP in RyR1, did not detect $Ca^{2+}$-dependent shifts in CaM position of a magnitude compatible with the results of cryo-EM data (69). However, $Ca^{2+}$-induced structural changes in both probe-carrying proteins are possible and might minimize FRET distances even in the presence of real shifts in binding position.

In conclusion, even if the detailed mechanism remains to be resolved, it is now accepted that direct regulation of RyR gating by CaM is $Ca^{2+}$-dependent (stimulatory to inhibitory) in RyR1 and $Ca^{2+}$-independent (always inhibitory) in RyR2. Formation of the $Ca^{2+}$-CaM complex does affect RyR2 gating significantly, but this occurs through an indirect mechanism, involving CaMKII activation.

CaMKII is a cytosolic serine-threonine kinase activated by $Ca^{2+}$ with a $K_d$ of 20-100 nM, which dramatically decreases (to 60 pM) after enzyme autophosphorylation (8). The $Ca^{2+}$-CaM complex activates kinase activity by binding to an enzyme regulatory region, located in the central protein domain. Enzyme activation occurs by displacement of an auto-inhibitory segment that occludes access of the substrate to the N-terminal catalytic domain. As for other targets, both N- and C-terminal CaM lobes are involved in activation of kinase activity (25), which is in this case strictly $Ca^{2+}$-dependent.

CaMKII mediates a number of $Ca^{2+}$-activated phosphorylations, including that of RyR2 at Ser2814 on the cytosolic surface of the channel (exclusively for CaMKII) and, additional serine residues (49, 70). Most of the evidence converges to show that CaMKII-dependent phosphorylation facilitates opening of RyR2 channels, thus increasing sensitivity of SR $Ca^{2+}$-release to cytosolic $Ca^{2+}$. This may be particularly relevant under pathological conditions (70).

CaM binding to RyRs also depends on factors other than $Ca^{2+}$, such as pH, $Mg^{2+}$ oxidation state (54, 62). In particular, oxidative modifications compromise the normal activity of RyR2 by influencing their luminal $Ca^{2+}$ regulation in a manner similar to that observed in heart failure (71).

Stabilization of RyR2 closed state by CaM is crucial in minimizing spontaneous (non-triggered) $Ca^{2+}$ release from the SR in the form of either "Ca-leak" (random release from individual RyRs) or "$Ca^{2+}$ spark" (synchronous release from a RyR2 cluster), a function pivotal to both contractile and electrical function of cardiomyocytes (63).

## PHENOTYPES IN CAM MUTATIONS AND UNDERLYING MECHANISMS

Mutations in one of the three CALM genes, even in the heterozygous form, have been described in patients with a severe cardiac phenotype, characterized by a high propensity to ventricular arrhythmias, syncopal episodes and sudden death at a young age (72).

Despite sharing strong electrical instability, two distinct phenotypes can be identified in carriers of CaM mutations: the long QT syndrome (LQTS) (9, 73), characterized by prolongation of repolarization, and catecholamine-induced ventricular tachycardia (CPVT), characterized instead by exercise-induced ventricular arrhythmias (74). In general, each specific CALM mutation is associated with one of the two phenotypes; nonetheless, mutations with mixed phenotypes have also been described (72). Such confounding complexity contrasts with an apparently sharp separation of the molecular mechanisms underlying the LQTS and CPVT patterns. A third,

less well-defined arrhythmia phenotype, idiopathic ventricular fibrillation (IVF), has also been associated with a CALM mutation (75) and will be addressed here in paragraph Mixed phenotype.

A point of interest in the interpretation of CALM mutations is their extremely high penetrance: 1 mutant allele in 6 encoding for the same amino acid sequence (as in heterozygous mutations) is sufficient to result in marked functional derangements.

Also in view of the multiplicity of functions exerted by CaM in many cell types, all this suggests that, for one reason or another, mutant CaMs must interact with their target with high specificity. In the following paragraphs we will describe the cellular functional derangements associated with the LQTS and CPVT phenotypes and address, as much as current knowledge allows, the mechanisms underlying target specificity of CaM mutations.

## LQTS Phenotype

Prolongation of action potential duration (APD), reflected as QT interval prolongation on the ECG, can result from loss of function of outward currents, or gain of function of inward ones; therefore, CaM abnormalities affecting modulation of $K_v7.1$ ($I_{Ks}$) and $Ca_v1.2$ ($I_{CaL}$) might theoretically be involved in prolongation of repolarization. Enhancement of the "window" ($I_{NaW}$) or "late" ($I_{NaL}$) components of the $Na^+$ current $I_{Na}$ ($Na_v1.5$ channel) might represent a further potential mechanism.

Nevertheless, gain of $Ca_v1.2$ function ($I_{CaL}$ enhancement) has emerged as the dominant mechanism in CALM gene mutations associated with delayed repolarization.

In 2013, Crotti et al. reported three *de novo* heterozygous missense CALM gene mutations in LQT-infants with recurrent cardiac arrest (73). In particular, the *CALM1*-p.D130G and *CALM2*-p.D96V mutations affect highly conserved aspartic acid residues (C-lobe EF IV and EF III, respectively) involved in $Ca^{2+}$ binding. The *CALM1*-p.F142L (next to C-lobe EF IV), albeit outside the EF-hand, is expected to alter the energetics of the conformational change associated to $Ca^{2+}$ binding (22). The p.D130G mutation, associated with the LQTS phenotype, has also been identified in the *CALM3* gene (76), thus reinforcing the concept that mutation effect may be independent of the gene affected. *In vitro* $Ca^{2+}$ binding studies revealed that all these three mutations are characterized by a 5- to 50-fold reduction in $Ca^{2+}$ binding affinity of the C-lobe, without affecting N-lobe affinity (73). Overexpression of these mutations in guinea-pig myocytes or an engineered cell line showed loss of $I_{CaL}$ CDI, leading to action potential prolongation with enhanced intercellular variability. The amplitude of $Ca^{2+}$ transients and its dispersion were also increased, likely secondary to increased $Ca^{2+}$ influx; notably, spontaneous $Ca^{2+}$ release events were not reported (77). Indeed, consistent with the LQTS phenotype, RyR2 function was unaffected. Binding of CaM mutants to $Ca_v1.2$ was tested by FRET and found to be enhanced for p.F142L and unaffected by the other mutations. On the other hand, titration of WT vs. mutant expression levels showed that a ratio (WT/mutant) of 7 (compatible with heterozygosity) was enough to impair CDI (77). Therefore, selectivity of mutant CaMs in altering $Ca_v1.2$ channel function can be explained by the fact that modulation of this target requires a pre-bound apo-CaM pool (containing mixtures of WT and mutant CaMs) and subsequent $Ca^{2+}$ binding to this pool (impaired in mutants by loss of $Ca^{2+}$ affinity). This interpretation would explain sparing of RyR2, whose modulation may not require $Ca^{2+}$ binding, and of CaMKII, which binds CaM directly in its holo-form (not represented if $Ca^{2+}$ affinity is reduced). Selective CDI impairment by additional mutations reducing C-lobe $Ca^{2+}$ affinity (*CALM2*-p.D132H and *CALM1*-p.D132V) has also been reported in transfection studies on human induced pluripotent stem cell-derived cardiomyocytes (78).

Other heterozygous LQTS mutations, *CALM2*-p.D130V and *CALM1*-p.E141G have been recently identified by Boczek et al. (79). As in p.D130G, the former involves replacement of aspartic acid by a neutral residue; therefore, loss of C-lobe $Ca^{2+}$ affinity is to be expected. *CALM1*-p.E141G has a phenotype closely resembling that of *CALM1*-p.F142L, indicating that residues 141 and 142 are both crucial for C-lobe $Ca^{2+}$ binding. Notably, when transfected in isolation, *CALM1*-p.E141G also enhanced $I_{NaL}$, but the effect disappeared when mutant and WT constructs were co-expressed. This is consistent with a role of CaM stabilizing $Na_v1.5$ inactivation (see above) and implies lack of functional dominance of the mutation for this target. However, at least according to a current model of CaM-$Na_v1.5$ interaction (48), reduced affinity of mutant CaM for $Ca^{2+}$ would not explain $I_{NaL}$ enhancement.

CaM mutations resulting in downregulation of $K^+$ currents have not been reported, even if $I_{Ks}$ function has been tested in some cases (*CALM1*-p.F142L) (80). Nonetheless, the $K_v7.1$ α-subunit mutation p.K526E, accounting for a case of LQT1, impairs interaction of the channel's helix B with CaM's N-lobe. This leads to $I_{Ks}$ downregulation and delayed repolarization (43). Considering that the mode of CaM–$K_v7.1$ interaction involves a pre-bound pool and $Ca^{2+}$-dependent C-lobe signaling (as for $Ca_v1.2$), it is surprising that CaM mutations with loss of C-lobe $Ca^{2+}$ affinity may not affect $I_{Ks}$. One tentative explanation is compensation of the loss of CaM-dependent regulation by PIP2 signaling; it would be therefore interesting to evaluate the effect of known CaM mutations on $I_{Ks}$ under conditions of PIP2 depletion.

## CPVT Phenotype

Catecholaminergic polymorphic ventricular tachycardias are malignant arrhythmias with an ECG pattern suggesting multifocal origin (unlike TdP), typically induced by exercise, or other conditions associated with enhanced adrenergic stimulation (81). The prototypical form of this arrhythmia has been associated with mutations of RyR2 channels, or of the proteins associated with them in a macromolecular complex (junction, triadin, calsequestrin, sorcin etc.). The electrical disturbance at the basis of CPVT originates from "$Ca^{2+}$ waves," i.e., macroscopic surges of cytosolic $Ca^{2+}$ resulting from spontaneous RyR opening at a point site, followed by auto-regenerative propagation (by $Ca^{2+}$-induced $Ca^{2+}$ release) of the ionic perturbation to the whole cell (82). The mechanism connecting the $Ca^{2+}$ wave to membrane potential is $Ca^{2+}$-induced activation of the electrogenic $Na^+/Ca^{2+}$ exchanger (NCX), which results in a depolarizing current, also referred

to as "transient inward current" ($I_{TI}$). While "$Ca^{2+}$ overload" facilitates $Ca^{2+}$ waves (by increasing RyRs open probability), it is neither necessary nor sufficient to induce them; indeed some degree of intrinsic RyR2 instability may be involved even in the prototypical case of digitalis toxicity (83).

CaM mutations associated with the CPVT phenotype are generally characterized by a relatively small impairment of C-lobe $Ca^{2+}$ binding (e.g., *CALM1*-p.N98S, *CALM1*-p.N54I, and *CALM3*-p.A103V) (84, 85), which (as shown for *CALM3*-p.A103V) (85) corresponds to a minor effect on $I_{CaL}$ CDI. Besides this, the relationship between mutation features and the CPVT phenotype is somewhat elusive. Nyegaard and colleagues tested *CALM1*-p.N54I and -p.N98S binding to a small RyR2 segment, found a decrease in *CALM1*-p.N98S affinity only at low $Ca^{2+}$ levels and explained mutation phenotype with loss of CaM-RyR2 complexing. These findings were later contradicted by studies using the entire RyR2 protein (86), that detected an increase in RyR2 affinity for both these mutations (also accounting for dominance of effects). Nonetheless, increased affinity for RyR2 may not be a prerequisite for channel destabilization; indeed the CPVT mutation *CALM3*-p.A103V, which strongly increased $Ca^{2+}$ release events, displayed normal RyR2 affinity (85). Notably, mutations sites N54 and N98, albeit affecting the N- and C-lobes, respectively, are not contained within any known protein-protein interaction sites (84).

In conclusion, the features of CPVT mutations may explain why they are not generally associated with an LQTS phenotype (however see below), but a general mechanism by which they induce RyR2 instability cannot be clearly envisioned. Since CaM interaction with RyR2 is essentially $Ca^{2+}$-independent, the mechanism must conceivably reside in a change of 3D protein conformations involved in CaM-RyR2 complexing; nonetheless, the nature of this change remains to be clarified.

### Mixed Phenotype

Notwithstanding the apparently sharp demarcation of CaM abnormalities affecting $Ca_v1.2$ and RyR2 channels, several mutations have been associated with both LQTS and CPVT phenotypes. CaM mutations were found in five subjects with QT prolongation; nonetheless, two of them (*CALM2*-p.D132E and –p.Q136P) were associated with arrhythmia features strongly suggestive of SR instability and thus were assigned to the CPVT phenotype (72). These mutations affect EF III and EF IV of the C-loop and displayed reduced $Ca^{2+}$ affinity; thus, even if $I_{CaL}$ CDI was not directly tested in this study, it may be tentatively considered responsible for the observed QT prolongation. Intriguingly, two different reports assign LQTS and CPVT phenotypes to the same mutation (p.N98S) occurring in genes *CALM2* (72) and *CALM* (84), respectively; since the CaM amino acid sequence encoded by the 2 genes is identical, other factors should account for the discrepancy.

The reason for SR instability in all these cases is as elusive as the properties of mutations that favor RyR2 dysfunction (see above). Nonetheless, it should be considered that impairment of $I_{CaL}$ CDI and the resulting APD prolongation are obviously stress conditions for intracellular $Ca^{2+}$ homeostasis, requiring robust compensatory mechanisms. Thus, albeit not observed in hiPSC-CMs from an LQTS case (80), SR instability secondary to defective CDI might occur in subjects (or conditions) in which such compensation is less efficient. Thus, assignment to an LQTS or CPVT clinical phenotype may not be always accurate in defining the mutation-induced abnormality accounting for arrhythmogenesis.

Marsman et al. have described the *CALM1*-p.F90L mutation in a patient with IVF, i.e., VF episodes without the features of either LQTS or CPVT (mild QT prolongation only during exercise recovery) (75). The mutation, which resides on the linker between EF III and EF IV, impairs C-lobe $Ca^{2+}$ affinity conformational stability and CaM-RyR2 interaction (87). In heterologous expression experiments, p.F90L also affects small-conductance $Ca^{2+}$-activated $K^+$ channels (SK channels) (88); nonetheless, the role of these channels in ventricular electrophysiology is unclear.

## EVALUATING CAM MUTATIONS IN PATIENT-DERIVED CARDIOMYOCYTES

Induced pluripotent stem cell-derived cardiomyocytes from mutation carriers (hiPSC-CMs) provide the means to test mutation effects in the context of each patient's genetic background. Recent studies have exploited this cellular model to test the effect of CaM mutations. Yamamoto et al. reported a typical LQTS phenotype for the heterozygous *CALM2*-p.N98S mutation and obtained reversal of the phenotype by knocking out the mutant allele by gene editing (89), thus supporting a causal relationship between mutation and phenotype. Notably, *CALM2*-p.N98S affinity for $Ca^{2+}$ is only mildly reduced, and a CPVT phenotype has also been reported for this mutation (84).

We recently investigated hiPSC-CMs from a patient with LQTS phenotype and heterozygous carrier of the *CALM1*-p.F142L mutation (80) (**Figure 4**). CDI of $I_{CaL}$ was severely impaired, thus accounting for APD prolongation (which was reversed by $I_{CaL}$ blockade) and its failure to shorten adequately at high pacing rates. As expected from the increase in $Ca^{2+}$ influx, the amplitude of V-triggered $Ca^{2+}$ transients was significantly increased; nonetheless, SR $Ca^{2+}$ content was normal and no spontaneous $Ca^{2+}$ release events were observed, thus suggesting preserved homeostatsis of intracellular $Ca^{2+}$. This argues against SR instability as the arrhythmogenic mechanism in this case and suggests a primary role of prolonged and "stiff" (non-rate-adaptive) repolarization instead (80). Other currents under CaM modulation were also evaluated in this study: $I_{Ks}$ was found to be unaffected and a persistent component of $I_{Na}$ (likely contributed by $I_{NaW}$) was significantly reduced (80). While this confirms loss of $I_{CaL}$ CDI as the sole mechanism of repolarization abnormality, $I_{NaW}$ reduction was unexpected; indeed, loss of CaM affinity for $Ca^{2+}$ should if anything, increase $I_{NaW}$ (48). Notably, CaMKII activity was preserved and even slightly enhanced, probably secondary to the increase in $Ca^{2+}$ transients amplitude. This supports the view that negative dominance of the mutation only applies to targets, as $Ca_v1.2$, binding CaM in its apo form.

Altogether, these findings clearly confirm loss of $I_{CaL}$ CDI as the mechanism underlying the LQTS phenotype in CaM

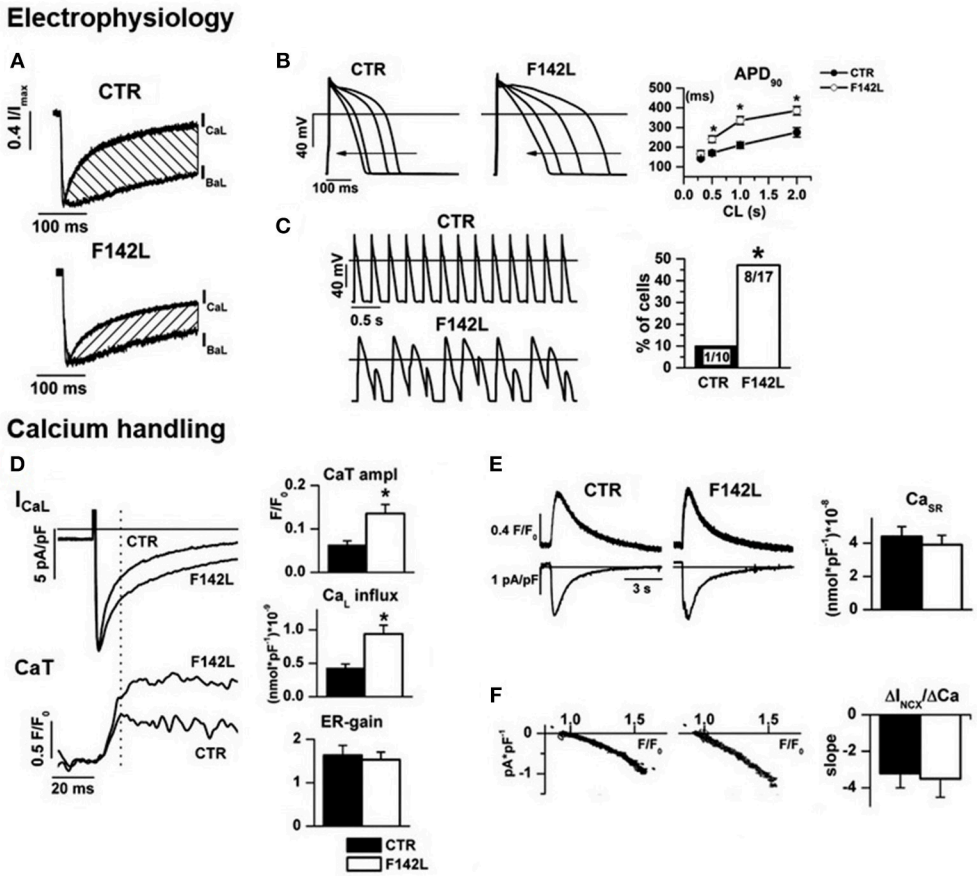


**FIGURE 4 |** Arrhythmogenic mechanism of CALM1 F142L from experiments in patient-derived hiPSC-CMs. *Electrophysiology:* **(A)** $I_{CaL}$ CDI (hatched area) was reduced; **(B)** CDI impairment led to APD prolongation and inadequate APD shortening at high pacing rate; **(C)** APD abnormalities led to loss of 1:1 response to fast pacing in a large % of F142L cells. *Calcium handling*: **(D)** Impaired $I_{CaL}$ CDI led to matching increments of $Ca^{2+}$ influx and of the amplitude of $Ca^{2+}$ transients (CaT); excitation/release gain (ER-gain) was unchanged, thus suggesting normal RyRs function. **(E)** In spite of enhanced $Ca^{2+}$ influx, SR $Ca^{2+}$ content was unchanged, thus implying compensation by homeostatic mechanisms. **(F)** The slope of the relationship between $Na^{+}/Ca^{2+}$ exchanger current ($I_{NCX}$) and $Ca^{2+}$ concentration was unchanged, to indicate that homeostatic compensation did not involve changes in the expression of the exchanger. Asterisks denote significance of changes. Modified from ref. Rocchetti et al. (80).

mutations with reduced $Ca^{2+}$ affinity. To our best knowledge, no hiPSC-CMs studies are thus far available for mutations with a clear-cut CPVT phenotype. It should be considered that, due to immaturity of the structures involved in intracellular $Ca^{2+}$ handling (e.g., lack of T-tubules) (90), hiPSC-CMs may be less suitable in evaluating CaM mutations leading to SR instability (CPVT phenotype).

## CONCLUSIONS AND THERAPEUTIC IMPLICATIONS

CaM functions as a $Ca^{2+}$ sensor to maintain physiological $Ca^{2+}$ levels in cells. In addition to this homeostatic role, CaM signal targeting is required to transduce fundamental cell processes, for which $Ca^{2+}$-CaM complexing is not necessarily involved, but may still have a modulatory effect. This is possible because of the presence of CaM-binding sequences suitable to allow CaM to bind multiple targets even in its "apo" form; this generates a quantitatively prevailing "pre-bound" CaM pool. CaM binding to targets occurs with very high specificity, which is required to explain restriction of CaM mutations phenotype to the myocardium and, within it, to specific subcellular targets.

Whereas mutation-induced loss of $Ca^{2+}$ sensing function is crucial in impairing CDI of sarcolemmal $Ca^{2+}$ channels (carrying $I_{CaL}$), it is not required for mutations associated with RyR2 instability. For the latter, changes in CaM affinity for RyR2 channels are apparently more important; however, the direction and even the need for such changes are still unclear. Possibly, mutations induce complex (3D) modifications in the protein-protein binding interface, of which changes in CaM affinity for the target are just a gross readout. This is a field in which new information is strongly required.

Whereas, "pure" LQTS and CPVT phenotypes suggest abnormal modulation of $I_{CaL}$ and RyR2, respectively, we hypothesize that coexistence of QT prolongation and SR instability (mixed phenotypes) might be accounted for by impaired $I_{CaL}$ CDI, possibly with the complement of (very

common) conditions weakening homeostatic control of intracellular $Ca^{2+}$.

Based on the information reviewed above, mechanism-guided therapeutic approaches to calmodulinopathies should ideally address the interaction of mutant CaM with its targets. Particularly in the case of LQTS-type mutations, this approach is justified by the role of the high target affinity of mutant CaMs in causing negative dominance of the mutation. Tools for this purpose are not available yet, but possibilities exist and are currently explored.

Therapy of CaM mutations with more classical approaches may depend on the phenotype. $I_{CaL}$ blockade seems a logical approach in the case of $I_{CaL}$ gain of function, resulting from loss of CDI (LQTS phenotype); indeed, verapamil did shorten the QT interval in hiPSC-CMs from *CALM1*-p.F142L carriers (80). Nonetheless, selective inhibition of the sustained $I_{CaL}$ component would be desirable and should be pursued by developing $I_{CaL}$ blockers with such a property; as suggested by availability of selective blockade of $I_{Na}$ sustained component (91), this should be seen as an achievable goal. Pharmacological treatment of CPVT-type CaM mutations may require RyR2 stabilization, or at least, blunting membrane electrical response to spontaneous $Ca^{2+}$ release events. This is a long-pursued goal for which no ideal tool has been thus far identified; while agents as flecainide or carvedilol may provide some protection [for review see Zaza and Rocchetti (82)], the search of clinically usable specific RyR2 blockers is currently ongoing.

Because calmodulinopathies have been recently described, information on the clinical efficacy of therapies is not available yet.

## FUTURE CHALLENGES

Calmodulinopathies have undoubtedly attracted high quality, multidisciplinary research; nonetheless, and rather unsurprisingly, many questions have yet to be addressed. The present review highlights a few that, in our view, might deserve particular attention.

The role and mechanism of $Na_V1.5$ dysregulation in CaM mutation-associated phenotypes is elusive. Notably, $I_{NaL}$ enhancement, a target for which therapeutic interventions are available, might have a role in both QT prolongation (LQTS phenotype) and SR instability (CPVT phenotype) (91).

The interplay between CaM- and PIP2-dependent modulation of $I_{Ks}$ suggests that factors affecting membrane PIP2 levels (e.g., phospholipase-C signaling) potentially influence CaM mutation penetrance. If this were the case, such factors might represent easily accessible therapeutic targets.

The ultimate mechanism of arrhythmia facilitation by loss of $I_{CaL}$ CDI, which seems to diverge from what would be expected, has thus far been only superficially addressed.

Finally, the molecular basis of RyR2 dysfunction in the context of CaM mutations remains largely unresolved, thus preventing identification of mechanism-specific targets.

## AUTHOR CONTRIBUTIONS

BB wrote a general manuscript draft. CR focused on the section about CaM modulation of voltage-gated channels. M-CK, LS, and AG provided text and discussion for integration with clinical and genetic aspects of calmodulinopathies. LC and AZ supervised the process and edited the manuscript to its final version.

## ACKNOWLEDGMENTS

This work has been supported by Fondo di Ateneo per la Ricerca (FAR, 2018) of Università Milano-Bicocca to AZ and by the DIMET Ph.D. program to BB.

## REFERENCES

1. Clapham DE. Calcium signaling. *Cell* (2007) 131:1047–58. doi: 10.1016/j.cell.2007.11.028
2. Ikura M. Calcium binding and conformational response in EF-hand proteins. *Trends Biochem Sci.* (1996) 21:14–7. doi: 10.1016/S0968-0004(06)80021-6
3. Luby-Phelps K, Hori M, Phelps JM, Won D. $Ca^{2+}$-regulated dynamic compartmentalization of calmodulin in living smooth muscle cells. *J Biol Chem.* (1995) 270:21532–8. doi: 10.1074/jbc.270.37.21532
4. Deisseroth K, Heist EK, Tsien RW. Translocation of calmodulin to the nucleus supports CREB phosphorylation in hippocampal neurons. *Nature* (1998) 392:198. doi: 10.1038/32448
5. Berchtold MW, Villalobo A. The many faces of calmodulin in cell proliferation, programmed cell death, autophagy, and cancer. *Biochim Biophys Acta Mol Cell Res.* (2014) 1843:398–435. doi: 10.1016/j.bbamcr.2013.10.021
6. Kotta M-C, Sala L, Ghidoni A, Badone B, Ronchi C, Parati G, Zaza A and Crotti L. Calmodulinopathy: A Novel, Life-Threatening Clinical Entity Affecting the Young. *Front Cardiovasc Med.* (2018). 5:175. doi: 10.3389/fcvm.2018.00175
7. Bers DM. Cardiac excitation–contraction coupling. *Nature* (2002) 415:198. doi: 10.1038/415198a
8. Maier LS, Bers DM. Calcium, calmodulin, and calcium-calmodulin kinase II: heartbeat to heartbeat and beyond. *J Mol Cell Cardiol.* (2002) 34:919–39. doi: 10.1006/jmcc.2002.2038
9. Schwartz PJ, Crotti L, Insolia R. Long-QT syndrome: from genetics to management. *Circ Arrhythm Electrophysiol.* (2012) 5:868–77. doi: 10.1161/CIRCEP.111.962019
10. Fischer R, Koller M, Flura M, Mathews S, Strehler-Page MA, Krebs J, et al. Multiple divergent mRNAs code for a single human calmodulin. *J Biol Chem.* (1988) 263:17055–62.
11. Crotti L, Kotta MC. The role of genetics in primary ventricular fibrillation, inherited channelopathies and cardiomyopathies. *Int J Cardiol.* (2017) 237:45–8. doi: 10.1016/j.ijcard.2017.03.119
12. Villarroel A, Taglialatela M, Bernardo-Seisdedos G, Alaimo A, Agirre J, Alberdi A, et al. The ever changing moods of calmodulin: how structural plasticity entails transductional adaptability. *J Mol Biol.* (2014) 426:2717–35. doi: 10.1016/j.jmb.2014.05.016
13. Malmendal A, Linse S, Evenäs J, Forsén S, Drakenberg T. Battle for the EF-hands: magnesium– calcium interference in calmodulin. *Biochemistry* (1999) 38:11844–50. doi: 10.1021/bi9909288
14. Tadross MR, Dick IE, Yue DT. Mechanism of local and global $Ca^{2+}$ sensing by calmodulin in complex with a $Ca^{2+}$ channel. *Cell* (2008) 133:1228–40. doi: 10.1016/j.cell.2008.05.025
15. Babu YS, Sack JS, Greenhough TJ, Bugg CE, Means AR, Cook WJ. Three-dimensional structure of calmodulin. *Nature* (1985) 315:37. doi: 10.1038/315037a0

16. Zhang M, Tanaka T, Ikura M. Calcium-induced conformational transition revealed by the solution structure of apo calmodulin. *Nat Struct Mol Biol.* (1995) 2:758. doi: 10.1038/nsb0995-758
17. Chou JJ, Li S, Klee CB, Bax A. Solution structure of Ca 2+-calmodulin reveals flexible hand-like properties of its domains. *Nat Struct Mol Biol.* (2001) 8:990. doi: 10.1038/nsb1101-990
18. Yamniuk AP, Vogel HJ. Calmodulin's flexibility allows for promiscuity in its interactions with target proteins and peptides. *Mol Biotechnol.* (2004) 27:33–57. doi: 10.1385/MB:27:1:33
19. Marshall CB, Nishikawa T, Osawa M, Stathopulos PB, Ikura M. Calmodulin and STIM proteins: two major calcium sensors in the cytoplasm and endoplasmic reticulum. *Biochem Biophys Res Commun.* (2015) 460:5–21. doi: 10.1016/j.bbrc.2015.01.106
20. Bähler M, Rhoads A. Calmodulin signaling via the IQ motif. *FEBS Lett.* (2002) 513:107–13. doi: 10.1016/S0014-5793(01)03239-2
21. Gellman SH. On the role of methionine residues in the sequence-independent recognition of nonpolar protein surfaces. *Biochemistry* (1991) 30:6633–6. doi: 10.1021/bi00241a001
22. Chin D, Means AR. Calmodulin: a prototypical calcium sensor. *Trends Cell Biol.* (2000) 10:322–8. doi: 10.1016/S0962-8924(00)01800-6
23. Stigler J, Rief M. Calcium-dependent folding of single calmodulin molecules. *Proc Natl Acad Sci USA.* (2012) 109:17814–9. doi: 10.1073/pnas.1201801109
24. O'Neil KT, DeGrado WF. How calmodulin binds its targets: sequence independent recognition of amphiphilic α-helices. *Trends Biochem Sci.* (1990) 15:59–64. doi: 10.1016/0968-0004(90)90177-D
25. Tidow H, Nissen P. Structural diversity of calmodulin binding to its target sites. *FEBS J.* (2013) 280:5551–65. doi: 10.1111/febs.12296
26. Valeyev NV, Bates DG, Heslop-Harrison P, Postlethwaite I, Kotov NV. Elucidating the mechanisms of cooperative calcium-calmodulin interactions: a structural systems biology approach. *BMC Syst Biol.* (2008) 2:48. doi: 10.1186/1752-0509-2-48
27. Beitner R. Calmodulin antagonists and cell energy metabolism in health and disease. *Mol Genet Metab.* (1998) 64:161–8. doi: 10.1006/mgme.1998.2691
28. Schumacher MA, Rivard AF, Bächinger HP, Adelman JP. Structure of the gating domain of a Ca2+-activated K+ channel complexed with Ca2+/calmodulin. *Nature* (2001) 410:1120. doi: 10.1038/35074145
29. Wagner S, Maier LS. Modulation of cardiac Na(+) and Ca(2+) currents by CaM and CaMKII. *J Cardiovasc Electrophysiol.* (2006) 17(Suppl. 1):S26–33. doi: 10.1111/j.1540-8167.2006.00382.x
30. Wang C, Chung BC, Yan H, Wang H-G, Lee S-Y, Pitt GS. Structural analyses of Ca 2+/CaM interaction with Na V channel C-termini reveal mechanisms of calcium-dependent regulation. *Nat Commun.* (2014) 5:4896. doi: 10.1038/ncomms5896
31. Jurado LA, Chockalingam PS, Jarrett HW. Apocalmodulin. *Physiol Rev.* (1999) 79:661–82. doi: 10.1152/physrev.1999.79.3.661
32. Maier LS, Ziolo MT, Bossuyt J, Persechini A, Mestril R, Bers DM. Dynamic changes in free Ca-calmodulin levels in adult cardiac myocytes. *J Mol Cell Cardiol.* (2006) 41:451–8. doi: 10.1016/j.yjmcc.2006.04.020
33. Kakiuchi S, Yasuda S, Yamazaki R, Teshima Y, Kanda K, Kakiuchi R, et al. Quantitative determinations of calmodulin in the supernatant and particulate fractions of mammalian tissues. *J Biochem.* (1982) 92:1041–8. doi: 10.1093/oxfordjournals.jbchem.a134019
34. Bers DM, Perez-Reyes E. Ca channels in cardiac myocytes: structure and function in Ca influx and intracellular Ca release. *Cardiovasc Res.* (1999) 42:339–60. doi: 10.1016/S0008-6363(99)00038-3
35. Lee K, Marban E, Tsien R. Inactivation of calcium channels in mammalian heart cells: joint dependence on membrane potential and intracellular calcium. *J Physiol.* (1985) 364:395–411. doi: 10.1113/jphysiol.1985.sp015752
36. Zygmunt AC, Maylie J. Stimulation-dependent facilitation of the high threshold calcium current in guinea-pig ventricular myocytes. *J Physiol.* (1990) 428:653–71. doi: 10.1113/jphysiol.1990.sp018233
37. Zuehlke RD, Pitt GS, Deisseroth K, Tsien RW, Reuter H. Calmodulin supports both inactivation and facilitation of L-type calcium channels. *Nature* (1999) 399:159. doi: 10.1038/20200
38. Erickson MG, Alseikhan BA, Peterson BZ, Yue DT. Preassociation of calmodulin with voltage-gated Ca(2+) channels revealed by FRET in single living cells. *Neuron* (2001) 31:973–85. doi: 10.1016/S0896-6273(01)00438-X
39. Liang H, DeMaria CD, Erickson MG, Mori MX, Alseikhan BA, Yue DT. Unified mechanisms of Ca2+ regulation across the Ca2+ channel family. *Neuron* (2003) 39:951–60. doi: 10.1016/S0896-6273(03)00560-9
40. Lee T-S, Karl R, Moosmang S, Lenhardt P, Klugbauer N, Hofmann F, et al. Calmodulin kinase II is involved in voltage-dependent facilitation of the L-type cav1. 2 calcium channel identification of the phosphorylation sites. *J Biol Chem.* (2006) 281:25560–67. doi: 10.1074/jbc.M508661200
41. Erxleben C, Liao Y, Gentile S, Chin D, Gomez-Alegria C, Mori Y, et al. Cyclosporin and timothy syndrome increase mode 2 gating of CaV1. 2 calcium channels through aberrant phosphorylation of S6 helices. *Proc Natl Acad Sci USA.* (2006) 103:3932–7. doi: 10.1073/pnas.0511322103
42. Shamgar L, Ma L, Schmitt N, Haitin Y, Peretz A, Wiener R, et al. Calmodulin is essential for cardiac IKS channel gating and assembly: impaired function in long-QT mutations. *Circ Res.* (2006) 98:1055–63. doi: 10.1161/01.RES.0000218979.40770.69
43. Tobelaim WS, Dvir M, Lebel G, Cui M, Buki T, Peretz A, et al. Ca(2+)-Calmodulin and PIP2 interactions at the proximal C-terminus of Kv7 channels. *Channels* (2017) 11:686–95. doi: 10.1080/19336950.2017.1388478
44. Chang A, Abderemane-Ali F, Hura GL, Rossen ND, Gate RE, Minor Jr DL. A calmodulin C-Lobe Ca2+-dependent switch governs Kv7 channel function. *Neuron* (2018) 97:836–52.e836. doi: 10.1016/j.neuron.2018.01.035
45. Ciampa EJ, Welch RC, Vanoye CG, George AL. KCNE4 juxtamembrane region is required for interaction with calmodulin and for functional suppression of KCNQ1. *J Biol Chem.* (2011) 286:4141–9. doi: 10.1074/jbc.M110.158865
46. Shugg T, Johnson DE, Shao M, Lai X, Witzmann F, Cummins TR, et al. Calcium/calmodulin-dependent protein kinase II regulation of IKs during sustained beta-adrenergic receptor stimulation. *Heart Rhythm* (2018) 15:895–904. doi: 10.1016/j.hrthm.2018.01.024
47. Kim J, Ghosh S, Liu H, Tateyama M, Kass RS, Pitt GS. Calmodulin mediates Ca2+ sensitivity of sodium channels. *J Biol Chem.* (2004) 279:45004–12. doi: 10.1074/jbc.M407286200
48. Shah VN, Wingo TL, Weiss KL, Williams CK, Balser JR, Chazin WJ. Calcium-dependent regulation of the voltage-gated sodium channel hH1: intrinsic and extrinsic sensors use a common molecular switch. *Proc Natl Acad Sci USA.* (2006) 103:3592–7. doi: 10.1073/pnas.0507397103
49. Lanner JT, Georgiou DK, Joshi AD, Hamilton SL. Ryanodine receptors: structure, expression, molecular details, and function in calcium release. *Cold Spring Harb Perspect Biol.* (2010) 2:a003996. doi: 10.1101/cshperspect.a003996
50. Soeller C, Crossman D, Gilbert R, Cannell MB. Analysis of ryanodine receptor clusters in rat and human cardiac myocytes. *Proc Natl Acad Sci USA.* (2007) 104:14958–63. doi: 10.1073/pnas.0703016104
51. Louch WE, Stokke MK, Sjaastad I, Christensen G, Sejersted OM. No rest for the weary: diastolic calcium homeostasis in the normal and failing myocardium. *Physiology* (2012) 27:308–23. doi: 10.1152/physiol.00021.2012
52. Franzini-Armstrong C, Protasi F, Ramesh V. Shape, size, and distribution of Ca2+ release units and couplons in skeletal and cardiac muscles. *Biophys J.* (1999) 77:1528–39. doi: 10.1016/S0006-3495(99)77000-1
53. Bers DM, Stiffel VM. Ratio of ryanodine to dihydropyridine receptors in cardiac and skeletal muscle and implications for EC coupling. *Am J Physiol Cell Physiol.* (1993) 264:C1587–93. doi: 10.1152/ajpcell.1993.264.6.C1587
54. Balshaw DM, Xu L, Yamaguchi N, Pasek DA, Meissner G. Calmodulin binding and inhibition of cardiac muscle calcium release channel (ryanodine receptor). *J Biol Chem.* (2001) 276:20144–53. doi: 10.1074/jbc.M010771200
55. Xiong H, Feng X, Gao L, Xu L, Pasek DA, Seok J-H, et al. Identification of a two EF-hand Ca2+ binding domain in lobster skeletal muscle ryanodine receptor/Ca2+ release channel. *Biochemistry* (1998) 37:4804–14. doi: 10.1021/bi971198b
56. Xu L, Gomez AC, Pasek DA, Meissner G, Yamaguchi N. Two EF-hand motifs in ryanodine receptor calcium release channels contribute to isoform-specific regulation by calmodulin. *Cell Calcium* (2017) 66:62–70. doi: 10.1016/j.ceca.2017.05.013
57. Gyorke S, Terentyev D. Modulation of ryanodine receptor by luminal calcium and accessory proteins in health and cardiac disease. *Cardiovasc Res.* (2008) 77:245–55. doi: 10.1093/cvr/cvm038
58. Li P, Chen SW. Molecular basis of $Ca^{2+}$ activation of the mouse cardiac Ca2+ release channel (ryanodine receptor). *J Gen Physiol.* (2001) 118:33–44. doi: 10.1085/jgp.118.1.33

59. Guo W, Sun B, Xiao Z, Liu Y, Wang Y, Zhang L, et al. The EF-hand Ca2+ binding domain is not required for cytosolic $Ca^{2+}$ activation of the cardiac ryanodine receptor. *J Biol Chem.* (2016) 291:2150–60. doi: 10.1074/jbc.M115.693325
60. Zalk R, Lehnart SE, Marks AR. Modulation of the ryanodine receptor and intracellular calcium. *Annu Rev Biochem.* (2007) 76:367–85. doi: 10.1146/annurev.biochem.76.053105.094237
61. Buratti R, Prestipino G, Menegazzi P, Treves S, Zorzato F. Calcium-dependent activation of skeletal-muscle $Ca^{2+}$ release channel (ryanodine receptor) by calmodulin. *Biochem Biophys. Res Commun.* (1995) 213:1082–90. doi: 10.1006/bbrc.1995.2238
62. Tripathy A, Xu L, Mann G, Meissner G. Calmodulin activation and inhibition of skeletal muscle $Ca^{2+}$ release channel (ryanodine receptor). *Biophys J.* (1995) 69:106–19. doi: 10.1016/S0006-3495(95)79880-0
63. Walweel K, Oo YW, Laver DR. The emerging role of calmodulin regulation of RyR2 in controlling heart rhythm, the progression of heart failure and the antiarrhythmic action of dantrolene. *Clin Exp Pharmacol Physiol.* (2017) 44:135–42. doi: 10.1111/1440-1681.12669
64. Xu L, Meissner G. Mechanism of calmodulin inhibition of cardiac sarcoplasmic reticulum Ca2+ release channel (ryanodine receptor). *Biophys J.* (2004) 86:797–804. doi: 10.1016/S0006-3495(04)74155-7
65. Yamaguchi N, Xu L, Pasek DA, Evans KE, Meissner G. Molecular basis of calmodulin binding to cardiac muscle $Ca^{2+}$ release channel (ryanodine receptor). *J Biol Chem.* (2003) 278:23480–6. doi: 10.1074/jbc.M301125200
66. Oda T, Yang Y, Nitu FR, Svensson B, Lu X, Fruen BR, et al. In cardiomyocytes, binding of unzipping peptide activates ryanodine receptor 2 and reciprocally inhibits calmodulin binding. *Circ Res.* (2013) 112:487–97. doi: 10.1161/CIRCRESAHA.111.300290
67. Oda T, Yang Y, Uchinoumi H, Thomas DD, Chen-Izu Y, Kato T, et al. Oxidation of ryanodine receptor (RyR) and calmodulin enhance Ca release and pathologically alter, RyR structure and calmodulin affinity. *J Mol Cell Cardiol.* (2015) 85:240–8. doi: 10.1016/j.yjmcc.2015.06.009
68. Gangopadhyay JP, Ikemoto N. Interaction of the Lys(3614)-Asn(3643) calmodulin-binding domain with the Cys(4114)-Asn(4142) region of the type 1 ryanodine receptor is involved in the mechanism of Ca2+/agonist-induced channel activation. *Biochem J.* (2008) 411:415–23. doi: 10.1042/BJ20071375
69. Huang X, Fruen B, Farrington DT, Wagenknecht T, Liu Z. Calmodulin-binding locations on the skeletal and cardiac ryanodine receptors. *J Biol Chem.* (2012) 287:30328–35. doi: 10.1074/jbc.M112.383109
70. Wehrens XH, Lehnart SE, Reiken SR, Marks AR. Ca2+/calmodulin-dependent protein kinase II phosphorylation regulates the cardiac ryanodine receptor. *Circ Res.* (2004) 94:e61–70. doi: 10.1161/01.RES.0000125626.33738.E2
71. Terentyev D, Gyorke I, Belevych AE, Terentyeva R, Sridhar A, Nishijima Y, et al. Redox modification of ryanodine receptors contributes to sarcoplasmic reticulum Ca2+ leak in chronic heart failure. *Circ Res.* (2008) 103:1466–72. doi: 10.1161/CIRCRESAHA.108.184457
72. Makita N, Yagihara N, Crotti L, Johnson CN, Beckmann B-M, Roh MS, et al. Novel calmodulin mutations associated with congenital arrhythmia susceptibilityclinical perspective. *Circ Genom Prec Med.* (2014) 7:466–74. doi: 10.1161/CIRCGENETICS.113.000459
73. Crotti L, Johnson CN, Graf E, De Ferrari GM, Cuneo BF, Ovadia M, et al. Calmodulin mutations associated with recurrent cardiac arrest in infants. *Circulation* (2013) 127:1009–17. doi: 10.1161/CIRCULATIONAHA.112.001216
74. Sondergaard MT, Sorensen AB, Skov LL, Kjaer-Sorensen K, Bauer MC, Nyegaard M, et al. Calmodulin mutations causing catecholaminergic polymorphic ventricular tachycardia confer opposing functional and biophysical molecular changes. *FEBS J.* (2015) 282:803–16. doi: 10.1111/febs.13184
75. Marsman RF, Barc J, Beekman L, Alders M, Dooijes D, van den Wijngaard A, et al. A mutation in CALM1 encoding calmodulin in familial idiopathic ventricular fibrillation in childhood and adolescence. *J Am Coll Cardiol.* (2014) 63:259–66. doi: 10.1016/j.jacc.2013.07.091
76. Reed GJ, Boczek NJ, Etheridge SP, Ackerman MJ. CALM3 mutation associated with long QT syndrome. *Heart Rhythm* (2015) 12:419–22. doi: 10.1016/j.hrthm.2014.10.035
77. Limpitikul WB, Dick IE, Joshi-Mukherjee R, Overgaard MT, George AL, Yue DT. Calmodulin mutations associated with long QT syndrome prevent inactivation of cardiac L-type Ca2+ currents and promote proarrhythmic behavior in ventricular myocytes. *J Mol Cell Cardiol.* (2014) 74:115–24. doi: 10.1016/j.yjmcc.2014.04.022
78. Pipilas DC, Johnson CN, Webster G, Schlaepfer J, Fellmann F, Sekarski N, et al. Novel calmodulin mutations associated with congenital long QT syndrome affect calcium current in human cardiomyocytes. *Heart Rhythm* (2016) 13:2012–9. doi: 10.1016/j.hrthm.2016.06.038
79. Boczek NJ, Gomez-Hurtado N, Ye D, Calvert ML, Tester DJ, Kryshtal D, et al. Spectrum and prevalence of CALM1-, CALM2-, and CALM3-encoded calmodulin (CaM) variants in long QT syndrome (LQTS) and functional characterization of a novel LQTS-associated CaM missense variant, E141G. *Circ Cardiovasc Genet.* (2016) 9:136–46. doi: 10.1161/CIRCGENETICS.115.001323
80. Rocchetti M, Sala L, Dreizehnter L, Crotti L, Sinnecker D, Mura M, et al. Elucidating arrhythmogenic mechanisms of long-QT syndrome CALM1-F142L mutation in patient-specific induced pluripotent stem cell-derived cardiomyocytes. *Cardiovasc Res.* (2017) 113:531–41. doi: 10.1093/cvr/cvx006
81. Priori SG, Napolitano C, Tiso N, Memmi M, Vignati G, Bloise R, et al. Mutations in the cardiac ryanodine receptor gene (hRyR2) underlie catecholaminergic polymorphic ventricular tachycardia. *Circulation* (2001) 103:196–200. doi: 10.1161/01.CIR.103.2.196
82. Zaza A, Rocchetti M. Calcium store stability as an antiarrhythmic endpoint. *Curr Pharm Des.* (2015) 21:1053–61. doi: 10.2174/1381612820666141029100650
83. Nishio M, Ruch SW, Kelly JE, Aistrup GL, Sheehan K, Wasserstrom JA. Ouabain increases sarcoplasmic reticulum calcium release in cardiac myocytes. *J Pharmacol Exp Ther.* (2004) 308:1181–90. doi: 10.1124/jpet.103.060004
84. Nyegaard M, Overgaard MT, Søndergaard MT, Vranas M, Behr ER, Hildebrandt LL, et al. Mutations in calmodulin cause ventricular tachycardia and sudden cardiac death. *Am J Hum Genet.* (2012) 91:703–12. doi: 10.1016/j.ajhg.2012.08.015
85. Gomez-Hurtado N, Boczek NJ, Kryshtal DO, Johnson CN, Sun J, Nitu FR, et al. Novel CPVT-associated calmodulin mutation in CALM3 (CALM3-A103V) activates arrhythmogenic Ca waves and sparks. *Circ Arrhythm Electrophysiol.* (2016) 9:e004161. doi: 10.1161/CIRCEP.116.004161
86. Hwang H-S, Nitu FR, Yang Y, Walweel K, Pereira L, Johnson CN, et al. Divergent regulation of RyR2 calcium release channels by arrhythmogenic human calmodulin missense mutants. *Circ Res.* (2014) 114:1114–24. doi: 10.1161/CIRCRESAHA.114.303391
87. Nomikos M, Thanassoulas A, Beck K, Vassilakopoulou V, Hu H, Calver BL, et al. Altered RyR2 regulation by the calmodulin F90L mutation associated with idiopathic ventricular fibrillation and early sudden cardiac death. *FEBS Lett.* (2014) 588:2898–902. doi: 10.1016/j.febslet.2014.07.007
88. Yu CC, Ko JS, Ai T, Tsai WC, Chen Z, Rubart M, et al. Arrhythmogenic calmodulin mutations impede activation of small-conductance calcium-activated potassium current. *Heart Rhythm* (2016) 13:1716–23. doi: 10.1016/j.hrthm.2016.05.009
89. Yamamoto Y, Makiyama T, Harita T, Sasaki K, Wuriyanghai Y, Hayano M, et al. Allele-specific ablation rescues electrophysiological abnormalities in a human iPS cell model of long-QT syndrome with a CALM2 mutation. *Hum Mol Genet.* (2017) 26:1670–7. doi: 10.1093/hmg/ddx073
90. Koivumäki JT, Naumenko N, Tuomainen T, Takalo J, Oksanen M, Puttonen KA, et al. Structural immaturity of human iPSC-derived cardiomyocytes: *in silico* investigation of effects on function and disease modeling. *Front Physiol.* (2018) 9:80. doi: 10.3389/fphys.2018.00080
91. Zaza A, Rocchetti M. The late Na+ current–origin and pathophysiological relevance. *Cardiovasc Drugs Ther.* (2013) 27:61–8. doi: 10.1007/s10557-012-6430-0


**Conflict of Interest Statement:** The authors declare that the research was conducted in the absence of any commercial or financial relationships that could be construed as a potential conflict of interest.

frontiers in Cardiovascular Medicine

REVIEW
published: 06 December 2018
doi: 10.3389/fcvm.2018.00175

# Calmodulinopathy: A Novel, Life-Threatening Clinical Entity Affecting the Young

*Maria-Christina Kotta[1†], Luca Sala[1†], Alice Ghidoni[1], Beatrice Badone[2], Carlotta Ronchi[2], Gianfranco Parati[3,4], Antonio Zaza[2‡] and Lia Crotti[1,3,4*‡]*

[1] Istituto Auxologico Italiano, IRCCS, Center for Cardiac Arrhythmias of Genetic Origin and Laboratory of Cardiovascular Genetics, Milan, Italy, [2] Department of Biotechnology and Bioscience, University of Milano-Bicocca, Milan, Italy, [3] Department of Medicine and Surgery, University of Milano-Bicocca, Milan, Italy, [4] Istituto Auxologico Italiano, IRCCS, Department of Cardiovascular, Neural and Metabolic Sciences, San Luca Hospital, Milan, Italy

Sudden cardiac death (SCD) in the young may often be the first manifestation of a genetic arrythmogenic disease that had remained undiagnosed. Despite the significant discoveries of the genetic bases of inherited arrhythmia syndromes, there remains a measurable fraction of cases where in-depth clinical and genetic investigations fail to identify the underlying SCD etiology. A few years ago, 2 cases of infants with recurrent cardiac arrest episodes, due to what appeared to be as a severe form of long QT syndrome (LQTS), came to our attention. These prompted a number of clinical and genetic research investigations that allowed us to identify a novel, closely associated to LQTS but nevertheless distinct, clinical entity that is now known as *calmodulinopathy*. Calmodulinopathy is a life-threatening arrhythmia syndrome, affecting mostly young individuals, caused by mutations in any of the 3 genes encoding calmodulin (CaM). Calmodulin is a ubiquitously expressed $Ca^{2+}$ signaling protein that, in the heart, modulates several ion channels and participates in a plethora of cellular processes. We will hereby provide an overview of CaM's structure and function under normal and disease states, highlighting the genetic etiology of calmodulinopathy and the related disease mechanisms. We will also discuss the phenotypic spectrum of patients with calmodulinopathy and present state-of-the art approaches with patient-derived induced pluripotent stem cells that have been thus far adopted in order to accurately model calmodulinopathy *in vitro*, decipher disease mechanisms and identify novel therapies.

**Keywords: CALM, calmodulin, long QT syndrome, sudden cardiac death, catecholaminergic polymorphic ventricular tachycardia**

OPEN ACCESS

***Edited by:***
*Gaetano M. De Ferrari, University of Pavia, Italy*

***Reviewed by:***
*Osmar Antonio Centurion, Universidad Nacional de Asunción, Paraguay*
*Daniel M. Johnson, University of Birmingham, United Kingdom*

***Correspondence:**
*Lia Crotti*
*l.crotti@auxologico.it*

*[†]These authors share the first authorship*

*[‡]These authors share the senior authorship*

***Specialty section:***
*This article was submitted to Cardiac Rhythmology, a section of the journal Frontiers in Cardiovascular Medicine*

***Received:*** *05 September 2018*
***Accepted:*** *22 November 2018*
***Published:*** *06 December 2018*

***Citation:***
*Kotta M-C, Sala L, Ghidoni A, Badone B, Ronchi C, Parati G, Zaza A and Crotti L (2018) Calmodulinopathy: A Novel, Life-Threatening Clinical Entity Affecting the Young. Front. Cardiovasc. Med. 5:175. doi: 10.3389/fcvm.2018.00175*

## INTRODUCTION

Sudden cardiac death (SCD) is an unexpected natural death due to cardiac causes that is responsible for up to 25% of all deaths in the Western world (1). While SCD as a term describes a final common clinical outcome, it does not by itself relay information on the pathophysiological mechanisms underlying its occurrence, which are quite distinct, especially when considering the age of the SCD victim. Indeed, in the young (<35 years), SCD is mainly the adverse outcome of inherited cardiac diseases, such as cardiomyopathies and channelopathies, with ventricular fibrillation (VF) being mostly the culprit arrhythmia (2). Unfortunately, SCD

may afflict even those in the perinatal, neonatal and early childhood period. We and others have shown that when post-mortem clinical investigations fail to identify the underlying causes ("mors sine materia" or "normal heart" SD) (3), channelopathies, and the long QT syndrome (LQTS) in particular, may contribute significantly to cases of sudden infant death syndrome (4), as well as intrauterine fetal death and stillbirth (5). In these cases, early-onset and highly malignant arrhythmias caused by penetrant genetic mutations in ion channel genes, or their accessory protein partners, often arising *de novo*, largely dictate SCD occurrence.

A few years ago, two infants having experienced recurrent VF episodes and suffering from what appeared to be as an unusually severe form of LQTS (QTc > 600 ms, intermittent 2:1 atrioventricular block and T wave alternans) came to our attention. Both were born to healthy parents and genetic testing of the major LQTS genes was negative. In order to identify what we presumed to be a novel underlying genetic cause of these severe arrhythmia manifestations, we performed whole-exome sequencing in both infants (as part of parent-child trios) and identified novel mutations in two of the three genes encoding the $Ca^{2+}$-signaling protein calmodulin (*CALM1*-p.D130G and *CALM2*-p.D96V) that were shown to have arisen *de novo*, thus explaining the parents' normal phenotype (6). This finding was further validated by expanding our search for calmodulin (CaM) mutations in a pool of unrelated LQTS patients that were genetically negative for mutations in the main LQTS genes. In doing so, we identified the same *CALM1*-p.D130G mutation as well as the novel *CALM1*-p.F142L mutation in two other unrelated LQTS cases with severe disease and recurrent cardiac arrest episodes (6). Shortly after, other investigators identified the same p.D130G mutation, albeit in the *CALM3* gene, as a novel genetic substrate of severe LQTS (7), thus completing the picture of a "genetic trilogy" for a new clinical entity that has been termed *calmodulinopathy* (8).

In the past few years our knowledge on calmodulinopathy has expanded and it is now known to be a severe arrhythmogenic condition that can manifest mainly as LQTS (6), catecholaminergic polymorphic ventricular tachycardia (9) or idiopathic VF (IVF) (10) caused by genetic mutations in any of the 3 calmodulin genes (*CALM1, CALM2, CALM3*). Calmodulin is a ubiquitously expressed protein that participates in a plethora of cellular processes, while acting intracellularly both as a $Ca^{2+}$ sensor and signal transducer. In the heart, CaM is a major player in the modulation of several ion channels such as the L-type calcium channel (LTCC), the sodium channel, different potassium channels, and the ryanodine receptor (RyR) (11).

In this review, we will provide an overview of currently available knowledge on this severe arrhythmogenic syndrome, termed calmodulinopathy. In particular, we will present in detail CaM's sequence, structure and function, the genetic spectrum of CaM mutations and the associated phenotypes, as well as available therapies. We will also overview the underlying disease mechanisms of calmodulinopathy (reviewed in detail in the accompanying article by Badone et al.) and present the thus far used *in vitro* methods for deciphering these disease mechanisms.

## CALMODULIN GENES AND PROTEIN

The first complementary DNA (cDNA) clone of human CaM was isolated from a human liver cDNA library in 1984 (12). Within a few years, two more human cDNA clones were isolated and characterized (13, 14) with diverse nucleic acid sequence identity but all encoding an identical CaM protein. These results suggested the existence of a multigene CaM family operating under selective pressure to regulate and express a protein with a prominent cellular role.

Calmodulin in humans is indeed encoded by three different genes (*CALM1*, *CALM2* and *CALM3*; NG_013338.1, NG_042065.1 and NG_051331.1 RefSeqGenes, respectively), located on three different chromosomes (14q32.11, 2p21 and 19q13.32, respectively). Although several splice variants exist, only few transcripts contribute to the full-length CaM protein with the principal ones being NM_006888.4, NM_001743.5 and NM_005184.3, respectively. The three genes have a similar exon-intron structure, with 6 coding exons (14–16). The CaM protein generated from the translation of each of the three main transcripts has a length of 149 amino acids and an identical amino acid sequence. Its evolutionary importance is highlighted not only by the presence of three different genes located on three different chromosomes encoding the same protein, but also by the extent of conservation of its protein sequence that is full across vertebrates and very high across all eukaryotes (17) (**Figure 1A**).

Despite CaM's significant conservation, the respective *CALM* genes share only approximately 80% sequence identity among their coding regions, while they have no significant homology in their non-coding regions (14). This shows that the *CALM* genes have diverged early during evolution (14) and are not the result of gene duplications as is often the case with multigene families, while operating under a strict evolutionary control that aims to maintain their structural integrity.

Although CaM's genetic redundancy may partly serve its ubiquitous nature and support its pivotal role in several processes essential for cell survival and functioning, little is known about *CALM* genes' differential expression. Gene expression analyses have shown that in mammalian cells (16) and human hearts at the fetal, infant and adult stages of development (6), significantly higher transcriptional levels of *CALM3* than *CALM2* and *CALM1* are observed, with the latter being the least transcribed. Data from the Expression Atlas (18) and the Human Protein Atlas (19) indicate that all three CaM genes are ubiquitously expressed in the majority of tissues, with high and medium levels of expression found in the brain and heart, respectively. At the protein level, the relative contribution of each transcript is still unclear. Upon the initial identification of different cDNA clones, suggesting the existence of three different genes, it was hypothesized that one gene could be the housekeeping gene, while the other two could be differentially expressed under conditions of particular stimuli (14). This however seems not to be the case and all transcripts contribute toward CaM's overall expression (20), albeit unclear to which extent.

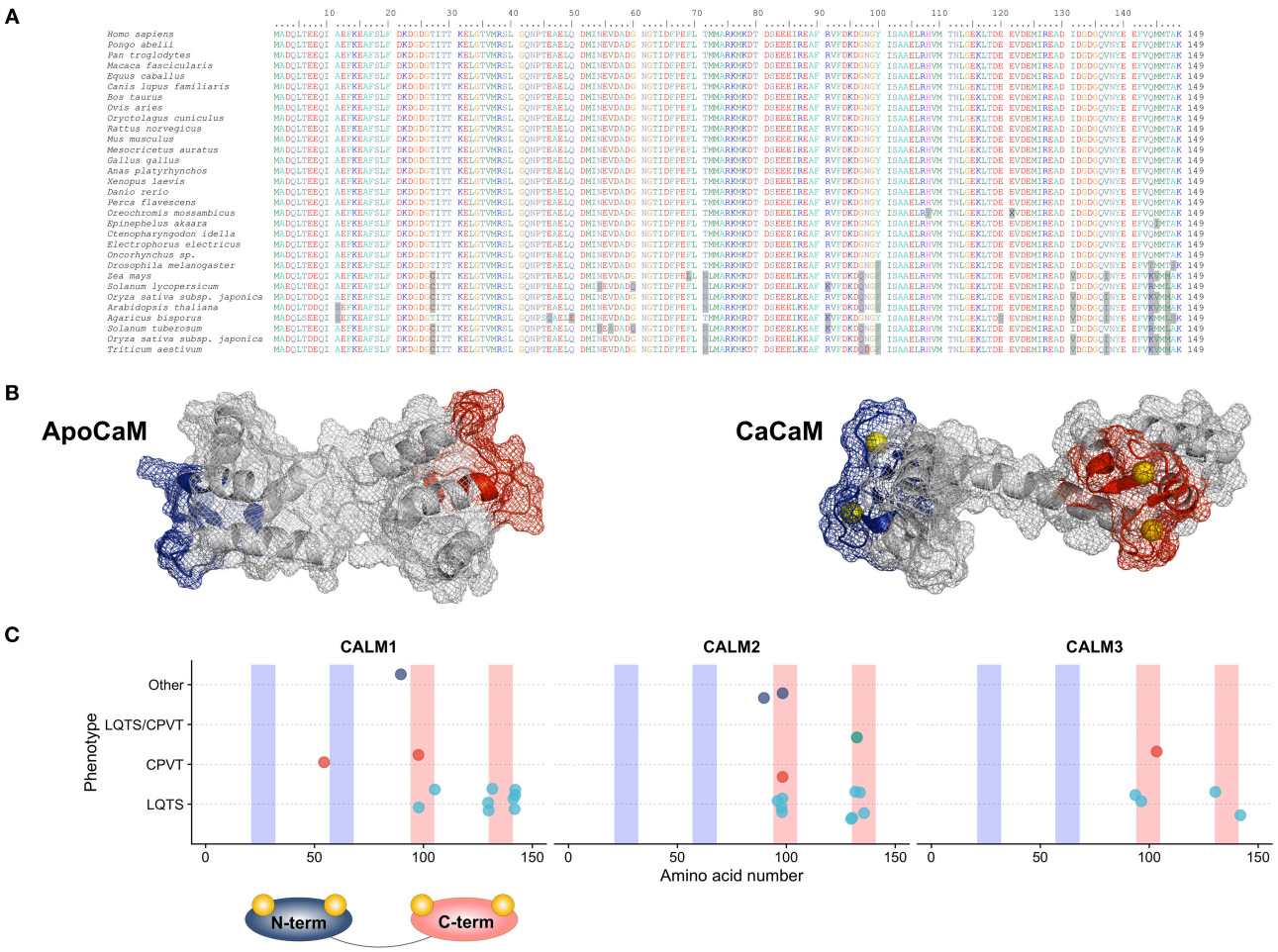


**FIGURE 1 | (A)** Multiple species alignment of the CaM protein sequence showing full sequence conservation across vertebrates and an impressive sequence conservation across lower eukaryotes. **(B)** CaM protein structure in the ApoCaM **(left)** and Holo- or CaCaM conformation **(right)**. The N-terminal and C-terminal $Ca^{2+}$ lobes are shown in blue and red, respectively. $Ca^{2+}$ ions are shown in yellow. PDB structures entries: ApoCaM PDB ID: 1CFD; CaCaM PDB ID: 1CLL. **(C)** Genotype-phenotype correlation graphic representation of published CaM mutations, with respect to the gene and domain in which the mutations reside. C-terminal $Ca^{2+}$-binding domains are shown in red and N-terminal $Ca^{2+}$-binding domains are shown in blue.

## CALMODULIN'S STRUCTURE

Human CaM is a small 149 amino acid protein with a length of 65 Angstroms (Å) that could be pictured in the shape of a dumbbell (21). It is comprised of two $Ca^{2+}$-binding lobes at its N- and C-terminus which are linked by a flexible helix, each containing two EF-hand (helix-loop-helix) structural motifs with $Ca^{2+}$-binding properties (**Figure 1B**). The lobes display cooperative $Ca^{2+}$-binding properties (22), with faster $Ca^{2+}$ binding at the N-terminal lobe and higher $Ca^{2+}$-binding affinity at the C-terminal lobe (23), thus allowing CaM to function either as a rapid or slow $Ca^{2+}$ sensor (24).

Within the cell, CaM may exist in multiple conformations that can be summarized in a six-state folding model, dependent on intracellular $Ca^{2+}$ levels (25). Calmodulin folding and regulation have been evolutionally selected as robust key mediators of multiple $Ca^{2+}$-based intracellular signals to control the activity of downstream targets in response to a broad range of intracellular $Ca^{2+}$ concentration changes and different states of energetic stability (25). At low intracellular $Ca^{2+}$ concentrations, the empty, $Ca^{2+}$-free form (ApoCaM) prevails; increasing $Ca^{2+}$ concentration leads to a progressive and cooperative occupation of the four $Ca^{2+}$-binding sites until the saturated form (CaCaM or *HoloCaM*) is reached. $Ca^{2+}$ binding and folding properties of each domain do influence both target binding and target regulation and confer to CaM the pliability to sense both local and global $Ca^{2+}$ levels (24).

## CALMODULIN'S INTERACTION NETWORK

Multiple cardiac ion channels and pumps are targeted and regulated by intracellular $Ca^{2+}$ through $Ca^{2+}$-sensing proteins, with CaM being the predominant and most widespread. This $Ca^{2+}$-dependent regulation acts on multiple levels and involves, among others, sarcolemmal ion channels responsible for the

L-type $Ca^{2+}$ current ($I_{CaL}$, $Ca_v1.2$), the peak sodium current ($I_{Na}$, $Na_v1.5$), the slow delayed rectifier potassium current ($I_{Ks}$, $K_v7.1$), the inward rectifier potassium current ($I_{K1}$, $K_{ir}2.1$) and sarcoplasmic reticulum (SR) proteins such as the cardiac ryanodine receptors (RyR2) and phospholamban (PLB) (11). The regulation of these targets by CaM can be primary, through a direct association of CaM to its target, or mediated by the activity of $Ca^{2+}$-CaM-dependent protein kinase II (CaMKII).

Different CaM pools do exist within the cell and the net result of this somehow unique protein distribution and equilibrium is that the vast majority (∼99%) of CaMs appear to be already pre-bound to targets (26, 27), thereby assigning a buffering capacity to the remaining tiny fraction of the total CaM pool. This means that the three different CaM genes encode for identical CaM proteins that will be mostly bound to their targets. This scenario dramatically reduces the competition for target binding and constitutes a vulnerable substrate toward genetic mutations.

Under certain conditions, when the ApoCaM configuration is adopted, the N-terminal lobe has higher stability than the C-terminal lobe (25), which allows the binding/pre-association to important biological targets such as the $Na_v1.5$ or $Ca_v1.2$ channels in the ApoCaM form (28, 29). In particular, ApoCaM pre-association to $Ca_v1.2$ is required since CaMs from the cytosolic bulk are unable to adequately access the binding site on $Ca_v1.2$ during $Ca^{2+}$ inflow (28); this property confers to the residual CaMs the ability to finely modulate substrate activities in response to local intracellular $Ca^{2+}$ concentration changes (30, 31) with such a precision and velocity that would not be possible if Ca-CaM would have to be recruited from the cytosolic CaM bulk.

A certain degree of cytosolic CaM–level dependency is nevertheless maintained in the cells as a mechanism of $Ca^{2+}$ homeostasis tuning other ion channels (32). Furthermore, according to modeling data published by Valeyev and coworkers, specificity and selectivity of CaM target regulation relies on target CaM-specific constants of dissociations and on the number of $Ca^{2+}$ ions required for CaM-target complex activation (33), with some interactions requiring a preferential $Ca^{2+}$ binding to the N-terminus (34), C-terminus or both.

Results by multiple groups have converged on deciphering the role of CaM's two main targets that underlie and define the main calmodulinopathy phenotypes, i.e., $Ca_v1.2$ and RyR2, encoded by *CACNA1C* and *RYR2*, genes with a previously established role in LQTS and CPVT pathogenesis, respectively.

## GENETICS OF CALMODULINOPATHY

Twenty three mutations in one of the three CaM genes have been identified so far in thirty index calmodulinopathy patients with different arrhythmic phenotypes (6, 7, 9, 10, 35–43) (**Table 1**). The mutations thus far described have mainly arisen *de novo*, as demonstrated by parental genetic screening in 23 families. In only three cases the mutation was inherited (*CALM3*-p.A103V, *CALM1*-p.N54I, *CALM1*-p.F90L (9, 10, 35) and was shown to co-segregate with an arrhythmic phenotype in the respective families.

All 23 mutations described are single nucleotide substitutions, leading to 18 distinct missense amino acid changes and are prevalently distributed in the *CALM1* ($n = 8$) and *CALM2* ($n = 10$) genes, while a few reside in the *CALM3* gene ($n = 5$). Interestingly, the majority of mutations (18/23, 78%) are localized in CaM's C-terminal $Ca^{2+}$-binding domains (EF-hands III and IV) (**Figure 1C**), and especially in the specific residues directly involved in $Ca^{2+}$ binding (16/23, 70%). Since the C-terminal EF-hands (III and IV) have been demonstrated to have a higher $Ca^{2+}$-binding affinity than those in the N-terminus (I and II), calmodulinopathy's mutation distribution strongly highlights the importance of $Ca^{2+}$-binding affinity for proper protein function and indicates specific topological domains that seem to be intolerant to genetic variation.

In support of the latter also come data on CaM genetic variation from the general population (genome aggregation database, gnomAD) (44). Not only thus far described calmodulinopathy-causative variants are absent from the general population, but also, the *CALM* non-synonymous genetic variants that are present ($n = 29$) have a different distribution within the CaM protein compared to the calmodulinopathy-causing mutations. In fact, the former are mainly localized outside the $Ca^{2+}$-binding domains, in the EF-hand linkers and in the N- and C-terminal ends of the protein. In addition, the C-terminal EF-hands III and IV host recurrent calmodulinopathy-causing mutations, such as the p.N98S, p.D130G, and p.F142L, identified thus far in 6, 4 and 4 index cases, respectively, further highlighting the functional importance and intolerance to variation of these topological domains within the CaM protein.

## CALMODULINOPATHY DISEASE MECHANISMS

Among all CaM mutations thus far described (45), 11 have been functionally investigated *in vitro,* mostly by $Ca^{2+}$-binding assays and/or electrophysiological studies. In our initial description of LQTS-associated calmodulinopathy (6) we provided preliminary evidence that the CaM mutations identified exhibited reduced affinity for $Ca^{2+}$ and were thereby predicted to interfere with CaM's ability to transduce $Ca^{2+}$-mediated signals. Diminished $Ca^{2+}$-binding capacity had also been previously demonstrated by *in vitro* overexpression of mutant CaM in mammalian cardiomyocytes (CMs), which resulted in severe action potential prolongation, i.e., a cellular recapitulation of LQTS (46). We have further validated this reduced affinity for $Ca^{2+}$ in the context of other LQTS-related CaM mutations (38, 39). Moreover, we have identified impaired $Ca^{2+}$-dependent inactivation (CDI) of the L-type $Ca^{2+}$ channel $Ca_v1.2$- with concordant disruption of cellular $Ca^{2+}$ homeostasis- as the prominent mechanism of LQTS-associated calmodulinopathy (39, 47) (**Figure 2A**). Our findings have been in accordance with those of other investigators.

Calcium-dependent inactivation is the mechanism by which conformational changes in CaM, driven by extracellular $Ca^{2+}$ inflow through $Ca_v1.2$, modulate part of the inactivation of the LTCCs. This mechanism acts as a negative feedback loop to precisely control the amount of $Ca^{2+}$ entering the cardiomyocyte at each heartbeat and it is deranged in the presence of certain CaM mutations associated with an LQTS

**TABLE 1 |** List of published CaM mutations associated with arrhythmic phenotypes.

| Gene | Nucleotide change | Amino acid change | Protein domain | N. of probands | Associated phenotype | References |
|---|---|---|---|---|---|---|
| *CALM1* | c.161A>T | p.N54I | inter-EF hand I-II linker | 1 | CPVT | (9) |
| *CALM1* | c.268T>C | p.F90L | inter-EF hand II-III linker | 1 | IVF | (10) |
| *CALM2* | c.268T>C | p.F90L | inter-EF hand II-III linker | 1 | SUD | (43) |
| *CALM3* | c.281A>C | p.D94A | EF-hand III | 1 | LQTS | (37) |
| *CALM3* | c.286G>C | p.D96H | EF-hand III | 1 | LQTS | (40) |
| *CALM2* | c.287A>T | p.D96V | EF-hand III | 1 | LQTS | (6) |
| *CALM1* | c.293A>G | p.N98S | EF-hand III | 2 | LQTS, CPVT | (9, 37) |
| *CALM2* | c.293A>G | p.N98S | EF-hand III | 4 | LQTS,CPVT,SUD | (36, 38, 43) |
| *CALM2* | c.293A>T | p.N98I | EF-hand III | 1 | LQTS | (38) |
| *CALM3* | c.308C>T | p.A103V | EF-hand III | 1 | CPVT | (35) |
| *CALM1* | c.314A>C | p.E105A | EF-hand III | 1 | LQTS | (42) |
| *CALM1* | c.389A>G | p.D130G | EF-hand IV | 2 | LQTS | (6) |
| *CALM2* | c.389A>G | p.D130G | EF-hand IV | 1 | LQTS | (41) |
| *CALM3* | c.389A>G | p.D130G | EF-hand IV | 1 | LQTS | (7) |
| *CALM2* | c.389A>T | p.D130V | EF-hand IV | 1 | LQTS | (41) |
| *CALM2* | c.394G>C | p.D132H | EF-hand IV | 1 | LQTS | (39) |
| *CALM1* | c.395A>T | p.D132V | EF-hand IV | 1 | LQTS | (39) |
| *CALM2* | c.396T>G | p.D132E | EF-hand IV | 1 | LQTS/CPVT Overlap | (38) |
| *CALM2* | c.400G>C | p.D134H | EF-hand IV | 1 | LQTS | (38) |
| *CALM2* | c.407A>C | p.Q136P | EF-hand IV | 1 | LQTS | (38) |
| *CALM1* | c.422A>G | p.E141G | EF-hand IV | 1 | LQTS | (41) |
| *CALM1* | c.426C>G | p.F142L | C-terminal region | 3 | LQTS | (6, 41) |
| *CALM3* | c.426T>G | p.F142L | C-terminal region | 1 | LQTS | (40) |
| Total | 23 | 18 | | 30 | | |

phenotype (LQTS-CaM), (**Figure 2A**). Multiple lines of evidence converge on the fact that LQTS-CaM mutations decrease CaM's affinity for $Ca^{2+}$ and lead to an impaired CDI, resulting in an increased and uncontrolled $Ca^{2+}$ inflow, action potential (AP) prolongation, QT interval prolongation and potentially lethal arrhythmogenic events. Conversely, other CaM mutations do not impair CaM's $Ca^{2+}$-binding properties, but, rather, they strengthen CaM's binding affinity to RyR2, thus promoting the open conformation of RyR2 and interfering with its fine regulation. When dysfunctional interactions between CaM and RyR2 occur, e.g., due to mutations associated to a CPVT phenotype (CPVT-CaM), SR $Ca^{2+}$ content, along with its feedback mechanism, are dysregulated, leading to premature and spontaneous $Ca^{2+}$ releases from the SR and arrhythmogenic propensity (48) (**Figure 2B**).

The polyhedral nature of CaM's interaction network certainly hampers the identification of straightforward links between clinical manifestations of calmodulinopathy and its underlying molecular bases. Although several hypotheses have been formulated, many of which by our group (6, 49), and calmodulinopathy's main molecular mechanisms delineated, a generalized consensus and in-depth understanding of the reasons leading to such severe clinical phenotypes, are still pending. The current hypothesis to explain the malignancy of the disease manifestations mainly relies on two mechanisms which might synergistically concur to shape the disease phenotype (**Figure 3**). Considering that 99% of CaMs are already pre-bound to their targets, this logically implies that also mutant CaMs will be bound to targets. However, this hypothesis alone, especially in the presence of a plethora of downstream mediators, may not fully explain the funneling of clinical manifestations into two main phenotypes, sometimes even in the presence of identical mutations.

The reason may partly rely also on a second mechanism, which involves the collateral consequences of ApoCaM's molecular interaction with its targets. Given that CaM pre-association to LTCC does not require $Ca^{2+}$, it is reasonable to speculate that mutations impacting on the $Ca^{2+}$-binding affinity of CaM should not theoretically alter ApoCaM's substrate-binding ability *per se*, but, on the contrary, they may indirectly enable it since mutant CaMs have a lower affinity for $Ca^{2+}$ in their C-terminus lobe and thus are more likely to be found in the ApoCaM form. The data generated by the Yue lab (50) demonstrated, through elegant FRET assays, that LQTS-CaMs have at least an equal affinity for LTCC in the ApoCaM form, with some LQTS-CaM mutations exhibiting even a higher affinity than WT-CaMs. Therefore, targets that require a pre-association of ApoCaM will be preferentially bound to LQTS-CaM mutants, which would explain both the fact that some targets seem unaffected by these mutations, as well as the dominant expression of the pathogenic phenotype despite the wild type-favoring (5:1) allelic balance (**Figure 3**).

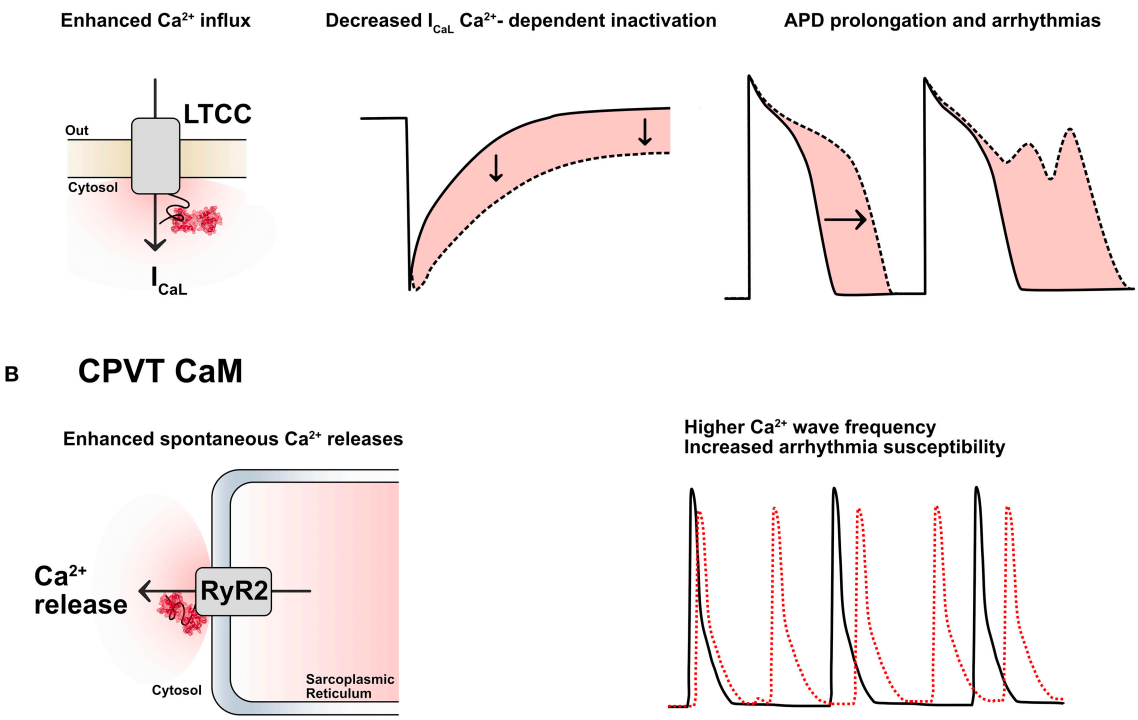


**FIGURE 2 | (A)** LQTS-CaMs induce an increased $Ca^{2+}$ influx via $I_{CaL}$ by decreasing its $Ca^{2+}$-dependent inactivation (CDI); this causes an enhanced $Ca^{2+}$ influx, a consequent action potential duration (APD) prolongation and arrhythmias. LTCC: L-type calcium channels. **(B)** CPVT-CaMs promote $Ca^{2+}$-release from the sarcoplasmic reticulum through the cardiac ryanodine receptors (RyR2). This leads to a higher frequency of $Ca^{2+}$ waves and to a higher arrhythmia susceptibility, especially in the presence of catecholamines.

## INDUCED PLURIPOTENT STEM CELL-DERIVED CARDIOMYOCYTE PLATFORMS FOR CALMODULINOPATHY MODELING *IN VITRO* AND TESTING OF THERAPEUTIC APPROACHES

Most of the studies that have aimed to characterize the relative effects of CaM mutations have used heterologous expression systems such as transient expression of CaM mutants in HEK293 (48, 50), tsA201 cells (41, 47), mammalian CMs (35, 41, 48, 50), or human induced pluripotent stem cells (hiPSCs) from healthy donors (39). Although these studies have provided insight into the prominent pathophysiological mechanisms of calmodulinopathy, they have had the major inherent limitation of not being able to faithfully recapitulate the *in vivo* effects by simply not respecting the native stoichiometry of mutant and wild-type CaM proteins. Having three different genes encoding the same CaM protein implies that in the presence of a mutation in a heterozygous state, there is a 5:1 wild-type:mutant allelic stoichiometry, with the quantitatively underrepresented mutant CaM still being able to confer its devastating effects. The redundancy of the CaM genes hampers also the generation of transgenic animal models, with diverse CaM gene copy numbers among species representing a substantial caveat for *in vivo* disease modeling.

In order to provide a more profound understanding of the effects conferred by CaM mutations in their native CM environment, multiple groups, including ours, generated hiPSCs from patients with CaM mutations (20, 49, 51). With the confidence of working in a physiologically relevant experimental model, CaM mutation rescue strategies have been recently attempted with multiple approaches. Limpitikul and coworkers used an elegant CRISPRi gene silencing approach to precisely suppress the transcription of the mutant *CALM2*$^{D130G}$ allele, allowing a complete rescue of the LQTS phenotype (20). Yamamoto and coworkers, instead, followed a gene editing approach to selectively knockout the *CALM2*$^{N98S}$ allele (51). Although not currently feasible in humans, this procedure demonstrated that the *CALM* loci can be realistic targets for gene correction approaches. Finally, Rocchetti and coworkers rescued the pathogenic LQTS phenotype caused by a *CALM1*$^{F142L}$ mutation investigated in detail in hiPSC-CMs from a calmodulinopathy patient (6) by blocking $I_{CaL}$ with verapamil (49). The field potential (FP) duration, measured with MEA, was rescued with acute exposure to verapamil, holding promise for a rapid implementation of this pharmacological approach in the clinical setting. This observation was immediately translated

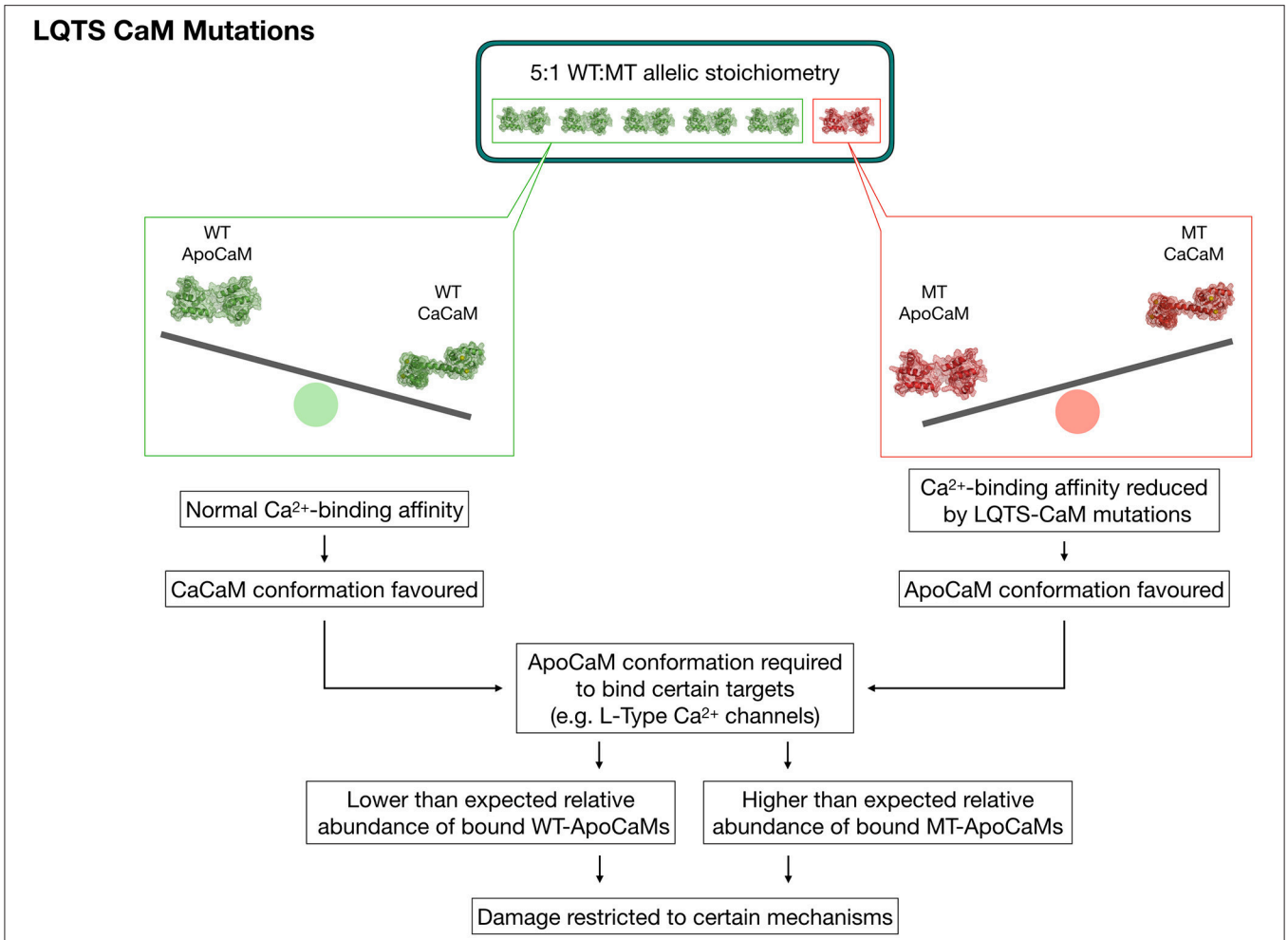


**FIGURE 3 |** Graphic representation depicting a theory to explain the strong phenotypic effect and allelic dominance of CaM mutants in the setting of heterozygous LQTS-CaM mutations. The lower $Ca^{2+}$ binding affinity of LQTS-CaMs creates a larger than expected pool of LQTS-ApoCaMs, i.e., the conformation that binds LTCCs, with a consequent higher-than-expected abundance of LQTS-CaM bound to LTCCs. Thus, LTCCs will have a high percentage of dysfunctional CaMs bound, which will significantly disrupt their activity despite the 5:1 WT:MT allelic stoichiometry.

by Webster and coworkers in clinical practice and in a single calmodulinopathy patient (52) verapamil showed some promising results.

Overall, these studies demonstrated the importance and feasibility of modeling calmodulinopathy in the setting of its native environment, provided insight into the pathophysiological mechanism underlying the respective life-threatening arrhythmias and validated calmodulinopathy patient-derived iPSC-CMs as a platform for precision medicine investigations.

## CALMODULINOPATHY PHENOTYPES AND CLINICAL FEATURES

The rapid emergence of the genetic discoveries related to calmodulinopathy has eclipsed the ability of the field to ascertain and compare in depth all the individual clinical features among different subjects thus far described in the literature. This has naturally led to the "lumping" of cases under existing clinical "umbrella" terms. Indeed, CaM mutations have been associated with a spectrum of arrhythmic phenotypes, including LQTS, CPVT, IVF, as well as LQTS/CPVT overlap and Sudden Unexplained Death (SUD) (6, 7, 9, 10, 35–43). From the thus far available descriptions, however, it seems to emerge that there is a novel constellation of symptoms, arrhythmia types, ECG features and response to therapy that are characteristic of calmodulinopathy as a clinical entity, closely-related, but nevertheless distinct, from other arrhythmia syndromes.

To this end, we have recently established an international registry of subjects with CaM mutations (ICalmR) (45), currently enrolling patients from overall 15 countries, in order to conduct a thorough ascertainment of the clinical spectrum, genotype-phenotype relationship, and treatment responses of these patients. In order to further aid the enrollment of new

cases and facilitate the discussion among experts, ICalmR has become a member of the European Reference Network on rare diseases of the heart (53), while, recently, the registry has been made available to the European Commission for online data submission and patient enrollment, according to EU requirements.

From the descriptions thus far available in the literature, the most prevalent phenotype is LQTS, observed in 73% (22/30) of index cases. All LQTS-associated CaM mutations are localized within CaM's EF-hands III ($n = 7$) and IV ($n = 9$) or in the C-terminal region ($n = 2$). The second most frequent arrhythmic phenotype observed is CPVT, with 4 index cases carrying the *CALM1*-p.N54I, *CALM1*-p.N98S, *CALM2*-p.N98S, or *CALM3*-p.A103V mutations. Much less represented phenotypes are LQTS/CPVT overlap (1 case, *CALM2*-p.D132E), IVF (1 case, *CALM1*-p.F90L), and SUD (2 cases, *CALM2*-p.F90L, *CALM2*-p.N98S). Interestingly, particular hotspot mutations, such as the p.N98S mutation, may give rise to diverse arrhythmic phenotypes (LQTS, CPVT, SUD), regardless of the gene in which the nucleotide substitution resides, whilst others, such as the p.D130G and p.F142L, always cause definite LQTS.

Irrespective of the associated phenotypes, a common feature of all CaM mutations identified so far is the extreme severity of disease manifestations and early occurrence with almost half of subjects having a perinatal presentation (28th week of gestation to 28th postnatal day) (12/28, 43%, with the exclusion of 2 SUDs), mainly among those with an LQTS phenotype. The latter often show 2:1 AV block, T wave alternans and QTc values above 550 ms (45).

As in other inherited arrhythmogenic conditions, SCD can be the first manifestation of the disease, but unfortunately SCD can also occur after diagnosis and establishment of antiarrhythmic therapies. Indeed, to provide some examples, in two patients, both carrying the *CALM1*-p.F142L mutation, the diagnosis of LQTS was made just after birth and beta-blocker therapy was immediately started. Later on, a pacemaker was implanted. Nevertheless, they both later died suddenly, at 2 and 1 years of age (41). Another LQTS subject, carrying the *CALM2*-p.Q136P mutation, came to medical attention at 8 years of age after an episode of syncope associated with a prolonged period of unconsciousness. At that time, she had a prolonged QTc of 500 ms with ventricular bigeminy, she was put on nadolol, but she died suddenly during a dancing competition at 11 years of age (38).

Unfortunately, half of calmodulinopathy patients will experience SCD (45) and may survive only if, often by chance, appropriate resuscitation will be provided in due time. Among those who will survive, many may end up neurologically compromised. Of note, in our original description of LQTS-associated calmodulinopathy (6), all patients presented with some neurodevelopmental/neurological features. However, it is still unclear whether neurological impairment may be an inherent feature of the disease spectrum, since CaM is also highly expressed in the brain, or such an impairment may be only the secondary result of multiple resuscitated cardiac arrests causing brain injury. By means of studying the disease systemically and by jointly examining a larger number of cases through the ICalmR (45), some light may be shed on whether CaM's non-cardiac expression may also give rise to concomitant non-cardiac phenotypes in the setting of calmodulinopathy.

## CALMODULINOPATHY THERAPY

Calmodulinopathy is a severe condition for which effective therapies are currently lacking. From the clinical data and descriptions available thus far in the literature, and from our own clinical experience (45), commonly used anti-arrhythmic therapies and procedures (i.e., left cardiac sympathetic denervation) largely fail to treat these young patients. Indeed, β blocker therapy- the mainstay treatment for LQTS and CPVT- seems to offer minimal benefit at controlling the life-threatening arrhythmias, while other antiarrhythmics, such as sodium channel blockers, have also not produced promising results (6, 52). $Ca^{2+}$ channel blockade may seem a rational therapeutic option since impaired CDI of the $Ca^{2+}$ channel $Ca_v1.2$ is the prominent underlying mechanism of LQTS related to CaM mutations (20, 49, 51). However, the $Ca^{2+}$ antagonist verapamil, despite some positive results in one case (52), largely fails to prevent cardiac event recurrences in other clinical cases (6, 45). This may be attributed to the fact that verapamil principally targets peak calcium current rather than modulating channel inactivation (52).

Although implantable cardioverter defibrillators (ICD) would be the treatment of choice for any patient surviving SCD due to VF (54), this type of intervention in these young patients imposes almost impossible clinical dilemmas. On one hand, the risk of complications is higher than in adults, but, on the other hand, these children are at very high risk of dying suddenly or having neurological sequelae due to brain injury secondary to multiple resuscitated cardiac arrests. Unfortunately, we have examples showing a premature death in both scenarios (i.e., death related to ICD complications or death related to VF when the ICD was not implanted).

These real life examples highlight the urgent need to identify appropriate management schemes and therapies for life-threatening calmodulinopathy.

## CONCLUSION

Genetic mutations in any of the 3 genes encoding the ubiquitous $Ca^{2+}$ signaling protein CaM cause calmodulinopathy, a recently identified severe arrhythmogenic entity, affecting very young individuals. Although more arrhythmic phenotypes have been associated to CaM mutations, LQTS is the predominant one, with CDI of the L-type $Ca^{2+}$ channel $Ca_v1.2$ and disruption of cellular $Ca^{2+}$ homeostasis being the main underlying mechanism. To date, no therapies exist that may effectively treat the life-threatening arrhythmias and prevent SCD occurrence, while ICD implantation in these young patients is frequently associated with complications.

State-of-the-art technologies such as patient-derived iPSC-CMs have been successfully thus far employed for

calmodulinopathy modeling, not only providing insight into the mechanistic bases but also showing promising results for future precision medicine investigations, e.g., through gene correction approaches.

Systematic clinical evaluation of a large number of patients and identification of new cases prospectively in combination with the most recent technological advancements in hiPSC-CM technology, pharmacological screenings (55), and tridimensional approaches (56, 57), hold promise in identifying effective therapeutic strategies for this devastating disease.

## AUTHOR CONTRIBUTIONS

M-CK wrote the manuscript and drew the protein alignments. LS wrote the manuscript and drew the figures. AG wrote the manuscript. BB, CR, GP, and AZ critically reviewed the manuscript. LC wrote and critically reviewed the manuscript.

## FUNDING

This work was originally supported by the Italian Ministry of Health (GR-2010-2305717).

## REFERENCES


1. Priori SG, Blomström-Lundqvist C, Mazzanti A, Blom N, Borggrefe M, Camm J, et al. ESC Guidelines for the management of patients with ventricular arrhythmias and the prevention of sudden cardiac death: the task force for the management of patients with ventricular arrhythmias and the prevention of sudden cardiac death of the European Society of Cardiology (ESC)endorsed by: Association for European Paediatric and Congenital Cardiology (AEPC). *Eur Heart J.* (2015) 36:2793–867. doi: 10.1093/eurheartj/ehv316
2. Crotti L, Kotta MC. The role of genetics in primary ventricular fibrillation, inherited channelopathies and cardiomyopathies. *Int J Cardiol.* (2017) 237:45–8. doi: 10.1016/j.ijcard.2017.03.119
3. Basso C, Carturan E, Pilichou K, Rizzo S, Corrado D, Thiene G. Sudden cardiac death with normal heart: molecular autopsy. *Cardiovasc Pathol.* (2010) 19:321–5. doi: 10.1016/j.carpath.2010.02.003
4. Arnestad M, Crotti L, Rognum TO, Insolia R, Pedrazzini M, Ferrandi C, et al. Prevalence of long-QT syndrome gene variants in sudden infant death syndrome. *Circulation* (2007) 115:361–7. doi: 10.1161/CIRCULATIONAHA.106.658021
5. Crotti L, Tester DJ, White WM, Bartos DC, Insolia R, Besana A, et al. Long QT syndrome – associated mutations in intrauterine fetal death. *JAMA* (2013) 309:1473–82. doi: 10.1001/jama.2013.3219
6. Crotti L, Johnson CN, Graf E, De Ferrari GM, Cuneo BF, Ovadia M, et al. Calmodulin mutations associated with recurrent cardiac arrest in infants. *Circulation* (2013) 127:1009–17. doi: 10.1161/CIRCULATIONAHA.112.001216
7. Reed GJ, Boczek NJ, Etheridge SP, Ackerman MJ. CALM3 mutation associated with long QT syndrome. *Heart Rhythm* (2015) 12:419–22. doi: 10.1016/j.hrthm.2014.10.035
8. George AL. Calmodulinopathy: a genetic trilogy. *Heart Rhythm* (2015) 12:423–4. doi: 10.1016/j.hrthm.2014.11.017
9. Nyegaard M, Overgaard MT, Søndergaard MT, Vranas M, Behr ER, Hildebrandt LL, et al. Mutations in calmodulin cause ventricular tachycardia and sudden cardiac death. *Am J Hum Genet.* (2012) 91:703–12. doi: 10.1016/j.ajhg.2012.08.015
10. Marsman RF, Barc J, Beekman L, Alders M, Dooijes D, van den Wijngaard A, et al. A mutation in CALM1 encoding calmodulin in familial idiopathic ventricular fibrillation in childhood and adolescence. *J Am Coll Cardiol.* (2014) 63:259–66. doi: 10.1016/j.jacc.2013.07.091
11. Ben-Johny M, Dick I, Yang W, Issa J, Sang L, Lee S, et al. Towards a unified theory of calmodulin regulation (calmodulation) of voltage-gated calcium and sodium channels. *Curr Mol Pharmacol.* (2015) 8:188–205. doi: 10.2174/1874467208666150507110359
12. Wawrzynczak EJ, Perham RN. Isolation and nucleotide sequence of a cDNA encoding human calmodulin. *Biochem Int.* (1984) 9:177–85.
13. Sen Gupta B, Detera-Wadleigh SD, McBride OW, Friedberg F. A calmodulin pseudogene on human chromosome 17. *Nucleic Acids Res.* (1989) 17:2868. doi: 10.1093/nar/17.7.2868
14. Fischer R, Koller M, Flura M, Mathews S, Strehler-Page MA, Krebs J, et al. Multiple divergent mRNAs code for a single human calmodulin. *J Biol Chem.* (1988) 263:17055–62.
15. Rhyner JA, Ottiger M, Wicki R, Greenwood TM, Strehler EE. Structure of the human CALM1 calmodulin gene and identification of two CALM1-related pseudogenes CALM1P1 and CALM1P2. *Eur J Biochem.* (1994) 225:71–82. doi: 10.1111/j.1432-1033.1994.00071.x
16. Toutenhoofd SL, Foletti D, Wicki R, Rhyner JA, Garcia F, Tolon R, et al. Characterization of the human CALM2 calmodulin gene and comparison of the transcriptional activity of CALM1, CALM2 and CALM3. *Cell Calcium* (1998) 23:323–38. doi: 10.1016/S0143-4160(98)90028-8
17. Halling DB, Liebeskind BJ, Hall AW, Aldrich RW. Conserved properties of individual $Ca^{2+}$-binding sites in calmodulin. *Proc Natl Acad Sci USA.* (2016) 113:E1216–25. doi: 10.1073/pnas.1600385113
18. Papatheodorou I, Fonseca NA, Keays M, Tang YA, Barrera E, Bazant W, et al. Expression Atlas: gene and protein expression across multiple studies and organisms. *Nucleic Acids Res.* (2018) 46:D246–51. doi: 10.1093/nar/gkx1158
19. Uhlen M, Fagerberg L, Hallstrom BM, Lindskog C, Oksvold P, Mardinoglu A, et al. Tissue-based map of the human proteome. *Science* (2015) 347:1260419. doi: 10.1126/science.1260419
20. Limpitikul WB, Dick IE, Tester DJ, Boczek NJ, Limphong P, Yang W, et al. A precision medicine approach to the rescue of function on malignant calmodulinopathic long-QT syndrome. *Circ Res.* (2017) 120:39–48. doi: 10.1161/CIRCRESAHA.116.309283
21. Babu YS, Bugg CE, Cook WJ. Structure of calmodulin refined at 2.2 A resolution. *J Mol Biol.* (1988) 204:191–204. doi: 10.1016/0022-2836(88)90608-0
22. Beccia MR, Sauge-Merle S, Lemaire D, Brémond N, Pardoux R, Blangy S, et al. Thermodynamics of calcium binding to the calmodulin N-terminal domain to evaluate site-specific affinity constants and cooperativity.*J Biol Inorg Chem.* (2015) 20:905–19. doi: 10.1007/s00775-015-1275-1
23. VanScyoc WS, Sorensen BR, Rusinova E, Laws WR, Ross JBA, Shea MA. Calcium binding to calmodulin mutants monitored by domain-specific intrinsic phenylalanine and tyrosine fluorescence. *Biophys J.* (2002) 83:2767–80. doi: 10.1016/S0006-3495(02)75286-7
24. Tadross MR, Dick IE, Yue DT. Mechanism of local and global $Ca^{2+}$ sensing by calmodulin in complex with a $Ca^{2+}$ channel. *Cell* (2008) 133:1228–40. doi: 10.1016/j.cell.2008.05.025
25. Stigler J, Rief M. Calcium-dependent folding of single calmodulin molecules. *Proc Natl Acad Sci USA.* (2012) 109:17814–9. doi: 10.1073/pnas.1201801109
26. Wu X, Bers DM. Free and bound intracellular calmodulin measurements in cardiac myocytes. *Cell Calcium* (2007) 41:35364. doi: 10.1016/j.ceca.2006.07.011
27. Maier LS, Ziolo MT, Bossuyt J, Persechini A, Mestril R, Bers DM. Dynamic changes in free Ca-calmodulin levels in adult cardiac myocytes. *J Mol Cell Cardiol.* (2006) 41:451–8. doi: 10.1016/j.yjmcc.2006.04.020
28. Erickson MG, Alseikhan BA, Peterson BZ, Yue DT. Preassociation of calmodulin with voltage-gated Ca(2+) channels revealed by FRET in single living cells. *Neuron* (2001) 31:973–85. doi: 10.1016/S0896-6273(01)00438-X
29. Shah VN, Wingo TL, Weiss KL, Williams CK, Balser JR, Chazin WJ. Calcium-dependent regulation of the voltage-gated sodium channel hH1: intrinsic and extrinsic sensors use a common molecular switch. *Proc Natl Acad Sci USA.* (2006) 103:3592–7. doi: 10.1073/pnas.0507397103

30. Mori MX, Erickson MG, Yue DT. Functional stoichiometry and local enrichment of calmodulin interacting with $Ca^{2+}$ Channels. *Science* (2004) 304:432–5. doi: 10.1126/science.1093490
31. Peterson BZ, DeMaria CD, Adelman JP, Yue DT. Calmodulin is the $Ca^{2+}$ sensor for $Ca^{2+}$-dependent inactivation of L-type calcium channels. *Neuron* (1999) 22:549–58. doi: 10.1016/S0896-6273(00)80709-6
32. Liu X, Zhang X, Herbert SJ. Feeding China's growing needs for grain. *Nature* (2010) 465:420. doi: 10.1038/465420a
33. Valeyev N V, Bates DG, Heslop-Harrison P, Postlethwaite I, Kotov N V. Elucidating the mechanisms of cooperative calcium-calmodulin interactions: a structural systems biology approach. *BMC Syst Biol.* (2008) 2:48. doi: 10.1186/1752-0509-2-48
34. Boschek CB, Jones TE, Squier TC, Bigelow DJ. Calcium occupancy of N-terminal sites within calmodulin induces inhibition of the ryanodine receptor calcium release channel. *Biochemistry* (2007) 46:10621–8. doi: 10.1021/bi700655h
35. Gomez-Hurtado N, Boczek NJ, Kryshtal DO, Johnson CN, Sun J, Nitu FR, et al. Novel CPVT-associated calmodulin mutation in CALM3 (CALM3-A103V) activates arrhythmogenic Ca waves and sparks. *Circ Arrhythm. Electrophysiol.* (2016) 9:e004161. doi: 10.1161/CIRCEP.116.004161
36. Jiménez-Jáimez J, Doza JP, Ortega Á, Macías-Ruiz R, Perin F, Rodríguez-Vázquez Del Rey MM, et al. Calmodulin 2 mutation N98S is associated with unexplained cardiac arrest in infants due to low clinical penetrance electrical disorders. *PLoS ONE* (2016) 11:e0153851. doi: 10.1371/journal.pone.0153851
37. Daly, A, Johnson, NM, Decker, E, Callis, TE, Tahiliani, J, Garcia, J, et al. Pathogenic variants in calmodulin associated with resuscitated childhood cardiac arrest (Abstract C-AB01-05). *Heart Rhythm* (2017) 14:S2. Available online at: https://www.heartrhythmjournal.com/article/S1547-5271(17)30422-8/pdf
38. Makita N, Yagihara N, Crotti L, Johnson CN, Beckmann B-M, Roh MS, et al. Novel calmodulin mutations associated with congenital arrhythmia susceptibility. *Circ Cardiovasc Genet.* (2014) 7:466–74. doi: 10.1161/CIRCGENETICS.113.000459
39. Pipilas DC, Johnson CN, Webster G, Schlaepfer J, Fellmann F, Sekarski N, et al. Novel calmodulin mutations associated with congenital long QT syndrome affect calcium current in human cardiomyocytes. *Heart Rhythm* (2016) 13:2012–9. doi: 10.1016/j.hrthm.2016.06.038
40. Chaix MA, Koopmann TT, Goyette P, Alikashani A, Latour F, Fatah M, et al. Novel CALM3 mutations in pediatric long QT syndrome patients support a CALM3-specific calmodulinopathy. *Heart Rhythm Case Rep.* (2016) 2:250–4. doi: 10.1016/j.hrcr.2016.02.002
41. Boczek NJ, Gomez-Hurtado N, Ye D, Calvert ML, Tester DJ, Kryshtal D, et al. Spectrum and prevalence of CALM1-, CALM2-, and CALM3-encoded calmodulin variants in long QT syndrome and functional characterization of a novel long QT syndrome-associated calmodulin missense variant, E141G. *Circ Cardiovasc Genet.* (2016) 9:136–46. doi: 10.1161/CIRCGENETICS.115.001323
42. Takahashi K, Ishikawa T, Makita N, Takefuta K, Nabeshima T, Nakayashiro M. A novel *de novo* calmodulin mutation in a 6-year-old boy who experienced an aborted cardiac arrest. *Heart Rhythm Case Rep.* (2017) 3:69–72. doi: 10.1016/j.hrcr.2016.09.004
43. Anderson JH, Tester DJ, Will ML, Ackerman MJ. Whole-exome molecular autopsy after exertion-related sudden unexplained death in the young. *Circ Cardiovasc Genet.* (2016) 9:259–65. doi: 10.1161/CIRCGENETICS.115.001370
44. Lek M, Karczewski KJ, Minikel E V., Samocha KE, Banks E, Fennell T, et al. Analysis of protein-coding genetic variation in 60,706 humans. *Nature* (2016) 536:285–91. doi: 10.1038/nature19057
45. Crotti L, Spazzolini C, Boczek N, Jimenez Jaimez J, Makita N, Tester D, et al. International Calmodulinopathy Registry (ICaMR). *Circulation* (2016) 134:A14840. doi: 10.1161/circ.134.suppl_1.14840
46. Alseikhan BA, DeMaria CD, Colecraft HM, Yue DT. Engineered calmodulins reveal the unexpected eminence of $Ca^{2+}$ channel inactivation in controlling heart excitation. *Proc Natl Acad Sci USA.* (2002) 99:17185–90. doi: 10.1073/pnas.262372999
47. Yin G, Hassan F, Haroun AR, Murphy LL, Crotti L, Schwartz PJ, et al. Arrhythmogenic calmodulin mutations disrupt intracellular cardiomyocyte $Ca^{2+}$ regulation by distinct mechanisms. *J Am Heart Assoc.* (2014) 3:e000996. doi: 10.1161/JAHA.114.000996
48. Hwang HS, Nitu FR, Yang Y, Walweel K, Pereira L, Johnson CN, et al. Divergent regulation of ryanodine receptor 2 calcium release channels by arrhythmogenic human calmodulin missense mutants. *Circ Res.* (2014) 114:1114–24. doi: 10.1161/CIRCRESAHA.114.303391
49. Rocchetti M, Sala L, Dreizehnter L, Crotti L, Sinnecker D, Mura M, et al. Elucidating arrhythmogenic mechanisms of long-QT syndrome CALM1-F142L mutation in patient-specific induced pluripotent stem cell-derived cardiomyocytes. *Cardiovasc Res.* (2017) 113:531–41. doi: 10.1093/cvr/cvx006
50. Limpitikul WB, Dick IE, Joshi-Mukherjee R, Overgaard MT, George AL, Yue DT. Calmodulin mutations associated with long QT syndrome prevent inactivation of cardiac L-type $Ca^{2+}$ currents and promote proarrhythmic behavior in ventricular myocytes. *J Mol Cell Cardiol.* (2014) 74:115–24. doi: 10.1016/j.yjmcc.2014.04.022
51. Yamamoto Y, Makiyama T, Harita T, Sasaki K, Wuriyanghai Y, Hayano M, et al. Allele-specific ablation rescues electrophysiological abnormalities in a human iPS cell model of long-QT syndrome with a CALM2 mutation. *Hum Mol Genet.* (2017) 26:1670–7. doi: 10.1093/hmg/ddx073
52. Webster G, Schoppen ZJ, George AL. Treatment of calmodulinopathy with verapamil. *BMJ Case Rep.* (2017) 2017:bcr-2017-220568. doi: 10.1136/bcr-2017-220568
53. *European Reference Networks, ERN GUARD-Heart*. Available online at: https://ec.europa.eu/health/ern/overview_en and http://guardheart.ern-net.eu/disease-registries/
54. Zipes DP, Wellens HJJ. Sudden cardiac death. *Circulation* (1998) 98:2334–51. doi: 10.1161/01.CIR.98.21.2334
55. Sala L, Bellin M, Mummery CL. Integrating cardiomyocytes from human pluripotent stem cells in safety pharmacology: has the time come? *Br J Pharmacol.* (2017) 174:3749–65. doi: 10.1111/bph.13577
56. Giacomelli E, Bellin M, Sala L, van Meer BJ, Tertoolen LGJ, Orlova VV, et al. Three-dimensional cardiac microtissues composed of cardiomyocytes and endothelial cells co-differentiated from human pluripotent stem cells. *Development* (2017) 144:1008–17. doi: 10.1242/dev.143438
57. Schaaf S, Shibamiya A, Mewe M, Eder A, Stöhr A, Hirt MN, et al. Human engineered heart tissue as a versatile tool in basic research and preclinical toxicology. *PLoS ONE* (2011) 6:e26397. doi: 10.1371/journal.pone.0026397


**Conflict of Interest Statement:** The authors declare that the research was conducted in the absence of any commercial or financial relationships that could be construed as a potential conflict of interest.